UNIVERSIDADE BEIRA INTERIOR

Development of new steroidal oximes as possible anticancer drugs

Catarina Sofia Simão Canário

Tese para obtenção do Grau de Doutor em
Ciências Farmacêuticas
(3º ciclo de estudos)

Orientador: Prof. Doutor Gilberto Lourenço Alves
Coorientador: Prof. Doutor Samuel Martins Silvestre
Coorientador: Prof. Doutor Amílcar Celta Falcão Ramos Ferreira

Júri:
Prof. Doutora Ana Paula Coelho Duarte
Prof. Doutor Samuel Martins Silvestre
Prof. Doutora Maria Manuel da Cruz Silva
Prof. Doutor Bruno Miguel Alves Fernandes do Gago
Prof. Doutor Nuno Filipe de Sousa Vale
Prof. Doutor Márcio José de Abreu Marques Rodrigues

15 de Novembro de 2022

Declaração de Integridade

Eu, Catarina Sofia Simão Canário, que abaixo assino, estudante com o número de inscrição D1312 do 3º Ciclo em Ciências Farmacêuticas da Faculdade de Ciências da Saúde, declaro ter desenvolvido o presente trabalho e elaborado o presente texto em total consonância com o **Código de Integridade da Universidade da Beira Interior**.

Mais concretamente afirmo não ter incorrido em qualquer das variedades de Fraude Académica, e que aqui declaro conhecer, e que em particular atendi à exigida referenciação de frases, extratos, imagens e outras formas de trabalho intelectual, e assim assumo na íntegra as responsabilidades da autoria.

Universidade da Beira Interior, Covilhã

Assinado por: **CATARINA SOFIA SIMÃO CANÁRIO**
Num. de Identificação: 13378841
Data: 2022.11.16 18:43:33+00'00'

CARTÃO DE CIDADÃO

The experimental work presented in this thesis was carried out at the Health Sciences Research Centre of the University of Beira Interior (CICS-UBI), under the scientific supervision of Professor Gilberto Lourenço Alves (CICS-UBI, Covilhã), Professor Samuel Martins Silvestre (CICS-UBI, Covilhã) and Professor Amílcar Celta Falcão Ramos Ferreira (CIBIT – Coimbra Institute for Biomedical Imaging and Translational Research of the University of Coimbra, Coimbra).

O trabalho experimental apresentado nesta tese foi realizado no Centro de Investigação em Ciências da Saúde da Universidade da Beira Interior (CICS-UBI), sob a orientação científica do Professor Doutor Gilberto Lourenço Alves (CICS-UBI, Covilhã), do Professor Doutor Samuel Martins Silvestre (CICS-UBI, Covilhã) e do Professor Doutor Amílcar Celta Falcão Ramos Ferreira (CIBIT – Centro de Imagem Biomédica e Investigação Translacional da Universidade de Coimbra, Coimbra).

À minha Tia Albertina.

Agradecimentos

A elaboração de uma tese académica não resulta exclusivamente do esforço solitário do seu autor, mas do contributo, estímulo e incentivo de algumas pessoas e entidades. A todas quero expressar, desde já, o meu reconhecimento e sincero agradecimento.

Em primeiro lugar, ao meu orientador, Professor Doutor Gilberto Alves, que me fez o convite para ingressar neste "Mundo" que é o doutoramento, aceitando orientar esta tese, entendendo as minhas dúvidas e forma de trabalhar. Nem sempre fácil, mas com as suas amáveis palavras e apoio constante, conseguimos hoje chegar aqui. O meu muito obrigado pela sua disponibilidade, apoio, amizade e ensinamentos prestados.

Ao Professor Doutor Samuel Silvestre, meu coorientador, cujas palavras serão sempre poucas para expressar o meu agradecimento. Obrigada pela sua presença assídua, sem a qual não seria possível desenvolver este trabalho. Agradeço o companheirismo, disponibilidade, ajuda, apoio, amizade e ensinamentos prestados.

Ao Professor Doutor Amílcar Falcão, meu coorientador, agradeço o seu apoio e ajuda que me foi dando ao longo da realização desta tese de doutoramento. A sua vasta experiência e reconhecimento científico foram fundamentais para chegar ao fim deste longo, mas recompensador caminho.

À Professora Doutora Adriana Santos, o meu muito obrigada pela sua disponibilidade constante e pelo seu enorme apoio na área da biologia celular. O seu conhecimento científico foi fundamental no apoio a esta tese.

À Vanessa de Brito pela sua grande ajuda na área do *docking* molecular e apoio prestado no laboratório.

À Patrícia Pires pela ajuda prestada no laboratório.

Ao Pedro Vicente pelo seu apoio na área de farmacocinética.

Ao Pedro Soeiro pelo seu apoio no laboratório.

O meu agradecimento especial à minha Amiga Mariana Matias pela amizade, palavras amigas, bem como toda a disponibilidade e entusiasmo enérgico e contagiante que sempre demonstrou. As longas conversas e desabafos, principalmente nas horas menos boas, mas também os bons momentos de descontração, em muito me ajudaram na

elaboração deste trabalho. Mais do que a nível profissional, é sobretudo a nível pessoal que gostaria de lhe manifestar o meu sincero reconhecimento.

Aos colegas do CICS, que percorreram os mesmos caminhos, os mesmos laboratórios, que partilharam os momentos de alegria, as mesmas dificuldades… a todos Vós, o meu muito obrigada.

À Universidade da Beira Interior que me possibilitou as condições necessárias para a realização deste trabalho.

Aos meus amigos, mas em especial às minhas Amigas Ana Sofia Rodrigues e Andreia Matos pela amizade de longos anos, pela vossa dedicação, disponibilidade, ajuda e por saberem e compreenderem tão bem o quanto é difícil acabar o doutoramento. O meu sincero agradecimento.

Aos meus colegas de trabalho da Mutualista Covilhanense, especialmente à Andreia Gaspar e Zenaide Fernandes e, aos meus colegas do Hospital Garcia de Orta.

Por último, gostaria de agradecer de uma forma muito especial e sentida à minha Família. De uma forma muito especial aos meus Pais, pelo Amor, confiança, estímulo e apoio incondicionais que sempre me deram, pelos valores morais que me incutiram. A vossa presença constante permitiu-me sentir sempre confiante e capaz de realizar todos os objetivos a que me propus. A vós vos agradeço tudo o que sou hoje, pois sem vocês nada disto seria possível. O meu mais sincero OBRIGADA.

Ao meu marido, Márcio Geraldes, pelo amor, amizade, dedicação, disponibilidade, por acreditar que seria possível e pela compreensão nos momentos de ausência a que me dedicava à realização deste projeto.

A todos os que acreditam que “tentar não significa conseguir, mas os que conseguiram tentaram”, o meu sincero e sentido OBRIGADA!

Preface

The present doctoral thesis intends to describe the main achievements of the project entitled *"Development of new steroidal oximes as possible anticancer drugs"*. The potential of oxime compounds based on estrone scaffold as cytotoxic drugs was addressed.

The thesis is organized in seven chapters reflecting the work strategy followed in this project.

The **first chapter** discusses the problematic of cancer disease and the current therapeutic challenges in this field. The hormonal therapy is often used in hormone-dependent cancers, where steroid hormones have a crucial role in cancer progression. The main enzymes involved in steroidogenesis as well as steroidal compounds with activity against them were described. In addition, a brief discussion of *in silico* and experimental tools used in the preclinical evaluation of promising anticancer drugs was also performed.

The **second chapter** describes the synthesis and biological evaluation of $\Delta^{9,11}$-estrone derivatives.

The **third chapter** describes the synthesis and biological evaluation of C-ring estrone derivatives.

The **fourth chapter** focuses on the synthesis and biological evaluation of estrone *p*-quinol.

The **fifth chapter** focuses on the synthesis and biological evaluation of new oximes estrone derivatives.

Finally, the **sixth chapter** presents an integrated discussion of the most relevant findings of the preceding chapters, and the **seventh chapter** focuses on the main conclusions and contextualizes them in a future work.

Resumo Alargado

O cancro é uma das principais causas de morte em todo o mundo, responsável por quase 10 milhões de mortes em 2020. Os dados apresentados em 2020 pelo GLOBOCAN (Agência Internacional de Investigação sobre o Cancro) mostraram que o cancro do pulmão foi a principal causa de morte por cancro, com uma estimativa de 1,8 milhões de mortes (18%), seguido pelo cancro colorretal (9,4%), cancro do fígado (8,3%), cancro do estômago (7,7%) e cancro da mama feminino (6,9%). A indústria farmacêutica tem trabalhado arduamente para desenvolver novas terapêuticas anticancerígenas, com maior seletividade e melhor perfil de segurança, permitindo um aumento na sobrevida e qualidade de vida dos doentes. Em geral, a terapêutica hormonal é altamente eficaz contra os cancros hormono-dependentes e é bem tolerada. Assim, ao longo dos anos, muitas moléculas esteroides foram sintetizadas e testadas contra diferentes células tumorais na tentativa de se identificarem novos candidatos a fármacos anticancerígenos.

O presente trabalho teve como objetivo desenvolver novas oximas esteroides, da série estrano, com potencial interesse antitumoral. Para isso, foram sintetizados vários intermediários, os quais foram usados na síntese de oximas em C17 através da reação da hidroxilamina com a 17-cetona dos derivados da estrona. Depois de sintetizados, todos os compostos foram purificados e caracterizados através de espetros de infravermelho e de ressonância magnética nuclear (protão e carbono-13); os espetros de massa de alta resolução também foram obtidos para os novos compostos. Posteriormente, a citotoxicidade foi avaliada em seis linhas celulares [mama (MCF-7, T47-D), próstata (LNCaP), fígado (HepaRG), intestino (Caco-2) e fibroblastos da derme (NHDF)] através do ensaio do brometo de 3-(4,5-dimetiltiazol-2-il)-2,5-difeniltetrazólio (MTT). Também foram efetuados ensaios de estrogenicidade em células T47-D, bem como a análise de distribuição do ciclo celular e de microscopia de fluorescência com Hoechst 33258 para os compostos mais promissores. Estudos *in silico* de *docking* molecular foram realizados contra o recetor de estrogénios α (ERα), a esteroide sulfatase, a 17β-hidroxiesteroide desidrogenase tipo 1 e a β-tubulina. As previsões computacionais das propriedades farmacocinéticas e de toxicidade também foram obtidas e estudadas. A redução mais relevante da proliferação celular foi observada com os compostos $\Delta^{9,11}$-estrona em células HepaRG, com a oxima da $\Delta^{9,11}$-estrona em células LNCaP e com o acetato de 9α-hidroxi-11β-nitrooxiestrona em células dependentes de hormonas (MCF-7, T47-D e LNCaP). A $\Delta^{9,11}$-estrona mostrou citotoxicidade contra as células cancerígenas HepaRG (IC_{50} = 6,67 μM) promovendo a paragem do ciclo celular na fase G_0/G_1. A atividade estrogénica foi observada para este

composto a 0,1 μM nas células T47-D e os estudos de *docking* molecular estimaram uma interação interessante entre este composto e o ERα. A presença do grupo 16*E*-benzilideno, nos derivados da estrona, aumentou o efeito antiproliferativo nas células MCF-7 e T47-D. A introdução do grupo iodo nas posições 2 e 4 da estrona pareceu induzir uma citotoxicidade seletiva para as células HepaRG. No entanto, a presença de iodo e bromo nas posições 2 e 4 da $\Delta^{9,11}$-estrona não foi uma alteração estrutural favorável para o desenvolvimento de potenciais agentes antiproliferativos. Já a presença simultânea dos grupos 9α-hidroxi e 11β-nitrooxi no acetato de estrona reduziu marcadamente a viabilidade das células HepaRG (~92%). O acetato de 9α-hidroxiestrona exibiu um efeito antiproliferativo seletivo nas células HepaRG, induzindo a paragem do ciclo celular em G_0/G_1 e não promoveu um efeito estrogénico nas células T47-D. O *docking* molecular estimou uma afinidade geralmente mais baixa dos compostos oxidados no anel C para o ERα. O derivado *p*-quinol da estrona (10β-hidroxiestra-1,4-dieno-3,17-diona) exibiu atividade citotóxica marcada, particularmente contra células hormono-dependentes e a análise dos estudos de citometria de fluxo revelou que este composto reduziu significativamente a viabilidade das células HepaRG. O *docking* molecular mostrou uma alta afinidade para o ERα e para a 17β-hidroxiesteroide desidrogenase tipo 1. Além disso, foi predito que esta molécula tem uma boa biodisponibilidade oral e uma dose máxima tolerada baixa em humanos. Relativamente às oximas, foram sintetizadas seis oximas da série estrano, cinco das quais pela primeira vez. A 2-nitroestrona-17-oxima mostrou maior citotoxicidade que o composto original nas células MCF-7. Além disso, as oximas que continham grupos halogénio no anel A evidenciaram seletividade para as células HepaRG. Notavelmente, a $\Delta^{9,11}$-estrona-17-oxima foi a mais citotóxica para as células LNCaP e induziu a paragem do ciclo celular na fase G_2/M. Os estudos de microscopia de fluorescência mostraram a presença de DNA condensado típico da prófase e núcleos condensados e fragmentados característicos da apoptose. No entanto, esta oxima promoveu a proliferação das células T47-D. Os estudos de *docking* molecular estimaram uma forte interação entre a $\Delta^{9,11}$-estrona-17-oxima e o ERα e a β-tubulina, o que pode justificar os efeitos citotóxicos descritos. Em suma, a presença de um grupo oxima em C17 no núcleo da estrona mostrou ser uma boa estratégia para a obtenção de novas moléculas com potenciais efeitos anticancerígenos.

Palavras-chave

Atividade antiproliferativa; Derivados da estrona; *Docking* molecular; Estudos *in silico*; Oximas.

Abstract

Cancer is a leading cause of death worldwide, accounting for nearly 10 million deaths in 2020. Therefore, it is urgent to find new anticancer treatments. This work aimed to develop new steroidal oximes of the estrane series with potential antitumor interest.
For this, several intermediates and respective C17 oximes were synthesized by reaction of hydroxylamine with the 17-ketone of estrone derivatives. Then, their cytotoxicity was evaluated in six cell lines (MCF-7, T47-D, LNCaP, HepaRG, Caco-2 and NHDF) by the 3-(4,5-dimethylthiazol-2-yl)-2,5-diphenyltetrazolium bromide (MTT) assay. Estrogenicity assays, cell cycle distribution analysis and fluorescence microscopy studies with Hoechst 33258 staining were also performed for the most promising compounds. In addition, molecular docking against estrogen receptor α (ERα), steroid sulfatase, 17β-hydroxysteroid dehydrogenase type 1 and β-tubulin were also accomplished. Computational predictions of their pharmacokinetics and toxicity properties were also performed.
$\Delta^{9,11}$-estrone has been shown to be cytotoxic against HepaRG cancer cells (IC_{50} = 6.67 μM) and promoted a cell cycle arrest at G_0/G_1 phase. Estrogenic activity was also observed for this compound at 0.1 μM in T47-D cells and molecular docking studies estimated a marked interaction between this compound and ERα. The presence of a 16*E*-benzylidene group increased the antiproliferative effect on MCF-7 and T47-D cells. Moreover, the introduction of iodine in positions 2 and 4 of estrone seemed to induce a selective cytotoxicity for HepaRG cells. The 9α-hydroxy,11β-nitrooxyestrone derivative markedly reduced HepaRG cells viability (~92%) and 9α-hydroxyestrone acetate exhibited a selective antiproliferative effect on HepaRG cells, inducing a cell cycle arrest at G_0/G_1, and did not promote an estrogenic effect on T47-D cells. Docking studies estimated a generally lower affinity of C-ring oxidized compounds to ERα. Estrone *p*-quinol (10β-hydroxyestra-1,4-diene-3,17-dione) displayed marked cytotoxic activity, particularly against hormone-dependent cancer cells and the flow cytometry analysis revealed that this compound markedly reduced the viability of HepaRG cells. Molecular docking studies suggested a high affinity towards ERα and 17β-hydroxysteroid dehydrogenase type 1. Moreover, it was predicted that this molecule has a good oral bioavailability and a low maximum tolerated dose in humans. Concerning oximes, six steroidal oximes in estrane series were synthesized, five of which for the first time. The 2-nitroestrone oxime showed higher cytotoxicity than the parent compound on MCF-7 cells. Furthermore, the oximes bearing halogen groups in A-ring evidenced selectivity for HepaRG cells. Remarkably, the $\Delta^{9,11}$-estrone oxime was the most cytotoxic and arrested LNCaP cells in the G_2/M phase. Fluorescence microscopy

studies showed the presence of condensed DNA typical of prophase and condensed and fragmented nuclei characteristic of apoptosis. However, this oxime promoted the proliferation of T47-D cells. Interestingly, molecular docking studies estimated a strong interaction between $\Delta^{9,11}$-estrone oxime and ERα and β-tubulin, which may account for the described effects.
Thus, the presence of an oxime group at C17 in functionalized estrone scaffold showed to be a good strategy to obtain new molecules with potential anticancer effects.

Keywords

Antiproliferative activity; Estrone derivatives; *In silico* studies; Molecular docking; Oximes.

Table of contents

List of figures and schemes

Schemes

List of tables

List of abbreviations

ADMET	Absorption, distribution, metabolism, excretion, and toxicity
ATP	Adenosine triphosphate
AR	Androgen receptor
Bcl-2	Protein B-cell lymphoma 2
CAN	Ceric ammonium nitrate
CDKs	Cyclin-dependent kinases
CNS	Central nervous system
CFSE	Carboxyfluorescein diacetate
CRPC	Castration-resistant prostate cancer
CYP19A1	Aromatase
CYP17A1	17α-Hydroxylase/17,20-lyase
CYP450	Cytochrome P450
d	Doublet
dd	Double doublet
DDQ	2,3-Dichloro-5,6-dicyano-1,4-benzoquinone
DHEA	Dehydroepiandrosterone
DHT	5α-Dihydrotestosterone
DMAP	4-Dimethylaminopyridine
DMEM	Dulbecco's modified Eagle medium
DMSO	Dimethyl sulfoxide
DNA	Deoxyribonucleic acid
E1	Estrone
E2	17β-Estradiol
EDTA	Ethylenediamine tetraacetic acid
EMA	European Medicines Agency
EMATE	Estrone-3-*O*-sulphamate
ER	Estrogen receptor
ESI-HRMS	High-resolution mass spectrometry
EtOH	Ethanol
FBS	Fetal bovine serum
FCM	Flow cytometry
FDA	Food and Drug Administration
FL	Fluorescence channel

FSC	Channels forward scatter
FSH	Follicle-stimulating hormone
5-FU	5-Fluorouracil
GEMMs	Genetically engineered mouse models
GLOBOCAN	Global Cancer Observatory
HEDD	10β-Hydroxyestra-1,4-diene-3,17-dione
HER2	Human epidermal growth factor receptor 2
17β-HSD	17β-Hydroxysteroid dehydrogenase
IR	Infrared spectroscopy
LH	Luteinizing hormone
LHRH	Luteinizing hormone-releasing hormone
2ME2	2-Methoxyestradiol
MeOH	Methanol
MTT	3-(4,5-dimethylthiazol-2-yl)-2,5-diphenyltetrazolium bromide
NADPH	Nicotinamide adenine dinucleotide phosphate
NMR	Nuclear magnetic resonance
OMATE	Estrone oxime 3-*O*-sulfamate
PARP	Poly (ADP-ribose) polymerase
PDX	Patient-derived xenograft
PBS	Phosphate buffer saline
PDB	Protein data bank
PE	Petroleum ether bp 40 - 60 °C
PhH	Benzene
PI	Propidium iodide
PSA	Prostate specific antigen
5α-R	5α-Reductase
RNA	Ribonucleic acid
s	Singlet
SAR	Structure-activity relationship
SERD	Selective estrogen receptor degrader
SERM	Selective estrogen receptor modulator

SI	Selectivity index
SSC	Side scatter
StAR	Steroidogenic acute regulatory protein
STS	Steroid sulfatase
t	Triplet
TLC	Thin layer chromatography
UV	Ultraviolet

List of publications

Papers related with this thesis

1. Canário C, Silvestre S, Falcão A, Alves G. 2018. Steroidal Oximes: Useful Compounds with Antitumor Activities. Curr Med Chem. 25(6):660–686.

2. Canário C, Matias M, Brito V, Santos AO, Falcão A, Silvestre S, Alves G. 2020. $\Delta^{9,11}$-Estrone derivatives as potential antiproliferative agents: synthesis, *in vitro* biological evaluation and docking studies. C R Chim. 23(2):201–217.

3. Canário C, Matias M, Brito V, Pires P, Santos AO, Falcão A, Silvestre S, Alves G. 2022. C-Ring oxidized estrone acetate derivatives: assessment of antiproliferative activities and docking studies. Appl Sci. 12(7): e3579.

4. Canário C, Matias M, Brito V, Cruz-Vicente P, Soeiro P, Santos AO, Falcão A, Silvestre S, Alves G. 2022. 10β-Hydroxyestra-1,4-diene-3,17-dione as potential antiproliferative agent: *in vitro* biological evaluation and *in silico* studies. Nat Prod Res. 15:1-5.

5. Canário C, Matias M, Brito V, Santos AO, Falcão A, Silvestre S, Alves G. 2021. New Estrone Oxime Derivatives: Synthesis, Cytotoxic Evaluation and Docking Studies. Molecules. 26(9):e2687.

Chapter 1
General introduction

1.1 Cancer

Cancer, neoplasm or malignant tumor are a group of diseases, in which, abnormal cells divide without control and can invade nearby tissues or spread to other parts of the body (WHO 2020). Cancer cells distinguish from normal cells due to uncontrolled proliferation, undifferentiated cells and loss of function, avoidance of apoptosis, invasive power and formation of metastases. The eight hallmarks of cancer comprise the acquired capabilities for sustaining proliferative signaling, evading growth suppressors, resisting cell death, enabling replicative immortality, inducing/accessing vasculature, activating invasion and metastasis, reprogramming cellular metabolism and avoiding immune destruction (Hanahan and Weinberg 2000; Hanahan and Weinberg 2011). Recently, unlocking phenotypic plasticity, non-mutational epigenetic reprogramming, polymorphic microbiomes and senescent cells were new proposed hallmarks of cancer (Hanahan 2022).

Cancer may be classified considering the primary site of origin, the histological or tissue types where it is originated, grade or stage. As examples of primary site of origin, a patient can have breast cancer, lung cancer or colon cancer, among others. The cancer classification by tissue types is based on the International Classification of Diseases for Oncology, Third Edition (ICD-O-3) (WHO 2013) as follows: carcinoma, sarcoma, myeloma, leukemia and mixed types.

Carcinoma originates from the epithelial layer of cells that form the lining of external parts of the body or the internal linings of organs within the body. Sarcoma originates in connective and supportive tissues including muscles, bones, cartilage, and fat. Myeloma originates in the plasma cells of bone marrow. Leukemia is a cancer of the blood, and mixed types have two or more components of the cancer (e.g., carcinosarcoma). Cancers can also be classified in different grades according to abnormality of the cells with respect to surrounding normal tissues (grade 1 to grade 4; i.e., increasing abnormality increases the grade). On the other hand, cancer can also be classified individually according to their stage, considering the tumor size (T), the degree of regional spread or node involvement (N), and distant metastasis (M) – the so-called TNM staging method (Mandal 2019). Nowadays, cancer taxonomy is very important for diagnosis, prognosis and therapeutics (Salto-Tellez and Cree 2019).

1.1.1 Highlights of cancer history

The description of cancer dates back to the beginning of humankind, where a osteosarcoma from Swartkrans Cave, South Africa, was found about 1.7 million years ago (Odes et al. 2016). Fossilized bone tumors and human mummies in ancient Egypt,

as well as the ancient manuscripts, which data backs to 3000 BC, evidenced the description of cancer disease in history (Hajdu 2011a). Interestingly, the "Edwin Smith" and "George Ebers" papyri documents described the first procedure to remove breast cancer by cauterization (Faguet 2015). The “Father of Medicine” - Hippocrates (460-370 BC) - proposed the Humoral Theory of Medicine, in which, cancer occurred due to an excess of black bile (ACS 2020). He used the terms *karkinos* and *karkinoma* to describe the malignant processes because in Greek these words refer to a crab, the image associated to cancer (Faguet 2015).

Through the centuries, cancer was described as a curable disease only in its earliest stage. From the 17th century, it became more acceptable for physicians to dissect bodies to study and discover the cause of death. In 1761, Giovanni Morgagni of Padua was the first doctor that performed autopsies routinely. Then, the autopsies contributed significantly to the medical knowledge and the foundation of scientific oncology due to the better discovery of the human body (Hajdu 2011b; Hajdu 2012a; ACS 2020). In the 18th century, with the widespread use of the microscopes, it was discovered that the 'cancer poison' spread from the primary tumor through the lymph nodes to other sites of the body, creating metastasis. This discovery was first formulated by the English surgeon Campbell De Morgan between 1871 and 1874 (Hajdu 2012a). Later, in the 19th century, the scientific oncology had a very marked development with the use of modern microscope that allowed to study the diseased tissues. Rudolf Virchow, often called the founder of cellular pathology, provided the scientific basis for the modern pathologic study of cancer (Hajdu 2012b).

Remarkably, the first nitrogen mustards drugs used to treat Hodgkin's disease, lymphosarcoma and leukemias appeared in 1946, through Louis Goodman (Freireich 1984). In the early 20th century, oncology was established as a science because technological advances enabled to understand the molecular biology of cells as well as the development of research and diagnostic techniques, recognition of chemical carcinogens and development of chemotherapeutic agents (Hajdu and Darvishian 2013). In fact, the deeper knowledge of cancer biology allowed to develop novel and improved treatments against this heterogeneous pathological condition that has increased significantly over the years.

1.1.2 Epidemiology of cancer

The global cancer burden is increasing. Worldwide, an estimated 19.3 million new cancer cases and 10 million deaths occurred in 2020. Overall incidence was from 2-fold to 3-fold higher in transitioned *versus* transitioning countries for both sexes. The last cancer statistic update was done in 2020 by GLOBOCAN. Accordingly, lung cancer

remained the leading cause of cancer death, with an estimated 1.8 million deaths (18%), followed by colorectal (9.4%), liver (8.3%), stomach (7.7%), and female breast (6.9%) cancers. In 2020, thirty nine percent of all cancers diagnosed in men were lung (14.3%), prostate (14.1%) and colorectal (10.6%) cancers. For women, the three most common cancers were breast (24.5%), colorectal (9.4%) and lung (8.4%) (Sung et al. 2021).

In Portugal, the most frequently diagnosed cancers were colorectal (17%), breast (12%) and prostate cancer (11%) (**Figure 1.1**). Also, each year are detected about 6000 new cases of breast cancer and, unfortunately, 1500 women die because of this pathology (Liga Portuguesa Contra o Cancro 2021). According to GLOBOCAN data, colorectal cancer was the second most deadly and the third most commonly diagnosed cancer in the world (Bray et al. 2018; Sung et al. 2021). Of the patients that are diagnosed with colorectal cancer, 90% are older than 50, with a median age of 64 years (Granados-Romero et al. 2017). Concerning hepatocellular carcinoma, the incidence of this cancer has been rising worldwide over the last 20 years and it is expected to increase until 2030 in some countries (Dasgupta et al. 2020). In fact, liver cancer was the sixth most commonly diagnosed cancer and the third leading cause of cancer death worldwide in 2020 (Sung et al. 2021). This type of malignancy is significantly more observable among males with its highest incidence in the age group of 45 to 60 years (Mohammadian et al. 2018). The incidence of hepatocellular carcinoma is higher in Asia and Africa, where the endemic high prevalence of hepatitis B and C strongly predisposes patients to the development of chronic liver disease and subsequent development of cancer (Balogh et al. 2016).

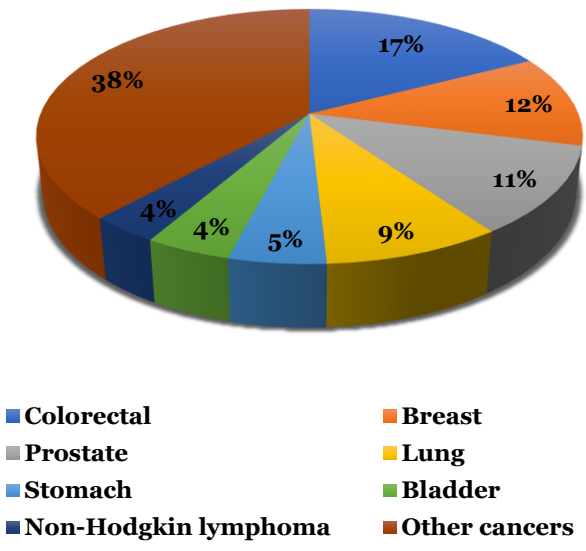

Figure 1.1 Cancer statistics in 2020 in Portugal (Sung et al. 2021).

In the future, if these trends remained, it is predicted there will be 28.4 million new cancer cases worldwide each year by 2040 (**Figure 1.2**). This represents an increase of 47% from 2020, with a larger increase in transitioning (64% to 95%) *versus* transitioned (32% to 56%) countries due to demographic changes (Sung et al. 2021).

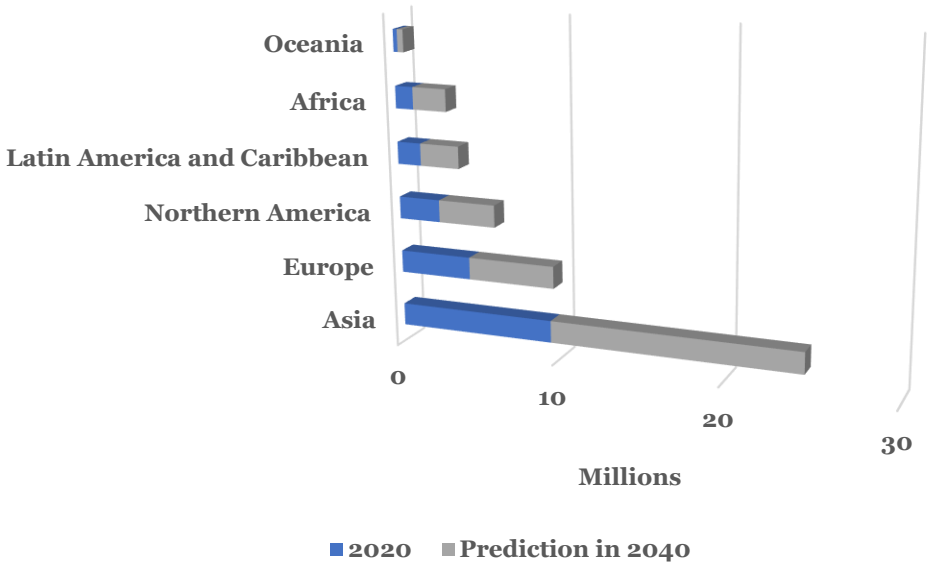

Figure 1.2 Forecast of cancer incidence worldwide in 2040 (Sung et al. 2021).

The interaction of many factors can contribute to cancer development. The recent global assessments of cancers have considered infections, diet, obesity, smoking and ultraviolet radiation as the main ones (Sung et al. 2021). Infections can increase cancer risk by several ways. Viral infections directly affect deoxyribonucleic acid (DNA), promote the tissue inflammation or suppress the immune system. As example, the human papilloma virus that causes genital warts has been shown to play an important role in cervical cancer development. A high-fat diet has also been associated with an increased risk for cancer of the prostate, endometrium and colorectal. It is believed that a high-fat diet is a cancer promoter because excess of fat seems to be involved in the production of free radicals. A diet based on plants, including vegetables, whole fruit, whole grains, and protein from peas and beans is better for reducing the risk of cancer (Stein and Colditz 2004). Also, cigarette smoking is the most significant cause of lung cancer and the leading cause of lung cancer death in both men and women. Smoking is also responsible for most cancers of the larynx, oral cavity and esophagus. The reduction of tobacco consumption is a good measure to reduce this major modifiable risk factor. The most common form of ultraviolet radiation exposure is from the sun. Then, avoiding an excess of sun exposure is important to prevent all skin cancers (Stein and Colditz 2004; Sung et al. 2021). Therefore, it is undoubtedly that, external and

internal factors (like genetic factors) may act together, or in sequence, to initiate or promote carcinogenesis.

1.1.3 Carcinogenesis

Carcinogenesis, also called oncogenesis or tumorigenesis, is the formation of a cancer, whereby normal cells are transformed into cancer cells and is closely related to DNA damage and tissue inflammation (Fishbein et al. 2021). A carcinogen is defined as any substance (chemical, physical or biological), which after inhalation, ingestion, dermal application or injection, can induce cancer, increase its incidence or shortens the time to tumor manifestation (Luch 2005). Some examples are tobacco compounds, alcohol, chemicals (e.g., aflatoxin, urethane, tryptophan metabolites, nitrosamines), radiation, viruses and environmental toxins. Also, carcinogens are classified as genotoxic and nongenotoxic (Fishbein et al. 2021). A genotoxic carcinogen is defined as a chemical that causes cancer by directly altering the genetic material of target cells and promoting DNA damage, while nongenotoxic carcinogens are chemicals that can induce cancer by other mechanisms, such as the promotion of chronic inflammation (Fishbein et al. 2021).

Carcinogenesis is a complex multistep process, which can be generally divided into three major stages: initiation, promotion, and progression. Initiation involves the alteration, change or mutation of genes that regulate cell division, apoptosis and DNA repair, arising spontaneously or induced by exposure to a carcinogenic agent [i.e., initiator agent, e.g. chemical (alkylating agents, polycyclic hydrocarbons, benzopyrene, aromatic amines, azo dyes), physical (ionizing and ultraviolet radiation) and biological carcinogens (*Helicobacter pylori*, Epstein-Barr virus, human papillomavirus)]. These modifications can result in dysregulation of biochemical signaling pathways associated with cellular proliferation, survival, differentiation or cellular death. The promotion stage is a reversible process in which actively proliferating preneoplastic cells accumulate. Examples of promoters include hormones, such as estrogens, drugs, chemicals and radiation. Progression is the last stage that involves a fast increase in the tumor size, where the cells may undergo further mutations with invasive and metastatic potential (Siddiqui et al. 2015).

The main genomic alterations that contribute to generation of cancer cells are mutations, DNA lesions, DNA strand breaks and DNA-protein links (Barnes et al. 2018). The failure of mechanisms of DNA repair involves the deregulation of proteins that control this process (e.g., DNA polymerases, serine/threonine protein kinases, checkpoint kinase 1) and the deregulation of biomolecules that control the cell cycle, such as proto-oncogenes and tumor suppressor genes (Wang et al. 2018; Kiwerska and

Szyfter 2019). Proto-oncogenes may function as growth factors, transducers of cellular signals and nuclear transcription factors. Mutations in proto-oncogenes originate oncogenes (e.g., mitogens, receptor tyrosine kinases, transcription factors), which promote cell proliferation. Examples of mutations that involved proto-oncogenes are point mutations of rat sarcoma virus (Ras) proto-oncogenes and chromosomal translocations that produce hybrid genes, such as the Philadelphia translocation (BRC-ABL). Also, lack or inactivation of tumor-suppressor genes (e.g., retinoblastoma 1 protein, pRb and tumor protein, p53) leads to cancer (Kontomanolis et al. 2020).

In hormone-dependent breast cancer, the main mutations involved in cancer development are mutations in breast cancer genes 1 and 2 (BRCA1 and BRCA2). Another highly important mutation can occur in tumor suppressor gene p53 resulting in a triple negative breast cancer. However, most breast cancer cases are not related to a mutated gene of high penetrance, but to genes of low penetrance such as checkpoint kinase 2 (CHEK2), cadherin-1 (CDH1), nibrin (NBS1), double strand break repair protein (RAD50), helicase (BRIP1) and partner and localizer of BRCA2 (PALB2) (Sheikh et al. 2015). In prostate cancer development, there are several genes involved, such as BRCA2, BRCA1, serine/threonine kinase (ATM), cyclin dependent kinase 12 (CDK12), protein for complementation group D2 (FANCD2) or Fanconi protein RAD51C (Dong 2006; Lozano et al. 2021).

Additionally, the continuous tissue inflammation could be a cause of cancer progression (Panigrahy et al. 2019). The carcinogen exposure can induce inflammatory pathways, which activate nuclear factor kappa-light-chain-enhancer of activated B cells (NF-κB), cytokines, eicosanoids production, inflammatory infiltrates (e.g., lymphocytes, neutrophils, eosinophils and Kupffer cells), pro-inflammatory and reactive oxygen species (Panigrahy et al. 2019). Resolution of inflammation promotes macrophage phagocytosis of cellular debris, inhibits the cytokine storm, suppresses inflammatory infiltration and, consequently, the inhibition of carcinogenesis (Fishbein et al. 2021).

Interestingly, cancer therapies either directly (chemotherapy and radiation) or indirectly (immunotherapy and antiangiogenic therapy) result in apoptotic tumor cell death (“debris”). However, these “debris” can paradoxically stimulate tumor growth and metastasis via pro-inflammatory mechanisms including a macrophage-secreted cytokine and eicosanoid “storm” of pro-angiogenic mediators (Chang et al. 2019; Fishbein et al. 2020).

1.1.4 Hormone-dependent cancers

A hormone-dependent cancer or hormone-sensitive cancer is a type of cancer that is dependent on hormones to grow and/or survive. Examples include the majority of breast cancers, some ovarian and some endometrial cancers, which are dependent on estrogens like 17β-estradiol (E2), and prostate cancers, which are dependent on androgens like testosterone (Henderson and Feigelson 2000; Herington et al. 2010).

1.1.4.1 Breast cancer

The development of breast cancer can occur in different areas of breast, such as in the ducts, the lobules or the tissue between them due to changes of stem cells function (**Figure 1.3**) (Feng et al. 2018).

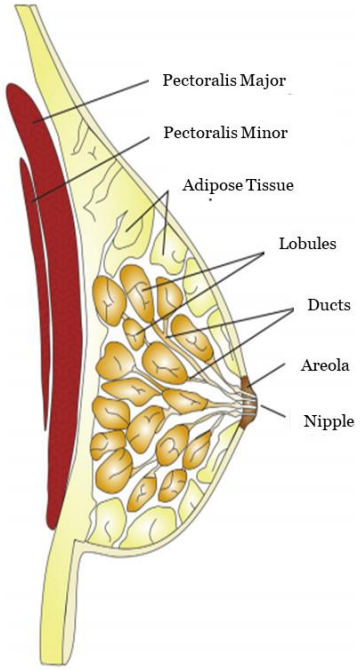

Figure 1.3 Breast tissue. Adapted from (Feng et al. 2018).

Normal breast tissue and mammary stem cells are regulated by several hormones [e.g., estrone (E1), E2]. E1 and E2 are hormones involved in cancer progression. Luteinizing hormone-releasing hormone (LHRH) from the hypothalamus stimulates the anterior pituitary to secrete luteinizing hormone (LH) and follicle-stimulating hormone (FSH). Then, LH stimulates androstenedione secretion from the ovarian and FSH controls the expression of both aromatase (CYP19A1) and 17β-hydroxysteroid dehydrogenase (17β-HSD) enzymes. In the granulosa cells, androstenedione is converted to E1 by the CYP19A1 enzyme pathway and 17β-HSD1 converts E1 to E2. Also, steroid sulfatase (STS) converts E1 sulfate into E1 (Fuentes and Silveyra 2019). Many signaling pathways

are also involved, such as estrogen receptors (ER), human epidermal growth factor receptor 2 (HER2), Wnt/β-catenin pathway, cyclin dependent kinases and by tubulin activity (Kamdje et al. 2014). Their deregulation contributes to cancer progression. Furthermore, recent reports showed that epigenetic regulations and noncoding ribonucleic acid (RNA) may play important roles in breast cancer development and may contribute to the heterogeneity and metastatic aspects of breast cancer, especially for triple-negative breast cancer (Feng et al. 2018). Nowadays, it is known that mutations in BRCA1 or BRCA2 are also related to this malignancy development (Allison 2012). In clinical practice, 70% of all breast cancers are characterized as positive for ER and/or progesterone receptors, HER2-negative and have low levels of antigen Ki-67. This type of cancer is characterized by low-grade slow growing and tends to have a good prognosis, with the treatment typically involving hormonal therapy (Veronesi et al. 2005; Feng et al. 2018).
Concerning pathological features and invasiveness, breast cancers can be divided into three major groups (Feng et al. 2018):

- non-invasive (or *in situ*);
- invasive (the most common type of breast cancer, accounting for 80% of all cases);
- metastatic.

The main metastases associated to breast cancer can be found in lymph nodes in the armpit and/or in distant sites such as the lung, liver, bone and brain (Feng et al. 2018).

Importantly, a high percentage of breast cancers is hormone-dependent (~70%), expressing ER. In addition, a significant portion (~90%) of ER-positive (ER^+) breast tumors are also androgen receptor-positive (AR^+) (Majumder et al. 2017). For this reason, a good treatment approach may possibly depend on lowering estrogen levels in cancer tissues rather than in the whole organism. In fact, a cancer that is hormone-dependent has a better prognosis concerning disease evolution and treatment than those that are hormone-independent and present ER-mutated or non-functional (Ulm et al. 2019).

1.1.4.2 Prostate cancer

The prostate gland is composed by luminal (columnar cells), basal (elongated cells) and neuroendocrine cells surrounded by stroma, which contains stem cells (**Figure 1.4**) (Schrecengost and Knudsen 2013). The luminal cells express prostate specific antigen (PSA), prostatic acid phosphatase (PAP), AR and keratins (K) 8 and 18. The basal

cells express K5 and 14, antigen CD44 and protein B-cell lymphoma 2 (Bcl-2) (Hudson et al. 2001). The androgens testosterone and 5α-dihydrotestosterone (DHT) are hormones involved in cancer progression. LHRH from the hypothalamus stimulates the anterior pituitary to secrete LH and FSH. Then, LH stimulates testosterone secretion from the testes. In the prostatic cells, the enzyme 5α-reductase (5α-R) converts testosterone to DHT (more active). Androgens bind to AR, with the complex then entering the nucleus to influence cell growth and their overexpression can originate cancer (Elder et al. 2021).

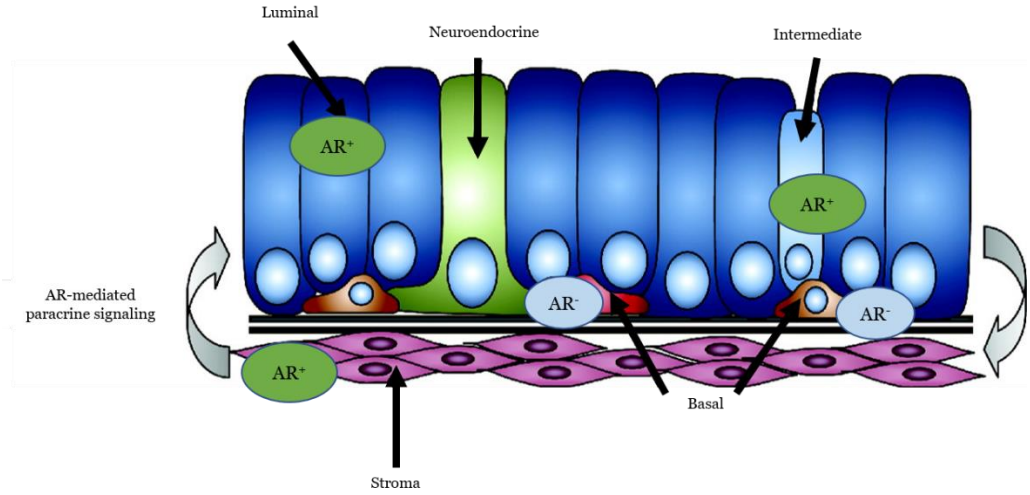

Figure 1.4 Prostate tissue. Adapted from (Taylor et al. 2010).

Carcinogenesis usually occurs in the prostatic epithelium and results in sequential disruption of coordinated reciprocal signaling between stroma and epithelium (Taylor et al. 2010). Growth of prostate cancer are regulated by several signaling pathways, such as Wnt/β-catenin pathway, AR signaling, NF-kB signaling, janus kinase-signal transducer and activator of transcription (JAK/STAT) signaling and receptor tyrosine kinase signaling (Ramalingam et al. 2017). The main mutations have occurred in AR, p53, pRb and Bcl-2 genes (Murray 2021; Mandigo et al. 2022).

Most prostate cancers (90%) are adenocarcinomas. Among these, 70% arise in the peripheral zone, 15-20% arise in the central zone and 10-15% arise in the transitional zone. Aggressiveness of the adenocarcinoma is reflected in the degree of differentiation on histology, which is graded using a Gleason Score grading system (Murray 2021).

Although androgen deprivation therapy is initially an effective treatment, the majority of patients develop resistance arising castration-resistant prostate cancer (CRPC) (Howard et al. 2019). The mechanisms associated with resistance may include gene amplifications, gene mutations, AR splice variants and changes in expression of AR co-regulatory proteins (Howard et al. 2019). Approximately, 80% of prostate cancer cases

are confined to the organ at the time of diagnosis, while 20% have metastasized locally or to distant organs (Ulm et al. 2019). Cancer cells may spread to other areas of the body, particularly the bones and distant lymph nodes (Buyyounouski et al. 2017).

1.1.5 Other cancers

Hepatocellular carcinoma is a primary malignancy of the liver that occurs predominantly in patients with liver cirrhosis, chronic hepatitis (B or C) and intoxication by alcohol, iron or aflatoxin-B1 (Balogh et al. 2016; Mazzanti et al. 2016). The development of hepatocellular carcinoma starts in both somatic (hepatocytes) and stem cells due to massive inflammation and fibrosis that are responsible for the deregulation of several signaling pathways and accumulation of genetic alterations in normal hepatocytes (Villanueva et al. 2007). The tyrosine kinase receptor pathways, the Ras mitogen-activated protein kinase (RAS/RAF/MAPK), the phosphatidylinositol 3-kinase (PI3K/AKT), the mammalian target of rapamycin (mTOR), the Wnt/β-catenin signaling pathway, the ubiquitin/proteasome degradation and the hedgehog signaling pathway are the critical pathways involved in the development of this type of cancer (Dimri and Satyanarayana 2020).

Colorectal cancer, also known as bowel or colon cancer, develops from the tissues of colon. Its incidence has been steadily rising in developed countries due to sedentary life, obesity, red meat consumption, alcohol and tobacco (Rawla et al. 2019). Colorectal cancer is a heterogeneous disease that develops via stepwise accumulation of well-characterized genetic and epigenetic alterations (Nguyen et al. 2020); it usually emerges from the epithelial cells of the large intestine and arise from precancerous polyps (growth on the inner lining of the colon or rectum) that are broadly categorized as either traditional tubular adenomas or serrated polyps (Nguyen et al. 2020). Different molecular mechanisms have been involved in the development and progression of colorectal cancer, such as the MAPK, cascades downstream of the epidermal growth factor receptor (EGFR), Notch pathway, PI3K/AKT pathway, transforming growth factor-β (TGF-β) and Wnt signaling pathways (Koveitypour et al. 2019).

1.1.6 Current therapeutic approaches in cancer

In recent years, remarkable progresses in cancer treatment occurred due to a better understanding of cancer biology. The therapy to be used may be selected according to the type of cancer, tumor size, tumor location, age of patient and comorbidities, but normally is used a combination of treatments. Current cancer therapeutic options

include surgery, radiotherapy, chemotherapy, immunotherapy, targeted therapy and hormonal therapy (Bidram et al. 2019).

Through surgery the damaged tissues can be removed. After surgical procedure, normally, the patients are treated with radiotherapy and/or chemotherapy. Despite the side effects, radiotherapy remains an important component of cancer treatment for at least 50% of all cancer patients and this technique use radiation to eliminate cancer cells (Baskar et al. 2012). On the other hand, chemotherapy utilizes cytotoxic drugs to kill cancer cells but, unfortunately, often also damages normal tissues, causing several side effects such as cardiotoxicity, neurotoxicity, infertility, nephropathy and chronic liver injury, among others (Lee et al. 2014; Pearce et al. 2017). Immunotherapy fights cancer by stimulating the innate or adaptive immune system of the patient (e.g., cancer vaccines, immune checkpoint inhibitors, chimeric antigen receptor (CAR)-T cells). The purpose of cancer immunotherapy is to improve the antigen presentation functions of dendritic cells, promote protective T cell response and overcome immunosuppression in the tumor (Meng et al. 2021).

Targeted cancer therapies inhibit growth, increase cell death and restrict the spread of cancer because drugs interfere with specific proteins involved in tumorigenesis. There are four main types of targeted cancer therapies: small molecule inhibitors, monoclonal antibodies, immunotherapeutic vaccines, and gene therapy (Baudino 2015). In fact, immunotherapy can also be considered a targeted therapy. Small molecules (< 900 Da) are able to penetrate into cells to target specific intracellular proteins. They can be used to target proteasomes, cyclin-dependent kinases (CDKs) and poly (ADP-ribose) polymerase (PARP) to activate cell-cycle checkpoints, promote apoptosis or manage DNA repair. Examples include imatinib, gefitinib, sunitinib, bortezomib, ribociclib and olaparib. Monoclonal antibodies are more specific, and they target only one protein. The target protein must be extracellular because antibodies cannot enter the cell. Bevacizumab, trastuzumab, brentuximab vedotin are some examples. Therapeutic cancer vaccines target specific tumor-associated antigens through T-cell stimulation to activate immune response (e.g., bacillus Calmette-Guérin vaccine for bladder cancer). Gene therapy involves the introduction of genetic material, consisting of either DNA or RNA, into cancerous cell, to destroy or inhibit their growth (Lee et al. 2018). One of the advantages of molecular targeted therapy is its ability to deliver drug effectively with high specificity and, therefore, it is less toxic compared to conventional chemotherapy. However, the treatment is only effective in patients with tumors that express the particular biomarker (Lee et al. 2018).

Lastly, hormonal therapy or endocrine therapy, is another therapeutic approach that slows or stops the growth of main breast, endometrium and prostate cancers that need specific hormones to grow. As previously mentioned, the sex steroid hormones (androgens, estrogens and progesterone) are important for the proliferation of some cancers and hormonal therapy targets the activity of their receptors, as well as the availability of these hormones (Elder et al. 2021). It is usually considered a standard therapeutic choice for patients with ER^+ or AR^+ cancers and for non-life-threatening advanced disease or for older patients that cannot receive chemotherapy. When compared with chemotherapy, endocrine therapy gives rise to less side effects, but the therapeutical action is slower than that achieved with chemotherapeutic agents. Interestingly, once a response to hormonal therapy has been achieved it tends to be more sustained and produce greater survival benefit. The main side effect of this treatment is bone loss, which may lead to an increased risk of fracture (Cheung 2007). Unfortunately, 25–30% of treated women acquired resistance to hormonal therapies. The mechanisms involved in such resistance are changes in transcription of ER and its co-regulators, epigenomic and post-translational modifications in ER, genetic polymorphisms that affect ER expression, mutations in ER pathway and genomic aberrations (Haque and Desai 2019). Concerning prostate cancer, mean time from hormonal therapy relapsing (assessed by increase in serum PSA levels) remains around 30 months for patients without metastases and half for patients with metastases (Maitland 2021). The development of CRPC entails both androgen-dependent and androgen-independent growth signaling pathways [e.g. fibroblast growth factor (FGF), transforming growth factor β (TGF-β), RAS/MAPK, Wnt-β pathways] (Crowley et al. 2021), although these mechanisms are not well understood.

Fortunately, several novel strategies have emerged aiming to reduce suffering and cancer-related death. However, they are not easily accessible due to their cost. These include (Bidram et al. 2019):

- Photodynamic therapy (technique that destroy tumor cells using a photosensitizing drug activated by specific wavelengths of light);
- Photothermal therapy (technique that use a photothermal agent activated by light producing heat to damage tumor cells);
- Nanoparticle-drug therapy (drugs incorporated in nanoparticles to more precisely target tumor cells; e.g., liposomal doxorubicin).

1.1.6.1 Breast cancer

Surgery, radiotherapy, chemotherapy and hormonal therapy are the main treatments applied against breast tumor disease (NCCN 2021). Concerning hormonal therapy, there are many ways of reducing the hormonal stimulation in breast cancers. These include (Elder et al. 2021):

- Suppression/ablation of ovarian function by:
    - Surgical oophorectomy;
    - Pelvic radiotherapy;
    - Use of LHRH agonists (e.g., goserelin).
- Use of selective estrogen receptor modulators (SERMs; e.g., tamoxifen).
- Use of aromatase inhibitors (e.g., anastrozole, exemestane, letrozole).

LHRH agonists causes a down-regulation of pituitary LHRH receptors, leading to a decrease in LH/FSH, which in turn leads to reduced serum E2 levels. These drugs are reserved for higher risk patients (young age, large tumor size, high grade, multiple lymph nodes positive) and for metastatic disease (Elder et al. 2021).
SERMs work by binding to activating regions of the ER by competitive antagonism. Tamoxifen, for example, is a first-line adjuvant treatment approach in premenopausal women. Normally, it is administered for 5 to 10 years. The main side effects include hot flushes, vaginal discharge/dryness, nausea and weight gain (NCCN 2021).
In addition, aromatase inhibitors reduce E2 production and are usually used in postmenopausal women. Their side effects include arthralgia, osteoporosis and hypercholesterolemia (NCCN 2021).

Examples of drugs available and approved for breast cancer treatment are described in **Table 1.1** (Ulm et al. 2019).

Table 1.1 Examples of drugs that have been used in breast cancer treatment.

Drugs	Class	Mechanism of action	Ref.
Paclitaxel, docetaxel, albumin-bound paclitaxel	Taxanes	Blocks the ability of cells to break down the internal 'skeleton' that allows them to divide	(EMA 2010; EMA 2015)
Doxorubicin, pegylated liposomal doxorubicin, epirubicin	Anthracyclines	Act mainly by intercalating with DNA and inhibit topoisomerase II	(Janssen 1996)
Cisplatin, carboplatin	Platinum	DNA damage	(Petrelli et al. 2014)
Vinorelbine	Vinca alkaloids	Microtubule inhibitor	(NCCN 2021)
Cyclophosphamide	Alkylating agents	Strand cross-linkage of DNA molecules	(NCCN 2021)
5-FU or capecitabine	Antimetabolites	Block thymidylate synthetase	(Ponce-Cusi and Calaf 2016)
Trastuzumab, pertuzumab	Monoclonal antibodies	Attach HER2 protein	(EMA 2018a)
Lapatinib	Kinase inhibitors	Block tyrosine kinase	(EMA 2018b)
Palbociclib, ribociclib	CDK4/6 inhibitors	Block cyclin-dependent kinases	(Pfizer 2016)
Olaparib	PARP inhibitors	Block the action of the enzyme PARP	(EMA 2020a)
Trastuzumab emtansine	Antibody-drug conjugates	Attach Her2 protein and blocks tubulin	(EMA 2016a; EMA 2020b)
Trastuzumab deruxtecan		Attach Her2 protein and blocks topoisomerase I.	
Hormonal therapy			
Tamoxifen	SERMs	Competes with E2 at the receptor site and blocks the promotional role of E2 in breast cancer	(Jones and Buzdar 2004)
Fulvestrant	ER antagonists	Inhibits receptor dimerization and promote degradation of ER	
Anastrozole, exemestane, letrozole	Aromatase inhibitor	Block the active site of enzyme	

CDK4/6, Cyclin-dependent kinase 4 and 6; DNA, Deoxyribonucleic acid; EGFR, Epidermal growth factor receptor; ER, Estrogen receptor; E2, 17β-Estradiol; 5-FU, 5-Fluorouracil; HER2, Human epidermal growth factor receptor 2; PARP, Poly (ADP-ribose) polymerase; SERM, Selective estrogen receptor modulator.

1.1.6.2 Prostate cancer

Surgery, radiotherapy, hormonal therapy and chemotherapy are the main therapeutic options toward prostate tumor disease (NCCN 2022a). Concerning hormonal therapy,

there are many ways of reducing the hormonal stimulation in prostate cancers (Elder et al. 2021). These include:

- LHRH agonists (e.g., goserelin, triptorelin).
- LHRH antagonists (e.g., degarelix);
- Cytochrome P450 (CYP) 17A1 inhibitor (e.g., abiraterone);
- Antiandrogens (e.g., bicalutamide, enzalutamide, apalutamide).

Hormonal therapy is the main treatment applied in AR^+ prostate tumor disease. It is the first line approach for regional or advanced disease and as neoadjuvant in combination with radiation in localized or locally advanced prostate cancers (NCCN 2022a).

LHRH agonists and antagonists cause a down-regulation of pituitary LHRH receptors, leading to a decrease in LH/FSH, which in turn leads to reduced serum testosterone levels. Antiandrogens, also known as androgen antagonists or testosterone blockers, are a class of drugs that prevents androgens, like testosterone and DHT, from mediating their biological effects in the body. They act by blocking the AR and/or inhibiting or suppressing androgen production. Enzalutamide can be used for castration-resistant prostate cancer that is not metastatic (has not yet spread) but has a high risk of metastasizing. Abiraterone acetate, a CYP17A1 inhibitor, is metabolized to abiraterone, which stops the body production of testosterone. It is used to treat men with metastatic prostate cancer. The main side effects of these drugs can include impotence, diarrhea, fatigue, rash, and worsening of hot flashes (Elder et al. 2021; NCCN 2022a).

Examples of drugs available and approved for prostate cancer treatment are described in **Table 1.2**.

Table 1.2 Examples of drugs that have been used in prostate cancer treatment.

Drugs	Class	Mechanism of action	Ref.
Docetaxel, Cabazitaxel	Taxanes	Blocks the ability of cells to break down the internal 'skeleton' that allows them to divide	(EMA 2010)
Olaparib Rucaparib	PARP inhibitors	Block the action of enzyme PARP	(Abida et al. 2020)
Hormonal therapy			
Bicalutamide Enzalutamide Apalutamide	AR antagonist	Blocks AR	(NCCN 2022a)
Abiraterone Acetate	CYP17A1 inhibitor	Blocks CYP17A1	

AR, Androgen receptor; CYP17A1, 17-α-hydroxylase/17,20-lyase; PARP, Poly (ADP-ribose) polymerase.

1.1.6.3 Drugs ongoing clinical trials for breast and prostate cancer

Cancer clinical trials are critical to bring new and potentially lifesaving treatments to more patients with cancer and may represent the greatest hope for those currently facing the disease. Some examples of ongoing clinical trials for breast and prostate cancer treatment are summarized in **Table 1.3**.

Table 1.3 Examples of drugs ongoing clinical trials for breast and prostate cancer treatment.

Drug candidate	Mechanism of action	Disease	Phase of development	Sponsor	Ref
Atezolizumab Plus Nab-Paclitaxel	PDL1 inhibitor plus taxane	Triple-negative breast cancer	Phase III	Hoffmann-La Roche	(Schmid et al. 2018).
Elacestrant	SERD	Breast cancer	Phase III	Radius Pharmaceuticals, Inc.	(Bardia et al. 2019)
Seviteronel	CYP17A1 inhibitor	Prostate and breast cancer	Phase II	Innocrin Pharmaceutical	(Madan et al. 2020)
Atezolizumab plus Trastuzumab plus Vinorelbine	PDL1 inhibitor plus targeted therapy plus microtubule destabilizing agent	Breast cancer	Phase II	SOLTI Breast Cancer Research Group	(Parsons et al. 2021)
LAE001	CYP17A1 inhibitor	Prostate cancer	Phase I and II	Laekna Limited	(Bessudo et al. 2021)

CYP17A1, 17α-hydroxylase/17,20 lyase; PDL1, Programmed death-ligand 1; SERD, Selective ER degrader.

1.1.6.4 Hepatocellular and colorectal cancer treatment

Nowadays, few options are clinically available to treat hepatocellular carcinoma. The main therapeutic options used to treat hepatocellular carcinoma are surgery, radiotherapy, chemotherapy, immunotherapy or transplantation. Atezolizumab plus bevacizumab, sorafenib, regorafenib or ramucirumab are some of the options used in chemotherapy. Liver transplantation remains the best option to cure. However, the supply of good-quality deceased-donor organs is limited (NCCN 2022b).

The main treatments used in colorectal cancer are surgery, radiotherapy, and combination chemotherapy. The main chemotherapy regimens available and approved for colorectal cancer treatment include FOLFOX [oxaliplatin plus leucovorin plus 5-fluorouracil (5-FU)], FOLFIRI (irinotecan plus leucovorin plus 5-FU), and XELOX (oxaliplatin plus capecitabine); trifluridine plus tipiracil; bevacizumab or EGFR inhibitors for KRAS/NRAS/BRAF mutations (cetuximab or panitumumab), which can be added for advanced or metastatic disease (Wolpin and Mayer 2008; NCCN 2022c).

When available therapeutic options are not successful, patients can be advised to participate in clinical trials, enabling the evaluation of new drug candidates, different

drug combinations, new approaches to radiation therapy or surgery and new methods of treatment.

1.1.7 Common therapeutic targets for anticancer steroids

In the last years, new anticancer drugs have been developed considering specific targets (Ulm et al. 2019). By molecular docking, predictive interactions with ERα, STS, 17β-HSD1 and β-tubulin targets were evaluated. These proteins are involved in steroidogenesis and cell cycle control.

1.1.7.1 Estrogen receptor α

ERα is a transcription factor that is involved in the regulation of many complex physiological processes in humans. The association between ERα activity and estrogens reveals that this receptor also regulates cell proliferation as well as therapeutic resistance (Lee et al. 2012; Begam et al. 2017; Miki et al. 2018). There are two subtypes of the nuclear ER, ERα and ERβ, which exhibit distinct cellular and tissue distribution in human body. ERα is mainly expressed in mammary gland, uterus, ovary (thecal cells), bone, male reproductive organs (testes and epididymis), prostate (stroma) and adipose tissue. In contrast, ERβ is predominant in prostate (epithelium), bladder, ovary (granulosa cells) and immune system (Farzaneh and Zarghi 2016).
The structure of ER is subdivided into six functionally distinct domains (**Figure 1.5**).

Figure 1.5 Human estrogen receptor (ER) ligand-binding domain in complex with 17β-estradiol (E2) (from PDB).

The ERα ligand binding domain has composed by 12 helices, which play a crucial role in determining interactions with coactivators and corepressors and, therefore, the respective agonist or antagonist effect of a ligand. Ligand recognition is achieved through hydrogen bonds and the complementarity with the hydrophobic residues that line the cavity to the non-polar nature of the ER ligands (Yaşar et al. 2017). Structure-

activity relationship (SAR) studies showed that effective binding requires the presence of polar hydroxyl groups at C3 and C17 of steroid nucleus (Palomino 1999). Small hydrophobic substituents at positions 4, 12β, 14 and 16α enhance binding affinity, whereas larger hydrophobic substituents are tolerated at positions 7α, 11β and 17α. The binding to ER is hampered with polar substituents (Anstead et al. 1997).
Nowadays, in cancer treatment a SERM like tamoxifen and ER antagonists (antiestrogens) like fulvestrant are used (Elder et al. 2021; NCCN 2021)

1.1.7.2 Steroid sulfatases

The sulfatase protein family includes 17 different human sulfatases, where only STS act on steroid sulfates. STS is an enzyme that converts E1 sulfate and dehydroepiandrosterone (DHEA) sulfate into E1 and DHEA, respectively, as well as cholesterol sulfate and pregnenolone sulfate to their corresponding unconjugated forms (Payne and Hales 2004). STS has been found in the membranes of the cellular endoplasmic reticulum in testis, ovary, adrenal glands, placenta, prostate, skin, brain, fetal lung, viscera, endometrium, peripheral blood lymphocytes, aorta, kidney and bone (Hernandez-Guzman et al. 2001; Reed et al. 2005). It is a monomer with a molecular mass of 63 kDa, a *N*-terminal signal peptide of 21–23 amino acids and two functional (Asn47, Asn259) glycosylation sites (Reed et al. 2005). The three-dimensional structure of STS (**Figure 1.6**) shows a globular polar domain with the catalytic site and the putative transmembrane domain, which consists of two antiparallel hydrophobic α-helices (Hernandez-Guzman et al. 2003). STS includes Ca^{2+} as a cofactor and ten catalytically important amino acid residues: Arg35, Arg36, ARG78, Arg342, Lys134, Lys368, His136, His290, Gln343 and a formylglycine (FGly75) (Rižner 2016).

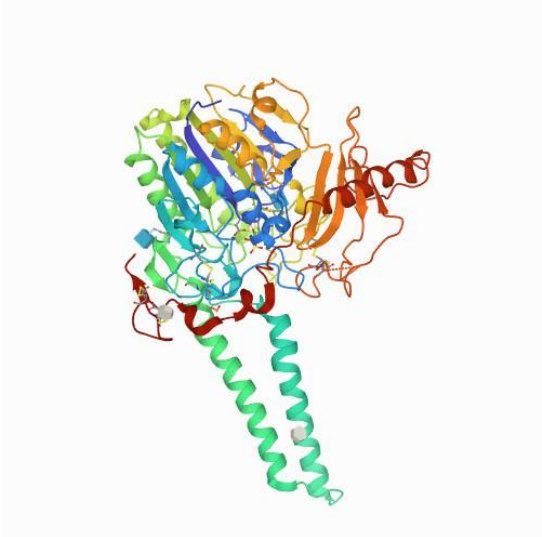

Figure 1.6 Structure of human placental estrone sulfatase (STS) (from PDB).

Estrone-3-*O*-sulphamate (EMATE) inhibited irreversibly STS enzyme (Purohit et al. 1995). Otherwise, irosustat is a non-steroid molecule that showed potent STS inhibitory effects (Palmieri et al. 2011).

1.1.7.3 17β-Hydroxysteroid dehydrogenase type 1

Human 17β-HSD catalyzes the interconversion of 17-ketosteroids (e.g., dehydroepiandrosterone, androstenedione and E1) to 17β-hydroxysteroids (e.g., androst-5-ene-3β,17β-diol (5-diol), testosterone and E2), using nicotinamide adenine dinucleotide phosphate (NADPH) as cofactor (Poirier 2011).

17β-HSD type 1 (**Figure 1.7**) is a cytosolic enzyme that belongs to the superfamily of short-chain dehydrogenases/reductases, which catalyzes the final step in the biosynthesis of estrogens promoting the activation of estrogens from weaker forms (E1 to E2 and 16α-hydroxyestrone to estriol). It is primarily expressed in the ovaries and placenta, but also at lower levels in the breast epithelium, and consists of 327 amino acid residues (34.9 kDa) and the active form exists as homodimer. 17β-HSD1 comprises a Rossmann fold (3-layer (αβα) sandwich), associated to cofactor binding ($NADP^+$/NADPH cofactor), and a steroid-binding cleft (Ghosh et al. 1995). The latter is described as a hydrophobic tunnel with polar residues at each end: His221/Glu282 on the C-terminal side, and Ser142/Tyr155, belonging to the catalytic tetrad (Peltoketo et al. 1988; Klein et al. 2011). Many 17β-HSD1 inhibitors have been developed and the compounds with a 16β-*m*-carbamoylbenzyl group at C16 position of E2 and E1 are considered highly potent compounds (Lespérance et al. 2021).

Figure 1.7 Crystal structure of human 17β-hydroxysteroid dehydrogenase type 1 (17β-HSD1) complexed with estrone (E1) (from PDB).

1.1.7.4 β-Tubulin

Tubulin (**Figure 1.8**) is a guanosine-5'-triphosphate-hydrolyzing globular protein constituted by α- and β-heterodimers that form the core of the microtubules (Nogales et al. 1998).

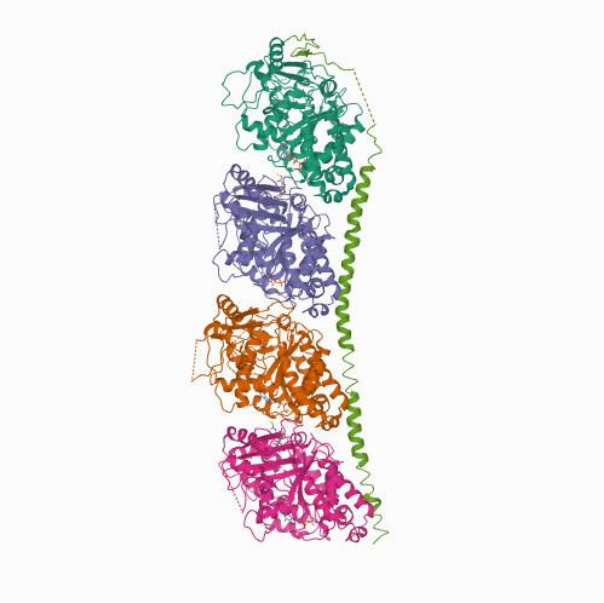

Figure 1.8 Tubulin-colchicine: stathmin-like domain complex (from PDB).

Both α and β tubulins have a mass of around 50 kDa. β-Tubulin is a protein that polymerizes into microtubules, which are involved in cell movement, intracellular trafficking and mitosis (Parker et al. 2014). Microtubule-active drugs mostly bind to one of three main sites on tubulin, the paclitaxel site, the Vinca domain or the colchicine domain (Jurášek et al. 2018). In clinical practice, taxanes (e.g., paclitaxel and docetaxel) bind to polymerized microtubules at the inner surface of the β subunit, and are widely used in the treatment of lung, breast, ovarian and bladder cancers. They promote tubulin stabilization, thereby interfering with tubulin dynamics. Otherwise, vinca alkaloids (e.g. vinblastine, vincristine and vinorelbine) promote depolymerization of microtubules (Lu et al. 2012). Also, 2-methoxyestradiol (2ME2) showed a weak competitive inhibition of colchicine binding site of tubulin with dual activity against cancer cell proliferation and angiogenesis (Lao et al. 2017). Since 2015, all clinical development of 2ME2 has been suspended. The reason was the very poor oral bioavailability of the molecule and also its extensive metabolism (Kumar et al. 2016).

1.1.7.5 Others

AR, 17α-hydroxylase/17,20 lyase (CYP17A1) and CYP19A1 are other enzymes involved in steroidogenesis and, consequently in cancer progression (Miller 2017).

AR is a ligand-dependent nuclear transcription factor, which is expressed in a diverse range of tissues including prostate, bone, muscle, adipose tissue, cardiovascular, immune system and hemopoietic systems (Kargbo 2020). It is a homodimer and consists in 919 amino acids with a molecular mass of 11 kDa (Fujita and Nonomura 2019). This receptor contains four main functional domains: the NH_2-terminal unstructured transcriptional activation domain (NTD), the central DNA binding domain (DBD), a hinge region and the carboxyl-terminal ligand binding domain (LBD). The NTD has glutamine repeats, which vary, and results in the variation of all amino acids in AR. Shorter glutamine repeats are associated with high transcriptional activity of AR and, consequently, men with shorter glutamine repeats have a higher risk for prostate cancer development. In the absence of hormones, the AR is associated with heat shock proteins and located in the cytoplasm in an inactive conformation (Feng and He 2019). Many AR antagonists were developed and are used in clinical practice. First-generation antiandrogens include cyproterone acetate, flutamide and bicalutamide. Enzalutamide represents a second-generation antiandrogen (Feng and He 2019).

CYP17A1 is an isoenzyme of the cytochrome P450 monooxygenase involved in corticoid and androgen biosynthesis, which catalysis both 17α-hydroxylase and 17,20-lyase activities. The 17α-hydroxylase activity of CYP17A1 is required for the hydroxylation of pregnenolone and progesterone at the C17 position to generate 17α-hydroxypregnenolone and 17α-hydroxyprogesterone, respectively. The 17,20 lyase activity follows with the cleavage of the C17-C20 bond of either 17α-hydroxypregnenolone or 17α-hydroxyprogesterone to form DHEA and androstenedione, respectively. It is a 57.4 kDa protein with 508 amino acid residues and has four important structural domains: a substrate-binding domain, a catalytic activity area, a haem-binding region and a redox-partner binding site. This enzyme is localized in the endoplasmic reticulum in the adrenal glands, testicular Leydig cells and ovarian thecal cells (Sivoňová et al. 2017). By 2011, the Food and Drug Administration (FDA) had approved abiraterone acetate as the first selective inhibitor of CYP17A1 to treat prostate cancer (Janssen 2018).

CYP19A1 is a key enzyme involved in the catalytic conversion of adrenal androgens (testosterone and androstenedione), via three consecutive hydroxylation reactions, to aromatic estrogens (E2 and E1, respectively). It also belongs to the CYP450 superfamily, which is characterized by the presence of a heme group. Aromatase is localized in the endoplasmic reticulum in the ovaries of premenopausal women, in the placenta of pregnant women, and in the adipose fibroblast cells of postmenopausal women (Chan et al. 2016). Third-generation aromatase inhibitors, including two triazole derivatives, anastrozole and letrozole, and one steroid analogue, exemestane,

are currently used clinically for the endocrine treatment of hormone-dependent breast cancer in postmenopausal patients (NCCN 2021).

1.2 Steroids

The importance of steroids in the treatment of hormone-dependent tumors is widely known. Due to its rigid structure, the possibility of several functionalizations, as well as the extended biological activity profile, the capacity to cross cell membranes and bind to specific receptors, steroids have been mainstays for the development of new bioactive molecules to be used in cancer therapy.

1.2.1 Characterization of steroids

A steroid is a lipophilic compound with low molecular weight, which can easily pass-through cell membranes, possessing the skeleton of cyclopentanoperhydrophenanthrene (**Figure 1.9**).

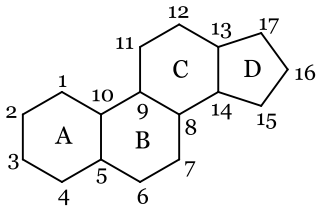

Figure 1.9 The simplest steroid nucleus, gonane.

They normally are white crystalline solids and they tend to be water insoluble. However, the addition of hydroxyls or other polar groups increases water solubility. The nucleus is composed by seventeen carbon atoms forming four fused rings in a three-dimensional shape. The three cyclohexane rings (A, B and C) form the skeleton of a perhydro derivative of phenanthrene. D ring is a cyclopentane structure. Because the steroid ring system is rigid, functional groups bonded to ring atoms have well-defined positions. Substituents below the plane of the ring are designated as α and above the plane of the ring are β (Karnik and Hasan 2021). The stereochemistry of double bonds in the side chain should be indicated using the *E* or *Z* convention. Methyl groups are normally present at C10 and C13. An alkyl side chain may also be present at C17. Sterols are steroids carrying a hydroxyl group at C3 and most have the cholestane skeleton (Moss 1989). The steroidal nucleus can be classified based on their total carbon number, as described in **Table 1.4**. In addition, modifications in C10, C13 and mainly in C17 are also relevant for steroid classification. For example, estrane (C18) is the 13β-methyl variant of gonane, androstane (C19) is the 10β,13β-dimethyl variant of gonane, and pregnane (C21) is the 10β,13β-dimethyl, 17β-ethyl variant of gonane (Noppe et al. 2008).

Table 1.4 Chemical classes of steroids, based on their total carbon number (Edgren and Stanczyk 1999).

Class	Number of carbon atoms
Cholestane	27
Cholane	24
Pregnane	21
Androstane	19
Estrane	18

Compounds can also differ in their characteristics because of the presence of different functional groups. Common functional groups include the ketone group, hydroxyl group and double bond (e.g. in cortisol). Other functional groups include carboxylic acids and aldehyde groups, which are present in the molecules such as bile acids and aldosterone. An important characteristic of the majority of C18 steroids is the presence of an aromatic ring that is found in estrogens (Stanczyk 2009).

The generic steroid structure without insaturations and with a hydrocarbon side chain at C17 has seven chiral stereocenters (carbons 5, 8, 9, 10, 13, 14 and 17), which means that 128 stereoisomers may be possible. Usually, all the three cyclohexane units of steroids are present in chair conformation. In some rare cases, the ring A of steroids, may assume boat conformation. The cyclopentane ring can be present in envelope or half-chair conformations. In most naturally occurring steroids, the stereochemistry of B/C/D rings is similar, being *trans*-fused. In this context, two families of steroids are common when double bonds involving C5 are absent; one is 5α-series with A:B rings fused in trans manner, and the other is 5β-series with A:B rings cis-fused (Karnik and Hasan 2021).

Steroid hormones are categorized in subgroups including corticosteroids (glucocorticoids and mineralocorticoids, produced in adrenal cortex), sex steroids (estrogens, androgens and progestagens, produced in the gonads or placenta) and vitamin D derivatives (Beato and Klug 2000; Hori-Tanaka et al. 2015). They have wide biological roles in organism, namely influencing metabolism, inflammation, immune function, reproduction and sex difference (Schäcke et al. 2002; Bereshchenko et al. 2018).

Human steroids are synthesized from cholesterol mainly in the adrenal gland and gonads in response to tissue-specific tropic hormones (e.g. adrenocorticotropic hormone, LH, and FSH). The cholesterol used for steroidogenesis is derived from a combination of sources: *de novo* synthesis in the endoplasmic reticulum, in which lanosterol (synthesized by triterpene squalene cyclization) is converted to cholesterol, or by uptake of plasma lipoprotein-derived cholesterol and lipoprotein-derived cholesteryl esters. Then, cholesterol is converted to pregnenolone by CYP11A1 enzyme localized in inner mitochondrial membrane (Hu et al. 2010).

Steroid hormones usually circulate in the blood bound to specific carrier proteins, such as sex hormone-binding globulin or corticosteroid-binding globulin (Holst et al. 2004). Their biosynthesis is controlled by the activity of several highly substrate-selective CYP450 enzymes and by steroid dehydrogenases, reductases and others (Schiffer et al. 2019). Their metabolism occurs in the liver, kidney and in peripheral tissues (Schiffer et al. 2019).

1.2.2 Biosynthesis and metabolism of steroids

Steroidogenesis is a multistep process for biosynthesis of steroid hormones from cholesterol, in which, cholesterol is converted into mineralocorticoids, glucocorticoids and sex hormones (pregnane, androstane and estrane hormones) through hydroxylation, oxidation and reduction steps in gonads, adrenal cortex and adipose tissue (**Figure 1.10**) (Miller 2017).

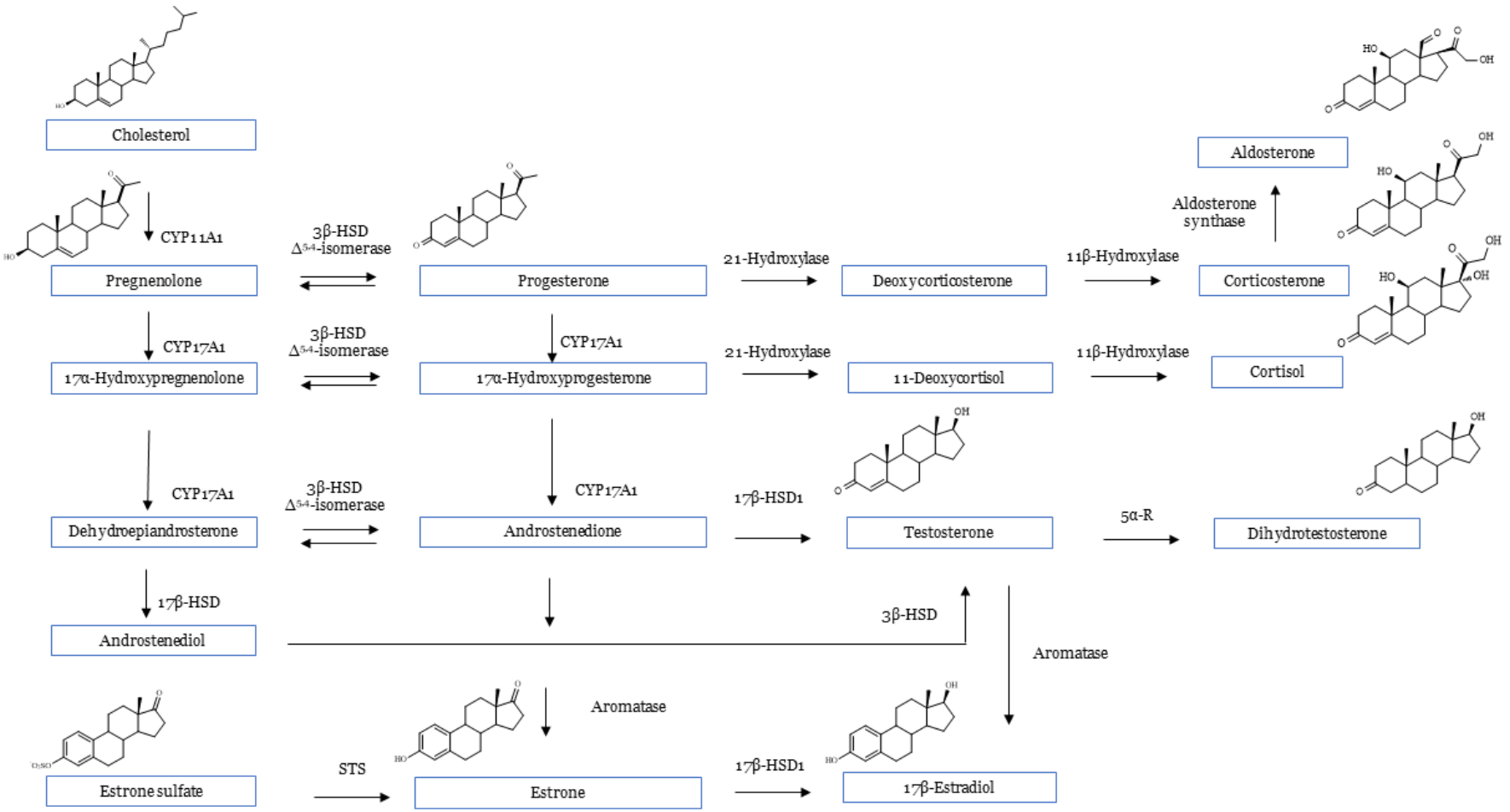

Figure 1.10 Scheme that represents steroidogenesis. CYP17A1, 17-α-hydroxylase/17,20-lyase; 3β-HSD, 3β-hydroxysteroid dehydrogenase; STS, steroid sulfatase; 17β-HSD1, 17β-hydroxysteroid dehydrogenase type 1; 5α-R, 5α-reductase. Adapted from (Miller 2017).

Firstly, occurs the translocation of cholesterol into the inner mitochondrial membrane, a process regulated by the steroidogenic acute regulatory protein (StAR) that is controlled by LH stimulation (Miller and Strauss 1999; Manna et al. 2009). Then, cholesterol is converted to pregnenolone, which is a precursor of all steroid hormones, by the enzyme CYP11A1 (Belfiore et al. 1994). In granulosa and theca cells of the ovary, androstenedione is obtained by CYP17A1 and 3β-hydroxysteroid dehydrogenase (3β-HSD) enzymes. Then, can be converted to other androgens, such as testosterone and DHT, or diffuse to the granulosa cells through the basal lamina. At the granulosa cells, androstenedione is converted to E1 by the CYP19A1 enzyme pathway. 17β-HSD1 converts E1 to E2. Also, the sulfatase pathway converts E1 sulfate into E1 (Hong and Chen 2011). In the granulosa cells, the expression of both aromatase and 17β-HSD1 is controlled by FSH stimulation (**Figure 1.11**).

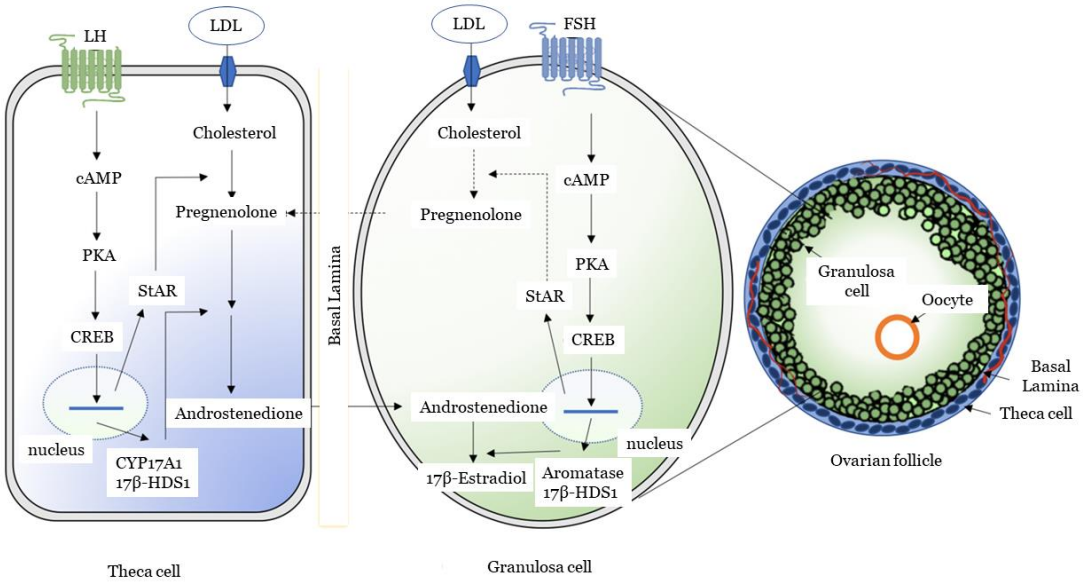

Figure 1.11 Synthesis of estrogens in ovarian cells. The luteinizing hormone (LH) induces the production of androgens in theca cells. The follicle-stimulating hormone (FSH) stimulates granulosa cells via aromatization of androgens to estrogens and by using cholesterol to produce pregnenolone. CREB, Cyclic AMP response element binding protein; PKA, protein kinase A; LDL, low density lipoproteins; cAMP, cyclic adenosine monophosphate; StAR, steroid acute regulatory protein; CYP17A1, 17α-hydroxylase/17,20-lyase; 17β-HSD1, 17β-hydroxysteroid dehydrogenase type 1. Adapted from (Fuentes and Silveyra 2019).

Overall, estrogens are normally produced by the ovaries and in smaller amounts by other tissues such as liver, pancreas, adrenal glands, adipose tissue and breast (Barakat et al. 2016). During pregnancy, estrogens are also synthesized by the placenta. E2, the predominant circulating estrogen in humans is mainly secreted by the granulosa cells of the ovarian follicles and the *corpora lutea*. In menopause, E1 is primarily produced by aromatization of androstenedione in extra-glandular tissues, where it can act locally as a paracrine or intracrine factor (Simpson 2003; Barakat et al. 2016). E1 can also be

transformed to E2 by the enzyme 17β-HSD1 in peripheral tissues, which include adipose and breast tissue, vascular endothelium, smooth muscle cells, brain tissue and bone cells, where it is metabolized or enters the circulation in small quantities (Simpson 2003).

In males, in the testis, steroidogenesis is restricted to Leydig cells, in which, after LH stimulation, cAMP/protein kinase A (PKA) promotes the transport of cholesterol into mitochondria and increases transcription of genes involved in testosterone biosynthesis. Cholesterol is converted to pregnenolone, which diffuses into the endoplasmic reticulum for testosterone biosynthesis via Δ^4 and Δ^5 pathways (Stanczyk 2009).

The Δ^4 pathway begins with the conversion of pregnenolone to progesterone through the action of two enzymes, 3β-HDS and $\Delta^{5,4}$-isomerase. In contrast to the reversible formation of androstenediol from DHEA, this reaction is not reversible to any significant extent. Once the ketone group is formed, the double bond between carbons 5 and 6 is rapidly shifted and becomes located between carbons 4 and 5 through the action of the isomerase enzyme. The Δ^5 pathway begins by formation of 17-hydroxypregnenolone from pregnenolone via the enzyme CYP17A1. DHEA is then transformed to androstenediol by 17β-HSD1. The conversion of DHEA to androstenediol is reversible. The Δ^5 pathway stops after androstenediol is formed. Testosterone is converted to DHT by 5α-R, which is a nicotinamide adenine dinucleotide phosphate dependent enzyme (Hanukoglu 1992; Miller and Auchus 2011), and some testosterone is aromatized to E2 (Ayaz and Howlett 2015). Interestingly, in peripheral tissues (adipose cells and bone) testosterone can be metabolized to E2 and E1 by aromatase activity (Simpson 2002). In male, Sertoli cells, Leydig cells and mature spermatocytes also produce local estrogen by aromatization (Fuentes and Silveyra 2019).

Concerning the steroid metabolism, phases 1 and 2 reactions are involved to increase their water-solubility and enable efficient excretion in urine and bile. The major phase 1 reactions for steroids are the reduction of the 3-keto-Δ^4 motif, the interconversion of hydroxy- and keto-groups by HSDs/oxoreductases and additional hydroxylations by CYPs, namely CYP3A4 (Schiffer et al. 2019). The major phase 2 reactions for steroids are the addition of sulfated and glucuronidated moieties by sulfotransferases (SULT1A1, SULT1E1 and SULT2A1) and UDP-glucuronosyltransferases (McNamara et al. 2013).

Although the liver undoubtedly makes the major contribution to steroid metabolism, most peripheral tissues also possess enzymatic machinery for both steroid activation

and subsequent inactivation through phases 1 (activation) and 2 (conjugation reactions) of metabolism (Schiffer et al. 2019).

1.2.3 Steroids with antitumor interest: emphasis on aromatic A-ring steroids and oxime derivatives

Throughout the years, modifications in the steroid structure have been carried out with the aim to obtain new molecules with anticancer activity. In fact, different endocrine therapies involving steroids (**Figure 1.12**) are available for clinical treatment of hormone-sensitive breast cancer, which include antiestrogen like fulvestrant, as well as third-generation aromatase inhibitors like exemestane (Zucchini et al. 2015). Cyproterone acetate was the first steroidal antiandrogen used for the treatment of prostatic cancer and more recently abiraterone acetate is used to treat metastatic prostate cancer (Lorente et al. 2021). Also in clinical practice are used corticosteroids (e.g. prednisolone and dexamethasone), which demonstrated anticancer effect (leukemia or lymphoma management), anti-swelling effect (brain tumor or brain metastases), and also to improve refractory symptoms such as dyspnea or gastrointestinal obstruction after chemotherapy (Lossignol 2016).

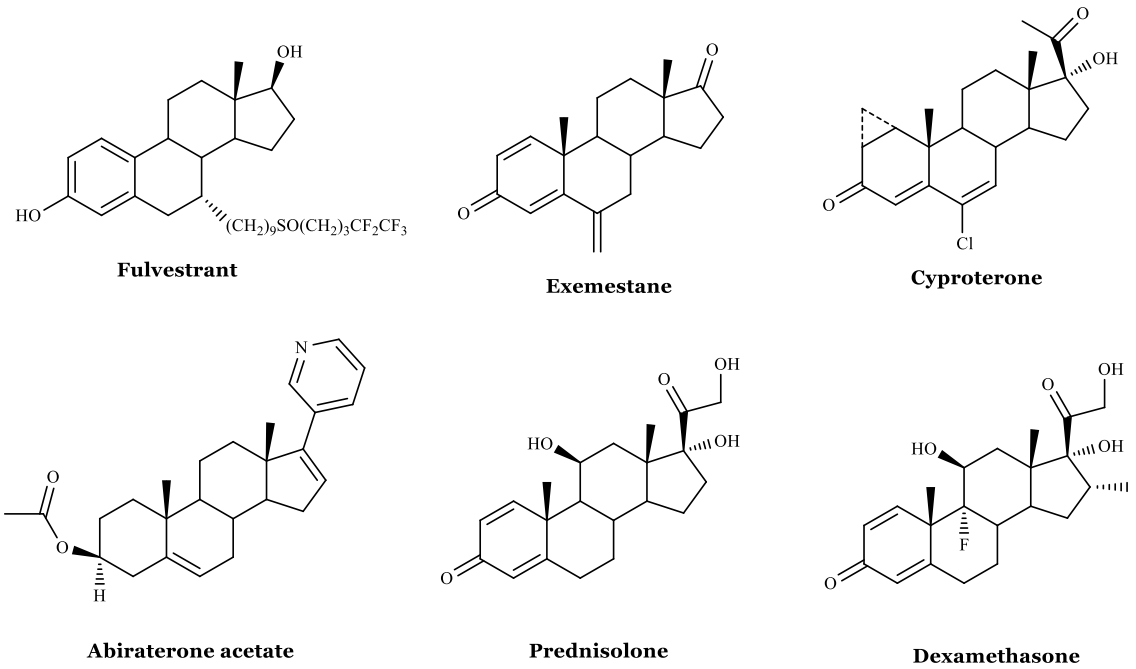

Figure 1.12 Steroids used in clinical practice to treat breast and prostate cancers (Zucchini et al. 2015; Lorente et al. 2021).

Otherwise, several steroidal molecules (examples in **Figure 1.13**) have been synthesized and evaluated as antiproliferative agents. For example, 16*E*-arylideneandrostane (compounds **1.1** and **1.2**) and 21*E*-arylidenepregnane (compound **1.3**) derivatives showed significant antiproliferative activities when compared to

reference compounds (Brito et al. 2021). An aminopyrazoloneandrostane derivative (compound **1.4**) showed to be cytotoxic against HepG2 cancer cells and *in silico* studies showed that this compound was a promising PI3K/AKT/mTOR inhibitor, and it induced a G_2/M cell cycle arrest, DNA fragmentation and apoptosis by inhibition of anti-apoptotic genes (Kattan et al. 2020). Also, 17α-modified-19-nortestosterone derivatives exhibited a remarkable inhibitory effect on the proliferation of HeLa cells with IC_{50} values lower than cisplatin (reference compound) with no associated undesired hormonal effects. A lactate dehydrogenase assay demonstrated a moderate cytotoxic effect and cell cycle disturbance and the elevation of the hypodiploid population were detected by flow cytometry. The proapoptotic effects were confirmed by fluorescent microscopy and a caspase-3 activity assay for compound **1.5** (Gyovai et al. 2018).

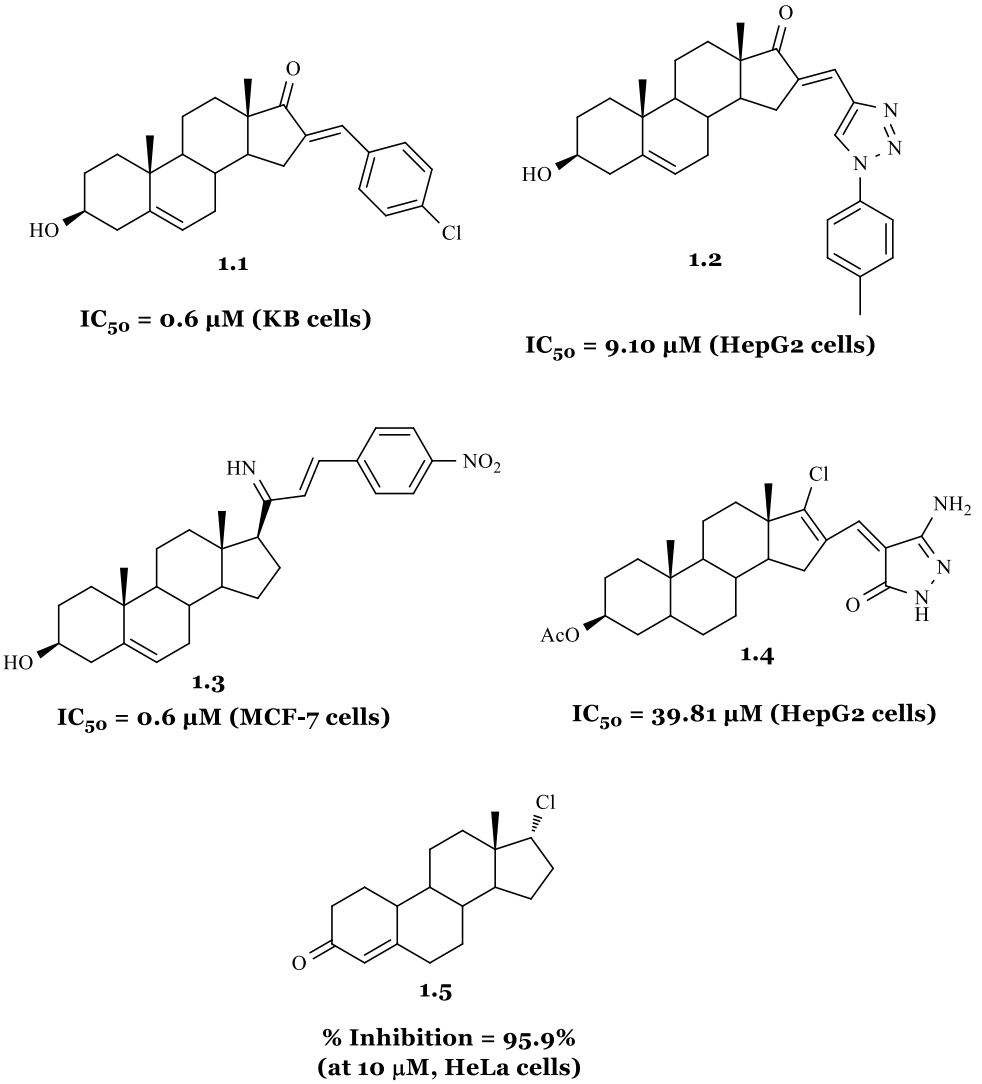

Figure 1.13 Examples of androstane and pregnane series with antiproliferative activity (Gyovai et al. 2018; Kattan et al. 2020; Brito et al. 2021).

Concerning steroidal oximes (**Figure 1.14**), it also has been shown that the introduction of a 20-oxime group on pregnane derivatives (Ling et al. 1998) markedly increased the CYP17A1 inhibitory effect as evidenced by the comparison of progesterone with the corresponding 20-oxime (compound **1.6**), and 16-dehydropregnenolone with its 20-oxime (compound **1.7**).

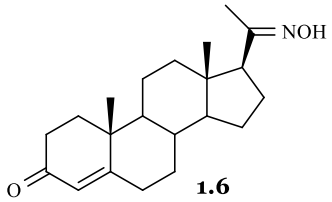

1.6

% Inhibition = 76.7 % (at 0.15 μM, CYP17A1)
IC_{50} = 0.063 μM (5α-R)

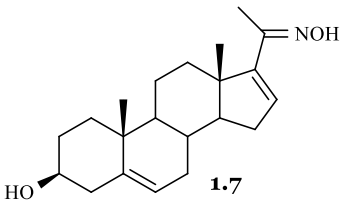

1.7

% Inhibition = 80.3 % (at 0.15 μM, CYP17A1)

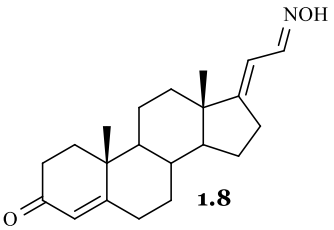

1.8

IC_{50} = 0.18 μM (CYP17A1)
IC_{50} = 0.43 μM (5α-R2)

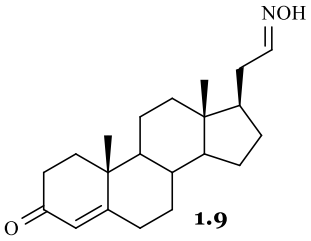

1.9

IC_{50} = 0.52 μM (CYP17A1)
IC_{50} = 1.95 μM (5α-R1)
IC_{50} = 0.3 μM (5α-R2)

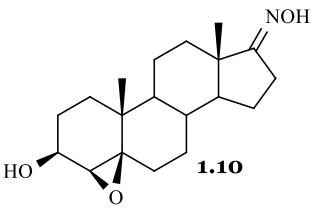

1.10

% Inhibition: 88.1 % (at 0.15 μM, CYP19A1)

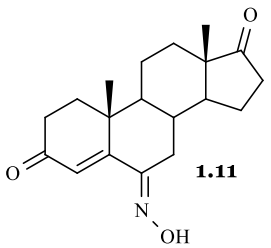

1.11

Ki = 0.08 μM (CYP19A1)

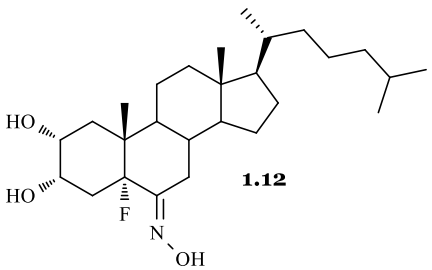

1.12

IC_{50} = 2.22 μM
(HCT-116 cells)

Figure 1.14 Examples of steroidal oximes in pregnane, androstane (Holland et al. 1992; Ling et al. 1998; Hartmann et al. 2000; Deive et al. 2001; Pokhrel and Ma 2011).

The inhibitory potency against CYP17A1 and 5α-R enzymes strongly depends on the position of the oxime group, being C21-oximes (e.g., compounds **1.8** and **1.9**) more

potent than C20-oximes (Hartmann et al. 2000). For androstane series, SAR analysis showed that the presence of a 3β-hydroxyl group and a β-configuration of the 4,5-epoxy ring (compound **1.10**) appeared to be important to achieve higher CYP19A1 inhibitory effects when compared with the corresponding compounds with a 3-ketone and a Δ^4 double bond (Pokhrel and Ma 2011). Also, 6-oximes (compound **1.11**) bind to the human placental CYP19A1 with high affinity (Holland et al. 1992). SAR study for 6*E*-hydroxyimino-4-ene steroids concluded that the presence of a cholesterol-type side chain is fundamental for their biological activity and the existence of a ketone functionality at C3 and a high degree of oxidation on ring A results in a greater bioactivity (compound **1.12**) (Deive et al. 2001).

The main modifications in estrane series to obtain 17β-HSD1, STS and β-tubulin inhibitors and cytotoxic molecules are described below.

1.2.3.1 Estrane steroids with activity against 17β-HSD1 enzyme

E1 and E2 derivatives are widely described as 17β-HSD1 inhibitors and, concerning the SAR studies, the main modifications are performed in A, B and D-ring of steroids (**Figure 1.15**) (Brozic et al. 2008; Poirier 2011; Salaha et al. 2019):

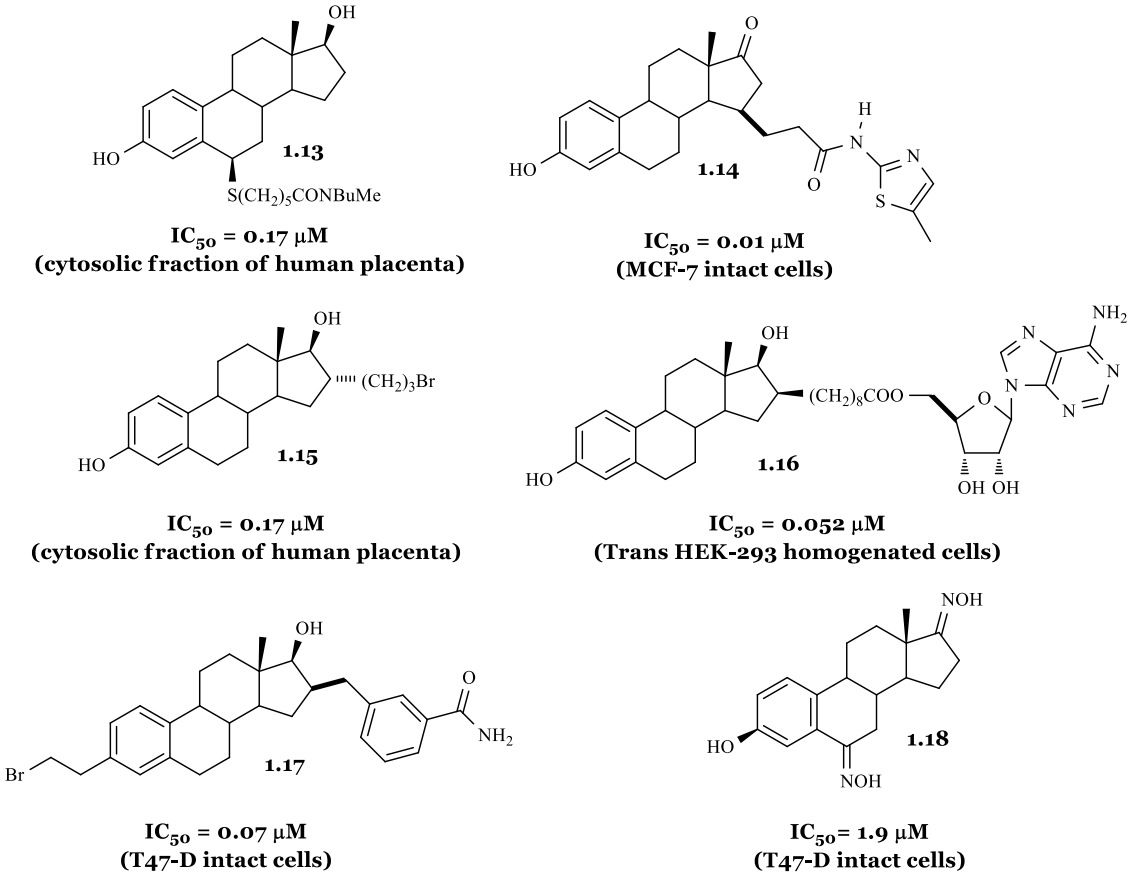

Figure 1.15 Examples of steroidal 17β-hydroxysteroid dehydrogenase (17β-HSD1) inhibitors (Allan et al. 2006; Lespérance et al. 2021; Poirier et al. 2021).

- A-Ring

Modifications at C2 are believed to reduce estrogenic activity (Brozic et al. 2008) and add some 17β-HSD1 inhibitory activity, especially with hydrophobic substitutions and small groups. The replacement of the 3-hydroxyl by a hydrogen atom was clearly unfavorable for the inhibition of 17β-HSD1 enzyme (Poirier et al. 1998; Tremblay et al. 2005; Brozic et al. 2008). Thus, generally, in all inhibitors, the moiety present in C3 is the hydroxyl. However, there are C3 substituted estrogens combined with substitutions on C2 and C15 and others and the moieties found are generally CH_3, CH_2Ph, SO_2NH_2 and SO_3OH. The sulfamates are weak inhibitors.

- B-ring

Concerning C6, some oxime and 6β-alkylamide derivatives are reported. In this last group of compounds, it was shown that the β-configuration is preferable than α to achieve better inhibition values. However, the compound with a thioether bond at C6 (compound **1.13**) promoted an estrogenic activity in breast T47-D cells (Poirier et al. 1998; Tremblay et al. 2005; Brozic et al. 2008). This occurred probably due to the instability of the thioether bond. The cleavage of the thioether bond was suspected to cause the formation of $\Delta^{6,7}$-E2, an estrogenic compound.

- D-ring

This ring is the most functionalized, presenting a variety of substitutions, combined or not with substitutions on the other steroid rings.

a) C15 modified derivatives: there are described large alkyl spacers linked to C15 that bear polar moieties (e.g., amide, ester, carbonyl, hydrazone, alcohol, ether, urea, carbamate, retroamide, sulfonylurea, sulfamide, sulfamate, retrosulfonamide, retrocarbamate, retroester or a sulfonylcarbamate type side chain), which can be found combined with substitutions at C2 and C3. Compound **1.14** (an amide) reversibly inhibited 17β-HSD1 without estrogenic effects (Messinger et al. 2009).

b) Modifications at C16: one of the most common substitutions. Better and irreversible enzyme inhibition was obtained for compounds having a good leaving group (F, Cl, Br, I) at the end of a short (three-carbon) side chain at C16-α (e.g. compound **1.15**) (Sam et al. 1998). However, these compounds showed proliferative effects on the breast cancer cell lines ZR-75-1 and T47-D (Tremblay et al. 1995). Then, the inhibitory activity of C16-substituted E2 derivatives was enhanced by designing and synthesizing a bifunctional hybrid inhibitor, combining an E2 and an adenosine moiety in a single compound (**1.16**) (Qiu et al. 2002). Recently, different C13 epimeric analogues of 16β-(*m*-carbamoylbenzyl)-E2 (e.g. compound **1.17**) also showed 17β-HSD1 inhibition and a weak estrogenic effect on breast T47-D cancer cells (Laplante et al. 2008). The bromoethyl side chain added at the C3-position of a 16β-(*m*-carbamoylbenzyl)-E2

nucleus showed to be crucial to covalently inhibit 17β-HSD1 without estrogenic effects with IC_{50} values within 0.05-0.5 μM (Lespérance et al. 2021; Poirier et al. 2021).
c) C17 modified derivatives: the most common changes involve the carbonyl moiety in C17, which mimics E1, or the hydroxyl moiety that mimics E2. Other substitutions include a 17-fluoro (a fluor can mimic the hydroxyl or carbonyl moieties because of its large electro-negativity and hydrogen-bond acceptor capacity) combined with substitutions at C14, C15 and C16, as well as at C2 and with double bonds at C8 and C9 (Deluca et al. 2006). NO-R groups were also described for estrogen derivatives (Allan et al. 2006). Compound **1.18** (a dual oxime) showed better inhibition when compared to the analogue only with a C17 oxime, indicating that the C6 oxime had a beneficial effect for binding to the active site of the enzyme, sufficient to substantially compensate the detrimental effect of the C17 oxime.

1.2.3.2 Estrane steroids with activity against STS enzyme

High estrogen levels produced by the STS pathway can contribute to the progression of several hormone-dependent cancers (e.g., of breast and endometrium). Then, STS inhibitors can be useful agents to stop the proliferation of cancer cells (**Figure 1.16**) (Gupta et al. 2013).

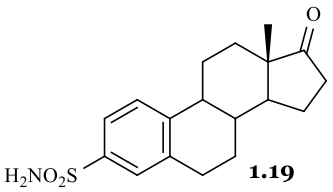

1.19

IC_{50}= 93 nM
(Placental microsomes)

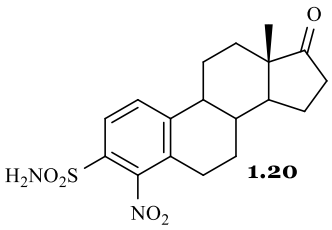

1.20

IC_{50}= 0.8 nM
(Placental microsomes)

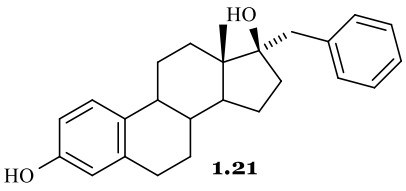

1.21

IC_{50}= 310 nM
(Homogenates of JEG-3 cells)

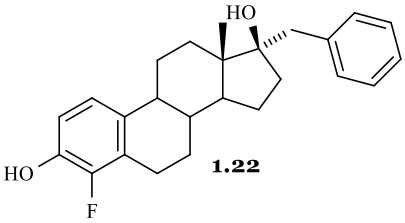

1.22

IC_{50}= 40 nM
(Placental microsomes)

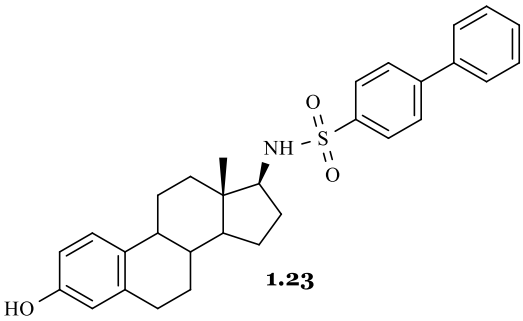

1.23

IC_{50}= 9 nM
(Purified enzyme)

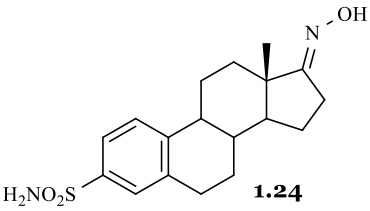

1.24

IC_{50}= 80 nM
(Placental microsomes)

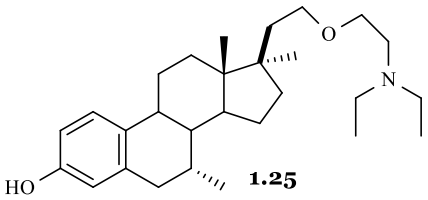

1.25

Figure 1.16 Examples of steroid sulfatase (STS) inhibitors (Hejaz et al. 1999; Rasmussen et al. 2007; Daśko et al. 2020).

One of the most active sulphamoylated aryl derivatives achieved was estrone-3-*O*-sulphamate (EMATE, **1.19**), which irreversibly inhibited STS enzyme in a time and concentration dependent manner on breast MCF-7 cancer cells (IC_{50} = 93 nM) (Purohit et al. 1995). Woo *et al* (Woo et al. 2012) synthesized various EMATE derivatives substituted at the 2- and/or 4-positions (e.g. with halogen atoms, nitro, propenyl, *n*-

propyl and cyano groups). Higher inhibition was observed for derivatives containing halogen atoms at the 4-position. In this context, 4-nitro-EMATE (compound **1.20**) was found to be the most potent derivative (IC_{50} = 0.8 nM). The removal of the 17-carbonyl group of EMATE is detrimental for activity. Other potent reversible STS inhibitors have also been developed, such as 17α-substituted E2 derivatives (compounds **1.21** and **1.22**) (Nussbaumer and Billich 2004). E2 derivatives substituted at the 4-position with a small electron withdrawing group such as a nitro group or a fluorine atom (compound **1.22**) showed good reversible and non-competitive inhibitory activity, which IC_{50} is seven-fold lower than compound **1.21** (Phan et al. 2011). Also, a series of *N*-17β-arylsulphonamides (e.g., compound **1.23**) and *N*-17β-alkylbenzenesulphonamides were synthesized and showed better STS inhibitory activity. Adding alkyl substituents into the arylsulphonamide group at C17 resulted in the improvement of STS inhibitory potency (the presence of a *n*-butyl chain was the most favorable) (Daśko et al. 2020). Hejaz and co-workers (Hejaz et al. 1999) synthesized estrone oxime 3-*O*-sulfamate (OMATE, **1.24**), among other compounds. This steroid inhibited the STS enzyme and showed a potency similar to the observed with the ketone analogue EMATE (Purohit et al. 1995; Purohit et al. 1999). The OMATE estrogenic activity was also evaluated by the ovariectomized rat uterine weight gain *in vivo* assay (initial weight = 0.036 g ±0.001). The results showed that this oxime displayed a stimulatory effect (0.15 g ± 0.01) on the uterine growth in ovariectomized rats, which was approximately 50 % higher than the observed for EMATE (0.11 g ± 0.02). Thus, this modification at C17 was identified as a useful route for estrogenicity enhancement in sulfamate-based estrogens (Hejaz et al. 1999; Woo et al. 2011). A steroid estrogen analogue modified at 7α position (compound **1.25**) (Rasmussen et al. 2007), without estrogenic properties, also possessed high STS inhibitory activity and blocked breast cancer cells growth with activity comparable to tamoxifen (Morozkina and Shavva 2016).

Some A-ring halogenated 13α-, 13β- and 17-deoxy-13α-E1 derivatives were also developed and showed inhibitory effects towards both 17β-HSD1 and STS enzymes (**Figure 1.17**). In this group, 4-halo-17-keto-13β compounds elicited submicromolar inhibitory effect towards both enzymes. In the 17-deoxy-13α-E1 series, the 2,4-bis-bromo (compound **1.26**) and 4-chloro (compound **1.27**) derivatives exerted potent low micromolar dual action. Also, 2-bromo- (compound **1.28**) and 2-chloro-13β-estrone (compound **1.29**) displayed considerable inhibition towards both enzymes. It is interesting to note that the position of iodine derivatives in the 13β-estrone series exhibited different effects. 2-Iodo compound was a highly specific 17β-HSD1 inhibitor,

whereas its 4-counterpart (compound **1.30**) presented dual STS and 17β-HSD1 inhibition (Bacsa et al. 2018).

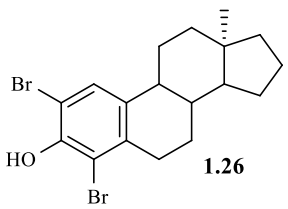

1.26

IC_{50}= 4.1 μM (17β-HSD1)
IC_{50}= 7.5 μM (STS)
(Placental microsomes)

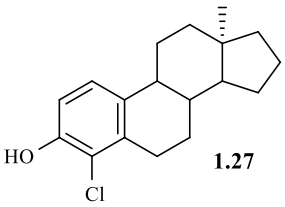

1.27

IC_{50}= 4.5 μM (17β-HSD1)
IC_{50}= 6.3 μM (STS)
(Placental microsomes)

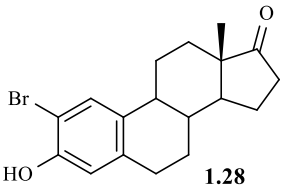

1.28

IC_{50}= 0.095 μM (17β-HSD1)
IC_{50}= 2 μM (STS)
(Placental microsomes)

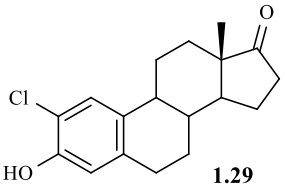

1.29

IC_{50}= 0.18 μM (17β-HSD1)
IC_{50}= 2.4 μM (STS)
(Placental microsomes)

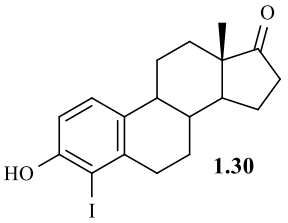

1.30

IC_{50}= 0.36 μM (17β-HSD1)
IC_{50}= 0.23 μM (STS)
(Placental microsomes)

Figure 1.17 Examples of dual steroid sulfatase (STS) and 17β-hydroxysteroid dehydrogenase (17β-HSD1) inhibitory compounds (Bacsa et al. 2018).

1.2.3.3 Estrane steroids with activity against β-tubulin

Drugs that disrupt microtubule/tubulin dynamics are widely used in cancer chemotherapy. Estramustine is an E2 synthetic conjugate bearing a nitrogen mustard system, exhibiting antitubulin activity and is used in the treatment of advanced prostate cancer (Lu et al. 2012). Interestingly, 2ME2 is a naturally occurring E2 derivative with antitumor and antiangiogenic properties, acting through the binding to β-tubulin near the colchicine-binding site (**Figure 1.18**).

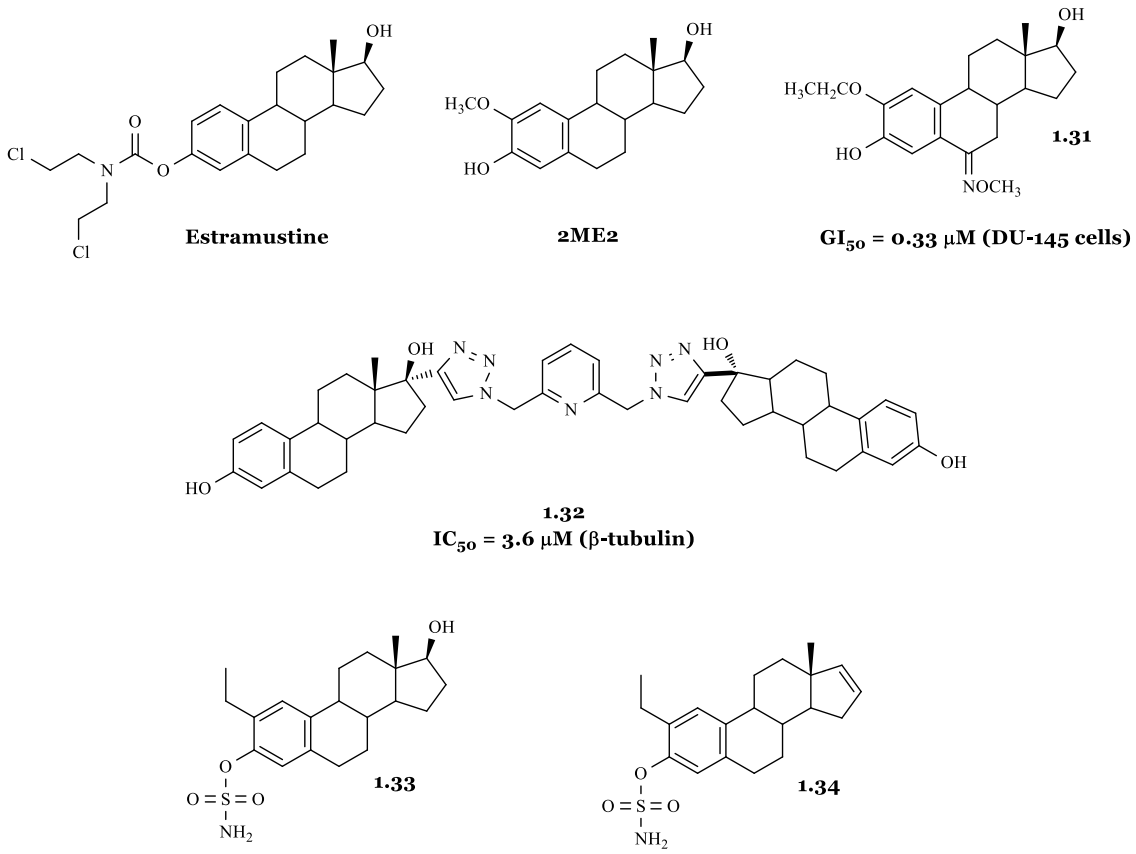

Figure 1.18 Examples of β-tubulin inhibitors (Cushman et al. 1997; Stander et al. 2011; Jurášek et al. 2018)

In fact, 2ME2 inhibited microtubule polymerization and induced mitotic arrest (Cushman et al. 1995; Lao et al. 2017). The 6-oxime of 2-ethoxyestradiol (compound **1.31**) clearly had higher antiproliferative effects than the ketone analogue against several cancer cell lines, including breast, prostate, and colon tumoral cells. In addition, this compound also inhibited tubulin polymerization and demonstrated low binding affinities to ERα (Cushman et al. 1997). Recently, E2 dimers bridged by 2,6-bis(azidomethyl)pyridine between D-rings also inhibited β-tubulin (e.g. compound **1.32**) (Jurášek et al. 2018). Also, the presence of 2-ethyl-3-*O*-sulphamoyl groups in estrane nucleus (compounds **1.33-1.34**) allowed an improvement of the antimitotic activity of E1 analogues (Stander et al. 2011). They interfere with the mitotic spindle with abnormal formation of mitotic spindles.

1.2.3.4 Estrane steroids with cytotoxic activities

Several studies have been showing the promissory cytotoxic effects of steroids based on estrane series (**Figure 1.19**).

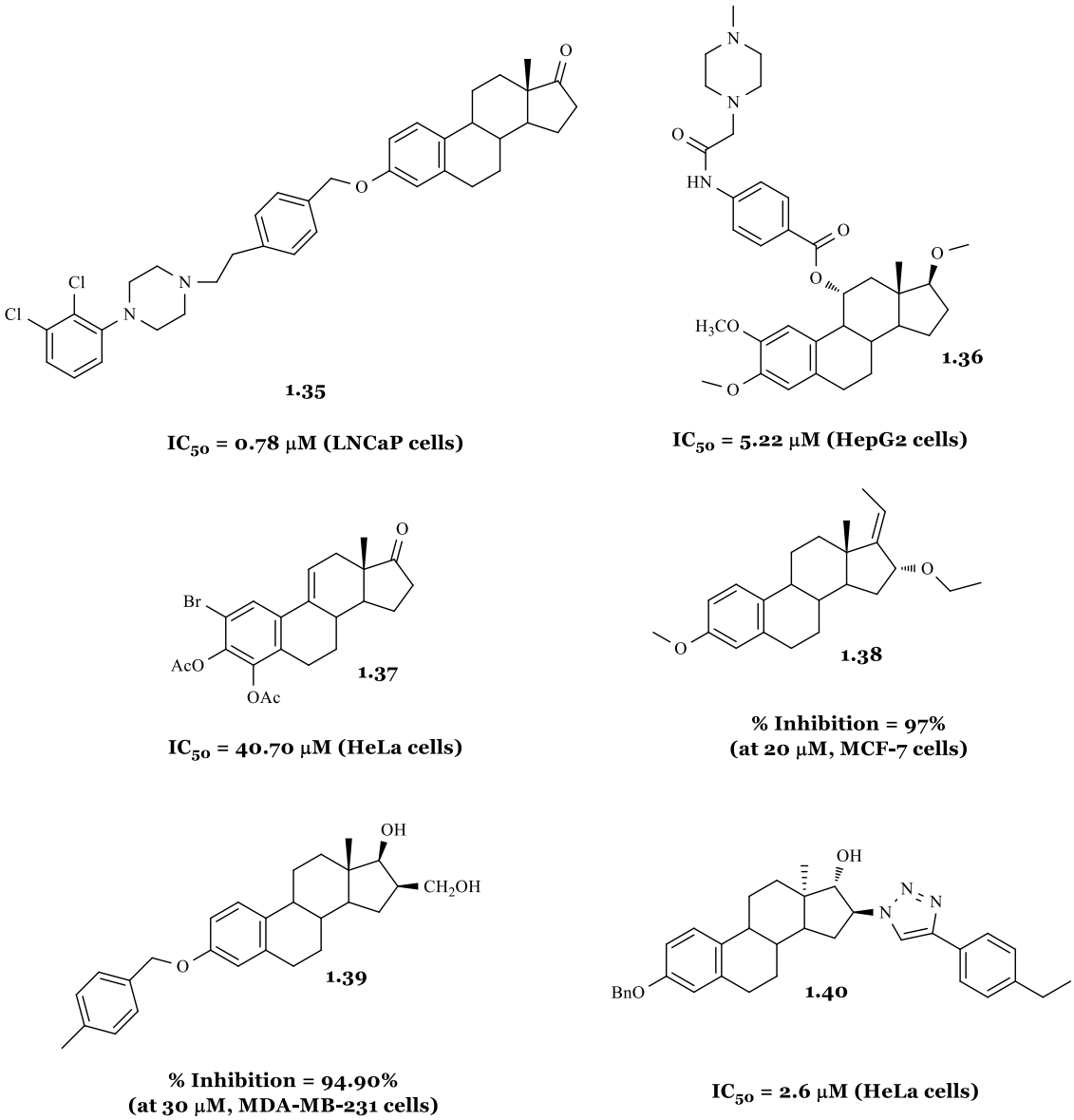

Figure 1.19 Examples of estrane derivatives with cytotoxic activities (Milić et al. 2005; Bacsa et al. 2015; Alsayari et al. 2017; Lao et al. 2017; Chen et al. 2018; Sinka et al. 2018).

As examples, E1 3-*O*-ether derivatives containing the piperazine ring exhibited a strong cytotoxic activity against prostate cancer cell lines (e.g., compound **1.35**) (Chen et al. 2018). Regarding C-ring modifications, several 11α-substituted 2ME2 analogs were synthesized and showed good cytotoxic activity against HepG2 cells, leading to a G_2/M cell cycle arrest, as well as significant antiestrogen activity (e.g. compound **1.36**) (Lao et al. 2017). Also, the presence of a double bond at C9=C11 combined with 2- and 4-substitutions originated significant activity against different cancer cell lines (e.g. compound **1.37**) (Milić et al. 2005). Concerning modifications at C16, the presence of a 16α-OEt in E1 derivatives appeared to be associated to a high cytotoxicity against MCF-7 cells without estrogenic effects and to a reduced interaction with ERα (compound

1.38) (Alsayari et al. 2017). Moreover, 3-substituted C16-hydroxymethyl-estradiols showed potent antiproliferative properties against breast triple-negative cancer cell lines (MDA-MB-231), causing programmed cell death and G_1 phase elevation (e.g. compound **1.39**) (Sinka et al. 2018). Furthermore, a 17α-hydroxy-13α-estradiol 3-benzyl ether derivative (compound **1.40**) demonstrated to be a promising scaffold for the design of hormonally inactive cytostatic derivatives, especially with a 16β-heterocyclic substituent that induces apoptosis via the intrinsic pathway in HeLa cells (Bacsa et al. 2015).

As described in Canário et al (Canário et al. 2018), many steroidal oxime derivatives in cholestane, pregnane, androstane and estrane series, were synthesized and showed interesting cytotoxic activities. The interest for this type of compounds emerged in the 90s of the last century because an abundant number of steroids having very unusual and interesting structures (oxime group) was isolated from *Cinachyrella* marine sponges (Rodriguez et al. 1997).
Concerning steroids with estrane scaffold (**Figure 1.20**), new estrone-16-oxime ethers were tested against human cervical (HeLa), breast (MCF-7), ovarian (A2780) and skin epidermoid carcinoma (A431) cell lines by the 3-(4,5-dimethylthiazol-2-yl)-2,5-diphenyltetrazolium bromide (MTT) assay and relevant results were observed.

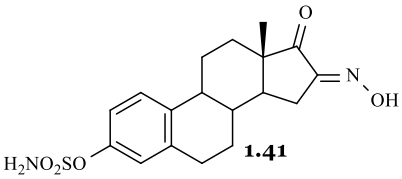

1.41

IC_{50} = 4.04 μM (HeLa cells)

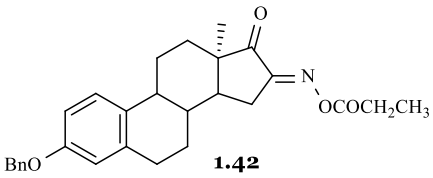

1.42

IC_{50} = 4.13 μM (MCF-7 cells)

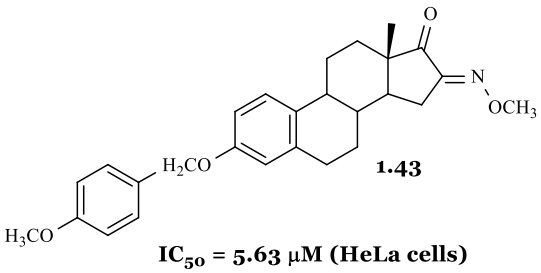

1.43

IC_{50} = 5.63 μM (HeLa cells)

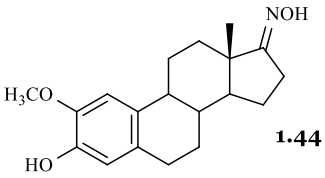

1.44

GI_{50} = 5.7 μM (MCF-7 cells)

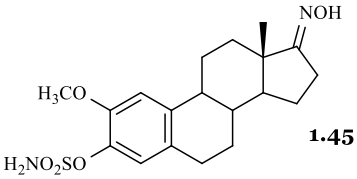

1.45

GI_{50} = 5.87 μM (MCF-7 cells)

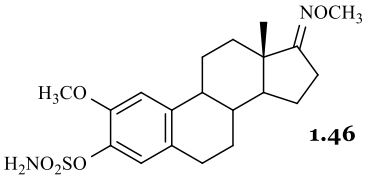

1.46

GI_{50} = 0.17 μM (MCF-7 cells)

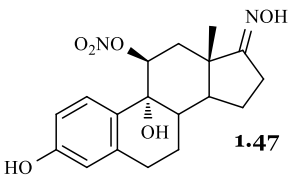

1.47

% inhibition = 72%
(Xenograph induced by Ca-755 cells)

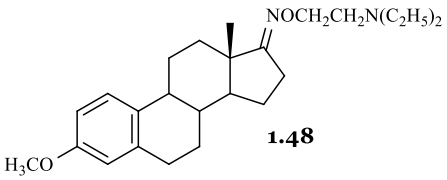

1.48

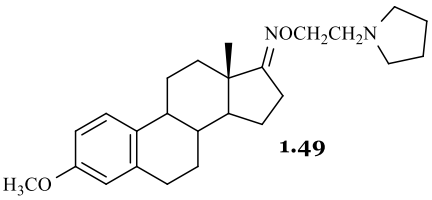

1.49

Figure 1.20 Examples of oximes in estrane series with cytotoxic activities (Jindal et al. 2003; Rzheznikov et al. 2003; Leese et al. 2005; Berényi et al. 2013).

SAR studies showed that a β orientation of the 13-methyl group is preferred. The best results were obtained with unsubstituted oximes (e.g., compound **1.41**), but an aromatic group (e.g., benzyl) may be considered at C16. The hydroxyl group on A-ring may be unsubstituted, sulfamoyloxylated (e.g., compound **1.41**) or substituted with an aromatic group (benzyl, compound **1.42** or *p*-methoxybenzyl, compound **1.43**) for

good cytotoxic activity. For these oximes, the possible mechanism of action involved apoptosis with cell cycle arrest at G_1 phase, leading to an increase in cellular shrinkage, nuclear condensation, membrane permeability, sub-diploid population and caspase-3 activity. However, relatively high concentrations are needed to exert substantial activity (30 μM) (Berényi et al. 2013).

Other study with new D-ring modified 2-substituted estrogen-3-*O*-sulfamates demonstrated that compound **1.44** (2-MeOE1 oxime) had higher antiproliferative activity than the corresponding ketone analogue (GI_{50} = 21.3 μM). In addition, the presence of the 3-*O*-sulfamoyl group led to a significant enhancement of the antiproliferative activity in MCF-7 cells (compound **1.45**). Also, *O*-substituted oximes, namely the *O*-methyl oxime (compound **1.46**), originated higher cytotoxic activity against MCF-7 cells (Leese et al. 2005).

Several steroidal 11β-nitrates were synthesized by Rzheznikov and co-workers (Rzheznikov et al. 2003) with the aim of studying their antitumor properties based on the fact that these compounds can generate nitric oxide and have potential cytotoxic activity. However, a C17-oxime (compound **1.47**) did not improve the cytotoxicity compared to the C17-ketone parent compound. Unfortunately, compounds tested showed an estrogenic effect, when studied in xenograft animal models of breast cancer, what has been observed by tumor growth after 15 days of treatment.

Using an *in vivo* hollow fiber assay, alkylaminoethyl derivatives of steroidal 17-oximes (compounds **1.48** and **1.49**) showed antiproliferative activities with interesting intraperitoneal and subcutaneous scores (Jindal et al. 2003). The activity of compounds can be due to their aromatic A-ring, which can bind to ER.

1.3 Discovery and development of new anticancer drugs

In anticancer drug discovery, the first breakthrough took place after the Second World War, with the discovery of nitrogen mustards and the birth of chemotherapy for the treatment of various hematological tumors. The second breakthrough on oncology took place at the beginning of the 1980s, with the development of the knowledge of molecular and cellular biology that allowed the development of drugs for specific targets, giving rise to targeted therapy. Chemotherapy and targeted therapies have significantly improved the survival and quality of life of cancer patients. Later, at the turn of the third millennium, using genetic engineering studies, there have been new advances in clinical oncology with the introduction of monoclonal antibodies and immune checkpoint inhibitors for the treatment of advanced or metastatic tumors, for which no effective treatment was available before (Falzone et al. 2018). Otherwise, natural products have played a major role in cancer chemotherapy for nearly half a century, both in terms of providing clinical drugs, new molecules for synthetic optimization or substances for probing cellular and molecular mechanisms of action relevant to cancer inhibition (Kinghorn et al. 2016). Some of the approved plant-derived chemotherapeutic agents used in clinical practice include the vinca alkaloids, the taxane diterpenoids and the camptothecin quinoline alkaloid derivatives (Pan et al. 2012). As examples of bacteria origin are anthracycline derivatives and mitomycin C. More recently, trabectedin drug was developed from marine sources (Kinghorn et al. 2016). Endocrine therapy emerged in 1896 with the discovery, by Beatson, that oophorectomy improved the treatment of advanced breast cancer due to the lack of estrogens (Sainsbury 2013).

Drug discovery and development is a complex process through which new drugs are identified, and new medicines are developed and launched into the market. It involves a wide range of scientific disciplines, including biology, chemistry and pharmacology (Mohs and Greig 2017). Also, its success is highly dependent on intense collaboration and interaction between many stakeholders such as industries, investigators, regulatory authorities, payers, academic experts, clinicians and patient organizations. Interestingly, the development of a drug from an initial idea to its entry into the market can take about 5-10 years and cost $1.7 billion.

1.3.1 Drug discovery and preclinical development

Drug discovery is a complicated, expensive and time-consuming process. More recently, computer-aided drug discovery (*in silico* studies) has emerged as a powerful

and promising technology for faster, cheaper and more effective drug design and it is increasingly used in the discovery of new drugs (Cui et al. 2020).
During the process of drug discovery, different strategies are followed or combined, which may involve the use of *in silico*, *in vitro*, *ex vivo* and *in vivo* animal models to gather basic information about the pharmacokinetics, safety and potential efficacy of a drug candidate (Muntha 2016).

1.3.1.1 *In silico* studies

In silico is a term usually used to describe computational studies that makes predictions, suggests hypotheses and ultimately provides discoveries of new drugs. These methods include databases, quantitative SAR, pharmacophores, homology models and other molecular modeling approaches, machine learning, data mining, network analysis tools and data analysis tools that use a computer (Ekins et al. 2007). These models frequently are used in the discovery and optimization of novel molecules and to study the drug affinity to a target, the prediction of absorption, distribution, metabolism, excretion and toxicity properties, as well as the physicochemical characterization. *In silico* assays reduce the need for animal models and human cohorts, decreasing the time and cost of studies (Saeidnia et al. 2013). Interestingly, they have potential to enable precision medicine for complex diseases with variable treatment response across the patient population (Zloh and Kirton 2018). Computational drug design has successfully promoted the discovery of several new anticancer drugs such as gefitinib, erlotinib, sorafenib, lapatinib, abiraterone acetate and crizotinib (Cui et al. 2020). On the other hand, they can be used to study the interaction of molecules with their potential targets. In some experimental works performed by us and presented later in this thesis, we focused on molecular docking studies and prediction of drug-likeness properties and pharmacokinetic properties of several compounds synthesized.

1.3.1.1.1 Molecular docking studies

Molecular docking is a typical structure-based protocol, which is used to study and predict the binding energies and interaction affinities between a ligand and a receptor (Ferreira et al. 2015). According to the flexibility of the ligands involved in the computational process, molecular docking could be categorized as rigid and flexible docking (Halperin et al. 2002). The rigid docking method is a binding model that only considers the static geometrical, physical and chemical complementarity between the ligand and the target proteins, ignoring the flexibility. This method is fast and highly effective. Otherwise, the flexible docking method considers more detailed and accurate

information (Salmaso and Moro 2018). There are different types of software available for docking, such as Glide, FlexX, DOCK, AutoDock, Discovery Studio and Sybyl (Cui et al. 2020).

The molecular docking process is mainly composed by three steps. First, the structures of molecules and target proteins should be prepared. Many structures of target proteins are available in the open access PDB database (http://www.rcsb.org). Second, the used program predict conformations, orientations and positional spaces in the ligand binding site (Raj et al. 2018). Docking calculations explore enthalpic and entropic contributions and components of molecular interactions that lead to the final free energy of binding (ΔG). Enthalpic contributions include electrostatic interactions (ionic bonds, charge-dipole and dipole-dipole interactions), dispersion forces (responsible for attractive interactions between non-polar molecules), hydrogen bonds and steric interactions (short-range repulsive forces), while entropic contributions are composed by translational and rotational energy (which means an interference in the degrees of freedom of the ligand after the formation of the ligand-receptor complex), hydrophobic effect and solvent reorganization. Finally, these programs evaluate the putative binding-free energy that associates the scoring function to determine which compounds are more likely to bind to targets (Huang et al. 2010).

1.3.1.1.2 Drug-likeness properties and pharmacokinetics and toxicity prediction

The early prediction of pharmacokinetics properties is very important to support decision making in drug discovery; indeed, the drug concentration-time profile in the body is determinant to obtain clinical efficacy, as well as a suitable safety profile. *In silico* technology has been widely used to evaluate the relevant properties of drugs in the preclinical stage and, for this, many databases and software programs have been developed (Wu et al. 2020). The use of computational tools to predict the absorption, distribution, metabolism, excretion and toxicity (ADMET) properties and to support the selection of compounds with higher potential to interact with protein targets is a widely used approach in modern medicinal chemistry (de Ruyck et al. 2016). The pkCSM web platform (http://biosig.unimelb.edu.au/pkcsm/prediction) is a free software that allows a fast prediction of the ADMET properties of compounds based on their simplified molecular input line entry specification (SMILES) strings. The program analyses, for example, Caco-2 permeability, intestinal absorption, central nervous system (CNS) permeability and hepatotoxicity. To evaluate drug-likeness or determine if a chemical compound with a certain biological activity has chemical and physical properties that would make it a likely orally active drug in humans, the Lipinski's rules

are employed. Traditionally, therapeutics are small molecules that fall within the Lipinski's rule of five: a molecule with a molecular mass less than 500 Da; no more than 5 hydrogen bond donors; no more than 10 hydrogen bond acceptors; and a calculated octanol–water partition coefficient (log $P_{o/w}$) not greater than 5. In this software (pkCSM web platform), the log $P_{o/w}$, the molecular weight (MW) and the number of hydrogen bond acceptors (HBA), hydrogen bond donors (HBD) and routable bonds (RB) are usually studied parameters (Pires et al. 2015). The number of rotatable bonds is a measure of molecular flexibility and it is also important namely for determining oral bioavailability of the drugs. The mean value for rotatable bonds per molecule in drugs is 6 (Khanna and Ranganathan 2009). In most cases, an orally active drug does not violate more than one Lipinski's rule (Lipinski 2000).

In vitro and *in vivo* studies are important tools in cancer research, used to better explain tumor behavior, to evaluate the effect of experimental drug and to study the efficacy of cytotoxic drugs. *In vitro* models provide a starting point for researchers to understand how a cell responds to a new drug in a controlled and isolated environment. They are low-cost assays used by pharmaceutical companies to study the biological effects of experimental drug candidates against cancer cell lines (Katt et al. 2016). The results from these studies show the possible molecular mechanisms involved and how these mechanisms may influence cancer cells under defined conditions. However, it is extremely difficult to extrapolate these effects for clinical practice. Once a drug candidate demonstrates effectiveness through a series of *in vitro* experiments, *in vivo* models can be employed to advance to drug development studies. These preclinical studies typically involve the use of animals to further evaluate the safety and efficacy of a drug candidate (Patil et al. 2019).

1.3.1.2 In vitro models

In vitro studies are important tools in cancer research, which are often used to better explain tumor behavior and to evaluate experimentally the efficacy of an anticancer drug candidate. *In vitro* models provide a starting point for researchers to understand how cancer cells respond to a new drug candidate in a controlled and isolated environment. They are low-cost assays largely used by pharmaceutical companies to study the biological effects of experimental drug candidates against cancer cell lines. The results from these studies show the possible molecular mechanisms involved and how these mechanisms may influence cancer cells proliferation under defined conditions (Katt et al. 2016).

In vitro is the latin word for “in glass”, which describes medical procedures, tests and experiments that researcher perform outside of a living organism in a test tube or petri dish. The greatest advantage of *in vitro* studies is that they offer the possibility to maintain cells in completely controlled environmental conditions, and it is possible to obtain results in a short time. Also, they are less expensive than animal models (Arantes-Rodrigues et al. 2013). However, they also have disadvantages such as *in vitro* cell growing cannot be representative of that occurs *in vivo*. Traditionally, *in vitro* drug studies are performed in bidimensional (2D) cultures, where cells are seeded on flat plates to form a monolayer. This technique is very used due to simplicity, but 2D models are unable to replicate the cell–cell signaling of complex three dimensional (3D) tissues (Valente et al. 2017). Also, *in vitro* studies do not predict the adverse effects of drugs (Arantes-Rodrigues et al. 2013). In order to better understand the progression and treatment of cancer, novel *in vitro* tumor models have been developed, such as models to the study of intravasation, extravasation, angiogenesis, matrix remodeling and tumor cell dormancy (Katt et al. 2016). In addition, sophisticated bioengineered microscale organotypic models defined in *in vitro* platforms that rely on the use of 3D environments (e.g., multicellular spheroids), 3D matrices (e.g., collagen) and the culture of one or multiple cell types (e.g., tumor cells) were also developed (Ayuso et al. 2021).

Accordingly, in cancer drug discovery a wide variety of methods have been used to study the bioactivity of new compounds:

- Cell viability/antiproliferation [based on cellular enzymes and proteins, DNA synthesis, cellular adenosine triphosphate (ATP), membrane integrity];
- Estrogenicity assays;
- Cell cycle distribution;
- Apoptosis;
- Cell migration and invasion;
- Angiogenesis;
- Antioxidant and oxidative stress markers;
- Cellular senescence;
- Gene mutations and chromosomal alterations;
- Gene and protein expression analysis;
- Energy metabolism in cancer cells.

In several experimental works performed in the scope of this thesis we utilized *in vitro* viability and proliferation assays, a preliminary estrogenic assay, cell cycle analysis by flow cytometry and fluorescence microscopy to understand in which phase the cells

were arrested, as well as what was the morphology of dying cells, and whether it was compatible with apoptosis.

1.3.1.2.1 Cell viability and cell proliferation assays

Viability levels and proliferation rates of cells are good indicators of "cell health". These assays are rapid and inexpensive and, therefore, they are routinely used in drug oncological research in order to evaluate the compounds cytotoxicity and tumor cell growth inhibition (Aslantürk 2018). Trypan blue, a dye exclusion assay, is frequently used in the laboratories for cell counting under the microscope. Only dead cells turn blue after dye application and live cells have a clear appearance. Cell viability is calculated using the ratio of total live/total cells (live and dead cells). It is an easy and cheap assay (Adan et al. 2016).

Using multi-well plates, tetrazolium reduction, resazurin reduction, protease markers and ATP detection are the most used assays to estimate cell viability. The tetrazolium reduction, resazurin reduction and protease activity assays measure cell metabolism. The reagent is incubated with viable cells that convert the substrate to a colored or fluorescent product that is detected with a plate reader. The signal is usually proportional to the number of viable cells present. However, in ATP assay it is not necessary an incubation period because this reagent immediately ruptures the cells (Markossian et al. 2016).

The 3-(4,5-dimethylthiazol-2-yl)-2,5-diphenyltetrazolium bromide (MTT) assay is one of most commonly used tetrazolium assays for anticancer drug screening and it was chosen by us to perform the studies. It is a colorimetric assay for assessing cell metabolic activity. NADPH-dependent oxidoreductases or dehydrogenases in viable cells can reduce MTT into purple colored formazan, which can then be solubilized for further spectrophotometric analysis at 570 nm (**Figure 1.21**) (Berridge and Tan 1993).

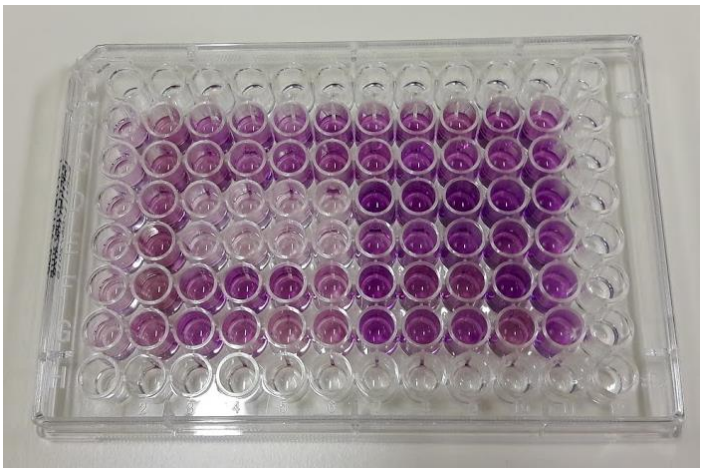

Figure 1.21 3-(4,5-Dimethylthiazol-2-yl)-2,5-diphenyltetrazolium bromide (MTT) assay after dissolution of formazan used in our laboratory.

The MTT method is easy to use, relatively safe, has a high reproducibility and is widely used to determine both cell viability and cytotoxicity activity. However, the amount of signal generated is dependent on several parameters, including the concentration of MTT, the length of the incubation period, the number of viable cells and their metabolic activity. Also, prior to measuring the absorbance, an organic solvent such as dimethyl sulfoxide (DMSO) or isopropanol is required to solubilize the formazan (Aslantürk 2018).

The sulforhodamine B assay is another common colorimetric assay that is used to investigate viability of cancer cells, which is similar to MTT assay (Skehan et al. 1990). Other tetrazolium compounds such as 3-(4,5-dimethylthiazol-2-yl)-5-(3-carboxymethoxyphenyl-2-(4-sulfophenyl)-2*H*-tetrazolium (MTS), 2,3-bis-2-methoxy-4-nitro-5-sulfophenyl)-2*H*-tetrazolium-5-carboxabilide (XTT) and 4-[3-(4-Iodophenyl)-2-(4-nitro-phenyl)-2*H*-5-tetrazolio]-1,3-benzene sulfonate (WST) were also used to generate formazan (Riss et al. 2013). Unlike the traditional MTT assay, the assays with these regents (MTS, XTT and WST) do not require the formazan solubilization step since solubilization occurs in the cell medium itself. Although these assays are cheap and easy to conduct, their major disadvantages are related to the damage of cells during washing steps (Wang et al. 2010).

Also, resazurin (Alamar Blue assay) is dissolved in physiological buffers (has a deep blue colored solution) and added directly to cells in culture. Viable cells can reduce resazurin into the resorufin product which is pink and fluorescent compound. The fluorescence signals can be measured at 570 and 630 nm. The major advantages of this assay are the inexpensive cost and sensitivity.

The protease activity is measured using a cell permeable fluorogenic protease substrate (glycylphenylalanylaminofluorocoumarin; GF-AFC) that generates a fluorescent signal proportional to the number of viable cells. The major advantage of this method is the short time of incubation (30 min to 1 h).
ATP assay has been widely accepted as a valid marker of viable cells. When cells lose membrane integrity, they lose the ability to synthesize ATP. In this method, it is not necessary an incubation time for viable cells convert the substrate into a colored compound and it is also a very sensitivity assay (Adan et al. 2016; Markossian et al. 2016)

Otherwise, cell proliferation assays analyze the growth rate of a cell population, detect daughter cells in a growing population or the proportions of cells in different stages of the cell cycle. Several methods can be used to study the cell proliferation. The incorporation of a radioisotope, [3*H*]-thymidine, into cellular DNA, followed by autoradiography can be used. Alternatively, bromodeoxyuridine (BrdU) may be used instead of thymidine. Cells that have incorporated BrdU into their DNA are easily detected using a monoclonal antibody against BrdU with an enzymatic (e.g., ELISA) or fluorometric technique. Ethynyldeoxyuridin (EdU) assay is similar to BrdU, but uses a fluorescent dye or biotin for colorimetric or fluorometric detection (Adan et al. 2016).
Other techniques often use membrane-impermeable fluorescent dyes (mostly DNA stains) that stain cells with damaged cell membranes. These dyes typically are not permeable to viable cells but can enter dead cells through damaged membranes. Propidium iodide (PI) is the mostly commonly used dye. In dye dilution assays, 5(6)-carboxyfluorescein diacetate *N*-succinimidyl ester (CFSE) is a popular choice for measuring the number of divisions undergone by a cellular population. Upon entering the cell, CFSE is cleaved by intracellular esterases to form the fluorescent compound. The dyes are retained within cells over multiple generations (Ediriweera et al. 2019).
In this thesis, we used flow cytometry (FCM) to analyze viability and cell proliferation. This technique allows the analysis of the size and complexity of cells, as well as fluorescence through electronic and optical detectors. PI, fluorescein diacetate, CFSE, 7-aminoactinomycin (7AAD), 4',6-diamidino-2-phenylindole (DAPI) are commonly dyes applied. PI cannot enter into viable cells, opposed to fluorescein diacetate or carboxyfluorescein diacetate that are able to enter into these cells (Boyd et al. 2008). In this process, a sample containing cells is suspended in a fluid and injected into the flow cytometer instrument. Cells are often labeled with fluorescent markers so light is absorbed and then emitted in a band of wavelengths. Forward *versus* side scatter (FSC vs SSC) and fluorescent (FL3, for PI) gating is commonly used to identify cells of

interest based on size and granularity. It is often suggested that forward scatter indicates cell size whereas side scatter relates to the complexity or granularity of the cell (**Figure 1.22**). Data analyzed by flow cytometers can be generated as histograms (2D or 3D plots) based on the fluorescence intensity (Adan et al. 2017).

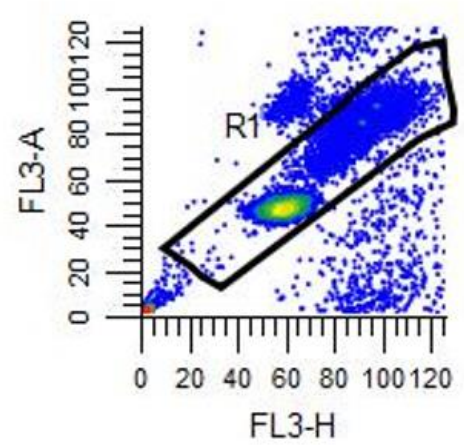

Figure 1.22 T47-D cells determined by forward scatter (FSC) and fluorescence channel-3 (FL3) are stained with propidium iodide (PI) to identify viable cells (R1).

1.3.1.2.2 Cell cycle assays

Cell cycle checkpoints can be analyzed by various assays, such as [3*H*]-thymidine incorporation, BrdU incorporation, staining the DNA using FCM and fluorescence microscopy techniques. Assays that use antibodies are also utilized such as Ki-67 antigen, proliferating cell nuclear antigen or phospho-histone H3 detection (Adan et al. 2016).

In this thesis we used DNA staining by FCM. Thus, cell cycle profile of a sample can be determined by staining the DNA with a fluorescent dye and measuring its intensity. The dye stains DNA stoichiometrically (in proportion to the amount of DNA present in each cell), allowing differentiation of cells in G_0/G_1, S phase and G_2/M, as well as identification of aneuploid populations. Some DNA dyes do not stain live cells. The sample must be fixed and permeabilized to allow the dye to enter the cells (e.g., PI and DAPI). Hoechst 33342 or DRAQ5^{Tm} are DNA dyes that are membrane-permeable and can be used to stain live and intact cells (Banfalvi 2017). Using FCM technique, there are standard modeling algorithms that can then be employed to determine the breakdown of cells in the G_0/G_1 phase *versus* S phase, G_2, or polyploidy state of the cell population (**Figure 1.23**).

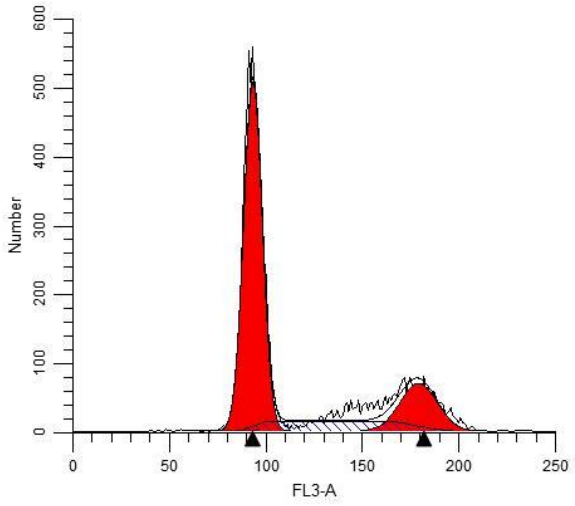

Figure 1.23 Histogram of T47-D cell cycle distribution using propidium iodide as dye.

1.3.1.2.3 Estrogenicity assays

The estrogenicity of a new compound is defined as the ability of a compound to bind to the ER and modulate the gene expression or transcriptional activity, and it can be evaluated by the bioluminescent assay (Prokai-Tatrai and Prokai 2019) or by the *E*-screening assay (Soto et al. 1995).

The main purpose of the reporter gene assay is to investigate the promoter of a gene of interest, i.e. the regulation of its expression. This can be done by linking the promoter of interest to an easily detectable gene, such as luciferase, which catalyzes a reaction that produces light. This light is detected with a luminometer, a device that precisely quantifies how much light is produced in each reaction tube. The amount of light produced provides a quantitative measure of the effect of the protein on expression of the target gene (Fan and Wood 2007).

The study of proliferative activity on estrogen-sensitive cells (*E-screening*), like breast T47-D, ZR-75-1 or MCF-7 cancer cells (endogenously expresses ERα) was firstly developed by Soto *et al* (Soto et al. 1995) and is based on the enhanced proliferation of human breast cancer cells in the presence of estrogen active substances. For assaying, a range of concentrations of the test compound is added to the experimental medium. In each experiment, the cells are exposed to a dilution series of E2 for providing a positive control (standard dose-response curve) and treated only with hormone-free medium as a negative control. After 6 days of exposure, the proliferation of cancer cells was estimated by the MTT assay. One of the limitations for determining estrogenicity of chemicals by checking the proliferation of ER positive cell line is that mitogens, other than estrogens, can also influence cell proliferation and, thus, rendering non-specific

responses by chemicals (Resende et al. 2013). Since *E-screening* assay is an easy and a cheaper procedure, it was applied in the experimental work supporting this thesis.

1.3.1.2.4 Apoptosis evaluation

Apoptosis is a reliable indicator of therapeutic efficacy in cancer and can be evaluated based on a variety of biochemical and morphological alterations using colorimetric, fluorometric, FCM and fluorescence microscopy techniques. An apoptosis assay detects and quantifies the cellular events associated with programmed cell death, including cell surface exposure of phosphatidylserine, caspase activation or DNA fragmentation. Early events can be detected using Annexin V, mid events using caspase-3 assays and late-stage of apoptosis using DNA fragmentation detection. PI is widely used in conjunction with Annexin V to determine if cells are viable, apoptotic or necrotic through differences in plasma membrane integrity and permeability by FCM (Banfalvi 2017). Caspase assay can be performed by the detection of cleavage of the fluorometric substrate with antibodies specifically recognizing the active form of caspases in FCM or microscopy. Fluorescence microscopy is an imaging technique used in light microscopes that allows the excitation of fluorophores (after incubation with sample) and subsequent detection of the fluorescence signal (Combs and Shroff 2017). A fluorophore is a fluorescence molecule, such as acridine, tetrapyrrole, arylmethine, anthracene, coumarin and cyanine derivatives, which possesses different excitation and emission wavelengths (Stockert and Blazquez-Castro 2017). Fluorescent dyes (fluorochromes) are commonly linked to mono- or polyclonal antibodies because it is beneficial for the detection of different apoptotic pathways (e.g. caspase-3 activity) (Gordon et al. 2018). One of the most used dyes in fluorescence microscopy is Hoechst 33258 or 33342. Hoechst 33258 is a lipophilic and cell permeable probe most frequently used in fluorescence microscopy for qualitative detection of nuclear morphology changes, primarily for detecting cell shrinkage, chromatin condensation, nuclear fragmentation and apoptotic bodies formation in various cell lines (Majtnerova et al. 2021). Hoechst 33342 is often used to distinguish condensed pyknotic nuclei in apoptotic cells (Tolosa et al. 2012). This is a simple and low cost technique (Bucevičius et al. 2018).

1.3.1.3 In vivo animal models

Once a drug candidate demonstrates effectiveness through a series of *in vitro* experiments, *in vivo* animal models can be employed to move towards preclinical drug development. These early preclinical studies typically involve the use of rodents (mice

and rats) to further evaluate the safety and efficacy of drug candidates (Patil et al. 2019).

Larger-scale screens of anticancer drugs emerged around 1955, with the discovery of nitrogen mustards that were used to treat malignant lymphomas (Patil et al. 2019). *In vivo* studies are undertaken to further define the antitumor activity and provide pharmacology and toxicology data needed for the subsequent clinical development (Stathis et al. 2012).

One of the first models used was the hollow fiber assay, which was developed by Hollingshead *et al* (Hollingshead et al. 1995). It is a fast *in vivo* assay to determine the cytotoxic effect of drugs as well as their pharmacodynamic effects on human tumor cell lines that grow in hollow fibers, which are implanted subcutaneously or intraperitoneally in mice or rats.

Another older method used is the chemically induced cancer model that is generated by the exposition of synthetic chemical compounds to the animal body via ingestion, inhalation, injection or dermal absorption. This model has several advantages including the easy procedures, fruitful tumor generation and high analogy to clinical human primary cancers. However, in addition to the time-consuming process, the major drawback of chemical carcinogenesis is the difficulty in noninvasive tumor burden assessment in small animals (Liu et al. 2015).

Other simple *in vivo* models were also developed and use spontaneous and transplanted murine tumors (syngeneic model) or human tumors (xenograft model). Cell lines are inoculated subcutaneously into the flank of a mouse and tumor growth is monitored with capillaries (Patil et al. 2019). Spontaneous tumor models are difficult to obtain and maintain, but they have some advantages over transplanted tumor cell lines (e.g., genetic diversity, growth in the original environment). Importantly, tumor characteristics and metastasizing depend on implantation site of tumors, where tumors injected orthotopically (organ of origin) behave more similarly to the clinical. Consequently, the response to anticancer drugs may depend on the implantation site (Patil et al. 2019). These assays are cheap, but they do not reflect the complexity of the cancer disease. Then, more complex models are being developed to be more predictive of the clinical efficacy. An example is the patient-derived xenograft (PDX) model, in which, freshly resected human tumors are implanted into immunosuppressed mice, which can reflect the heterogeneity and diversity of the human patient population. However, the cost of using and maintaining PDX panels is high and could not be used to study immunomodulatory agents. Personalized PDX models are also developed and use cells from the patient's primary tumor site for xenotransplantation into immunosuppressed mice (**Figure 1.24**).

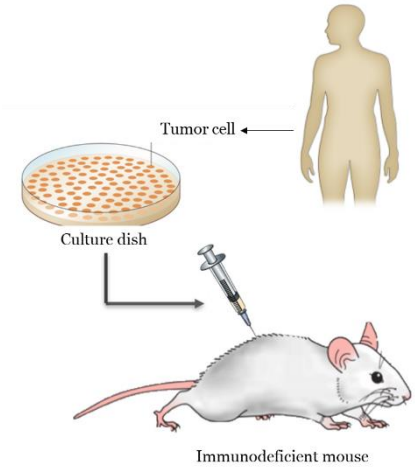

Figure 1.24 *In vivo* patient-derived xenograft (PDX) model. Adapted from Creative Biolabs®.

Organoid xenografts are 3D *in vitro* models generated from patient tumor tissue that is been previously incorporate into murine models for expansion. This model overcomes some of the limitations associated with modelling the tumor microenvironment. In addition, genetically engineered mouse models (GEMMs) were also developed. These models successfully predicted clinical events, but the main limitation of GEMMs is that it targets a few numbers of genes, which is normally not insightful of the complicated heterogeneity of human tumor cells. The establishment of GEMMs is expensive and tedious, frequently required long periods of work before validation. Tumor evolution in animals is variable and slow. They have different biochemistry, physiology and anatomy compared to humans (Ireson et al. 2019; Sajjad et al. 2021). Other complex models have been developed such as drosophila, pig cancer model or zebrafish model (Sajjad et al. 2021). Thus, testing compound in a disease-relevant environment saves substantial time and money during preclinical phase and the choice of the best *in vivo* model is fundamental to achieve good results.

1.3.2 Clinical development for anticancer drugs

The clinical development of a drug is a complex process and usually involves a lot of different clinical trials, which are included in different phases depending on the objectives of the trials (phase I, phase II, phase III and phase IV). Phase I clinical trials are carried out to investigate the pharmacokinetics and safety in humans and to determine the maximum tolerated dose of the drug candidate and usually are performed in healthy volunteers (Kunnumakkara et al. 2019). However, for anticancer drugs, these phase I clinical trials are not usually carried out in healthy volunteers due to ethical reasons and include a small number of patients (up to a few dozen). In these clinical trials, patients with any type of advanced cancer can be included, usually after trying treatment with all available alternatives. The phase I clinical trials also include

dose escalation studies. Phase II clinical trials have the purpose to determine if the new treatment has an effect on a certain cancer and to see how the new treatment affects the body and helps fight cancer. Each of these trials typically includes less than 100 patients. Later, phase III clinical trials compare the safety and effectiveness of the new treatment (or new use of a treatment) with the current standard treatment and may include several hundred to thousands of patients with a particular cancer type. Some clinical trials combine two phases (phase I/II or phase II/III) in a single protocol. In these combined study designs, there is a seamless transition between trial phases, which may allow questions under investigation to be answered more quickly or with fewer patients (NIH 2022).

The European Medicines Agency (EMA) in Europe or FDA in United States of America provide guidance and support to medicines developers, which include scientific and regulatory information on how to design and conduct clinical trials, compliance standards and obligations for developers of new drugs. Based on the assessment of non-clinical, clinical and quality data submitted, these regulators have to make sure that only products with a positive benefit–risk balance are launched into the market (EMA 2016b).

In phase IV or pharmacovigilance studies the side effects caused over time by a new treatment after its approval are collected and analyzed. Pharmacovigilance may detect side effects that were not identified in earlier trials and may also study how well a new treatment works over a long period of time (Suvarna 2010).

Overall, only 55% of all the drugs that achieve the phase III of clinical trials reach the market (Mould and Hutson 2017).

In anticancer drug development, the relatively high failure rate in phase III clinical trials results in high development costs (Mould and Hutson 2017). Concerning preclinical studies, numerous factors contribute for this hard process. The new modern biological techniques and systems to evaluate toxicity are very expensive and low-efficient, for example, to study metastasis. Nowadays, it is also well recognized that more than 95% of the drugs that kill either cancer cells in culture or that induce tumor regression in animals, fail in phase I clinical trials, indicating that most preclinical models of cancer are inadequate (Kunnumakkara et al. 2019). Also, the development of new anticancer drugs is a slow process due to inefficient trial design such as lack of randomization, lack of overall survival data, inappropriate use of crossover, use of suboptimal control arms, difficulties in recruitment, data collection and interpretation, complexity in maintaining and monitoring safety and economic constraints on the conduct of the trials (Ajithkumar and Gilbert 2017; Hilal et al. 2020). Otherwise,

current policy of anticancer drug licensing is that new compounds must be more effective than the already licensed ones. This is not always possible because many cancers have to be treated with multiple drugs. Thus, the rigid drug evaluation and regulatory rules have hampered anticancer drug development (Lu et al. 2017).

1.4 Aims

The incidence of cancer has increased over the years and, consequently, the academia and pharmaceutical industry have been worked hardly to develop anticancer therapies with higher selectivity and improved safety profiles. The main goal of the present work was the discovery of new oxime derivatives based on estrone scaffold with antiproliferative properties that should be developed and elected for further development.

To this end, the following specific objectives were outlined for the implementation of this doctoral work:

- Design, synthesis, purification and structural characterization of new oxime derivatives based on the structure of E1. For that, modifications at C2, C3, C4, C9, C10, C11 and C16 were performed through iodination, bromination, nitration, oxidation, alkylation, condensation and acetylation to obtain intermediates, which were used when possible to synthesize C17 E1 oximes.
- *In vitro* screening of cytotoxicity of the synthesized compounds. The well-established MTT assay was used to evaluate the antiproliferative activities of synthesized compounds. The cancer cells used were breast (MCF-7 and T47-D), prostatic (LNCaP), hepatic (HepaRG) and intestinal (Caco-2) cell lines; in addition, normal human dermal fibroblasts (NHDF) were also used for the evaluation of selectivity.
- *In vitro* estrogenicity assay analyzing the estrogen-sensitive (ER^+) breast (T47-D) cell proliferation, which indicates the estrogenic potential of new compounds. In the treatment of cancer are expected that compounds are devoid of estrogenicity.
- *In vitro* screening of cell viability and cell cycle distribution through flow cytometry for the most promising compounds. To estimate the percentages of a cell population in the different phases of the cell cycle is important to understand the possible mechanism of action.
- *In vitro* fluorescence microscopy to analyze condensed DNA and apoptosis.
- *In silico* predictions of binding energies and binding mode through molecular docking studies against the main targets of cancers: ERα, ST, 17β-HSD1 and β-tubulin. Also, *in silico* predictions of ADMET properties were also performed. Pharmacokinetic properties were estimated using a predictive computational tool (pkCSM web platform) in order to better understand the drug-likeness of tested compounds.

Chapter 2
$\Delta^{9,11}$-Estrone derivatives

The content of this chapter is included in the following article:

Canário C, Matias M, Brito V, Santos AO, Falcão A, Silvestre S, Alves G. 2020. $\Delta^{9,11}$-Estrone derivatives as potential antiproliferative agents: synthesis, *in vitro* biological evaluation and docking studies. C R Chim. 23(2):201-217.

2.1 Introduction

The incidence of cancer has been increasing over the years. It is predicted that 27.5 million new cancer cases will appear worldwide each year by 2040. This represents an increase of 61.7% from 2018 and is expected to be higher in males (67.6% increase) than in females (55.3% increase) (Global Cancer Observatory 2018). Therefore, several classes of drugs have been developed over the years to treat cancer. For example, taxanes, monoclonal antibodies and steroids are used in clinical practice (Archampong and Sweetland 2014; Abou-Salim et al. 2019; Liu et al. 2019).

Steroid hormones are involved in many physiologic responses and pathologic conditions mainly by binding to their intracellular receptors, namely estrogen receptors (ERs), which are transcription factors. For example, the importance of androgens in prostatic cancer and estrogens in breast cancer led to the development of therapies that block their action in these tumors (Groner and Brown 2017). In this context, exemestane (an aromatase inhibitor) (Kümler et al. 2016) and fulvestrant (a selective ERα antagonist) (Lee et al. 2017) (**Figure 2.1**) are molecules of clinical interest in the treatment of hormone-dependent breast cancers (Salvador et al. 2013; Chuffa et al. 2017).

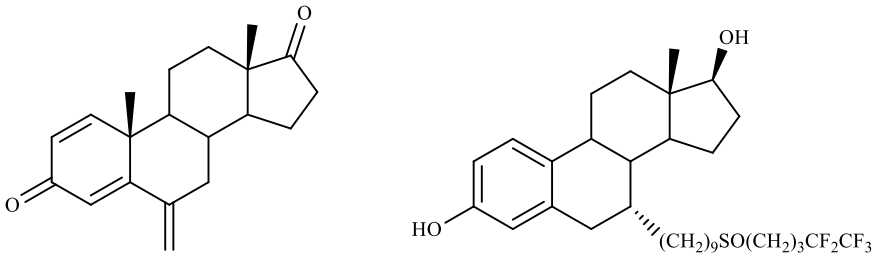

Exemestane **Fulvestrant**

Figure 2.1 Relevant steroids used in clinical practice as anticancer agents.

Therefore, developing safer and more effective ways of preventing and treating these hormone-dependent cancers is crucial, given the significant impact that these diseases have on human health and their economic and social importance (ACS 2018). Although the use of steroid hormones and analogues has been associated with hormone-dependent cancers, evidence also suggests that they can be important in the treatment of other kind of tumors such as lung, brain and liver cancers (Kumar et al. 2016; Chuffa et al. 2017).

Taking into account the importance of steroids in cancer treatment, and as has been widely demonstrated in the literature, estrone (E1) and 17β-estradiol (E2) have been used as starting materials for the design and development of new and more promising anticancer drug candidates with different targets of action (Salvador et al. 2013; Dutour et al. 2018; Amr et al. 2019; Salaha et al. 2019). For instance, the presence of a 16α-

hydroxyl in E1 derivatives appeared to be associated with a high cytotoxicity and a reduced interaction with ERα (Alsayari et al. 2017). In addition, the introduction of aryl groups in C-16 of steroidal scaffold led to higher antiproliferative effects (Bansal et al. 2011; Vosooghi et al. 2013). Furthermore, the presence of 2-ethyl-3-*O*-sulphamoyl groups in estrane nucleus allowed an improvement of the antimitotic activity of E1 analogues (Stander et al. 2011). E1 3-*O*-ether derivatives containing the piperazine ring also exhibited a strong cytotoxic activity against prostate cancer cell lines (Chen et al. 2018). Interestingly, different C-13 epimeric analogues of 16β-(*m*-carbamoylbenzyl)-E2 showed 17β-hydroxysteroid dehydrogenase type 1 (17β-HSD1) inhibition and a weak estrogenic effect on estrogen-sensitive breast cancer cells (Maltais et al. 2016). Regarding C-ring modifications, for example, the presence of a $\Delta^{9,11}$ double bond combined with 2- and 4-substitutions in E1 nucleus was also relevant to develop promising antiproliferative agents (Milić et al. 2005).

These findings, in addition to our continuous interest in steroidal chemistry and bioactivity (Salvador et al. 2013; Dias et al. 2015; Jesus et al. 2016; Canário et al. 2018; Brito et al. 2019) and the need to develop improved anti-cancer agents, motivated us to prepare and evaluate in *in vitro* the cell proliferation effects of E1 derivatives. Specifically, we report herein the chemical synthesis of $\Delta^{9,11}$-E1 derivatives with A-(2,4-diiodo and 2,4-dibromo) and D-ring (16-benzylidene) modifications and their biological evaluation (cell proliferation and viability assays, *E*-screening assay and cell cycle distribution analysis). Docking studies on ERα, steroid sulfatase (ST) and 17β-HSD1, which are relevant potential targets of these $\Delta^{9,11}$-E1 derivatives, were also performed.

2.2 Experimental section

2.2.1 Chemistry

All chemicals received from suppliers were used without further purifications. The reagents were purchased from the following suppliers: E1: Cayman Chemical (Michigan, USA); methanol (MeOH): Fisher Chemical (MA, USA); *N*-bromosuccinimide (NBS): Alfa Aesar (Massachusetts, USA); benzene (PhH): Merck (NJ, USA); benzaldehyde (BZ): Acros Organics (New Jersey, USA); ethanol (EtOH) 99.9%: Manuel Vieira & Ca (Torres Novas, Portugal). The reagents 2,3-dichloro-5,6-dicyano-*p*-benzoquinone (DDQ), morpholine, E2, 5-fluorouracil (5-FU) and dimethyl sulfoxide (DMSO) as well as the remaining chemical products referred to in the text, including petroleum ether (PE) 40 - 60 °C, were obtained from Sigma-Aldrich (St. Louis, MO, USA). Deuterated DMSO

(DMSO-d_6) and deuterated chloroform ($CDCl_3$) were purchased from Armar Chemicals (Leipzig, Germany). All reactions were monitored by thin layer chromatography (TLC) using Al-backed aluminum/silica gel plate 0.20 mm (Macherey-Nagel 60 F254, Duren, Germany) and, after elution, the plates were visualized under ultraviolet (UV) radiation (254 nm) in a CN-15.LC UV chamber. EtOH/concentrated sulfuric acid (95:5, v:v) mixture was used to process the plates, followed by heating at 120 ˚C. The evaporation of solvents was achieved by using a rotary vacuum drier from Büchi (R-215). Melting points (mp) were recorded on a Büchi B-540 melting point apparatus and are uncorrected. Infrared (IR) spectra were collected on a Thermoscientific Nicolet iS10 equipped with a diamond attenuated total reflectance crystal at room temperature in the 4000-400 cm^{-1} range by averaging 16 scans at a spectral resolution of 2 cm^{-1}. Nuclear magnetic resonance (NMR) spectra (^{1}H-NMR and ^{13}C-NMR) were acquired on a Bruker Avance 400 MHz spectrometer and were processed with the software TOPSPIN 4.07 (Bruker, Fitchburg, WI, USA). Chemical shifts are reported in parts per million (ppm) relative to tetramethylsilane (TMS) or solvent as an internal standard. Coupling constants (*J* values) are reported in hertz (Hz) and splitting multiplicities are described as s=singlet; brs=broad singlet; d=doublet; dd=double doublet and m=multiplet. High resolution mass spectrometry (ESI-HRMS) was performed by the microanalysis service on a QSTAR XL instrument (Salamanca, Spain).

*2.2.1.1 Synthesis of 3-hydroxyestra-1,3,5(10),9(11)-tetraen-17-one (**2.1**)*

A stirred solution of **1** (540.8 mg, 2 mmol) in MeOH (80 mL) was heated at 45 ˚C. DDQ (680.9 mg) was added in one portion and the resulting solution was vigorously stirred for 5 h at 45 ˚C under nitrogen (N_2) atmosphere. After completion of the reaction (TLC control), MeOH was evaporated and the residue was diluted in 300 mL of dichloromethane (CH_2Cl_2), washed with 100 mL of aqueous 10% sodium sulfite (Na_2SO_3), 100 mL of a saturated aqueous solution of sodium hydrogen carbonate ($NaHCO_3$) and 100 mL of water (H_2O) and dried over anhydrous sodium sulfate (Na_2SO_4), filtered and evaporated under reduced pressure to yield the crude product, which was recrystallized from MeOH to give compound **2.1** (Gabbard et al. 1981; Stéphan et al. 1995) as beige crystals (223.5 mg, 42% yield); mp 235.2-237 °C (lit (Alvarez and Watt 1972) 243-246 °C). IR (υ_{max}, cm^{-1}): 814, 1224, 1453, 1605, 1615, 1715, 2832-2964, 3019, 3255; ^{1}H-NMR (400 MHz, DMSO-d_6) δ: 0.82 (s, 3H, C18-CH_3), 6.05 (m, 1H, C11-H), 6.46 (d, 1H, J = 2.5 Hz, C4-H), 6.55 (dd, 1H, J_1 = 8.6 Hz, J_2 = 2.5 Hz, C2-H), 7.43 (d, 1H, J = 8.7, C1-H), 9.28 (brs, 1H, 3-OH); ^{13}C-

NMR (100 MHz, DMSO-d_6) δ: 14.21, 22.05, 27.31, 29.20, 33.56, 35.72, 37.69, 45.45, 47.02, 113.82, 114.79, 115.22, 125.03, 125.11, 135.24, 137.19, 156.23, 220.42.

*2.2.1.2 Synthesis of 3-hydroxy-16-phenylmethylidene-estra-1,3,5(10),9(11)-tetraen-17-one (**2.2**)*

To a solution of compound **2.1** (134.2 mg, 0.5 mmol) in MeOH (3.8 mL) was added BZ (76.4 µL) and potassium hydroxide (KOH) (192 mg). The reaction mixture was stirred during 4.5 h at room temperature. After completion (TLC control), the reaction mixture was diluted in 150 mL of CH_2Cl_2 and washed with 50 mL of H_2O, dried over anhydrous Na_2SO_4 and concentrated under reduced pressure to yield the crude product, which was recrystallized from MeOH to give compound **2.2** as brown crystals (57.2 mg, 32% yield); mp 263.1-265.2 °C. IR (υ_{max}, cm^{-1}): 809, 1285, 1360, 1447, 1496, 1604, 1698, 2829-2958, 3021, 3060, 3324; ^{1}H-NMR (400 MHz, DMSO-d_6) δ: 0.91 (s, 3H, C18-CH_3), 6.09 (m, 1H, C11-H), 6.49 (d, 1H, J = 2.3 Hz, C4-H), 6.56 (dd, 1H, J_1 = 8.7 Hz, J_2 = 2.4 Hz, C2-H), 7.34 (brs, 1H, H-vinyl), 7.46 (m, 4H, C1-H, H_3', H_4', H_5'); 7.67 (d, 2H, J = 7.5 Hz, H_2', H_6'), 9.30 (s, 1H, 3-OH); ^{13}C-NMR (100 MHz, DMSO-d_6) δ: 14.89, 27.36, 29.21, 29.47, 33.60, 37.35, 45.03, 45.36, 113.86, 114.83, 115.32, 125.01, 125.11, 128.81, 129.45, 130.41, 132.07, 135.08, 135.41, 136.01, 137.19, 156.28, 208.72. HRMS (ESI-TOF): *m/z* $[M + Na]^+$ calcd for $C_{25}H_{24}O_2$: 356.1776; found 356.1771.

*2.2.1.3 Synthesis of 2,4-diiodo-3-hydroxyestra-1,3,5(10)-trien-17-one (**2.3**)*

To a solution of E1 **1** (270.4 mg, 1 mmol) in PhH (56 mL) were added 302.8 mg of iodine (I_2) and 1536 µL of morpholine. The solution was stirred under room temperature for 17 h. After this time, 60 ml of 5% aqueous HCl solution was added and it was concentrated under reduced pressure. The result was diluted in 150 mL of CH_2Cl_2, washed with 50 mL of saturated aqueous solution of $NaHCO_3$, 50 mL of H_2O and dried over anhydrous Na_2SO_4 and evaporated under reduced pressure. Then, the residue was purified by column chromatography [ethyl acetate (EA)/PE, 1:5] to obtain compound **2.3** (Bacsa et al. 2018) as a beige solid (271 mg, 68% yield); mp 180.1-183 °C (lit (Bacsa et al. 2018) 200-202 °C). IR (υ_{max}, cm^{-1}): 794, 1011, 1083, 1258, 1450, 1707, 1737, 2858-2961, 3296, 3439; ^{1}H-NMR (400 MHz, $CDCl_3$) δ: 0.88 (s, 3H, C18-CH_3), 7.60 (s, 1H, C1-H); ^{13}C-NMR (100 MHz, $CDCl_3$) δ: 13.96, 21.74, 26.41, 27.47, 31.61, 36.05, 37.28, 37.59, 44.09, 48.03, 50.35, 78.56, 92.19, 136.07, 136.15, 140.83, 151.70, 220.61.

*2.2.1.4 Synthesis of 2,4-diiodo-3-hydroxyestra-1,3,5(10),9(11)-tetraen-17-one (**2.4**)*

A stirred solution of **2.3** (131.1 mg, 0.25 mmol) in MeOH (9.8 mL) was heated at 45 °C. DDQ (85.1 mg) was added in one portion and the resulting solution was vigorously stirred for 4 h at 45 °C under N_2 atmosphere. After completion (TLC control), MeOH was evaporated and the residue was diluted in 150 mL of EA and washed with 50 mL of Na_2SO_3 (10%, aqueous), 50 mL of saturated aqueous solution of $NaHCO_3$ and 50 mL of H_2O, dried over anhydrous Na_2SO_4 and concentrated under reduced pressure. This product was purified by column chromatography (eluent: EA/PE, 1:1) to afford compound **2.4** as brown solid (72.1 mg, 55% yield); mp 225.1-227.2 °C. IR (υ_{max}, cm^{-1}): 794, 1014, 1258, 1447, 1711, 1732, 2920-2961, 3442; ^{1}H-NMR (400 MHz, $CDCl_3$) δ: 0.89 (s, 3H, C18-CH_3), 6.12 (m, 1H, C11-H), 7.91 (s, 1H, C1-H); ^{13}C-NMR (100 MHz, $CDCl_3$) δ: 14.57, 22.65, 28.35, 34.22, 36.42, 36.81, 37.23, 46.38, 47.94, 79.52, 91.76, 119.27, 131.26, 134.43, 135.31, 140.06, 152.52, 221.24. HRMS (ESI-TOF): *m/z* $[M + Na]^+$ calcd for $C_{18}H_{18}I_2O_2$: 519.9396; found 519.9396.

*2.2.1.5 Synthesis of 2,4-dibromo-3-hydroxyestra-1,3,5(10)-trien-17-one (**2.5**)*

To a solution of E1 **1** (540.7 mg, 2 mmol) in EtOH (27.0 mL) was added 1.1 g of NBS. The solution was stirred under room temperature for 29 h. After this time, the solvent was evaporated under reduced pressure. The residue was diluted in 150 mL of CH_2Cl_2, washed with 50 mL of saturated aqueous solution of $NaHCO_3$, 50 mL of H_2O and dried over anhydrous Na_2SO_4 and concentrated under reduced pressure. Then, the product was recrystallized from MeOH to give compound **2.5** (Page et al. 1991) as white crystals (353 mg, 41% yield); mp 228.2-229 °C (lit (Page et al. 1991) 235-236 °C). IR (υ_{max}, cm^{-1}): 899, 1164, 1304, 1462, 1543, 1712, 2869-2936, 3235; ^{1}H-NMR (400 MHz, $CDCl_3$) δ: 0.88 (s, 3H, C18-CH_3), 7.38 (s, 1H, C1-H); ^{13}C-NMR (100 MHz, $CDCl_3$) δ: 13.95, 21.73, 26.33, 26.69, 31.12, 31.59, 36.03, 37.54, 44.13, 48.00, 50.39, 106.68, 113.42, 128.75, 135.23, 136.66, 147.47, 220.61.

*2.2.1.6 Synthesis of 2,4-dibromo-3-hydroxyestra-1,3,5(10),9(11)-tetraen-17-one (**2.6**)*

A stirred solution of **2.5** (53.5 mg, 0.125 mmol) in MeOH (4.9 mL) was heated at 45 °C. DDQ (42.6 mg) was added in one portion and the resulting solution was vigorously stirred for 5.30 h at 45 °C under N_2 atmosphere. After completion (TLC control), MeOH was evaporated and then the residue was diluted in 150 mL of EA, 50 mL of Na_2SO_3 aqueous solution (10%), 50 mL of saturated aqueous solution of $NaHCO_3$ and 50 mL of H_2O and then dried over anhydrous Na_2SO_4 and concentrated under reduced pressure

to obtain compound **2.6** as beige solid (38 mg, 71% yield); mp 200.4-202.9 °C. IR (υ_{max}, cm^{-1}): 796, 1011, 1064, 1260, 1463, 1540, 1717, 2836-2960, 3286; ^{1}H-NMR (400 MHz, $CDCl_3$) δ: 0.89 (s, 3H, C18-CH_3), 6.13 (m, 1H, C11-H), 7.69 (s, 1H, C1-H); ^{13}C-NMR (100 MHz, $CDCl_3$) δ: 14.59, 22.65, 27.60, 30.70, 34.19, 36.41, 37.25, 46.35, 47.95, 107.59, 113.14, 119.49, 127.81, 130.32, 134.47, 135.98, 148.30, 221.27. HRMS (ESI-TOF): *m/z* $[M + H]^+$ calcd for $C_{18}H_{18}Br_2O_2$: 423.9674; found 423.9644.

*2.2.1.7 Synthesis of 3-hydroxy-16-phenylmethylidene-estra-1,3,5(10)-tetraen-17-one (**2.7**)*

To a solution of **1** (135.2 mg, 0.5 mmol) in MeOH (3.8 mL) were added BZ (76.4 μL) and KOH (192 mg). The mixture was stirred at room temperature for 4 h. After MeOH evaporation, the reaction mixture was diluted in 150 mL of CH_2Cl_2 and washed with 50 mL of H_2O, dried over anhydrous Na_2SO_4 and concentrated under reduced pressure to yield the crude product, which was recrystallized from MeOH to give compound **2.7** (Poirier et al. 2006; Ispán et al. 2018) as white crystals (162 mg, 90% yield); mp 247.5-249.7 °C (lit (Ispán et al. 2018) 248-250 °C). IR (υ_{max}/cm^{-1}): 790, 1276, 1373, 1445, 1612, 1699, 2858-2920, 3019, 3053, 3350; ^{1}H-NMR (400 MHz, $CDCl_3$) δ: 1.00 (s, 3H, C18-CH_3), 4.82 (brs, 1 H, 3-OH), 6.60 (brs, 1H, C4-H), 6.66 (d, 1H, *J* = 9.1 Hz, C2-H), 7.17 (d, 1H, *J* = 9.1 Hz, C1-H), 7.39 (m, 3H, $H_{3'}$, $H_{4'}$, $H_{5'}$); 7.48 (brs, 1H, H-vinyl), 7.57 (d, 2H, *J* = 8.3 Hz, $H_{2'}$, $H_{6'}$); ^{13}C-NMR (100 MHz, $CDCl_3$) δ: 14.78, 26.19, 27.01, 29.37, 29.68, 31.90, 38.20, 44.26, 48.08, 48.81, 113.10, 115.53, 126.71, 128.91, 129.49, 130.56, 132.33, 133.56, 135.82, 136.20, 138.19, 153.77, 210.04.

2.2.2 Bioactivity assays

2.2.2.1 Cell culture

Human breast (MCF-7, T47-D), prostatic (LNCaP), colon (Caco-2) and fibroblast (NHDF) cell lines were obtained from American Type Culture Collection (ATCC; Manassas, VA, USA) and hepatic (HepaRG) cell line was acquired from Life Technologies – Invitrogen™ (through Alfagene, Portugal). They were cultured in 75 cm^2 culture flasks at 37 ˚C in a humidified air incubator with 5% CO_2. High-glucose Dulbecco's modified Eagle medium (DMEM) supplemented with 10% fetal bovine serum (FBS; Sigma-Aldrich, St Louis, MO, USA), and 1% antibiotic/antimycotic (10,000 units/mL penicillin G, 100 mg/mL streptomycin and 25 μg/mL amphotericin B) (Ab; Sigma-Aldrich, St Louis, MO, USA) was

used to culture MCF-7 cells. For Caco-2 cells, high glucose DMEM supplemented with 10% FBS and 1% of the antibiotic mixture of 10,000 units/mL penicillin G and 100 mg/mL of streptomycin (sp; Sigma-Aldrich, St Louis, MO, USA) was used. LNCaP and T47-D cells were cultured in RPMI 1640 medium with 10% FBS and 1% sp. Fibroblasts grew in RPMI 1640 medium supplemented with 10% FBS, 2 mM *L*-glutamine, 10 mM HEPES, 1 mM sodium pyruvate and 1% Ab. Finally, HepaRG cells were seeded in Williams' E medium supplemented with 10% FBS, 1% sp, 5 μg/mL insulin, and 5×10^{-5} M hydrocortisone hemisuccinate (Sigma–Aldrich, St Louis, MO, USA).

2.2.2.2 Preparation of compounds solutions

Stock solutions of compounds were prepared in DMSO at 10 mM and stored at 4-8 ˚C. The maximum DMSO concentration in cell studies was 1% and previous experiments revealed that this solvent level has no significant effects on cell proliferation (data not shown).

2.2.2.3 Antiproliferative assays

Cytotoxicity of compounds **1, 2.1-2.7** was evaluated by the 3-(4,5-dimethylthiazol-2-yl)-2,5-diphenyltetrazolium bromide (MTT; Sigma-Aldrich, St Louis, MO, USA) assay against MCF-7, T47-D, LNCaP, HepaRG, Caco-2 and NHDF cells. After reaching near confluence, cells were trypsinized and counted with a hemocytometer by means of the trypan-blue exclusion of dead cells. Then, 100 μL of cell suspension (2×10^4 cells/mL) were seeded in 96-well culture plates and left to adhere for 48 h. After adherence, the medium was replaced by several solutions of the compounds in study (30 μM for screening assays and 0.1, 1, 10, 25, 50 and 100 μM for concentration-response studies) in the appropriate culture medium for approximately 72 h. After this period, cells were washed with 100 μL of phosphate buffer saline (PBS; NaCl 137 mM, KCl 2.7 mM, Na_2HPO_4 10 mM and KH_2PO_4 1.8 mM, pH 7.4), and then 100 μL of the MTT solution (5 mg/mL), prepared in the appropriate serum-free medium, was added to each well, followed by incubation for approximately 4 h at 37 ˚C. Then, MTT containing medium was removed and formazan crystals were dissolved in DMSO. Absorbance was measured at 570 nm using a microplate reader Bio-rad Xmark spectrophotometer. After background subtraction, cell proliferation values were expressed as percentage relative to the absorbance determined in negative control cells. Untreated cells were used as the negative control and the

clinical drug 5-FU was used as positive control. Each experiment was performed in quadruplicate and independently repeated.

2.2.2.4 E-screening assay

T47-D cells (2×10^4 cells/mL) were seeded in 96-well culture plates in 100 µM of RPMI 1640 medium supplemented with 10% FBS and allowed to attach. After overnight incubation, the medium was replaced every 3 days with fresh phenol red free RPMI 1640 medium supplemented with 5% of dextran-coated charcoal-treated fetal calf serum (DCC-FCS) and containing the compounds under study. After 6 days of exposure, the proliferation of T47-D cells was estimated by the MTT assay described in the previous section. 0.1, 0.01 and 0.001 µM were the concentrations tested for E2 and for the synthesized selected compounds. Each experiment was performed in quadruplicate and independently repeated. After background subtraction, cell proliferation values were expressed as percentage relative to the absorbance determined in negative control cells.

2.2.2.5 Flow cytometric analysis of cell viability

The analysis of cell viability on HepaRG cells was performed by flow cytometry after staining dead cells with propidium iodide (PI) (solution of PI 1 mg/ml in 0.1% of sodium azide and water; Sigma Aldrich, St Louis, MO, USA). Briefly, 3 mL of cells suspension were seeded in 6-well plates (5×10^4 cells/mL) in complete culture medium. After 48 h they were treated with 50 µM of compound **2.1**. Untreated cells were used as negative control and 5-FU was used as positive control. Each experiment was performed in duplicate and independently repeated. At the end of 24 h of incubation, the supernatant of each well was collected; cells were harvested by trypsinization and pooled with the supernatants. The resulting cell suspension was kept on ice, pelleted by centrifugation and resuspended in 400 µL of complete medium. Afterwards, 395 µL of the cell suspension was transferred to a FACS tube and 5 µL of PI with EDTA (0.5 µL at 0.123 M) was added. A minimum of 20000 events was acquired using a BD Accuri C6 (San Jose, USA) flow cytometer in the channels forward scatter (FSC), side scatter (SSC) and fluorescence channel-3 (FL3, for PI). Acquisition and analysis were performed with BD Accuri Software. In the FSC/FL3 contour plot, three regions were created, one corresponding to viable cells (R1), another to dead cells (R2) and a third to an indeterminate cell population between the other two regions (R3) excluding debris that were not considered in the analysis (data not shown). The percentage of viability is the

percentage of cells in R1 as compared to the total number of events in R1, R2 and R3.

2.2.2.6 Flow cytometric analysis of cell cycle

After 24 h of treatment with 50 μM of compound **2.1** (6-well plates, 5 × 10^4 cells/mL), HepaRG cells were collected and washed with PBS and resuspended in 450 μL of a cold solution of 0.5% bovine serum albumin (BSA; Amresco, USA) in PBS with EDTA (204 μL in 25 mL), followed by fixation with 70% of EtOH and incubation at -20 ˚C. After, at least, 2 days at -20 ˚C, fixed cells were washed twice with PBS and resuspended in a solution of PI (50 μg/mL) prepared in 0.5% BSA in PBS with EDTA and then incubated with Ribonuclease A from bovine pancreas at a final concentration of 0.5 μg/μL (solution in 50% glycerol, 10 mM Tris-HCl, pH 8; Sigma Aldrich, St Louis, MO, USA) for 15 min in the dark. For comparison, untreated cells were used as negative control and cells treated with 5-FU at 50 μM were used as positive control. Each experiment was performed in duplicate and independently repeated. A minimum of 10000 events was acquired using BD Accuri Software and analysis was performed by Modfit software (Becton Dickinson, San Jose, CA, USA).

2.2.2.7 Flow cytometry carboxyfluorescein succinimidyl ester assay

HepaRG cells were trypsinized, counted and seeded in two 12-well culture plates (1 mL/well; 8 × 10^4 cells/mL) and left to adhere for 48 h. After this period, cells were rinsed twice with PBS and then carboxyfluorescein succinimidyl ester (CFSE; BD Horizon, San Jose, USA) was added at 10 μM and incubated for 15 or 30 min. After incubation, the wells were rinsed with PBS, and medium with compound **2.1** (50 μM) was added, followed by an incubation during approximately 48 and 72 h. Untreated cells were used as the negative control in each plate. For 15 min of CFSE incubation each experiment was performed in duplicate. For 30 min of incubation, one experiment was performed for 48 and another for 72 h. At the end of incubation period, cells were trypsinized, centrifuged and resuspended in 300 μL of medium with 5 μL of EDTA. A minimum of 20000 events was acquired using a BD Accuri C6 flow cytometer in the channels forward scatter (FSC), side scatter (SSC) and fluorescence channel-1 (FL1, for CFSE). Acquisition and analysis were performed with BD Accuri Software.

2.2.2.8 Statistical analysis

Data were expressed as mean ± standard deviation (SD). Comparison among groups was performed by using the *t*-Student test (two groups) and one-way ANOVA (three groups) followed by Bonferroni *post hoc* tests to determine statistically significant differences among the means. Difference between groups was considered statistically significant for a *p*-value lower than 0.05 ($p < 0.05$). The determination of IC_{50} was carried out by sigmoidal fitting analysis considering a confidence level of 95%.

2.2.3 Molecular docking studies

2.2.3.1 Preparation of proteins for molecular docking

The crystal structures of ERα, ST and 17β-HSD1 were obtained from protein data bank (PDB code: 1A52, 1P49 and 3KLM, respectively) (Tanenbaum et al. 1998; Hernandez-Guzman et al. 2003; Aka et al. 2010). The coordinates of all non-standard residues were deleted using the software Chimera (v. 1.10.1). Then, non-polar hydrogens were merged in AutoDockTools (v. 1.5.6) and Kollman and Gasteiger partial charges were added. Finally, the prepared structure was converted from the PDB format to PDBQT for posterior use in the docking study.

2.2.3.2 Preparation of ligands

All ligands were constructed using Chem3D (v. 12.0) software. Energy minimization and geometry optimization were performed by the same software and the final structures were saved as PDB file format. The process of energy minimization was applied in a range from -20 to -40 kcal.mol^{-1}. Then, the ligands were completely prepared choosing torsions and the structures were converted from PDB to PDBQT format, in the software AutoDockTools.

2.2.3.3 Grid parameters

The grid parameters were calculated using AutoDock vina and AutoDockTools based on the coordinates of the ligand crystalized for each case: E2, *N*-acetyl-*D*-glucosamine and 5α-dihydrotestosterone (DHT), with the respective macromolecule. The grid box was centered on the ligand with the following coordinates: for ERα, the coordinates were x=107.27, y=13.94, z=96.38; for ST were x=62.033, y=-12.215, z=52.512; and for 17β-HSD1 were x=11.643, y=9.297, z=-11.887. The size of grid box was 20x20x20 with a spacing of 1.0 Å.

2.2.3.4 Docking simulations

After ligands and protein preparation, molecular docking was performed by AutoDock vina executable, which uses an iterated local search global optimizer. The parameter exhaustiveness of performed experiments was defined as 8 (default). The results of molecular docking were visualized in Discovery Studio Visualizer program from BIOVIA and in PyMOL software.

2.2.3.5 Validation of the molecular docking performance

Scoring functions are essential for molecular docking performance. In order to verify those functions, it is necessary to validate the docking performance of AutoDock vina. This step is required to verify the performance by analysis of the difference between the real and best-scored conformations. For the docking process to be considered successful, the root-mean-square distance (RMSD) value between those two conformations must be less than 2.0 Å. In this case, the method validation was performed by re-docking ERα with E2, ST with *N*-acetyl-*D*-glucosamine and 17β-HSD1 with DHT. Low RMSD values were obtained for all cases, which means that docking process was reliable and validated.

2.3 Results and discussion

2.3.1 Chemistry

Four $\Delta^{9,11}$-E1 derivatives were synthesized by the general synthetic procedure described in **Scheme 2.1.** To the best of our knowledge, three of these derivatives have been synthesized for the first time (compounds **2.2**, **2.4** and **2.6**).

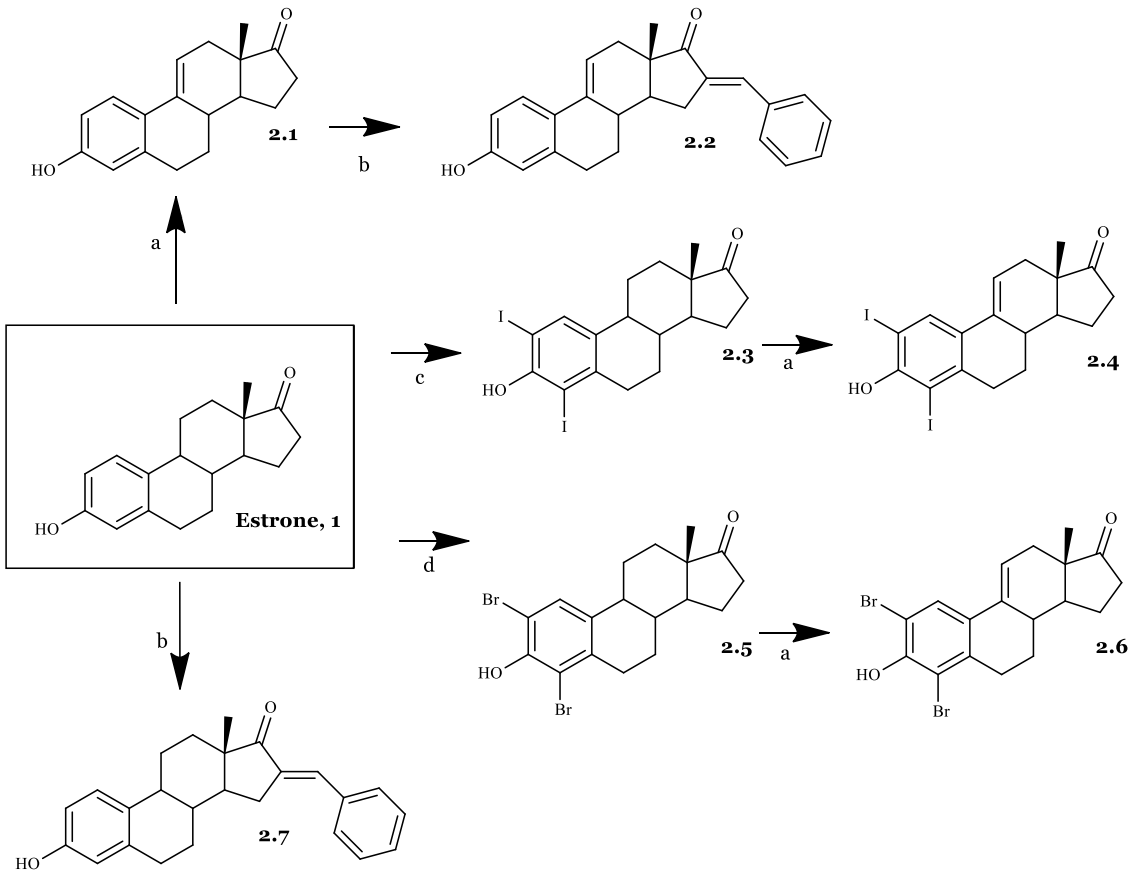

Scheme 2.1 Synthetic route to prepare $\Delta^{9,11}$-estrone derivatives. Reagents and conditions: (a) DDQ, MeOH, reflux; (b) benzaldehyde, KOH, MeOH, room temperature; (c) I2, morpholine, PhH, room temperature; (d) NBS, EtOH, room temperature.

All compounds were characterized by spectral analysis (IR, ^{1}H- and ^{13}C-NMR) and HRMS was also obtained for the new steroids prepared. All spectral data are in agreement with the presented structures. For example, the presence of $\Delta^{9,11}$ double bond was observed by the signal of C-11 proton that appeared between 6.05 and 6.13 ppm in the ^{1}H-NMR spectra, in accordance with the described in the literature (Stéphan et al. 1995).

The synthesis of $\Delta^{9,11}$-E1 derivatives can be performed using adamantyl carbonium ion as dehydrogenating agent (Lunn and Farkas 1968). In addition, Brown *et al* (Brown et al. 1968) described a simpler route using DDQ to obtain these compounds from E1 in high yield. Later, this last procedure was improved by other research groups (Stéphan et al. 1995). Although the preparation of $\Delta^{9,11}$-estrane derivatives has been known since the 1960´s, the biological activities of this group of compounds, specifically their potential anticancer activity, continue to be relatively unexplored. In this context, Milic *et al* (Milić et al. 2005) described promising cytotoxicity results of 2- and 4-substituted $\Delta^{9,11}$-E1 derivatives in different cancer cell lines, evidencing the interest for this modification in the C-ring of E1. Based on this information, in order to obtain compounds with promising cytotoxic effects, modifications in A-ring (2- and 4-

positions) of E1 were combined with the $\Delta^{9,11}$ double bond. In addition, due to the fact that the presence of a 16-arylidene group in the steroid skeleton is also associated with notable cytotoxic properties in several cell lines (Aka et al. 2010; Vosooghi et al. 2013), this modification was likewise explored by us.

Thus, the introduction of the $\Delta^{9,11}$ double bond in E1 yielded compound **2.1.** This process was successfully carried out using DDQ, as described in literature (Stéphan et al. 1995). Then, using BZ and KOH, compound **2.2** was easily synthesized through a base-mediated aldol reaction (Guo et al. 2011), where the corresponding 16*E*-benzylidene steroid was obtained (Brito et al. 2019). In this context, the signal of the methine-bridged proton at C-16 appeared at 7.34 ppm in the ^{1}H-NMR spectra (Bansal and Guleria 2008) and an *E*-configuration was assigned to this double bond based on previous reports (Brito et al. 2019). E1 A-ring iodination (using I_2) and bromination (using NBS) were performed to obtain 2,4-diiodoestrone (compound **2.3**) (Egan and Filer 2013) and 2,4-dibromoestrone (compound **2.5**) (Page et al. 1991), respectively. Among these two types of aromatic halogenations, bromination was simpler to perform than iodination. In fact, two other greener strategies were tried before the successful use of I_2/morpholine/PhH for the iodination (Egan and Filer 2013). This last procedure was preferable instead of the combination of sodium iodide and sodium chlorite (Lista et al. 2008), which only allowed the synthesis of 2-iodoestrone in low yields. In addition, on using I_2 and copper (II) chloride di-hydrate ($CuCl_2.2H_2O$) (Cushman et al. 1995), after the reaction, it was very difficult to separate the isomers 2- and 4-iodoestrone by column chromatography. This iodination also needs a non-oxidant atmosphere, which is more time-consuming. Then, the intermediates **2.3** and **2.5** were used to prepare the two new $\Delta^{9,11}$ derivatives **2.4** and **2.6** by DDQ, as described above. Interestingly, under similar reaction conditions, a higher yield of product was observed in the dehydrogenation of 2,4-dibromoestrone. Finally, compound **2.7** was also prepared from E1 by aldol condensation aiming to improve structure-relationship data by comparing its bioactivity with the observed for compounds **2.2** and even E1.

2.3.2 Biological testing

2.3.2.1 Cell growth effect

The MTT colorimetric assay was performed to evaluate the cytotoxicity of compounds **1**, **2.1**-**2.7** on hormone-dependent (MCF-7, T47-D and LNCaP) and hormone-independent (HepaRG and Caco-2) cancer cells and on normal dermal fibroblasts (NHDF). First, a screening at 30 μM was performed for all compounds in all cell lines (**Figure 2.2**).

When a reduction of cell proliferation was higher than 50%, the IC_{50} was determined. As shown in **Table 2.1**, the most relevant reduction of cell proliferation was observed with compound **2.1** in HepaRG cells (IC_{50} = 6.67 μM). Interestingly, the introduction of the $\Delta^{9,11}$ double bond in E1 increased the cytotoxic effects for all cell lines studied, except for T47-D cells. The presence of the 16*E*-benzylidene group (compound **2.2**) augmented the cytotoxic effects on MCF-7 (IC_{50} = 25.14 μM) and T47-D cells (IC_{50} = 25.06 μM) when compared with compound **2.1**. When comparing the bioactivity of compounds **2.2** and **2.7**, it was interesting to note that the presence of the $\Delta^{9,11}$ double bond in these 16*E*-benzylidenes also led to an increase in the cytotoxicity in breast cell lines but not in HepaRG and Caco-2 cells. In addition, the introduction of iodine in positions 2 and 4 of E1 (compound **2.3**) allowed a selective cytotoxicity against HepaRG cells (IC_{50} = 29.67 μM). The dibrominated steroid **2.5** generally had a higher cytotoxicity than the corresponding iodinated analogue **2.3**. On the other hand, no pronounced reduction of cell proliferation was observed for compounds **2.4** and **2.6** in all cell lines tested. Therefore, contrary to what was observed for E1 and compound **2.1**, the presence of iodine and bromine in positions 2 and 4 of $\Delta^{9,11}$-E1 was not a favorable structural change for the development of potential antiproliferative agents.

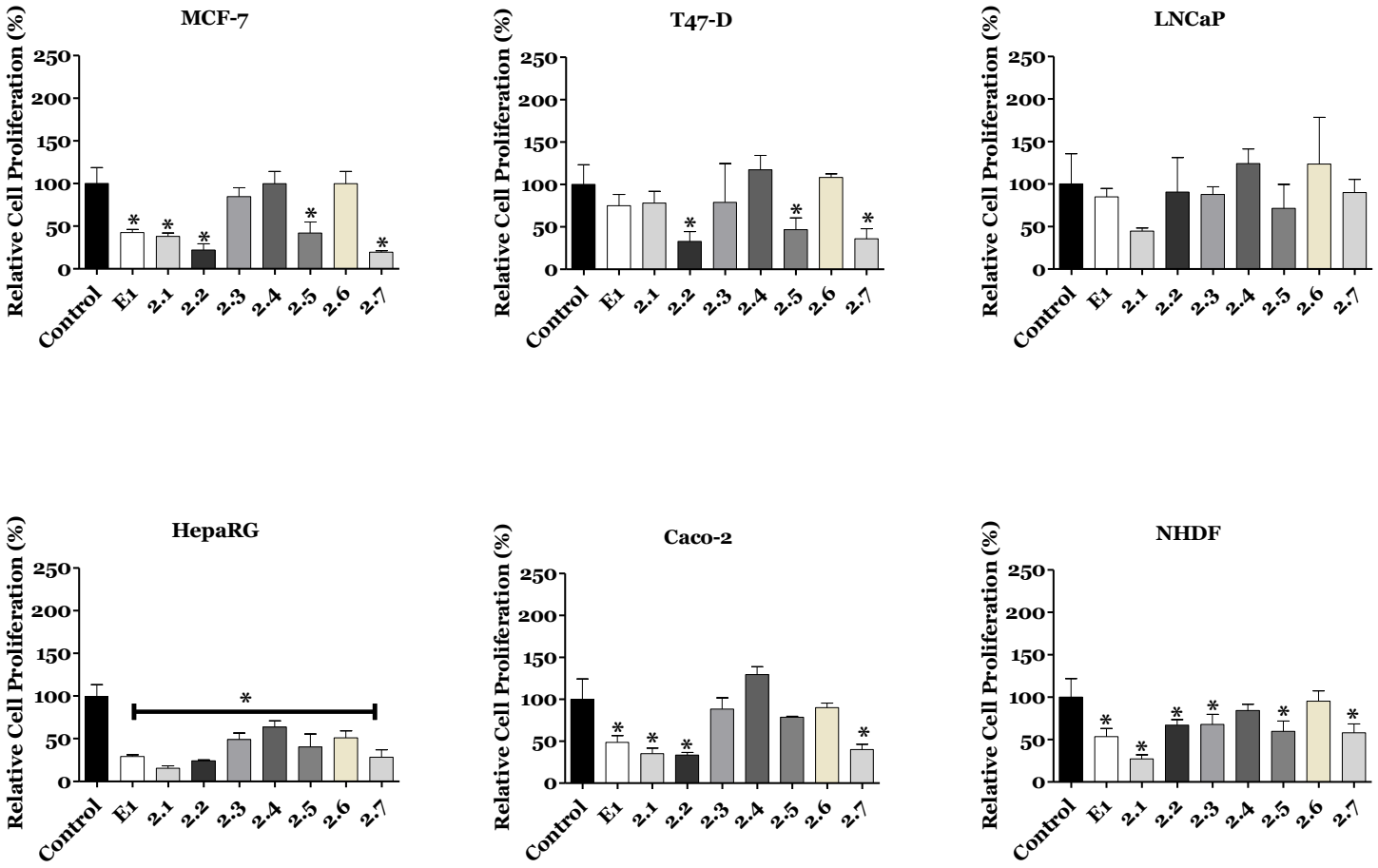

Figure 2.2 Relative cell proliferation of MCF-7, T47-D, LNCaP, HepaRG, Caco-2 and NHDF cells incubated with the synthesized compounds, for 72 h at 30 μM concentration, determined by the MTT assay, spectrophotometrically quantifying formazan at 570 nm. Data are expressed as a percentage of cell proliferation relative to the negative control and are indicated as means ± SD and are representative of at least two independent experiments. $^{*}p < 0.05$ *vs* control.

Table 2.1 Cytotoxicity (IC_{50} in μM) of the synthesized compounds (**1**, **2.1**–**2.7**) as well as 5-fluorouracil (5-FU) against breast (MCF-7 and T47-D), prostatic (LNCaP), hepatic (HepaRG) and colon (Caco-2) cancer cell lines and normal human dermal fibroblasts (NHDF)[a].

Compounds	MCF-7	T47-D	LNCaP	HepaRG	Caco-2	NHDF
	IC_{50}	IC_{50}	IC_{50}	IC_{50}	IC_{50}	IC_{50}
1	41.93	ND	ND	29.53	42.69	61.82
2.1	40.87	ND	32.30	6.67	39.17	20.83
2.2	25.14	25.06	ND	27.07	46.31	ND
2.3	ND	ND	ND	29.67	ND	ND
2.4	ND	ND	ND	ND	ND	ND
2.5	47.89	51.41	ND	18.46	ND	ND
2.6	ND	ND	ND	ND	ND	ND
2.7	26.70	34.27	ND	23.15	35.54	ND
5-FU	1.71	0.54	7.79	1.78	1.31	3.61

[a]Cells were treated with different concentrations (0.1, 1, 10, 25, 50 and 100 μM) for 72 h. The cell proliferation effects were determined by the MTT assay. The data shown are representative of at least two independent experiments. ND: not determined.

Regarding the values of selectivity index (SI) (**Table 2.2**), it is known that a value of 2 or greater indicates high selectivity for cancer cells (Bézivin et al. 2003). According to this information, the selectivity of compound **2.1** against HepaRG cell line is very interesting (SI > 3).

Table 2.2 – Selectivity index[a] of compounds **1**, **2.1** and 5-FU.

Compounds	MCF-7	T47-D	LNCaP	HepaRG	Caco-2
1	1.47	ND	ND	2.09	1.45
2.1	0.51	0.53	0.64	3.12	0.53
5-FU	2.11	0.49	0.46	2.03	2.76

[a]Selectivity index is the ratio of the IC_{50} values of the treatments of non-tumor cells (NHDF) and tumor cells (MCF-7, T47-D, LNCaP, HepaRG and Caco-2). ND: not determined.

A new drug candidate should be devoid of estrogenic activity as a pre-requisite for use in cancer therapy. In order to investigate the potential estrogenic profile of the synthesized compounds with the most relevant anti-proliferative activities (steroids **2.1** and **2.2**), their effect on cell growth was measured on the estrogen-sensitive breast cancer T47-D cells (ER^+) in serum-free culture medium. This proliferative/estrogenic activity was expressed as the difference between the cell proliferation (in percentage) caused by a given compound and the basal cell proliferation fixed at 100% (**Figure 2.3**) (Ayan et al. 2012; Cortés-Benítez et al. 2017). The natural estrogen E2 was also tested as reference compound. As expected, E2 had a proliferative effect on T47-D cells in all concentrations tested.

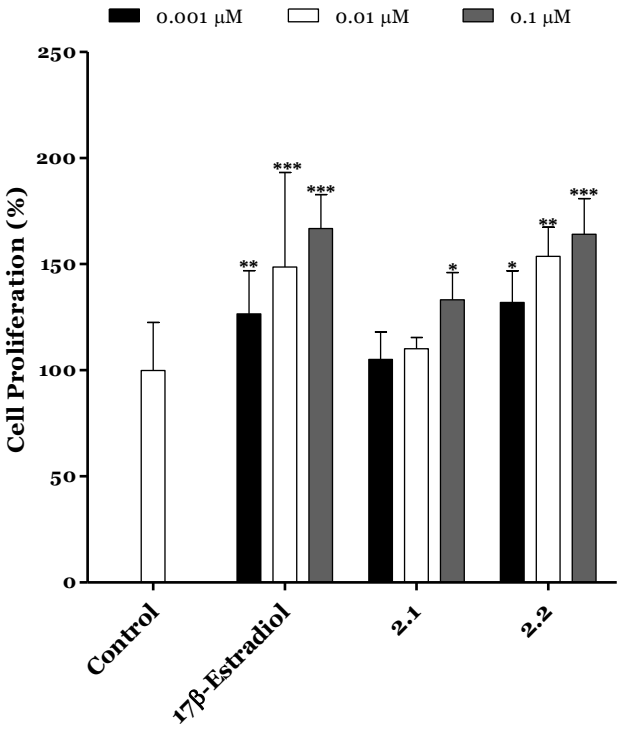

Figure 2.3 Proliferation of estrogen-sensitive T47-D cells after treatment with 17β-estradiol and compounds **2.1** and **2.2** for 24 h. Each bar represents the mean ± SD (originated from two independent experiments). $^{*}p < 0.05$ *vs* control; $^{**}p < 0.01$ *vs* control; $^{***}p < 0.001$ *vs* control.

Unfortunately, compound **2.1** also stimulated the cell proliferation at 0.1 µM (133%) when compared with the negative control. Compound **2.2** also favored cell proliferation in all concentrations tested. In this context, Palomino *et al* (Palomino et al. 1994), using X-ray crystallography and molecular modeling studies, showed that the $\Delta^{9,11}$ unsaturation in E2 (receptor binding affinity, RBA = 1000) caused a flattening of B, C and D rings and consequently reduced the binding to ER by one-fifth (RBA = 196). Although the presence of the $\Delta^{9,11}$ double bond can change the spatial conformation and reduce the interaction with ER, it did not eliminate the estrogenic effect characteristic of these compounds as evidenced by our results. In addition, Sakac *et al* (Sakač et al. 2005) confirmed the estrogenic effect of compound 3,6β-dihydroxyestra-1,3,5(10),9(11)-tetraene-17β-yl propionate using an immature rat uterine weight assay (approximately 73% of uterus proliferation compared with control). The antiestrogenic activity of this compound was also assessed using an anti-uterotrophic method that showed a weak effect (3.22% of antagonism effect *versus* 62.80% for reference drug tamoxifen) (Alsayari et al. 2017). Novel C-16 and C-17 modified E1 derivatives were synthesized by Alsayari group (Alsayari et al. 2017) showing potent inhibition of cell growth stimulated by E2 and high selective affinity to ERα. In addition, 2-methoxyestra-1,3,5(10),9(11)-tetraen-17-one, which has a $\Delta^{9,11}$ double bond, showed

estrogenic activity and displayed good binding affinities to ERα (4.09 μM) and ERβ (19.19 μM). It was also demonstrated that a 2-bromoethyl side chain at C-3 and that a carbamoylbenzyl chain at C-16 removed the residual estrogenic activity associated with estrogen nucleus (Laplante et al. 2008; Maltais et al. 2011; Ayan et al. 2012). However, our data showed that the introduction of benzylidene group at C-16 was not sufficient to reduce the estrogenic effect of this E1 derivative on T47-D cells.

2.3.2.2 Cell survival and cell cycle distribution evaluation

Compound **2.1** was further tested to evaluate its possible mechanism of action by flow cytometry after PI staining. This assay was performed in HepaRG cells and 5-FU was used as the positive control. In this cell line, it was observed that compound **2.1** led to a 34% reduction in cell viability after 24 h of treatment (**Figure 2.4**). This effect was higher than that caused by 5-FU. In addition to this flow cytometry study, cells were also observed with an optic microscope (**Figure 2.5**) and, after 24 h of treatment with compound **2.1**, it was possible to see small modifications in HepaRG cells. The cells lost their shape, becoming more rounded.

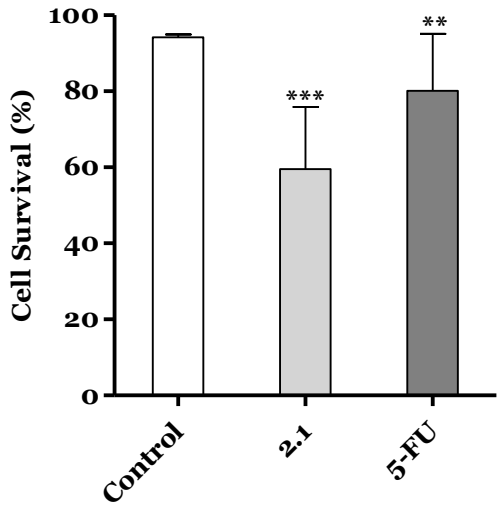

Figure 2.4 Percentage of HepaRG viable cells after 24 h treatment with 50 μM of compound **2.1** evaluated through propidium iodide (PI) flow cytometry assay. Control corresponds to untreated cells and 5-FU (50 μM) was used for comparison. The percentage of survival is the percentage of cells in R1 (live cells) as compared to the total number of events in R1, R2 (dead cells) and R3 (undetermined cells). Each bar represents the mean ± SD (originated from two independent experiments). $^{**}p < 0.01$ *vs* control; $^{***}p < 0.001$ *vs* control.

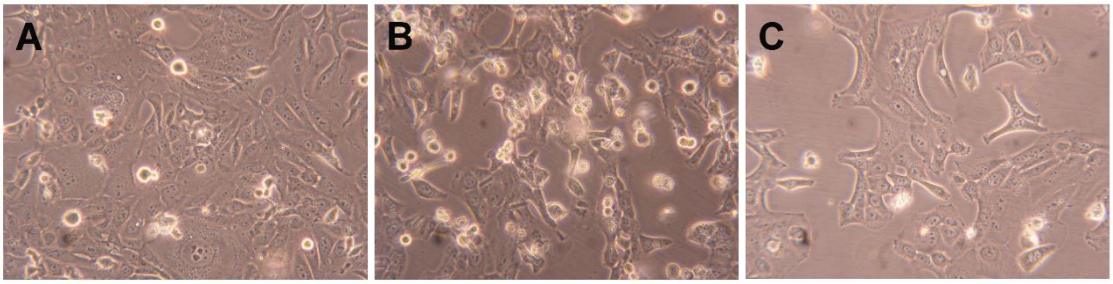

Figure 2.5 Photographs of the HepaRG cells (A) treated with 50 µM of compound **2.1** (B) and 5-fluorouracil (5-FU, C) for 24 h. Amplification of 100x.

Some studies showed that different steroids led to cell cycle blockage and inhibited some enzymes important for cell cycle regulation. For instance, 16β-triazolyl-17α-estradiol 3-benzyl ethers of the 13α-E2 series showed G_2/M cell cycle arrest and caspase inhibition (Mernyák et al. 2015). In addition, new 3-benzyloxy-16-hydroxymethylene-estradiol derivatives led to a G1 phase accumulation and to a proapoptotic effect through the elevation of the apoptotic subG1 phase on MDA-MB-231 cells after 24 h treatment (0.1-30 µM). In addition, these compounds were observed to have an antimetastatic activity by inhibition of kinases phosphorylation in a concentration-dependent manner (Sinka et al. 2018). Taking into account this information, the interference of compound **2.1** in cell cycle distribution was evaluated by flow cytometry. Interestingly, it was found that the treatment with compound **2.1** (50 µM, 24 h) induced an apparent G_0/G_1 cell cycle arrest (**Figure 2.6**), reducing the percentage of cells in S phase (DNA replication).

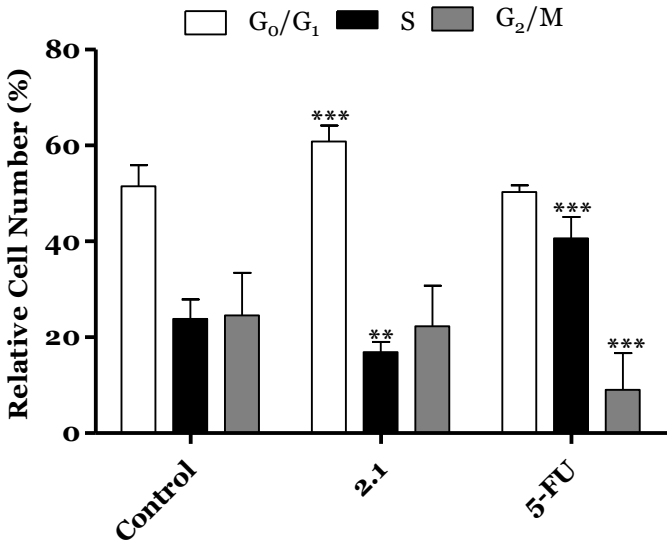

Figure 2.6 Cell cycle distribution analysis of HepaRG cancer cells after treatment with compound **2.1** (at 50 µM) for 24 h. A negative control (untreated cells) and a positive control [5-fluorouracil (5-FU), 50 µM] were included. The analysis of cell cycle distribution was performed after propidium iodide (PI) staining and then by flow cytometry. Each bar represents the mean ± SD (originating from two independent experiments). $^{**}p < 0.01$ *vs* control; $^{***}p < 0.001$ *vs* control.

The observed cell cycle arrest in G_0/G_1 phase can be related with the interference with one or more of the many proteins that participate in the highly regulated cellular mechanisms which delay or initiate DNA replication (Icard et al. 2019). Further studies will be necessary to elucidate which are the signaling pathways that are affected and to ascertain whether other mechanisms are involved in the cytotoxicity of these compounds.

Regarding the effect of compound **2.1** in HepaRG cell cycle we also decided to study the HepaRG cell proliferation after 72 h using an adapted protocol with carboxyfluorescein succinimidyl ester, a dye that labels cell cytoplasm and is diluted on cell division (Sánchez-Sánchez et al. 2016). HepaRG cells treated with compound **2.1** had higher intensity signal than control cells (**Figure 2.7)** meaning they accumulated a lower number of cell divisions, and therefore are less proliferative. Decreased proliferation confirms that cell accumulation in G_0/G_1 is due to arrest in the cell cycle rather than faster cell cycle progression through S and G_2/M phases.

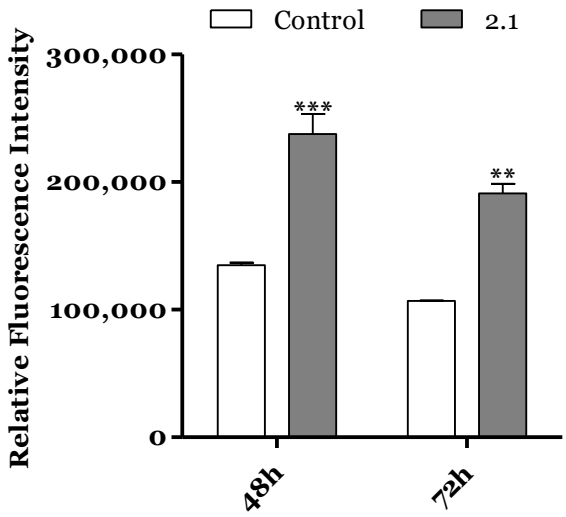

Figure 2.7 Relative fluorescence intensity of carboxyfluorescein succinimidyl ester (CFSE) of HepaRG cells, evaluated by flow cytometry after treatment with compound **2.1** (50 μM) for 48 and 72 h. Each bar represents the median with range of two samples. $^{**}p < 0.01$ *vs* control; $^{***}p < 0.001$ *vs* control.

2.3.3 Molecular docking studies

Molecular docking studies are a determinant in structure-based drug design, as it is possible to predict the binding-conformation of small molecule ligands to appropriate target binding sites, binding energies and binding mode in the target. In this context, characterization of the binding behavior plays an important role in rational drug design and helps us to elucidate fundamental biochemical processes (Kitchen et al. 2004). This study aimed to evaluate the existence of potential interactions between these $\Delta^{9,11}$-estrone derivatives and proteins that are known to interact with these types of steroids.

ERα is a transcription factor that is involved in the regulation of many complex physiological processes in humans. The association between ERα activity and cell cycle reveals that this receptor also regulates cell proliferation as well as therapeutic resistance (Lee et al. 2012; Begam et al. 2017; Miki et al. 2018). ST and 17β-HSD type 1 are enzymes also involved in cell proliferation (Cornel et al. 2017). In fact, ST converts estrone sulfate into E1 and 17β-HSD type 1 reduce the 17-ketone of androstane and estrane steroids to the corresponding 17β-hydroxylated derivatives, leading to estrogenic activity (Payne and Hales 2004). Therefore, their deregulation can contribute to the progression of several hormone-dependent cancers. Three-dimensional structural coordinates of these three protein receptors were obtained from PDB and molecular docking was performed using the program AutoDock vina. To validate the docking method, simulations were carried out and compared to crystallized ligands/drugs complexed with the respective proteins: all control re-docking simulations were able to reproduce the ligand-protein interaction geometries presented in the respective crystal structures with a RMSD ≤2.0 Å. All compounds were docked for ERα, ST and 17β-HSD1 as observed in **Table 2.3**.

Table 2.3 Predicted binding energies of compounds **1, 2.1-2.7** calculated against ERα, ST and 17β-HSD1 by AutodockTools with vina executable. Binding energies of ligand present in the X-ray crystal structures were calculated by re-docking.

Compounds	Lowest energy (kcal.mol^{-1})		
	ERα	**ST**	**17β-HSD1**
1	-10.3	-6.2	-8.1
2.1	-10.9	-5.9	-8.2
2.2	-6.9	-6.3	-9.8
2.3	-4.3	-6.0	-7.7
2.4	-4.1	-6.5	-8.0
2.5	-6.8	-6.3	-8.1
2.6	-6.3	-6.3	-8.3
2.7	-8.3	-6.9	-8.5
17β-estradiol	-9.9 [a]	-	-
N-acetyl-*D*-glucosamine	-	-7.2 [a]	-
DHT	-	-	-8.3 [a]

[a]The RMSD between re-docked ligands and the corresponding X-ray crystal structure coordinates was ≤ 2.

Interestingly, the results revealed that compound **2.1** can bind ERα in a lower energy than the control, 17β-estradiol. From **Figure 2.8** and regarding the ERα target, compound **2.1** exhibits two hydrogen bonds between ketone group at C-17 and Hist 524 and between hydroxyl group at C-3 and Glu 353.

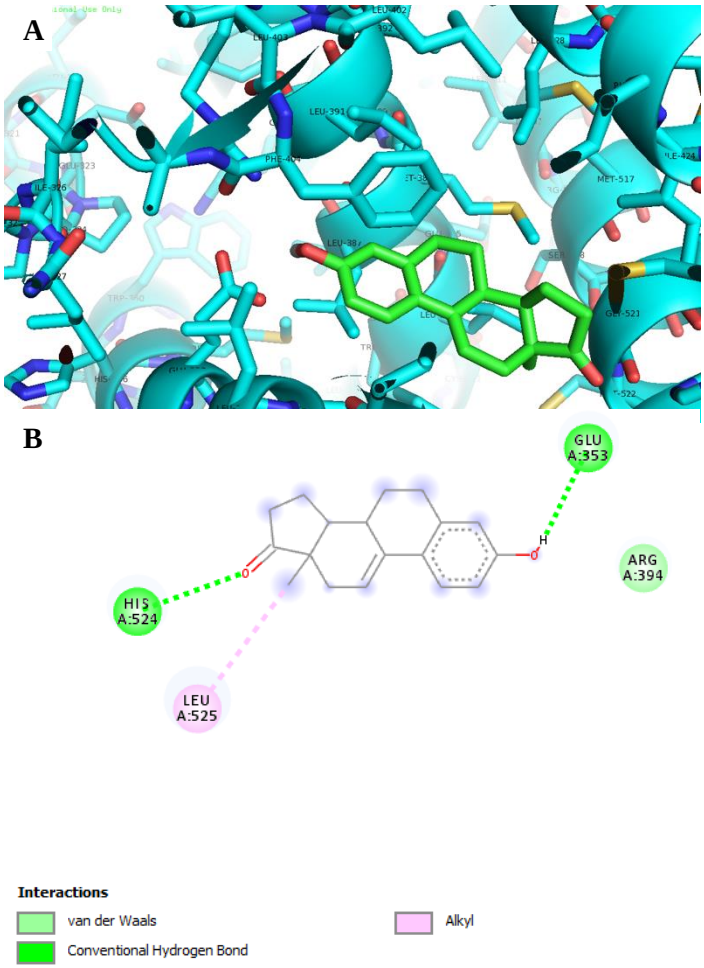

Figure 2.8 Analysis of predicted ERα binding orientations for the best ranked compound, **2.1** (binding energies lower than re-docking energies). (**A**) 3D and (**B**) 2D docking results showing the main interactions, H bonds with Hist 524 and Glu 353.

These interactions are similar to the observed for E2. As was expected, regarding 17β-HSD1, the lowest energy compared to control DHT was obtained with compound **2.2**, followed by compound **2.7**. In fact, many studies were published involving modifications at C-16 of E1 and C-2 of E2 to develop 17β-HSD 1 inhibitors (Poirier et al. 2006; Laplante et al. 2008; Maltais et al. 2011; Salaha et al. 2019). Compound **2.2** has a 16*E*-benzylidene group at C-16, which contributes to the interaction with 17β-HSD 1 target. In this context, it was demonstrated that a flexible linker in C-16 position gave better 17β-HSD1 inhibition than those with a rigid alkene linker (Allan et al. 2006). In addition, Bacsa *et al* (Bacsa et al. 2018) showed that 2- and/or 4-halogenated 13*β* or 13*α*-estrone derivatives led to a competitive reversible inhibition of 17β-HSD1 and ST enzymes. Regarding the ST enzyme, none of the studied compounds showed relevant interaction with this target. It is known that the presence of a free or *N*-unsubstituted sulfamate group ($H_2NSO_2O–$) is a pre-requisite for potent and irreversible ST inhibition as shown by inhibitors like EMATE (Woo et al. 2012).

2.4 Conclusion

In summary, several estranes with A-, C- and D-ring modifications, including three new $\Delta^{9,11}$-E1 derivatives, were prepared under mild reaction conditions. The introduction of a $\Delta^{9,11}$ double bond and a 16*E*-benzylidene group in E1 increased the cytotoxic activity on hormone-dependent breast (MCF-7 and T47-D) cancer cells when compared with E1. The introduction of 2,4-diiodo groups in E1 seemed to favor a selectivity for HepaRG cells. However, the presence of 2,4-diiodo and 2,4-dibromo groups in $\Delta^{9,11}$-E1 seemed to have no benefit for antiproliferative activities in all cell lines studied. The most promising result was observed with $\Delta^{9,11}$-E1, which exhibited a relevant antiproliferative activity against HepaRG cancer cells and presented moderate cytotoxicity on normal human cells. Nevertheless, this compound also showed an estrogenic effect on T47-D cells at 0.1 μM and flow cytometry analysis revealed a cell cycle arrest at G_0/G_1 phase of HepaRG cells. Molecular docking studies estimated a strong interaction between this compound and ERα. In conclusion, the presence of a $\Delta^{9,11}$ double bond in estrane derivatives can be of interest in the development of new and interesting antitumor agents.

Chapter 3
C-Ring oxidized estrone acetate derivatives

The content of this chapter is included in the following manuscript:

Canário C, Matias M, Brito V, Pires P, Santos AO, Falcão A, Silvestre S, Alves G. 2022. C-Ring oxidized estrone acetate derivatives: assessment of antiproliferative activities and docking studies. Appl Sci. 12(7): e3579.

3.1 Introduction

Steroids are natural products that play a central physiological role in metabolism, immune and sexual functions (Miller and Auchus 2011). They are also important in several pathological conditions, such as the maintenance and progression of hormone-dependent cancers (Soronen et al. 2004), mainly through estrogen (ER) and androgen receptors (AR) activation, which are transcription factors that regulates gene expression events that culminate in cell division (Capper et al. 2016). Therefore, modifications to the chemical structure of steroidal hormones, such as estrone (E1) or 17β-estradiol (E2) has been considered a relevant strategy to develop new therapeutic agents such as ethinylestradiol (Evans and Sutton 2015) or antitumor agents (Lao et al. 2017), particularly against hormone-dependent breast cancers, such as fulvestrant (Salvador et al. 2013; Chuffa et al. 2017; Groner and Brown 2017; Lee et al. 2017; Bray et al. 2018).

These structural modifications have been performed, mainly, in A-, B-, and, more frequently, in D-rings. Regarding the C-ring, modifications at this level have been less exploited primarily due to steric reasons. However, the importance of position 11 in estrogens structure for ER binding has been well documented by several research groups (examples in **Figure 3.1**), which makes its C-ring an important point for chemical alterations.

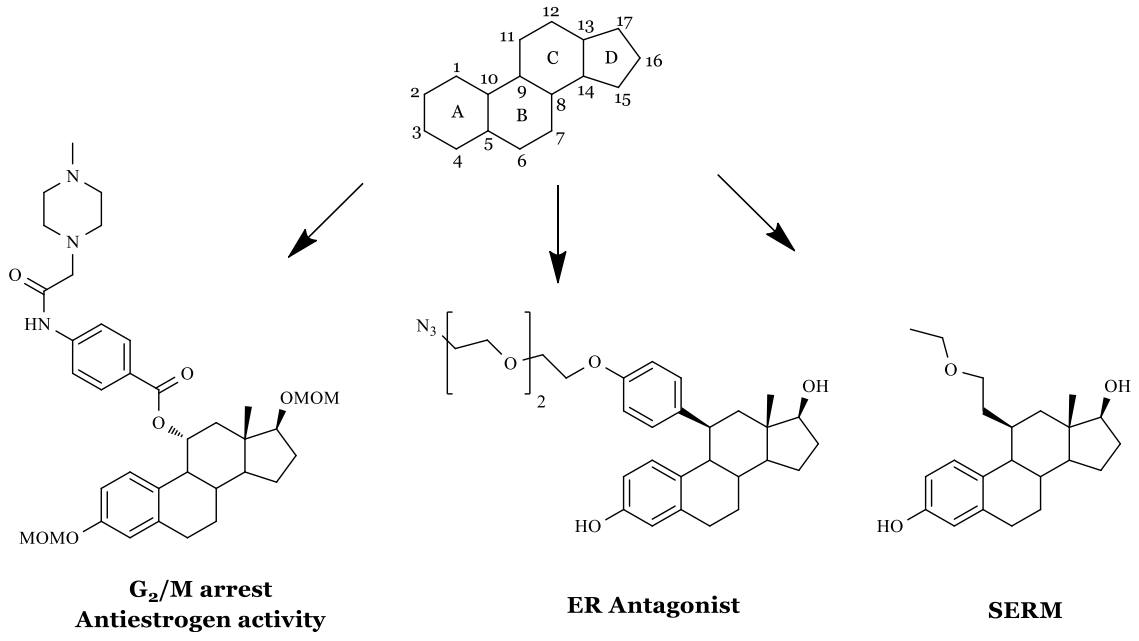

Figure 3.1 Some examples of C-ring modifications in estrane series with biological activities (Zhang et al. 2005; Hanson et al. 2012; Lao et al. 2017). ER, estrogen receptor; SERM selective estrogen receptor modulator.

Firstly, it was demonstrated that an enhancement of binding to ER can be achieved with short and nonpolar groups at 11β-position (Napolitano et al. 1995). It was also

evidenced that larger hydrophobic substituents in the same position are also tolerated (Anstead et al. 1997). In fact, E2 derivatives with an undecanamide side chain at 11β-position (Claussner et al. 1992) were devoid of *in vitro* estrogenic activity (e.g. proliferation of ER^+ cells) but maintained high ER binding affinity (Poirier et al. 1996). Interestingly, 11β-ethyl, 11β-butyl and 11β-decyl E2 derivatives (Lobaccaro et al. 1997) showed affinity constants for ER binding ranging from 0.4 to 37%. The authors of this work observed that the two 11β-ethyl compounds studied were mainly estrogenic while the three 11β-butyl and the 11β-decyl derivatives were essentially antiestrogenic. Additional studies also evidenced that the antagonistic activity of these compounds seemed to be more dependent on the size of the 11β-substituent than its nature (Aliau et al. 2000; Hanson et al. 2012). Moreover, several 11*β*-modified E2 derivatives (Zhang et al. 2005) were synthesized and it was showed that nonpolar groups in this position led to an antiestrogen effect. In fact, the estrogen stimulation in endometrial adenocarcinoma Ishikawa cells was inhibited when the 11β-side chain was an ether function with five non-hydrogen atoms. In addition, in *in vivo* studies using immature rats, the 2-ethoxyethyl derivative inhibited the uterotrophic stimulation of E2, with a useful estrogenic effect in liver and bone. Therefore, this compound was considered a selective estrogen receptor modulator (SERM). Other 11-substituted E2 derivatives (e.g. allyl and benzyl halides) also exhibited significant contraceptive activity (Dwivedy et al. 2008). However, 11α-hydroxy-E2 and 11β-hydroxy-E2 (Wang et al. 2013) had a weak relative binding affinity to ERα.

Concerning both C9 and C11 modifications, for example, the 9α-hydroxymethyl,11-ketone derivative of E1 showed poor affinity to ERα and was devoid of cytotoxic activity (Alsayari et al. 2017). However, some 9α-hydroxy-11β-nitrate esters (Peters et al. 1989) displayed higher estrogenic potency and postcoital antifertility activity than ethinylestradiol. Interestingly, many 11β-nitrates also showed antitumor activity against xenograft animal models of breast cancer (Rzheznikov et al. 2003). Unfortunately, these compounds also showed an estrogenic effect, being observed a tumor growth after 15 days of treatment. Recently, 11α-substituted 2-methoxyestradiol derivatives were prepared and showed relevant cytotoxic activity against hepatic HepG2 cells, promoting a G_2/M arrest and showing antiestrogen activity (Lao et al. 2017).

In this context, in a previous work, we prepared and evaluated several $\Delta^{9,11}$-E1 derivatives as antiproliferative agents and demonstrated that the presence of this C-ring modification was relevant for their effects on cell proliferation (Canário et al. 2020). Therefore, considering our continuous interest in developing antiproliferative steroids (Salvador et al. 2013; Brito et al. 2019), namely belonging to the estrane series

(Canário et al. 2018; Canário et al. 2020; Canário et al. 2021), in this work we synthesized C-ring oxidized derivatives of E1 acetate and analyzed their cytotoxic effects in breast, prostatic, colon, and hepatic cancer cell lines, as well as in normal fibroblast cells. The cell viability and cell cycle distribution were also studied for the most relevant compounds. An *in silico* study (molecular docking) was performed for ERα, steroid sulfatase (ST) and 17β-hydroxysteroid dehydrogenase type 1 (17β-HSD1).

3.2 Experimental section

3.2.1 Chemical synthesis and structural characterization

2,3-Dichloro-5,6-dicyano-*p*-benzoquinone (DDQ), tetrahydrofuran (THF), 4-(dimethylamino)pyridine (DMAP), potassium peroxymonosulfate (Oxone™), ammonium cerium(IV) nitrate (CAN), tetraethylammonium chloride (TEAC), E2, 5-fluorouracil (5-FU) and dimethyl sulfoxide (DMSO) were acquired from Sigma-Aldrich (St. Louis, MO, USA). E1 was purchased from Cayman Chemical (Ann Arbor, MI, USA), acetic anhydride (Ac_2O) from Fluka, methanol (MeOH) and acetic acid from Fisher Chemical (Waltham, MA, USA), acetone 99% from José Manuel Gomes dos Santos, Lda (Odivelas, Portugal), ethanol (EtOH) 99.9% from Manuel Vieira & C^a (Torres Novas, Portugal) and deuterated DMSO (DMSO-d_6) and deuterated chloroform ($CDCl_3$) were acquired from Armar Chemicals (Leipzig, Germany). Thin layer chromatography (TLC) with an al-backed aluminum/silica gel plate 0.20 mm (Macherey-Nagel 60 F254, Duren, Germany) was used to control all reactions. The CN-15.LC UV chamber (254 nm) was used to visualize TLCs before chemical revelation, which was performed using EtOH/concentrated sulfuric acid (95:5, v:v) and then heating at 120 °C. A rotary vacuum drier from Büchi (R-215) was used to evaporate solvents. The Infrared (IR) spectra were acquired on a Thermoscientific Nicolet iS10 at room temperature in the 4000-400 cm^{-1} range by averaging 16 scans (spectral resolution of 2 cm^{-1}). ^1H and ^{13}C nuclear magnetic resonance (NMR) spectra were acquired in Bruker Avance 400 MHz and the TOPSPIN 4.07 software (Bruker, Fitchburg, WI, USA) was used. Chemical shifts are reported in parts per million (ppm) relative to tetramethylsilane (TMS) or solvent as an internal standard. Coupling constants (*J* values) are reported in hertz (Hz) and splitting multiplicities are described as s=singlet; brs=broad singlet; d=doublet; dd=double doublet and t=triplet.

*3.2.1.1 Synthesis of 17-oxoestra-1,3,5(10)-trien-3-yl acetate (estrone acetate, **3.1**)*

The synthesis was carried out in accordance with a protocol previously described (Simeón et al. 2004). Briefly, 60 mg of DMAP and 200 µL of Ac_2O were added to a solution of E1 **1** (540.7 mg, 2 mmol) in THF (10.8 mL) and the mixture was stirred for 24 h at room temperature (r.t.). Then, the reaction solvent was evaporated and the crude was diluted in CH_2Cl_2, washed with 10% HCl, saturated solution of $NaHCO_3$ and H_2O and dried over anhydrous Na_2SO_4, filtered and finally the solvent was evaporated to afford compound **3.1** as a white solid (600 mg, 96%) (Simeón et al. 2004). IR ($\upsilon_{max,}cm^{-1}$): 820, 1007, 1204, 1366, 1491, 1605, 1732, 1759, 2876, 2930, 3055; ^{1}H-NMR (400 MHz, $CDCl_3$) δ: 0.89 (s, 3H, C18-CH_3), 2.26 (s, 3H, $COCH_3$), 6.79 (d, 1H, *J* = 2.6 Hz, C4-H), 6.83 (dd, 1H, J_1 = 8.6 Hz, J_2 = 2.6 Hz, C2-H), 7.27 (d, 1H, *J* = 8.6 Hz, C1-H); ^{13}C-NMR (100 MHz, $CDCl_3$) δ: 14.0, 21.3, 21.8, 25.9, 26.5, 29.6, 31.7, 36.0, 38.2, 44.3, 48.1, 50.6, 118.9, 121.8, 126.6, 137.6, 138.2, 148.7, 170.0, 220.9.

*3.2.1.2 Synthesis of 9α-hydroxy-17-oxoestra-1,3,5(10)-trien-3-yl acetate (**3.2**)*

The synthesis was carried out in accordance with a protocol previously described (Quinkert et al. 1982; D'Accolti et al. 2008). Briefly, H_2O (3.94 mL), $NaHCO_3$ (1.142 g), acetone (3.16 mL) and TEAC (2 mg) were added to a solution of compound **3.1** (156.18 mg, 0.5 mmol) in CH_2Cl_2 (3.56 mL). Then, Oxone™ (2.36 g) was added every 15 minutes for 2 hours followed by stirring on ice for 7 h. After, the crude was diluted in ethyl acetate (EA), washed with 10% Na_2SO_3 and H_2O, dried over anhydrous Na_2SO_4 and filtered under suction. After solvent evaporation, purification was performed by column chromatography [eluent: EA/petroleum ether (PE) 40 - 60 °C, 1:4] to yield compound **3.2** (Quinkert et al. 1982; D'Accolti et al. 2008) (beige solid, 90 mg, 55%). IR (υ_{max},cm^{-1}): 800, 902, 1013, 1196, 1372, 1448, 1606, 1723, 2832, 2938, 3060, 3351, 3564; ^{1}H-NMR (400 MHz, $CDCl_3$) δ: 0.88 (s, 3H, C18-CH_3), 2.26 (s, 3H, $COCH_3$), 6.83 (d, 1H, *J* = 2.4 Hz, C4-H), 6.89 (dd, 1H, J_1 = 8.5 Hz, J_2 = 2.4 Hz, C2-H), 7.52 (d, 1H, *J* = 8.5 Hz, C1-H); ^{13}C-NMR (100 MHz, $CDCl_3$) δ: 13.1, 20.2, 21.3, 21.6, 27.8, 29.6, 32.4, 36.1, 41.3, 43.3, 47.8, 70.2, 119.8, 122.5, 126.7, 138.6, 139.3, 150.2, 169.9, 220.7.

*3.2.1.3 Synthesis of 9α-hydroxy-11β-nitrooxy-17-oxoestra-1,3,5(10)-trien-3-yl acetate (**3.3**)*

The synthesis was carried out in accordance with a protocol previously described (Peters et al. 1989). Briefly, a solution of CAN (2.52 g, 4.6 mmol) in 2 ml of H_2O was

added dropwise to a solution of compound **3.1** (317.6 mg, 1 mmol) in acetic acid (15 ml). The resulting orange solution was maintained under vigorous stirring for 6 h at r.t. and then was diluted two-fold with H_2O and extracted with EA. The organic solution was then washed with saturated $NaHCO_3$ solution, brine and H_2O, dried using anhydrous Na_2SO_4 and filtered under suction. After solvent evaporation, a purification with column chromatography (eluent: gradient of EA/PE 40 - 60 °C, 1:4 to 1:2) and recrystallization (MeOH) was performed to afford compound **3.3** (Peters et al. 1989) as light brown solid (128.7 mg, 34%). IR (υ_{max},cm^{-1}): 853, 970, 1050, 1151, 1207, 1279, 1370, 1493, 1633, 1728, 1750, 2893, 2962, 3447; ^{1}H-NMR (400 MHz, $CDCl_3$) δ: 1.00 (s, 3H, C18-CH_3), 2.26 (s, 3H, $COCH_3$), 5.79 (t, 1H, J = 3 Hz, $CHONO_2$), 6.89 (brs, 1H, C4-H), 6.91 (d, J = 8.3 Hz, 1H, C2-H), 7.28 (d, 1H, J = 8.3 Hz, C1-H); ^{13}C-NMR (100 MHz, $CDCl_3$) δ: 15.3, 20.1, 21.3, 21.3, 29.7, 31.3, 35.5, 38.2, 42.2, 46.4, 71.9, 81.4, 120.5, 123.1, 126.3, 134.9, 139.9, 150.6, 169.7, 217.9.

*3.2.1.4 Synthesis of 17-oxoestra-1,3,5(10),9(11)-trien-3-yl acetate (**3.4**)*

The synthesis was carried out in accordance with a protocol previously described (Bovicelli et al. 1992; Stéphan et al. 1995). Briefly, 37.5 µL of Ac_2O and 11.8 mg of DMAP were added to a solution of compound **2.1** (107.4 mg, 0.4 mmol), prepared as previously described (Stéphan et al. 1995; Canário et al. 2020), in 2.14 mL of THF and the resulting mixture was stirred for 1 h at r.t. Afterwards, THF was partially evaporated and the crude was diluted in EA, washed with 10% HCl, saturated $NaHCO_3$ and H_2O, dried using anhydrous Na_2SO_4 and filtered under suction. After solvent evaporation, compound **3.4** (Bovicelli et al. 1992) was isolated as a beige solid (110 mg, 89%). IR (υ_{max}, cm^{-1}): 809, 1019, 1062, 1201, 1368, 1449, 1492, 1606, 1647, 1732, 2213, 2925, 3050, 3265; ^{1}H NMR ($CDCl_3$, 400 MHz): δ 0.90 (s, 3H, C18-CH_3), 2.26 (s, 3H, $COCH_3$), 6.21 (m, 1H, C11-H), 6.80 (d, 1H, J = 2.3 Hz, C4-H), 6.84 (dd, 1H, J_1 = 8.6 Hz, J_2 = 2.3 Hz, C2-H), 7.57 (d, 1H, J = 8.7 Hz, C1-H); ^{13}C NMR ($CDCl_3$, 100 MHz): δ 14.5, 21.1, 22.5, 27.6, 29.6, 34.0, 36.2, 37.9, 46.2, 47.8, 119.1, 119.4, 121.8, 125.3, 132.0, 135.2, 137.4, 149.4, 169.7, 221.5.

3.2.2 Bioactivity assays

3.2.2.1 Cell culture

For this study, MCF-7, LNCaP, NHDF, T47-D and Caco-2 cells were acquired from American Type Culture Collection (ATCC; Manassas, VA, USA) and HepaRG from Life Technologies – Invitrogen™ (through Alfagene, Carcavelos, Portugal). They grew in 75 cm^2 culture flasks at 37 ºC in a humidified air

incubator under a 5% CO_2 atmosphere. High-glucose Dulbecco's modified Eagle medium (DMEM) containing 10% fetal bovine serum (FBS; Sigma-Aldrich, St Louis, MO, USA), and 1% antibiotic/antimycotic (10.000 units/mL penicillin G, 100 mg/mL streptomycin and 25 µg/mL amphotericin B) (Ab; Sigma-Aldrich, St Louis, MO, USA) was used to culture MCF-7 cells. DMEM supplemented with 10% FBS and 1% of the antibiotic mixture of 10.000 units/mL penicillin G and 100 mg/mL of streptomycin (sp; Sigma-Aldrich, St Louis, MO, USA) was used to culture Caco-2 cells. LNCaP and T47-D cells grew in RPMI 1640 medium with 10% FBS and 1% sp. RPMI 1640 medium supplemented with 10% FBS, 2 mM *L*-glutamine, 10 mM HEPES, 1 mM sodium pyruvate and 1% Ab was used to culture fibroblasts (NHDF). Finally, HepaRG cells were cultured in Williams' E medium supplemented with 10% FBS, 1% sp, 5 µg/mL insulin, and 5×10^{-5} M hydrocortisone hemisuccinate (Sigma–Aldrich, St Louis, MO, USA).

3.2.2.2 Stock solutions

All synthesized compounds and 5-FU (positive control) were dissolved in DMSO in a concentration of 10 mM and stored at 4-8 ºC. For use, they were diluted in the corresponding fresh culture medium. The maximum DMSO concentration in the *in vitro* assays was 1%. Previous experiments revealed that this solvent level has no significant effects in cell proliferation (data not shown).

3.2.2.3 Antiproliferative assay

Molecules **1**, **2.1**, **3.1-3.4** were tested against the previously referred cell lines by the 3-(4,5-dimethylthiazol-2-yl)-2,5-diphenyltetrazolium bromide (MTT) (Sigma-Aldrich, St Louis, MO, USA) assay (Canário et al. 2020). Briefly, cells suspensions (2×10^4 cells/mL) were seeded in 96-well culture plates followed by 48 h of adherence before exposition to compounds for 72h. It was used a 30 µM concentration for preliminary assays and 0.1, 1, 10, 25, 50 and 100 µM for concentration-response studies. Negative control was the untreated cells and 5-FU was used as the positive control. After exposition to compounds and cells washing (100 µL of phosphate buffer saline, PBS), was added 100 µL of the MTT solution (5 mg/mL), prepared in the appropriate serum-free medium. Then, after incubation (4 h at 37 ˚C) and MTT removal, DMSO was added to dissolve formazan crystals. The absorbance was determined by using a Bio-rad Xmark spectrophotometer (570 nm). Percentages of cell proliferation were expressed relatively to the absorbance determined in negative control cells (after

background subtraction). Each assay was performed in quadruplicate (n=4) and independently repeated.

3.2.2.4 E-screening assay

This assay was performed as previously reported (Ayan et al. 2012; Canário et al. 2020). Briefly, ER^+ breast T47-D cancer cells (2×10^4 cells/mL) were cultured in 96-well culture plates. After 24 h, the complete medium was replaced by the experimental medium [freshly prepared phenol red free RPMI medium supplemented with 5% of dextran-coated charcoal-treated fetal calf serum (DCC-FCS)] containing the compounds under study (**3.2** and **3.3**) for 6 days (replaced every 3 days). The tested concentrations were 0.1, 0.01 and 0.001 μM. Untreated cells served as negative control and cells treated with 17β-estradiol were used as positive control. The above described MTT assay was used to estimate the percentage of cell proliferation. After background subtraction, cell proliferation values were expressed as percentage relative to the absorbance determined in negative control cells. Again, each experiment was performed in quadruplicate and independently repeated.

3.2.2.5 Cell viability evaluation

In 6-well plates, HepaRG cells (5×10^4 cells/mL; 48 h of attachment) were treated with experimental molecules (compounds **3.2** and **3.3;** 50 μM, 24 h). Untreated cells were used as negative control, and cells treated with 5-FU served as the positive control. Each assay was performed in duplicate and independently repeated. After the treatment, supernatants were collected, and the trypsinization was performed. Then, the obtained cell suspensions were kept on ice, pelleted, and resuspended in complete medium (400 μL). Subsequently, cell suspension (395 μL) was transferred to a FACS tube, and propidium iodide (PI, 5μl at 1 mg/ml) and EDTA (0.5 μL at 0.123 M) were added. A BD Accuri C6 (San Jose, CA, USA) flow cytometer was used in the channels forward scatter (FSC), side scatter (SSC), and fluorescence channel-3 for PI (FL3) to achieve a minimum of 20000 events. The Modfit LT software (v. 4.1.7) was used to analyze the results: three regions were created, (FSC/FL3 contour plot); R1 (viable cells); R2 (dead cells); and R3 (indeterminate cell population between the other two regions), excluding debris. The percentage of cells in R1 in comparison with total number of events in R1, R2, and R3 was considered the percentage of viability.

3.2.2.6 Cell cycle distribution study

In 6-well plates, HepaRG cells (5 × 10^4 cells/mL; 48 h of attachment) were treated with molecule **3.2** (50 μM, 24 h). After collecting and washing with PBS, the cells were resuspended with a cold solution of 0.5% bovine serum albumin (BSA; Amresco, Atlanta, GA, USA) in PBS containing EDTA (204 μL) (450 μL), and then fixed with 70% of EtOH and incubated at -20 ºC (during 2 days or more). After washing with PBS, fixed cells were resuspended in a PI solution (50 μg/mL; solution in 0.5% BSA in PBS with EDTA) and incubated for 15 min in the dark with Ribonuclease A (0.5 μg/μL; solution in 50% glycerol, 10 mM Tris-HCl, pH 8; Sigma Aldrich, St Louis, MO, USA). Negative control was untreated cells and 5-FU was used as positive control. BD Accuri C6 flow cytometer and Modfit software (v. 4.1.7) (Becton Dickinson, San Jose, CA, USA) were used for dada acquisition and analysis, respectively. Each experiment was performed in duplicate and independently repeated.

3.2.2.7 Cell proliferation analysis by the carboxyfluorescein succinimidyl ester assay

This assay was performed as previously described (Canário et al. 2020). HepaRG cells (12-well plates, 1 mL/well; 8 × 10^4 cells/mL) were incubated for 15 min or 30 min with carboxyfluorescein succinimidyl ester (CFSE; 10 μM, BD Horizon, San Jose, CA, USA). After being washed, cells were treated with molecule **3.2** (50 μM; 48 and 72 h). After incubation, cells were trypsinized, pelleted and resuspended with fresh medium (300 μL) containing EDTA (5 μL). Negative control was the untreated cells. BD Accuri C6 flow cytometer and BD Accuri Software were used for acquisition and analysis, respectively. The channels FSC, SSC and fluorescence channel-1 (FL1, for CFSE) were selected. Each experiment was performed in duplicate and independently repeated for 15 min studies and it was done one experiment for 48 and 72 h for 30 min assays.

3.2.3 Molecular docking

3.2.3.1 Preparation of proteins for molecular docking

ERα (PDB ID: 1A52), ST (PDB ID: 1P49) and 17β-HSD1 (PDB ID: 3KLM) crystal structures were obtained from protein data bank (PDB) (Tanenbaum et al. 1998; Hernandez-Guzman et al. 2003; Aka et al. 2010). These crystal structures were selected mainly due to the fact that these enzymes were complexed with endogenous molecules

such as E2 and DHT, which are also structurally similar to the tested compounds, and also considering their high resolution.

Software Chimera (v. 1.10.1) was used to delete the coordinates of all non-standard residues, including the co-crystalized ligand. Using AutoDockTools (v. 1.5.6) software, non-polar hydrogens were merged and Kollman and Gasteiger partial charges were added. Then, prepared structures were converted from the PDB format to PDBQT for docking studies.

3.2.3.2 Preparation of ligands

ChemDraw and Chem3D (v. 12.0) were used to build all ligands. In Chem3D were performed the energy minimization and geometry optimization, and the final structures were saved as PDB file format. The energy minimization was performed in the range from -20 to -40 kcal.mol^{-1}. AutoDockTools software converted PDB to PDBQT format.

3.2.3.3 Grid parameters

AutoDock vina and AutoDockTools were used to calculate the grid parameters, which were based on the coordinates of the adequate co-crystalized ligand: E2, *N*-acetyl-*D*-glucosamine and 5α-dihydrotestosterone (DHT). The grid box (its size was 20 x 20 x 20 with 1.0 Å of spacing) was centered on the ligand with the following coordinates: for ERα, the coordinates were x=107.27, y=13.94, z=96.38; for ST were x=62.033, y=-12.215, z=52.512; and for 17β-HSD1 were x=11.643, y=9.297, z=-11.887.

3.2.3.4 Docking simulations

AutoDock vina executable was used to perform molecular docking (Meng et al. 2011). The parameter exhaustiveness used was 15. Discovery Studio Visualizer program from BIOVIA and in PyMOL software were used to analyze and visualize the results.

3.2.3.5 Validation of the molecular docking performance

To validate docking process, the root-mean-square distance (RMSD) value should be less than 2.0 Å (Carugo 2003). In this study, re-docking ERα with E2, ST with *N*-acetyl-*D*-glucosamine and 17β-HSD1 with DHT were performed for method validation. As expected, low RMSD values (<2) were obtained for all the cases, which validated the docking process.

3.2.4 Statistical analysis

IC_{50} estimation was performed by sigmoidal fitting analysis (95% confidence level). Results were expressed as mean ± standard deviation (SD) and statistical significance was analyzed through the *t*-Student test (two groups) and one-way ANOVA (three groups) followed by Bonferroni post hoc tests. Results were considered statistically significant when $p < 0.05$.

3.3 Results

3.3.1 Chemistry

Scheme 3.1 represents the performed synthesis of the three C-ring oxidized E1 acetate analogs explored in the present study as previously described (Sykes et al. 1971; Stéphan et al. 1995; Schwarz et al. 1999; Murugan and Scriven 2003).

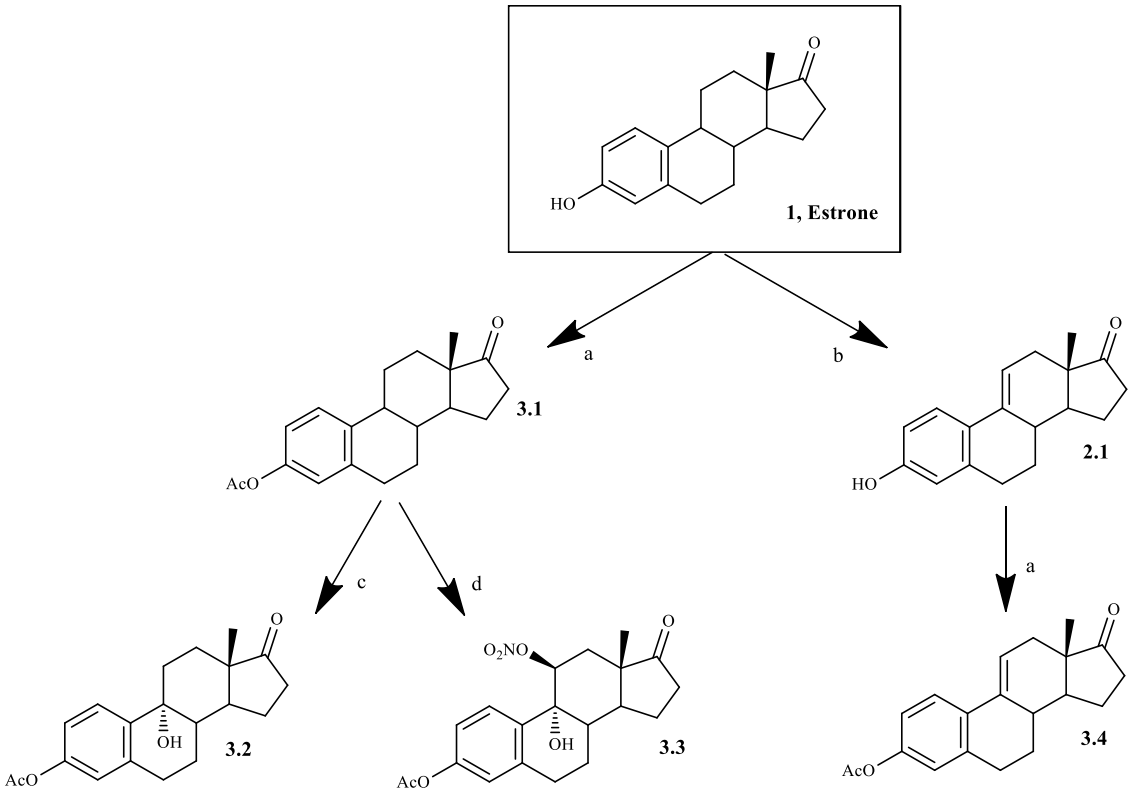

Scheme 3.1 Synthetic route to prepare the C-ring oxidized estrone acetate derivatives **3.2**, **3.3** and **3.4**. Reagents and conditions: (a) acetic anhydride, DMAP, THF, rt; (b) DDQ, MeOH, reflux; (c) Oxone™, acetone, CH_2Cl_2, H_2O, $NaHCO_3$, TBAHS, 15°C; (d) CAN, H_2O, acetic acid, rt.

The acetylation of compound E1 (96% yield) was successfully achieved using Ac_2O and DMAP (Murugan and Scriven 2003). Compound **3.2** was synthesized at an acceptable yield through the 9α-hydroxylation procedure involving the *in situ* formation of dimethyldioxirane as described in literature (Schwarz et al. 1999). The oxidation of E1

acetate using CAN (Sykes et al. 1971) allowed the preparation of 9α-hydroxy-11β-(nitrooxy)-17-oxoestra-1,3,5(10)-trien-3-yl acetate (compound **3.3**). The preparation of steroid **3.4** was firstly attempted by means of a DDQ-mediated dehydrogenation of estrone acetate **3.1** (Stéphan et al. 1995). However, in addition to incomplete substrate consumption, a mixture of inseparable products was obtained. Therefore, we decided to start the synthesis of compound **3.4** by the successful transformation of estrone E1 into $\Delta^{9,11}$-estrone **2.1**, again by using DDQ, as previously described (Stéphan et al. 1995; Canário et al. 2020). Then, the acetylation of compound **2.1** allowed the preparation of compound **3.4** with 89% yield. Starting from this 3-acetylated compound, two additional C-ring oxidized E1 derivatives were also tried to prepare. For this, by application of allylic oxidation reaction conditions, previously described by some of us (Salvador and Silvestre 2005), we attempted to synthesize 12-oxo-$\Delta^{9,11}$-estrone acetate. However, low reactivity was observed accompanied by the formation of a complex mixture of products (TLC control). In addition, by using *m*-chloroperoxybenzoic acid (Liang and Baran 1976), we could prepare 9α,11α-epoxy-estrone acetate. However, in the purification step to isolate the pure 9α,11α-diastereoisomer we found that this compound was unstable and was quickly transformed into several products (TLC control). This fact was also previously reported (Gao 1997). Therefore, this compound was not included in the present study.

Spectral analysis (IR, ^{1}H- and ^{13}C-NMR) for all prepared compounds are in agreement with the literature (Quinkert et al. 1982; Peters et al. 1989; Bovicelli et al. 1992; Simeón et al. 2004). The existence of acetate group in compounds **3.1** and **3.4** was evidenced by a signal near 2.26 ppm (^{1}H-NMR). The presence of the 9α-hydroxyl functional group of compound **3.2** was detected by the appearance of OH signals in the IR spectrum as well as by a signal at 70.21 ppm in the ^{13}C-NMR spectra, when compared with spectral data for compound **3.1**. In addition, the signal of C11 proton (compound **3.4**) at 6.21 ppm indicated the presence of the $\Delta^{9,11}$ double bond. Moreover, the triplet at 5.79 ppm corresponds to the typical signal of the 11α-hydrogen of the 9α-hydroxy-11β-nitrooxy derivative **3.3** (Peters et al. 1989).

3.3.2 Cell proliferation

The antiproliferative activity was studied on MCF-7, T47-D, LNCaP, HepaRG and Caco-2 cancer cells and on normal fibroblasts (NHDF) by the MTT assay (Mosmann 1983). **Figure 3.2** summarized the results of the initial screening at 30 μM for all compounds.

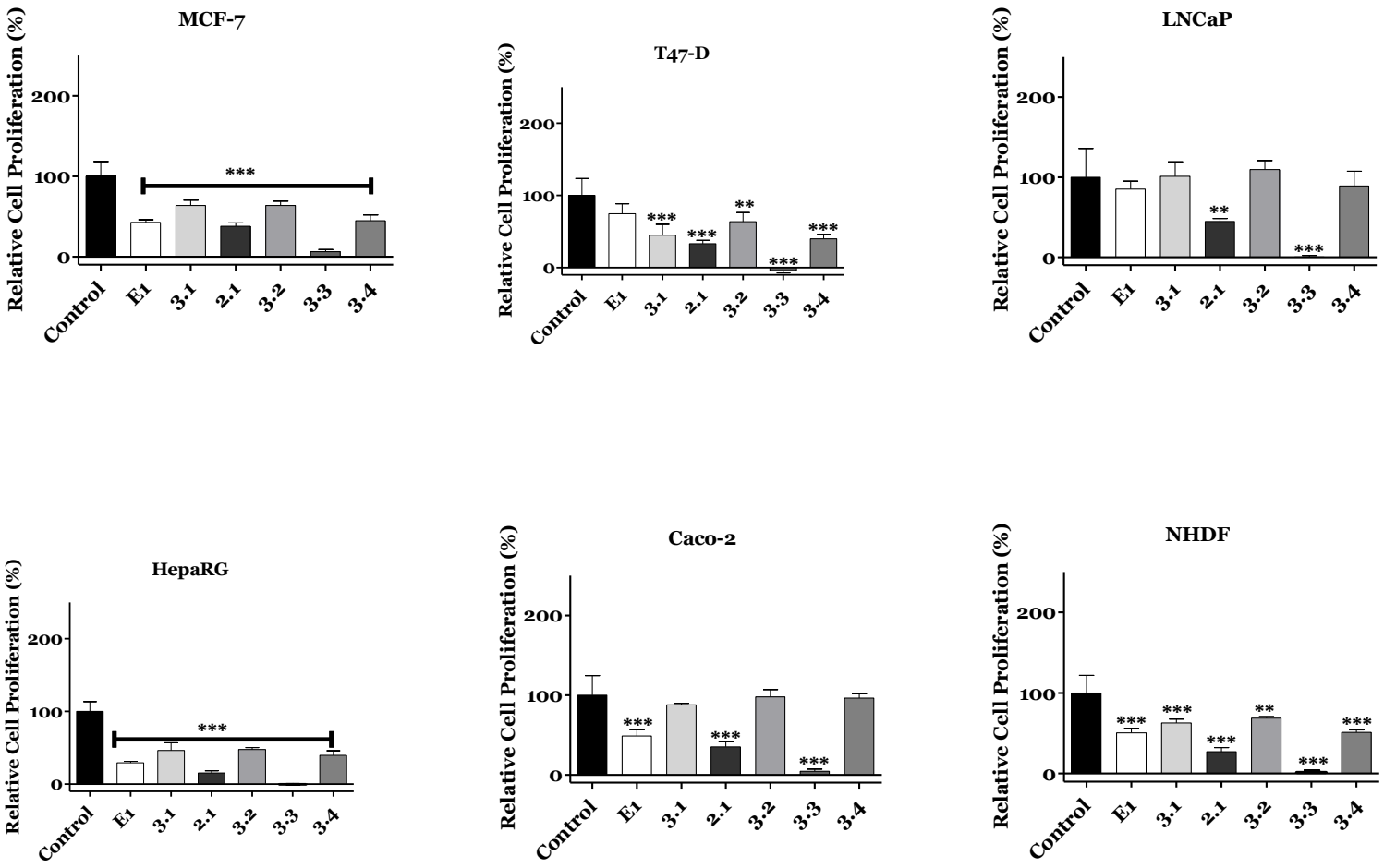

Figure 3.2 Relative cell proliferation of MCF-7, T47-D, LNCaP, HepaRG and Caco-2 cancer cells and normal fibroblasts (NHDF) exposed to the tested compounds for 72 h at 30 μM (MTT assay). Data are expressed as a percentage of cell proliferation relative to the negative control and are presented as mean ± SD and are representative of at least two independent experiments. $^{**}p < 0.01$ *vs* control; $^{***}p < 0.001$ *vs* control (Student t-test).

IC_{50} was calculated when a reduction of cell proliferation was higher than 50% (**Table 3.1**). The most cytotoxic compound was molecule **3.3**, with the lowest determined IC_{50} values for all tested cells. Interestingly, higher selectivity index (SI) was determined for compound **3.3** (**Table 3.2**) in hormone-dependent (MCF-7, T47-D and LNCaP) cancer cells. A SI value higher than 2 indicates a high selectivity for cancer cells (Bézivin et al. 2003).

Table 3.1 IC_{50} (μM) of compounds **1**, **3.1-3.4** and 5-fluorouracil (5-FU) against MCF-7, T47-D, LNCaP, HepaRG and Caco-2 cancer cells and normal fibroblasts (NHDF)[a].

Compounds	MCF-7	T47-D	LNCaP	HepaRG	Caco-2	NHDF
E1	41.93	ND	ND	29.53	42.69	61.82
3.1	ND	29.24	ND	46.54	ND	ND
3.2	ND	ND	ND	32.04	ND	ND
3.3	5.87	7.40	5.30	10.91	14.12	12.14
3.4	53.59	44.56	ND	36.06	ND	ND
5-FU	1.71	0.54	7.79	1.78	1.31	3.61

[a]Results from MTT assay using different concentrations (0.1, 1, 10, 25, 50 and 100 μM) for 72 h. The data shown are representative of at least two independent experiments. ND: not determined.

Table 3.2 Selectivity index (SI)[a] of compounds **1**, **3.3** and 5-fluorouracil (5-FU).

Compounds	MCF-7	T47-D	LNCaP	HepaRG	Caco-2
E1	1.47	ND	ND	2.09	1.45
3.3	2.07	1.64	2.29	1.11	0.86
5-FU	2.11	0.49	0.46	2.03	2.76

[a]Calculated by dividing the IC_{50} value in non-tumoral cells (NHDF) by the value of IC_{50} in cancer cell lines. [b]ND: not determined.

In addition, compounds **3.2** and **3.3** were tested on T47-D (ER^+) cells to evaluate their potential estrogenic capability (**Figure 3.3**) (Ayan et al. 2012; Cortés-Benítez et al. 2017), in comparison with E2, which led to increase in proliferation of T47-D cells in all concentrations studied. Unfortunately, compound **3.3** also led to cell proliferation at 0.1 μM (140%) when compared with the negative control. On the other hand, and interestingly, compound **3.2** did not exhibit proliferative action.

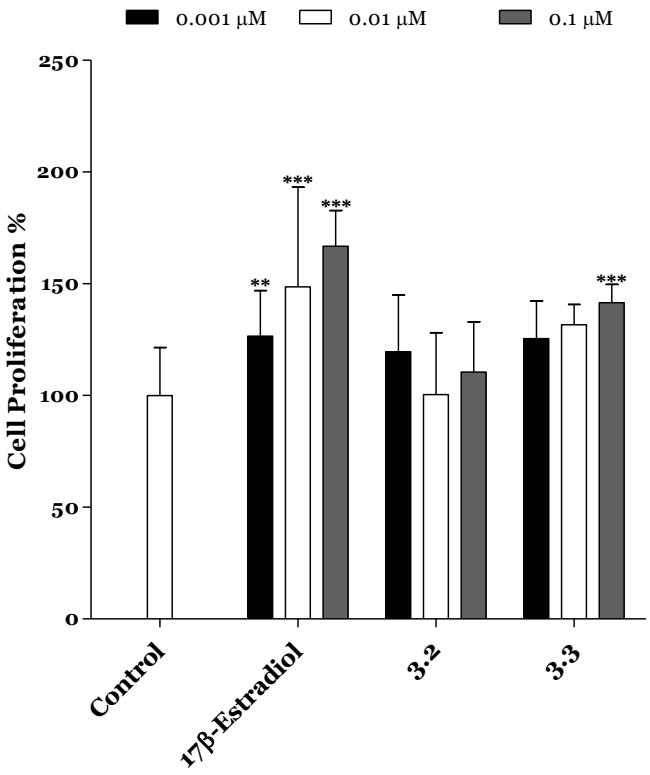

Figure 3.3 *E-screening* assay of compounds **3.2** and **3.3** in T-47D cells. Each bar represents the mean ± SD (two independent experiments). $^{**}p < 0.01$ *vs* control; $^{***}p < 0.001$ *vs* control (one way ANOVA post-hoc Bonferroni test).

3.3.3 Flow cytometry experiments

HepaRG cell survival was evaluated by flow cytometry (PI staining) for the compounds with the highest interest (**Figure 3.4**). The reduction on cell viability for compound **3.2** was not statistically significant at 24 h. However, compound **3.3** led to a drastic reduction of cell viability (92%). Additionally, in **Figure 3.5** are presented images of HepaRG cell after the treatment with this compound.

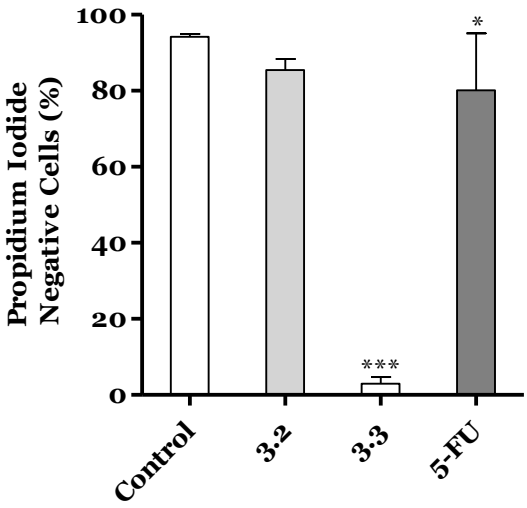

Figure 3.4 Percentage of viable HepaRG cells treated with steroids **3.2** and **3.3** (50 μM, for 24 h) by flow cytometric assay with propidium iodide (PI) staining. Untreated cells were used as the control. The percentage of cells in R1 (live cells, PI negative) as compared to the total number of events in R1, R2 (dead cells) and R3 (undetermined cells) was considered the percentage of viability. Each bar represents the mean ± SD (originated from two independent experiments). *$p < 0.05$ *vs* control; ***$p < 0.001$ *vs* control (two-way ANOVA post-hoc Bonferroni test).

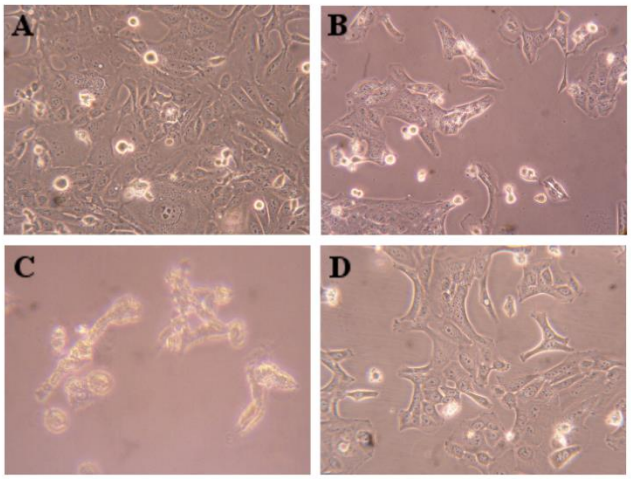

Figure 3.5 Microscopic visualization of HepaRG cells (A, control) treated with compound **3.2** (B), compound **3.3** (C) and 5-fluorouracil (D) at 50 μM for 24 h. Amplification of 100x.

Despite the interesting IC_{50} and SI values determined for compound **3.3** (**Tables 3.1** and **3.2**), and the drastic reduction in cell viability, this compound had a potential estrogenic effect (**Figure 3.3**), which is not interesting for the development of anticancer drugs. Therefore, it was decided to explore the effects of compound **3.2** in cell cycle progression by flow cytometry as well as by the carboxyfluorescein succinimidyl ester assay. By means of cell cycle distribution study, it was evidenced that steroid **3.2** (50 μM) induced a G_0/G_1 cell cycle arrest at 24 h post-treatment (**Figure**

3.6), being evident an increase in cell percentage in G_0/G_1 and a reduction of the percentage of cells in S phase.

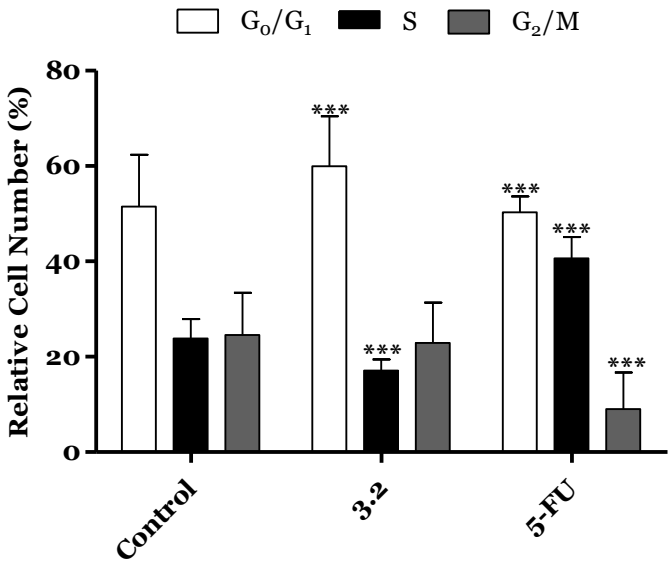

Figure 3.6 HepaRG cycle distribution after treatment with compound **3.2** (at 50 μM) for 24 h. 5-Fluorouracil [(5-FU), 50 μM] was used as positive control and untreated cells as negative control. Each bar represents the mean ± SD (originating from two independent experiments). ***p < 0.001 *vs* control (two-way ANOVA post-hoc Bonferroni test).

Using an adapted carboxyfluorescein succinimidyl ester assay, the cell proliferation after 48 and 72 h was also studied (Sánchez-Sánchez et al. 2016). Interestingly, compound **3.2** led to a higher intensity signal than control cells due to a lower number of cell replications (**Figure 3.7**).

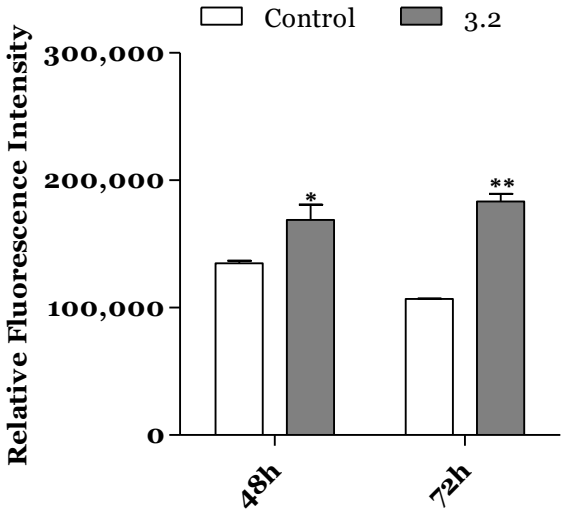

Figure 3.7 HepaRG relative fluorescence intensity after treatment with compound **3.2** (50 μM) for 48 and 72 h, obtained by the carboxyfluorescein succinimidyl ester assay. Each bar represents the median with range of two samples. *p < 0.01 *vs* control; **p < 0.01 *vs* control (two-way ANOVA post-hoc Bonferroni test).

Furthermore, from 48 to 72h control cell median fluorescence diminished (evidence of cell division), but fluorescence of treated cells remained unchanged, suggesting that no cell division occurred during this time period.

3.3.4 Molecular docking

The knowledge of the target and respective binding site of the molecule under study is essential in drug development (Makar et al. 2020). Three steroidal targets have been studied by molecular docking: ERα, ST and 17β-HSD type 1. ERα is involved in the control of many physiological processes such as cell proliferation (Miki et al. 2018). ST and 17β-HSD type 1 are also relevant for the regulation of cell replication by adjusting steroid hormone levels (Cornel et al. 2017). In fact, ST makes the conversion of 3-sulfated steroids into their hydroxylated analogs, including the transformation of E1 sulfate into E1. In addition, 17β-HSD type 1 reduces the 17-carbonyl group of androstane and estrane molecules to more potent 17β-hydroxysteroids (Payne and Hales 2004). Therefore, their deregulation is involved in cancer development, particularly of hormone-dependent breast cancers.

Molecular docking studies were made against ERα, ST and 17β-HSD1 by means of AutoDock vina executable. The results obtained for compounds **3.1-3.4** are summarized in **Table 3.3**.

Table 3.3 Predicted affinity energies of compounds **E1**, **3.1-3.4** calculated from molecular docking against known protein targets of steroidal molecules (ERα, ST and 17β-HSD1).

Compounds	Lowest energy (kcal.mol^{-1})		
	ERα	**ST**	**17β-HSD1**
E1	-10.3	-6.2	-8.1
3.1	-7.2	-6.2	-8.3
3.2	-7.3	-5.9	-8.2
3.3	-7.4	-6.9	-8.0
3.4	-7.0	-6.3	-8.3
17β-estradiol (E2)	-9.9 [a]	-	-
N-acetyl-*D*-glucosamine	-	-7.2 [a]	-
5α-Dihydrotestosterone (DHT)	-	-	-8.3 [a]

[a] The RMSD between re-docked ligands and the corresponding X-ray crystal structure coordinates was ≤ 2. (ERα+E2 = 0.103; ST+*N*-acetyl-*D*-glucosamine = 0.98; 17β-HSD1+DHT = 0.18). The standard error was +1 -1.5 kcal/mol.

For all the tested compounds, binding energy values were similar for ERα and higher than those determined for E2, which suggests a weak affinity to this target. In addition, by analyzing the interactions between these compounds and the macromolecule, marked differences were observed when compared with the interactions performed by E2. However, regarding the results for compound **3.3**, which presented the best affinity

value, it is possible to verify some common interactions between this compound and the reference compound (E2). In fact, although compound **3.3** does not establish the essential conventional hydrogen bonds with His524 and Glu353 residues, there are some interactions in common, such as Van der Waals interactions with Leu387, Met388 and Leu391 residues and alkyl and pi-alkyl interactions with Phe404, as it is shown in **Figure 3.8**. In addition, despite the absence of interaction with Glu353, this compound establishes a Van der Waals interaction with His524, a weaker interaction when comparing with the conventional hydrogen bond. Concerning 17β-HSD1 enzyme, the lowest energy was obtained with compounds **3.1** and **3.4** (**Figure 3.9**). Although the energy values were similar to the previously obtained with the ligand DHT, these compounds do not perform the essential interaction for inhibitory activity, which is the hydrogen bond with His221 (Day et al. 2008). However, both compounds seem to interact with Leu149, Pro187 and Val143 residues through alkyl and pi-alkyl interactions, similarly to DHT. In addition, compounds **3.1** and **3.4** establish a conventional hydrogen bond with Ser222, although the biological significance of this interaction is unclear. Furthermore, their binding mode is very similar and both structures are practically overlapping in within the macromolecule. Concerning ST enzyme, in addition to the weak affinity energies obtained, no relevant interactions with the amino acid involved in the binding site (Leu74, Arg98, Thr99, Val101, Leu103, Leu167, Val177, Phe178, Thr180, Gly181, Thr484 and Phe488) (Daśko et al. 2020) were observed.

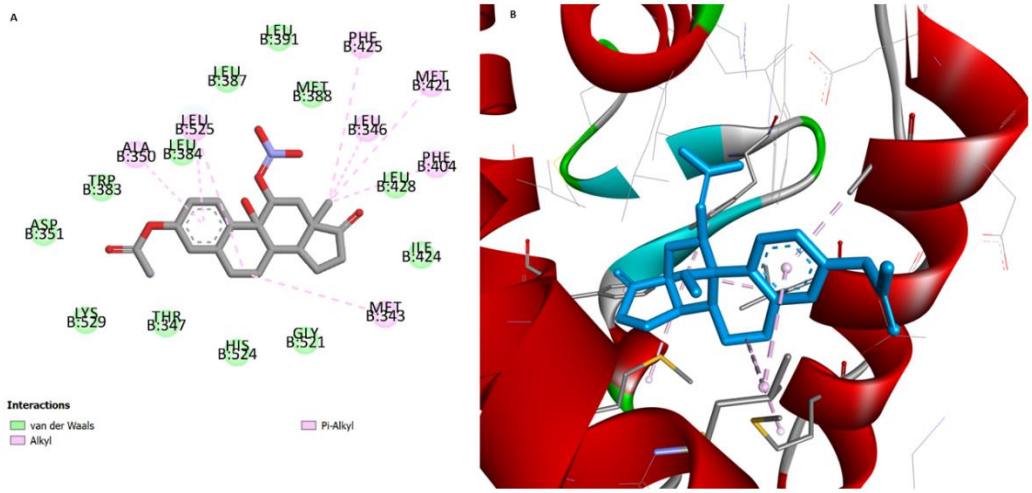

Figure 3.8 Predicted interactions and binding mode of the best ranked and synthetized compound **3.3**, with ERα in 2D (panel **A**) and 3D (panel **B**). (**A**) Van der Waals interactions are displayed in green and alkyl and pi-alkyl interactions in soft pink. (**B**) Binding mode of compound **3.3** in active site of ERα. Van der Waals interactions are displayed in green and alkyl and pi-alkyl interactions in soft pink.

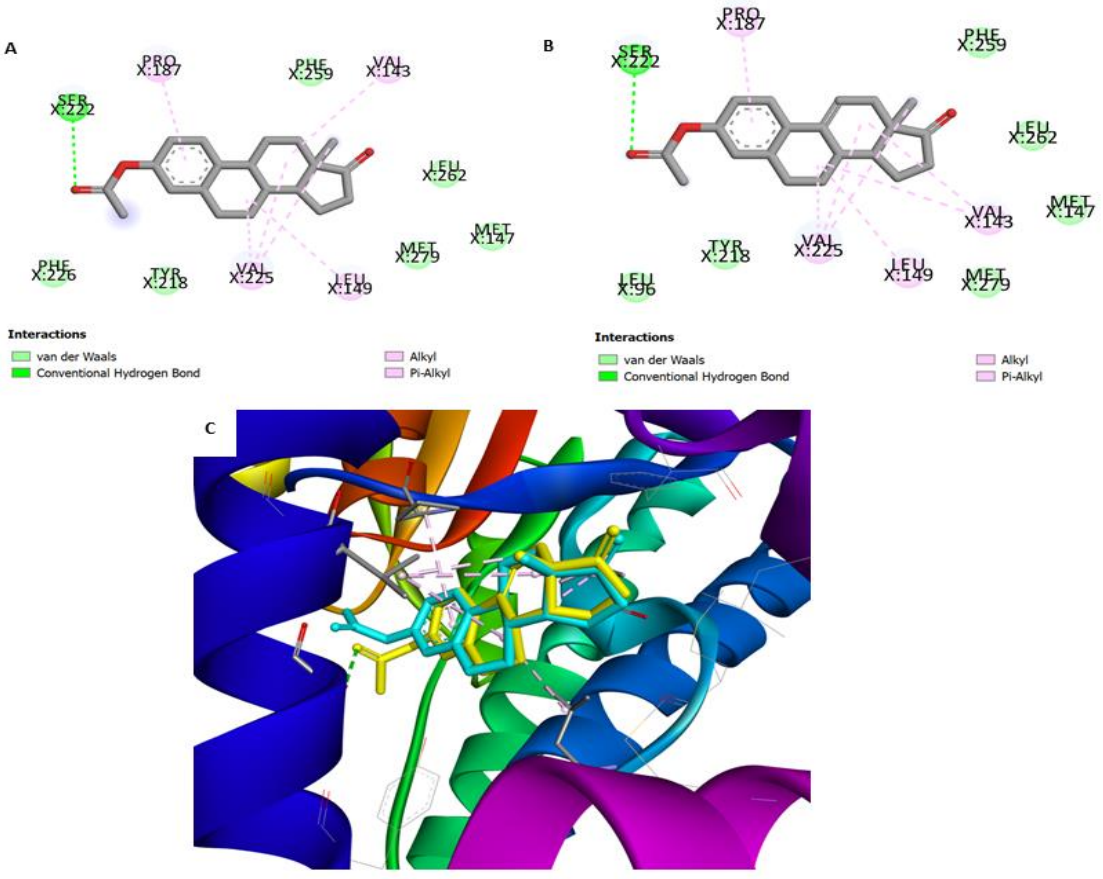

Figure 3.9 Predicted interactions of the best ranked and synthetized compounds **3.1** and **3.4**, with 17β-HSD1 in 2D (panel **A** and **B**) and 3D (panel **C**). (**A**) Van der Waals interactions are displayed in light green, conventional hydrogen bonds in green and alkyl and pi-alkyl in pink. Both compounds, as co-crystalized ligand DHT, present alkyl and pi-alkyl interactions with Pro187, Val143 and Leu149. (**B**) Van der Waals interactions are displayed in light green, conventional hydrogen bonds in green and alkyl and pi-alkyl in pink. (**C**) 3D representations of overlapping of compound **3.1** (in turquoise) and **3.4** (in yellow) in the macromolecule binding pocket.

3.4 Discussion

The chemical synthesis was performed under relatively mild reaction conditions. The use of CAN as oxidant originated compound **3.3** in 34% yield (Sykes et al. 1971). In fact and interestingly, in A-ring aromatic steroid derivatives, CAN leads to hydroxylation of the C9 benzyl atom and nitration of the C11 homobenzyl position (Golubovskaya and Rzheznikov 2007). The mechanism possibly involves the dehydration at C9-C11 followed by a nucleophilic addition at C11 and formation of a radical at C9, which reacts with cerium (IV) to form a carbon cation, which can react with a second nucleophile, giving rise to hydroxyl group (Peters et al. 1989). Steroid **3.4** was synthesized (89% yield) by the successful transformation of estrone E1 into $\Delta^{9,11}$-estrone **2.1** by DDQ followed by its acetylation (Murugan and Scriven 2003). Dehydrogenation using DDQ is widely used to obtain aromatic and α,β-unsaturated carbonyls. The mechanism includes the hydride transfer to the quinone oxygen with formation of a carbocation in the substrate, followed by the transference of a proton to the phenolate ion and concomitant formation of a double bond (Batista et al. 2012). Isolated or *in situ* formed dioxiranes have been used as oxidants because they are selective and can allow mild reaction conditions (Salvador et al. 2012). In this context, the hydroxylation of E1 acetate by dimethyldioxirane enabled the selective oxyfunctionalization at C9α (Schwarz et al. 1999), affording steroid **3.2** (55% yield). The reaction involves the *in situ* formation of dimethyldioxirane by the reaction of Oxone™ with acetone and subsequent oxidative attack involving the tertiary carbon.

Concerning the cell viability studies and structure-activity relationship data, the introduction of a 9α hydroxyl group to E1 acetate (compound **3.2**) did not enhance the antiproliferative activity in hormone-dependent cancer cells when compared with E1 acetate (compound **3.1**). However, this hydroxylation led to a higher antiproliferative activity against HepaRG cells (IC_{50} = 32.04 μM) than the observed with E1 acetate (compound **3.1**) and $\Delta^{9,11}$-E1 acetate (compound **3.4**). Interestingly, the existence of 11β-nitrooxy group, in addition to the 9α-hydroxyl (compound **3.3**), markedly increased the antiproliferative effect against all cell types studied (**Table 3.1**). These are relevant results because in literature, *in vitro* studies for compounds **3.2** and **3.3** are not known, to our knowledge. However, it was already evidenced that 11-nitrates of 9α,11β-dihydroxyestratrienes containing various substituents at positions 3 and 17 showed interesting antitumor activity in mongrel rats bearing a model of alveolar breast cancer (Rzheznikov et al. 2003). In addition, stimulation of the tumor growth was observed after 15 days of treatment, probably due to estrogenic effect inherent of steroidal molecules (Rzheznikov et al. 2003). In addition, the 11β-nitrate of 17α-ethynylestradiol-3,17-diacetate also exhibited antiestrogen activity in an assay with

uterus of immature animals (Golubovskaya et al. 2009). Our results for compound **3.3** showed an antiproliferative effect more pronounced in hormone-dependent cells (IC_{50} = 5.87 μM for MCF-7 cells; IC_{50} = 7.40 μM for T47-D cells; IC_{50} = 5.30 μM for LNCaP cells). However, in the *E-screening* assay compound **3.3** also revealed estrogenic activity in T47-D cells, which seems to be in concordance with the literature (Peters et al. 1989; Golubovskaya et al. 2009). In this context and as example, Zhang *et al* (Zhang et al. 2005) synthesized 11β-estradiol carboxylates, esters and ethers and showed that when the 11β-chain had four or five non-hydrogen atoms, the estrogenic effect diminished and a SERM (selective estrogen receptor modulator) was obtained. In addition, other structure–activity relationship studies showed that large hydrophobic substituents at 11β side chain originated anti-estrogenic compounds and that different chemical groups in this chain promoted different affinities to ER (Aliau et al. 2000; Hanson et al. 2012). Thus, the potential estrogenic activity associated with compound **3.3** can be explained by the small size of 11β-nitrooxy group. On the other hand, in our study, compound **3.2**, which only has a 9α-hydroxyl group, did not show a T47-D proliferation. Interestingly, Alsayari and co-workers (Alsayari et al. 2017) demonstrated that 3-methoxyestra-1,3,5(10),9(11)-tetraen-17-one was a estrogenic compound with affinity to ERα and ERβ. Otherwise, the 9-hydroxymethyl-11-keto analogue showed low cytotoxicity against MCF-7 cells and also was an estrogenic compound. Thus, the size of the group at C9 seems to be important for estrogenic and cytotoxic activities. Concerning the cell cycle effects of these compounds, some studies showed that several steroids (Berényi et al. 2013; Morozkina and Shavva 2016) as well as non-steroids (Mirzaei et al. 2020; Shen et al. 2020; Bader et al. 2021) lead to cell cycle arrest. In this context and as example, 11α-substituted 2-methoxyestradiol derivatives lead to a cell cycle arrest at G_2/M and demonstrated an important anti-estrogenic effect (Lao et al. 2017). In addition, as an example of non-steroidal compounds interfering in cell cycle, 2-benzyl-1-(3,4,5-trimethoxyphenyl)-1*H*-naphtho[1,2-*e*][1,3]oxazin-3(2*H*)-one also induced G_2/M phase arrest on A2780 cancer cell line and *in silico* studies showed a relevant molecular interaction with tubulin (Mirzaei et al. 2020). Remarkably, in our study, compound **3.2** induced a G_0/G_1 phase arrest, probably because it interferes with many proteins of the cell cycle such as cyclin-dependent kinases and others (Deshpande et al. 2005; Romagosa et al. 2011), which are important for the cellular regulation of DNA replication. However, additional studies are required to clarify the biological mechanisms. The estrogenicity absence of compound **3.2** associated with an arrest in G_0/G_1 showed that this steroid may be a suitable starting point to develop potentially improved anticancer drugs. In addition, the CFSE assay showed that compound **3.2** promoted a low number of cell divisions of HepaRG cancer

cells, being less proliferative. This result is in agreement with the cell cycle analysis results. Finally, $\Delta^{9,11}$-E1 acetate (compound **3.4**) showed weaker antiproliferative activity in all studied cell lines when compared with analogue **2.1**, which has a 3-hydroxyl group (Canário et al. 2020).

Molecular docking studied the interactions between these C-ring oxidized E1 acetate analogs and proteins that interact with them (Woo et al. 2012; Lespérance et al. 2018). Few studies were reported including docking with C-ring modified steroids (Alsayari et al. 2017; El-Kady et al. 2019). Concerning ERα results, weaker binding energies for compound **3.4** were observed, compared with E2, and with compound **2.1**, according to our previous report (Canário et al. 2020). In addition, compounds **3.2** and **3.3** also had weaker binding energies to ERα than E1 and E2. These results were expected because non-polar groups are preferable in C9 and C11 positions for the interaction with ERα (Napolitano et al. 1995; Palomino 1999). Thus, the cytotoxicity originated by compound **3.3** can be associated with another mechanism of action than the interaction with ERα. In this context, another possible reason is the generation of nitric oxide, which has a cytotoxic effect (Kerwin et al. 1995). As some compounds structurally similar to the described in this work were reported as 17β-HSD1 (Day et al. 2008) and ST (Nussbaumer and Billich 2004; Daśko et al. 2020) inhibitors, we also included these two proteins in our molecular docking study. Concerning 17β-HSD1 enzyme, for compounds **3.1** and **3.4**, although the binding energies were similar to DHT, there is a lack of the important conventional hydrogen bonds present in the binding mode of DHT, as described above. In fact, typical steroidal 17β-HSD1 E1/E2 inhibitors had modifications in D-ring at C16 and C17 positions of steroid nucleus (Maltais et al. 2014; Maltais et al. 2016). However, Deluca *et al* (Deluca et al. 2006) showed that an estratriene derivative with a C9 modification and fluorine-substitution in position 17 had a relevant 17β-HSD1 inhibitory activity. So, modifications only in C9 are not enough to inhibit this enzyme.

Taking into account ST enzyme, these experimental compounds should not markedly bind and interact with this protein with energy lower than the control, *N*-acetyl-*D*-glucosamine. Among ST inhibitors based on E1 skeleton, previous reports showed that 17α-benzyl-derivatives, 17β-arylsulfonamides, 17-diisopropylcarbamoyl-3-*O*-sulfamates, 2-methoxy-3-*O*-sulfamates and 2-methoxy-3,17β-bissulfamates are potent ST inhibitors (Morozkina and Shavva 2016). However, our results suggested that C-ring modifications tested in the present work were no useful to improve the binding energy to ST enzyme. Globally, docking results for the prepared compounds with these three targets revealed similar or lower binding energies than the co-crystalized ligands as well as the absence of some relevant binding points. Therefore, despite that with these

docking results it is not possible to exclude that these compounds can act by interacting with the three explored proteins, other targets should be considered in further docking studies. These include not only other proteins influencing hormonal biosynthesis and effects but also proteins and other biomolecules affecting the cell cycle, considering that compound **3.2** lead to an arrest at G_0/G_1 phase. Therefore, further *in silico* and experimental studies would be necessary to further elucidate the activity of these compounds.

3.5 Conclusion

C-ring modifications in E1 acetate scaffold originated molecules with higher cytotoxic activities than E1 acetate. Of these, the 9α-hydroxy,11β-nitrooxy derivative **3.3** showed to be the most cytotoxic molecule against hormone-dependent cancer cells. In addition, the introduction of 11β-nitrooxy group originated a drastic reduction in HepaRG cell viability and increased the proliferation of T47-D cells in *E-screening assay*. Therefore, similarly to previous studies, it was difficult to dissociate the estrogenic effect from the cytotoxic activity. Importantly, 9α-hydroxyestrone acetate **3.2** promoted a selective cytotoxic effect on HepaRG cells, induced an arrest at G_0/G_1 phase and, interestingly, did not promote T47-D proliferation. This last finding is of major importance since it has been described that usually estrogen derivatives could stimulate cell proliferation through the interaction with their receptors and consequently stimulate tumor growth. Overall, this preliminary study demonstrated that this structural modification can be of interest to develop new anticancer estrane derivatives without estrogenic activity.

Chapter 4
Estrone *p*-quinol

The content of this chapter is included in the following manuscript:

Canário C, Matias M, Brito V, Cruz-Vicente P, Soeiro P, Santos AO, Falcão A, Silvestre S, Alves G. 2022. 10β-Hydroxyestra-1,4-diene-3,17-dione as potential antiproliferative agent: *in vitro* biological evaluation and *in silico* studies. Nat Prod Res. 15: 1-5.

4.1 Introduction

Steroids play a crucial physiological role in metabolism and neuroprotection (Simpkins et al. 2004). 10β-Hydroxyestra-1,4-diene-3,17-dione (**HEDD**) is a steroidal *para*-quinol formed in the human body which can be considered a estrone prodrug in the central nervous system (CNS) without ER affinity in the peripheral tissues (Prokai et al. 2003; Prokai-Tatrai and Prokai 2019). Interestingly, **HEDD** was screened against melanoma (Fem-X), cervix carcinoma (HeLa) and leukemia (K_{562}) cells, displaying a weak antiproliferative effect (IC_{50} > 100 μM) (Milić et al. 2001). However, in CCRF-CEM leukemia cells some cytotoxicity (IC_{50} = 26.4 μM) was found (Milić et al. 1999). Taking into account these results, we prepared **HEDD** and *in vitro* explored its cytotoxic effects against six cell lines. In addition, an estrogenicity assay and a flow cytometry study were performed. Based on the results observed, we also performed molecular docking studies, including the estrogen receptor (ERα), androgen receptor (AR), 17β-hydroxysteroid dehydrogenase type 1 (17β-HSD1), aromatase (CYP19A1) and 17α-hydroxylase/17,20-lyase (CYP17A1). Furthermore, a computational prediction of the most relevant pharmacokinetic and toxicity properties was also carried out.

4.2 Experimental section

4.2.1 Chemistry

All chemicals were purchased from commercial suppliers and used without further purifications. The reaction was monitored by thin layer chromatography (TLC) using a Al-backed aluminum/silica gel plate 0.20 mm (Macherey-Nagel 60 F254, Duren, Germany). A visualization was performed under ultraviolet (UV) radiation (254 nm) in a CN-15.LC UV chamber and then plates were revealed using the mixture EtOH/concentrated sulfuric acid (95:5, *v*:*v*), followed by heating at 120 °C. The Infrared (IR) spectra were collected on a Thermoscientific Nicolet iS10 with a diamond attenuated total reflectance crystal at room temperature in the 4000-400 cm^{-1} range by averaging 16 scans at a spectral resolution of 2 cm^{-1}. Nuclear magnetic resonance (NMR) spectra (^{1}H-NMR and ^{13}C-NMR) were run on a Bruker Avance 400 MHz. The software used was TOPSPIN 4.07 (Bruker, Fitchburg, WI, USA). Chemical shifts are reported in parts per million (ppm) relative to tetramethylsilane (TMS) or solvent as an internal standard. Coupling constants (*J* values) are reported in hertz (Hz) and splitting multiplicities are described as s=singlet; d=doublet; and dd=double doublet and t =triplet.

*4.2.1.1 Synthesis of 10β-hydroxyestra-1,4-diene-3,17-dione (**HEDD**, compound **4.1**)*

To a solution of E1 (136 mg, 0.5 mmol) in ethyl acetate (21.62 mL) was added a solution of $KMnO_4$ (156.756 mg) in HCl (21.6 mL, 0.05 M). The solution was mixed under room temperature for 30 s. The reaction was monitored by TLC. To stop the reaction, 10 ml of water was added and then the solution was filtered through Celite®. The crude was diluted in 150 mL of CH_2Cl_2, washed with 50 mL of saturated aqueous solution of $NaHCO_3$, 50 mL of H_2O, dried over anhydrous Na_2SO_4 and evaporated under reduced pressure using a rotary vacuum drier from Büchi (R-215). Then, the crude was purified by column chromatography [ethyl acetate (EA)/petroleum ether (PE), 40 - 60 ˚C, 3:1] to afford compound **4.1** as light brown solid (32%) (Milić et al. 1997; Lista et al. 2006). IR (υ_{max}/cm^{-1}): 1208, 1292, 1457, 1633, 1728, 1750, 2893-2962, 3447; ^{1}H-NMR (400 MHz, $CDCl_3$) δ: 0.97 (s, 3H, CH3-18), 6.01 (t, 1H, J = 1.8 Hz, C4-H), 6.19 (dd, 1H, J1 = 10.2 Hz, J2 = 2.0 Hz, C2-H), 7.07 (d, 1H, J = 10.2 Hz, C1-H); ^{13}C-NMR (100 MHz, $CDCl^3$) δ: 13.89, 22.06, 22.16, 31.19, 31.96, 32.35, 34.74, 35.78, 47.91, 50.26, 54.34, 70.27, 123.26, 128.47, 150.37, 165.20, 185.67, 220.47.

4.2.2 Bioactivity assays

4.2.2.1 Cell culture

MCF-7, T47-D, LNCaP, Caco-2 and NHDF cell lines were obtained from American Type Culture Collection (ATCC; Manassas, VA, USA) and HepaRG cells were acquired to Life Technologies – Invitrogen™ (through Alfagene, Portugal) and were cultured in 75 cm^2 culture flasks at 37 ˚C in a humidified air incubator with 5% CO_2. MCF-7 cells were cultured in high-glucose DMEM medium supplemented with 10% fetal bovine serum (FBS) (Sigma-Aldrich, Inc., St. Louis) and 1% antibiotic/antimycotic (10.000 units/mL penicillin G, 100 mg/mL streptomycin and 25 μg/mL amphotericin B; Ab) (Sigma-Aldrich, Inc., St. Louis). Caco-2 cells were cultured in high-glucose DMEM medium supplemented with 10% FBS and 1% antibiotic (10.000 units/mL penicillin G and 100 mg/mL streptomycin; Sp) (Sigma-Aldrich, Inc., St. Louis). LNCaP and T47-D cells were cultured in RMPI 1640 medium supplemented with 10% FBS and 1% Sp. NHDF cells were cultured in RMPI 1640 medium supplemented with 10% FBS, 2 mM *L*-glutamine, 10 mM HEPES, 1 mM sodium pyruvate and 1% Ab. HepaRG cells were cultured in Williams' E medium supplemented with 10% FBS, 1% Sp, 5 μg/mL insulin, and 5×10^{-5} M hydrocortisone hemisuccinate (Sigma-Aldrich, Inc., St. Louis).

4.2.2.2 Preparation of compound solution

A stock solution of **HEDD**, E1 and 5-fluorouracil (5-FU) were prepared in DMSO at 10 mM and stored at 4 ºC. From the stock solution several diluted solutions of the compounds were prepared at different concentrations in complete cell medium before each experiment.

4.2.2.3 Antiproliferative assay

The cell proliferation was evaluated by quantifying the extent of the reduction of 3-(4,5-dimethylthiazol-2-yl)-2,5-diphenyltetrazolium bromide (MTT) (Sigma-Aldrich, Inc., St. Louis) assay by the studied cell lines. When cells reached approximately 90-95% confluence, they were gently detached by trypsinization (trypsin-EDTA solution, 0.125 g/L of trypsin and 0.02 g/L of EDTA) and the viable cells were counted with a hemocytometer by means of the trypan-blue exclusion assay. Then, 100 µL of cell suspension (2×10^4 cells/mL) were seeded in 96-well culture plates and left to adhere for 48h. After the cell adherence, the medium was replaced by the compounds' solution (30 µM for the screening assays and 0.1, 1, 10, 25, 50 and 100 µM for concentration-response studies) in the appropriate culture medium for approximately 72 h. After this period, compounds' solutions were removed and the cells were washed with 100 µL of phosphate buffer saline (137 mM NaCl, 2.7 mM KCl, 10 mM Na_2HPO_4 and 1.8 mM KH_2PO_4, in deionized water and pH adjusted to 7.4) and 100 µL of the MTT solution (5 mg/mL), previously prepared in the appropriate serum-free medium, were added to each well, followed by incubation at 37 ºC for 4h. Hereafter, the MTT-containing medium was removed and the formed formazan crystals were dissolved in DMSO. The absorbance was measured at 570 nm using a microplate reader spectrophotometer BIO-RAD xMark™. Cell viability values were expressed as percentages relatively to the absorbance determined in the cells used as negative control. 5-FU was used as positive control and untreated cells were used as negative control. Each experiment was performed in quadruplicate and independently repeated.

4.2.2.4 E-screening assay

T47-D cells (2×10^4 cells/mL) were seeded in 96-well culture plates in 100 µL of the appropriate cell medium and left to adhere. After overnight incubation, the medium was replaced every 3 days with fresh phenol red free RPMI 1640 medium supplemented with 5% of dextran-coated charcoal-treated calf serum

and the studied compounds' solutions (0.001, 0.01 and 0.1 μM). After 6 days of exposure, the cell proliferation was estimated by an MTT assay as described in the previous section. Each experiment was performed in quadruplicate.

4.2.2.5 Flow cytometry

HepaRG cells (5×10^4 cells/mL) were seeded in 6-well plates in 100 μL of the appropriate cell medium and left to adhere. After 48h of attachment, they were treated with **HEDD** (50 μM) for 24h. After this period, the medium of each well was collected and the cells were also collected by trypsinization and resuspended with the appropriate cell medium. The resulting cell suspension was kept on ice, centrifugated and the resulting pellet resuspended in 400 μL of complete medium. Then, 395 μL of the cell suspension was transferred to a FACS tube and 5 μL of propidium iodide (PI) (1 mg/ml in 0.1% of sodium azide in water) (Sigma-Aldrich, Inc., St. Louis) and EDTA (5 μL at 0.123 M). A minimum of 20.000 events were acquired using a BD Accuri C6 (San Jose, USA) flow cytometer in the channels forward scatter (FSC), side scatter (SSC) and fluorescence channel-3 (FL3, for PI) and the data was analyzed with the BD Accuri software. In the FSC/FL3 contour plot, three regions were created, one corresponding to viable cells (R1), another to dead cells (R2) and a third to an indeterminate cell population between the other two regions (R3) excluding debris that were not considered in the analysis (data not shown). The percentage of viable cells is represented by the percentage of cells in the R1 region as compared to the total number of events in all three regions. 5-FU was used as positive control and untreated cells were used as negative control. Each experiment was performed in quadruplicate and independently repeated at least 2 times.

4.2.2.6 Statistical analysis

The data is expressed as mean ± standard deviation (SD) in MTT, *E-screening* and flow cytometry assays. Comparison among group was performed by using the *t*-Student test (two groups) and one-way ANOVA (three groups) followed by Bonferroni *post hoc* tests to determine statistically significant differences among the means. Difference between groups was considered statistically significant for a *p*-value lower than 0.05 ($p < 0.05$). The determination of IC_{50} was done by sigmoidal fitting analysis considering a confidence level of 95%.

4.2.3 In silico studies

4.2.3.1 Molecular docking

4.2.3.1.1 Preparation of the macromolecules

The three-dimensional (3D) structural coordinates of ERα (PDB#1A52) (Tanenbaum et al. 1998), 17β-HSD1 (PDB#3KLM) (Aka et al. 2010), aromatase (PDB#3EQM) (Ghosh et al. 2009), CYP17A1 (PDB#3RUK) (DeVore and Scott 2012) and AR (PDB#2AMA) (Pereira de Jésus-Tran et al. 2006) were obtained from PDB (www.rcsb.org). The coordinates of the ligands co-crystallized and water molecules were removed using the software Chimera (v 1.10.1) and the final structures were saved in .pdb format. The non-polar hydrogen atoms were merged in AutoDock Tools (v. 1.5.6) and the Kollman and Gasteiger partial charges were added using the same software. Finally, the prepared structures were converted to .pdbqt format for further use in the docking study.

4.2.3.1.2 Preparation of ligands

The studied ligands were drawn in ChemDraw (v. 12.0) software, followed by energy minimization and geometry optimizations in Chem3D (v. 12.0) software (Cambridge ChemBioOffice 2010). The obtained structure was prepared for docking in Chimera (v. 1.10.1), saved in .pdb format and converted into pdbqt format in AutoDock Tools.

4.2.3.1.3 Grid parameters

AutoDock grid maps were calculated for each macromolecule based on the coordinates of their active site. The size of all grid boxes was 20 x 20 x 20 with 1.0 Å of spacing and centered in the following coordinates: for ERα, the coordinates were x=107.27, y=13.94, z=96.38; for 17β-HSD1 were x=11.643, y=9.297, z=-11.887; for aromatase were x=86.071, y=54.241, z=46.085; for CYP17A1 were x=27.256, y=-0.978, z=33.104, and for AR were x=27.603, y=1.834, z=4.722.7.

4.2.3.1.4 Molecular docking simulations

Molecular docking studies were performed using AutoDock vina executable, which uses an iterated local search global optimizer (Trott and Olson 2010). The parameter exhaustiveness of performed experiments was defined as 15. The obtained results from these docking simulations were visualized and analyzed in Discovery Studio Visualizer software (BIOVIA). To validate the methodology used, a re-docking with the co-crystalized ligand present in the crystal structures was performed and the root-mean-

square deviation (RMSD) values obtained between ligand conformations (docked ligand and crystallized ligand) was less than 2.0 Å, validating the approach used.

4.2.3.2 Prediction of pharmacokinetic and toxicity properties

ChemBioDraw 13.0 software was used to draw the structure of 10β-hydroxyestra-1,4-diene-3,17-dione and then the SMILES notation was obtained and used to predict the parameters of Lipinski's rule of five, pharmacokinetic and toxicity properties in pkCSM online software (available from http://bleoberis.bioc.cam.ac.uk/pkcsm/prediction) (Pires et al. 2015).

4.3 Results and discussion

The cytotoxic effects of **HEDD** were only barely studied and therefore, this work was designed to improve the current knowledge of its bioactivity and potential toxicity. **HEDD** (compound **4.1**) was prepared by our research group by the general synthetic procedure described in **scheme 4.1** and was structurally characterized by spectral analysis (IR, ^{1}H- and ^{13}C-NMR). In the present work we used potassium permanganate to prepare this product in relatively good yields and in a short time, similarly to which was previously described (Lista et al. 2006).

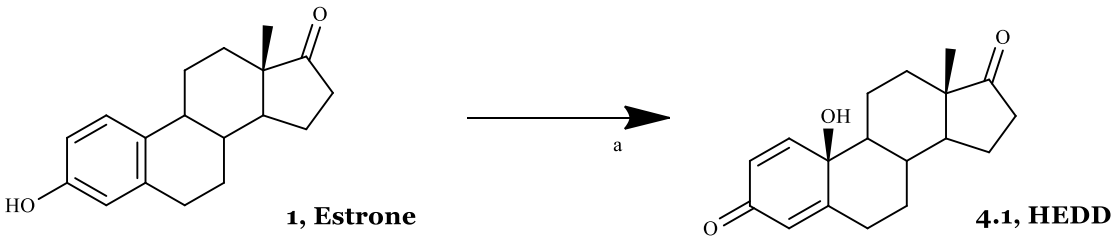

1, Estrone **4.1, HEDD**

Scheme 4.1 Synthetic route to prepare quinol **HEDD**, compound **4.1**. a) Reagents and conditions: $KMnO_4$, HCl, ethyl acetate, room temperature.

Using the 3-(4,5-dimethylthiazol-2-yl)-2,5-diphenyltetrazolium bromide (MTT) colorimetric assay, a first screening at 30 μM showed a very high cytotoxicity of **HEDD** in all cell lines [breast (MCF-7 and T47-D), prostate (LNCaP), hepatic (HepaRG), colon (Caco-2) and normal human dermal fibroblasts (NHDF)] tested (**Figure 4.1**). Then, a relevant anti-proliferative effect was observed for **HEDD** (IC_{50} values ranging from 4.11 to 18.64 μM) (**Table 4.1**) when compared with the parent compound, estrone (IC_{50} values between 29.53 and 61.82 μM).

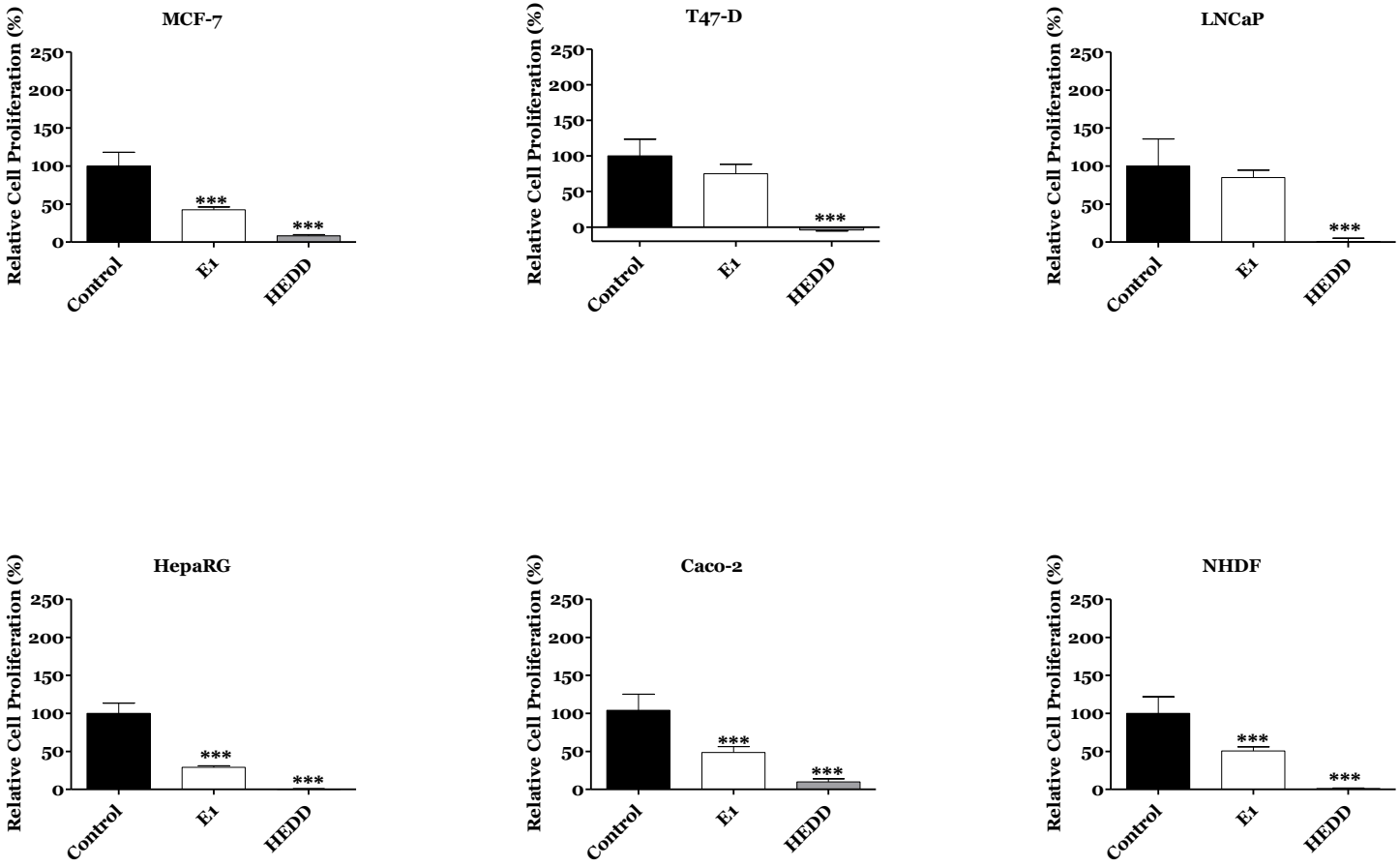

Figure 4.1 Relative cell proliferation screening assay. MCF-7, T47-D, LNCaP, HepaRG, Caco-2 and NHDF cells were treated with estrone (E1) or **HEDD** for 72 h at 30 µM, and relative viable cell number determined by the MTT assay, spectrophotometrically quantifying formazan at 570 nm. Data are expressed as a percentage of cell proliferation relative to the negative control (untreated cells) and are indicated as means ± SD and are representative of at least two independent experiments. ***$p < 0.001$ *vs* control (Student t-test).

Table 4.1 Estimated IC_{50} values (μM) for **HEDD** in breast (MCF-7, T47-D), prostate (LNCaP), hepatic (HepaRG), colon (Caco-2) cancer cells and normal dermal NHDF cells[a].

Compounds	MCF-7	T47-D	LNCaP	HepaRG	Caco-2	NHDF
E1	41.93	ND	ND	29.53	42.69	61.82
HEDD	5.79	7.72	4.11	10.68	18.64	12.57
5-FU	1.71	0.54	7.79	1.78	1.31	3.61

[a]Cells were treated with different concentrations (0.1, 1, 10, 25, 50 and 100 μM) during 72 h. The cell proliferation effects were determined by the MTT assay. The data shown are representative of at least two independent experiments. 5-FU: 5-fluorouracil; ND: not determined.

These results are new and very interesting because no relevant cytotoxicity (IC_{50} > 100 μM) was observed by Milic *et al.* (Milić et al. 2001). Our results also evidenced that **HEDD** has higher cytotoxicity against hormone-dependent cancer cells. Hepatic and colon cancer cells were less affected by this compound, as well as NHDF cells. In this context, it is important to mention that estrone can be converted, particularly in the liver, into the corresponding quinol **4.1** by CYP1A1, CYP2B6 and CYP2E1 isoenzymes (Ohe et al. 2000), which reinforces the importance of study its cytotoxic effect in hepatic cells. The selectivity index (SI) for **HEDD** (**Table 4.2**) was higher in LNCaP cells (SI > 3).

Table 4.2 Selectivity index[a] of estrone (E1), **HEDD** and 5-Fluorouracil (5-FU).

Compounds	MCF-7	T47-D	LNCaP	HepaRG	Caco-2
E1	1.47	ND	ND	2.09	1.45
HEDD	2.18	1.63	3.06	1.18	0.67
5-FU	2.11	0.49	0.46	2.03	2.76

[a]Selectivity index is the ratio of the IC_{50} values of the treatments of non-tumoral cells (NHDF) and tumoral cells (MCF-7, T47-D, LNCaP, HepaRG and Caco-2); ND: not determined.

Additionally, **HEDD** did not exhibit a proliferative action for 0.001 and 0.01 μM concentrations in *E-screening* assay (**Figure 4.2**).

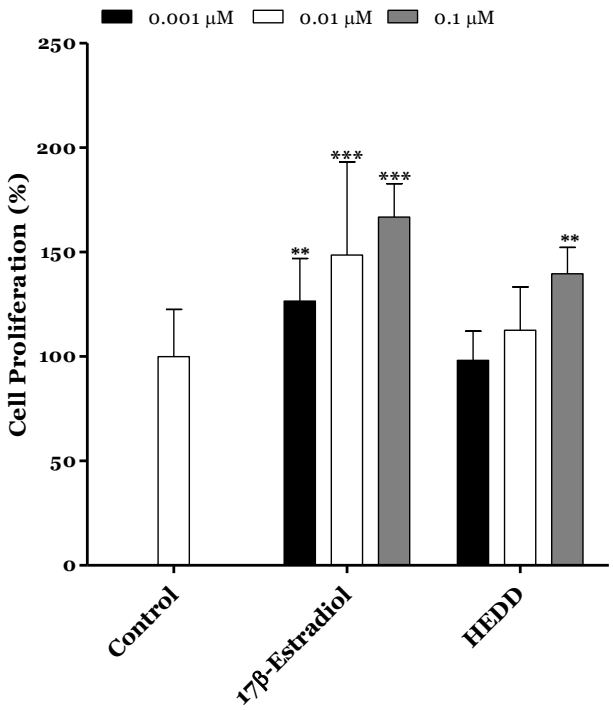

Figure 4.2 Proliferation of estrogen-sensitive T47-D cells after treatment with 17β-estradiol and **HEDD** for 24 h. Each bar represents the mean ± SD (originated from one experiment). $^{**}p < 0.01$ *vs* control; $^{***}p < 0.001$ *vs* control (one way ANOVA post-hoc Bonferroni test).

Therefore, it can be considered that this compound in low concentrations has probably reduced or null estrogenic effects, similarly to which was previously demonstrated for DHED and other analogues (Prokai-Tatrai and Prokai 2019). A flow cytometry assay using propidium iodide evidenced that **HEDD** led to a drastic reduction (approximately 83% after 24 h of treatment at 50 µM) of HepaRG cells viability (**Figure 4.3**). Consequently, no further studies have been done to explore the effects of **HEDD** on the cell cycle.

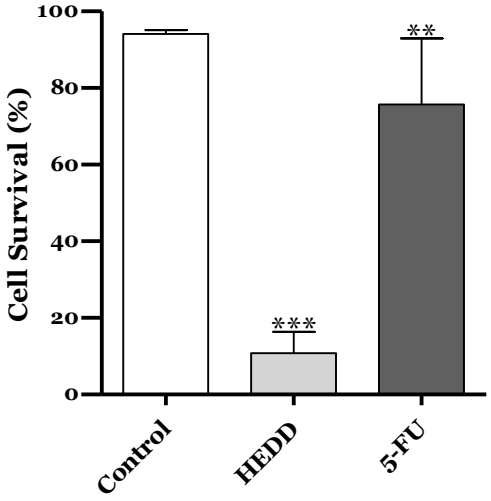

Figure 4.3 Cell viability assay. Percentage of HepaRG viable cells after 24 h treatment with 50 μM of **HEDD** was evaluated through propidium iodide staining by flow cytometry. Control corresponds to untreated cells and 5-Fluorouracil (5-FU, 50 μM) was used for comparison. The percentage of viability is the percentage of cells in R1 (live cells) as compared to the total number of events in R1, R2 (dead cells) and R3 (intermediate region of cells of undetermined state). Each bar represents the mean ± SD (originated from two independent experiments). $^{**}p < 0.01$ *vs* control; $^{***}p < 0.001$ *vs* control (one way ANOVA post-hoc Bonferroni test).

ERα, AR, 17β-HSD1, aromatase and CYP17A1 were included in this study because **HEDD** was more active against hormone-dependent cancer cells (Payne and Hales 2004; Amelichev et al. 2011; Hong and Chen 2011). These results are displayed in **Table 4.3**.

Table 4.3 Predicted lowest energies of **HEDD** (kcal.mol^{-1}) calculated in the molecular docking simulations, with vina executable, against well-known protein targets of steroid compounds: estrogen receptor α (ERα), 17β-hydroxysteroid dehydrogenase type 1 (17β-HSD1), aromatase (CYP19A1), 17α-hydroxylase/17,20-lyase (CYP17A1) and androgen receptor (AR). Binding energies of co-crystallized ligands were determined by re-docking the ligand structure and the respective macromolecule.

Compounds	Lowest energy (kcal.mol^{-1})				
	ERα	**17β-HSD1**	**Aromatase**	**CYP17A1**	**AR**
HEDD	-10.1	-8.8	-8.3	-9.0	-6.7
17β-Estradiol	-9.9	-	-	-	-
5α-Dihydrotestosterone	-	-8.3	-	-	-11.2
Androstenedione	-	-	-10.1	-	-
Abiraterone	-	-	-	-10.2	-

Interestingly, higher binding energy and potential stronger interaction for ERα and 17β-HSD1 proteins were predicted for **HEDD (Figures 4.4** and **4.5)**. Concerning ERα, **HEDD** shares with 17β-estradiol some hydrophobic interactions, involving particularly the residues Leu387, Met388, Leu391 and Phe404. However, the conventional hydrogen bonds with the residues Glu353 and His524 are absent (Fukuzawa et al. 2006). Instead, Van der Waals interactions with these residues and a

hydrogen bond with the amino acid Arg394 were predicted. When merging the docked 3D structures of 17β-estradiol and **HEDD**, it is possible to verify that these molecules are partially overlapped. The evaluation of **HEDD** binding mode with 17β-HSD1 also showed similar atomic interactions with the observed for DHT, the co-crystallized ligand, including hydrophobic interactions with the residues Val143, Leu149 and Pro187. However, when comparing the binding modes of both ligands, **HEDD** does not interact by a hydrogen bond with the essential amino acid His221 forming instead two hydrogen bonds with the residues Tyr218 and Ser222 (Day et al. 2008).

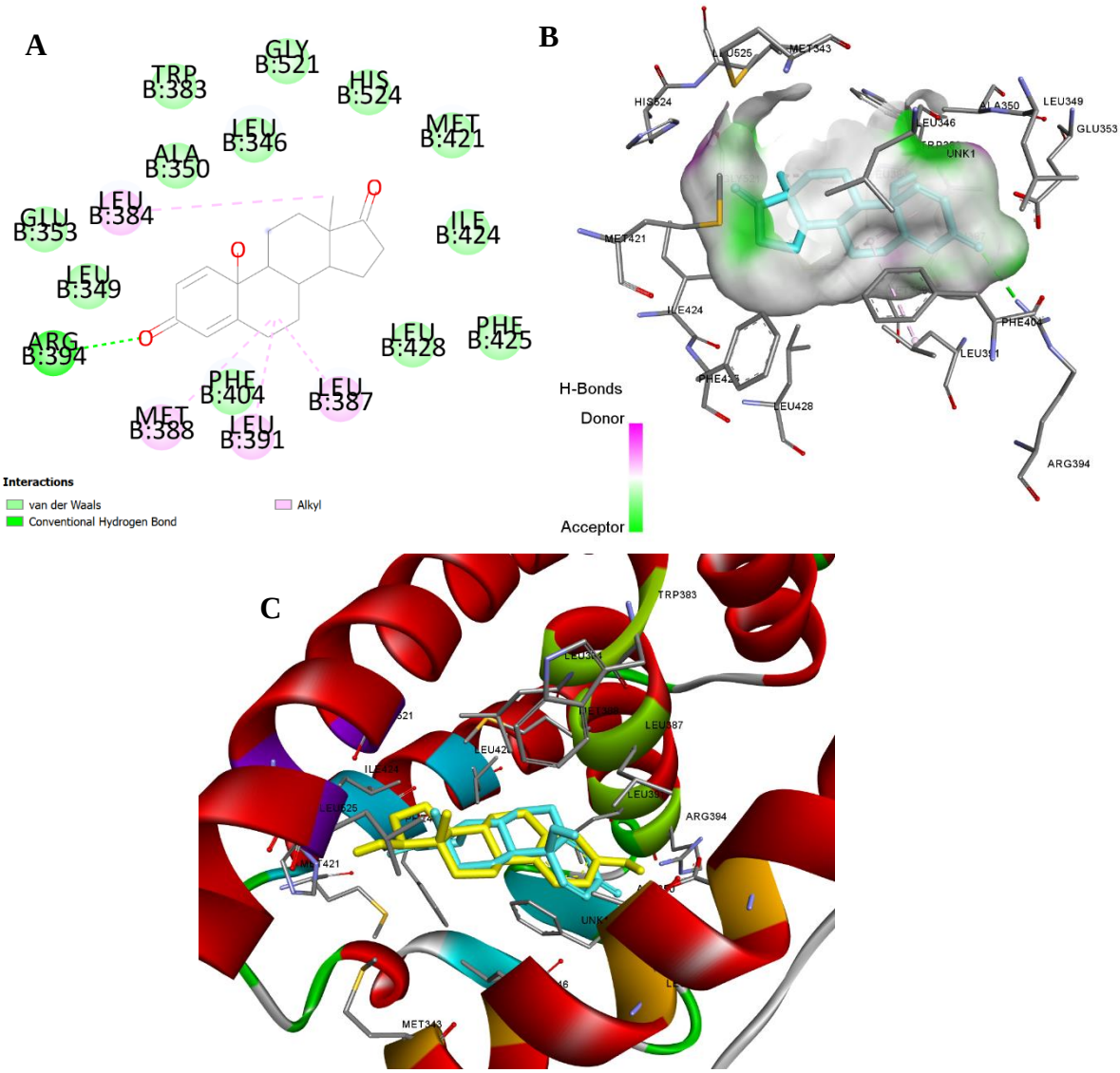

Figure 4.4 Analysis of predicted ERα binding mode for **HEDD** in 2D and in 3D representations. (**A** and **B**) Van der Waals interactions are displayed in light green, conventional hydrogen bound in green and alkyl interaction are displayed in pink. All contact and hydrogen bonds are shown as dotted lines and represented with same colors described. The H-bond surface diagram displays at green the areas containing H-bond acceptors and at pink H-bond donors. (**C**) 3D representation of overlapping of the co-crystallized ligand, 17β-estradiol (in yellow), and compound **4.1** (in turquoise) in the macromolecule binding pocket.

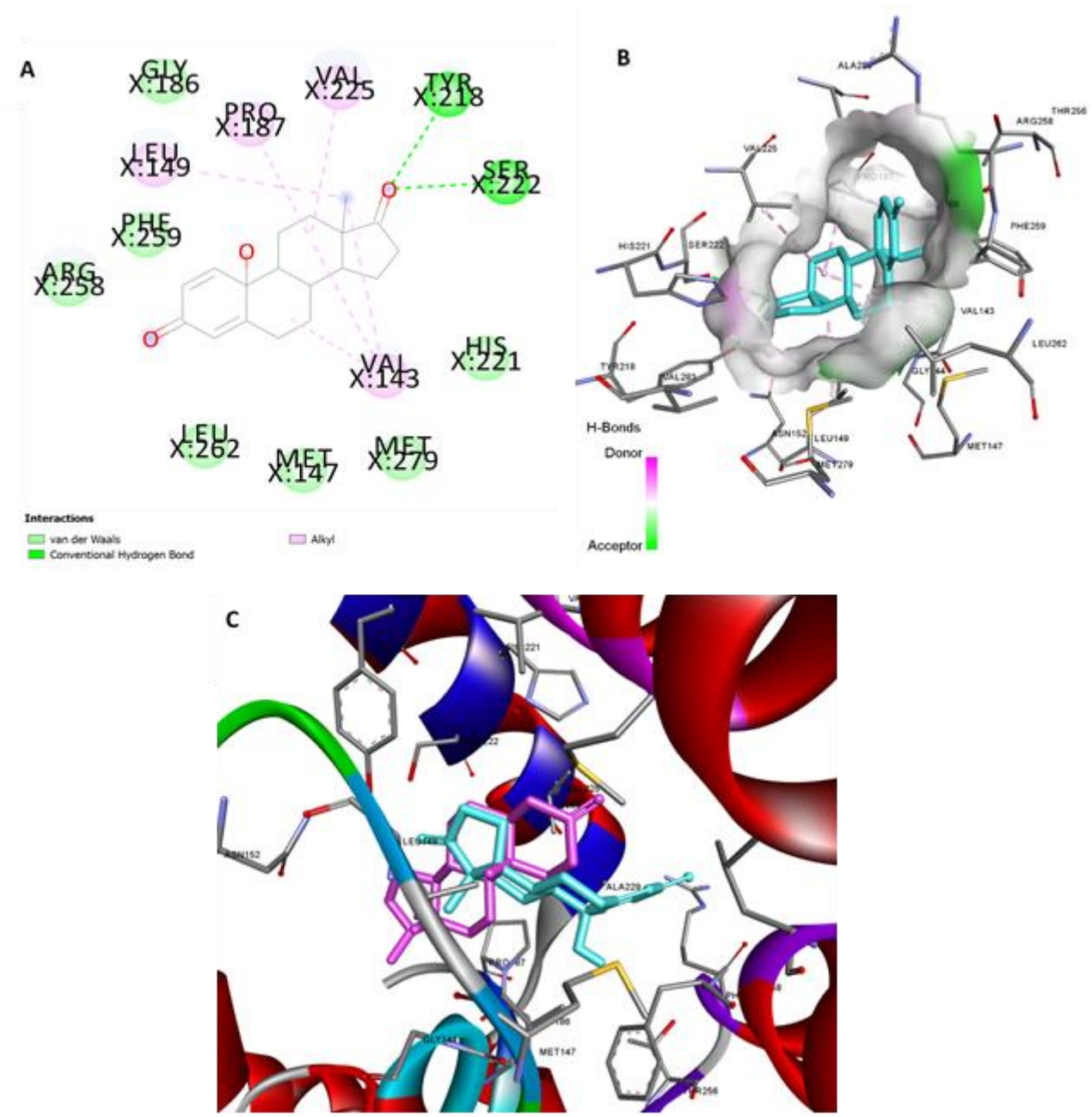

Figure 4.5 Predicted 17β-HSD1 binding mode for **HEDD** in 2D and in 3D representations. (**A** and **B**) Van der Waals interactions are displayed in light green, conventional hydrogen bound in green and alkyl interaction are displayed in pink. All contact and hydrogen bonds are shown as dotted lines and represented with same colors described. The H-bond surface diagram displays at green the areas containing H-bond acceptors and at pink H-bond donors. (**C**) 3D representation of overlapping of the co-crystallized ligand, DHT (in pink), and compound **4.1** (in turquoise) in the macromolecule binding pocket.

Also, an *in silico* evaluation of drug-likeness properties, specifically the Lipinski's rule of five, and a prediction of the ADMET properties were performed for the tested compound (**Table 4.4** and **Table 4.5).**

Table 4.4 Calculated molecular properties by pkCSM online software for **HEDD.**

Compound	log$P_{o/w}$	MW	HBA	HBD	RB
HEDD	2.59	286.37	3	1	0

log$P_{o/w}$, *n*-octanol-water partition coefficient; MW, the molecular weight; HBA, the number of hydrogen bond acceptors; HBD, hydrogen bond donors and RB, routable bonds.

Table 4.5 Predicted pharmacokinetic and toxicity properties by pkCSM online software for **HEDD.**

	Model Name	HEDD	Software criteria
Absorption	Caco2 permeability (log P_{app} in 10^{-6} cm/s)	1.25	> 0.90 → high Caco-2 permeability
	Intestinal absorption (% Absorbed)	97.56	< 30% → poorly absorbed
	P-glycoprotein substrate	No	
	P-glycoprotein I inhibitor	No	
	P-glycoprotein II inhibitor	No	
Distribution	BBB permeability	-0.08	> 0.3 → crosses the blood-brain barrier < −1 → poorly distributed to the brain
	CNS permeability	-2.82	> -2 → penetrates the CNS < -3 → unable to penetrate the CNS
Metabolism	CYP2D6 substrate	No	
	CYP3A4 substrate	Yes	
	CYP1A2 inhibitor	No	
	CYP2C19 inhibitor	No	
	CYP2C9 inhibitor	No	
	CYP2D6 inhibitor	No	
	CYP3A4 inhibitor	No	
Excretion	Renal organic cation transporter (OCT) 2 substrate	No	
Toxicity	AMES toxicity	No	
	Max. tolerated dose (log mg/kg/d)	-0.66	≤ 0.48 → low, 0.48 → high.
	Human Ether-à-go-go-Related Gene (hERG) I inhibitor	No	
	hERG II inhibitor	No	
	Hepatotoxicity	No	

The Ames test is a method to test whether a given chemical can cause mutations in the DNA.

The results showed a high Caco-2 permeability; high intestinal absorption; not be a P-glycoprotein substrate or inhibitor; not interact with the renal protein organic cation transporter 2 (OCT2); low probability to penetrate into the CNS; be a substrate of CYP3A4 isoform and low maximum tolerated dose in humans.

4.4 Conclusion

The anticancer potential of the quinol **HEDD** had been rarely explored and in this study was evaluated the *in vitro* cytotoxic properties of this compound. Interestingly, **HEDD** showed significant antiproliferative effects, mainly against hormone-dependent (MCF-7, T47-D and LNCaP) cancer cells. Furthermore, this steroidal quinol caused a drastic reduction in the hepatic HepaRG cell viability and did not promote the proliferation of estrogen-sensitive T47-D cells at low concentrations. *In silico* studies suggested strong interactions with ERα and 17β-HSD1 and a relatively low maximum tolerated dose, relevant data to be considered in future studies involving this compound.

Chapter 5
Oxime estrone derivatives

The content of this chapter is included in the following article:

Canário C, Matias M, Brito V, Santos AO, Falcão A, Silvestre S, Alves G. 2021. New Estrone Oxime Derivatives: Synthesis, Cytotoxic Evaluation and Docking Studies. Molecules. 26(9): e2687.

5.1 Introduction

Cancer is a major public health problem and is one of the leading causes of death worldwide (Siegel et al. 2020). Therefore, over the years, medicinal chemists and other researchers have been working in the development of new drugs with antitumor activity, namely starting from molecules that already exist in nature (Guo 2017). In this context, steroids are natural compounds that are usually involved in cell proliferation and consequently in cancer development (Sutherland et al. 1995). In the 90s, several steroids having very unusual and interesting structures were isolated from marine sponges. Among these, steroidal oximes isolated by Rodriguez *et al.* (Rodriguez et al. 1997) from *Cinachyrella* sponges showed relevant antiproliferative activity against several types of cancer cells (Deive et al. 2001). The interesting results observed in these studies stimulated researchers to prepare different series of steroidal oximes with potential anticancer interest. Classically, the oxime functional group is usually introduced by condensation of an aldehyde or a ketone, including of steroidal origin, with hydroxylamine affording, respectively, aldoximes and ketoximes (Ãbele and Lukevics 2000).

Among the different groups of steroidal oximes developed as anticancer agents, several of them have endocrine activity, acting by inhibition of steroid sulfatase (ST), aromatase, 17α-hydroxylase-17,20-lyase (CYP17A1), 5α-reductase (5α-R) or 17β-hydroxysteroid dehydrogenase type 1 (17β-HSD1) enzymes (Hejaz et al. 1999; Hartmann et al. 2000; Fischer et al. 2005; Allan et al. 2006; Pokhrel and Ma 2011; Canário et al. 2018). ST converts estrone sulfate into estrone (E1) and therefore its inhibition can be of interest in breast cancer treatment. In this context, Hejaz and co-workers (Hejaz et al. 1999) synthesized the estrone oxime sulfamate (OMATE), which inhibited the ST enzyme and showed a potency similar to the observed with the ketone analogue estrone sulfamate (EMATE). Later, modified 2-substituted estrogen-3-*O*-sulfamate 17-oximes have also been prepared and showed significant antiproliferative activity against breast MCF-7 cells (Leese et al. 2005). 17β-HSD type 1 enzyme reduce the 17-ketone of estrane steroids to the corresponding 17β-hydroxylated derivatives (Payne and Hales 2004). Relevant 17β-HSD1 inhibition was also demonstrated by Allan *et al* for 16-oxime and 6,17-oximes of E1 (% inhibition = 96% and 83%, respectively, at 10 μM) (Fischer et al. 2005; Allan et al. 2006). Interestingly, docking studies performed by these authors showed that both the presence of 16 and 17-oximes were associated to an improved 17β-HSD1 inhibition (Allan et al. 2006). Also, estrone (E1)-16-oxime ethers showed antiproliferative activities against cervix (HeLa), ovarian (A2780), MCF-7 and epidermoid (A431) cancer cell lines, promoted an apoptotic cell death and modulated the cell cycle progression (arrest at phase G_1) (Berényi et al.

2013). Estrogen receptor (ER), which is a transcription factor, was also involved in cell proliferation. Wendlandt *et al* (Wendlandt et al. 2010) showed that oxime estrogen dimers are able to effectively enter cells and modulate ERα-mediated genomic signaling. Otherwise, 2-methoxyestradiol (2ME2) is a naturally occurring E2 derivative with antitumor and antiangiogenic properties, acting through the binding to β-tubulin near the colchicine-binding site. In fact, 2ME2 inhibited microtubule polymerization and induced mitotic arrest (Cushman et al. 1995; Lao et al. 2017).

In another series of steroids, pregnenolone 20-oxime derivatives showed relevant activity as CYP17A1 and 5α-R enzyme inhibitors (Haidar et al. 2001; Kim and Ma 2009; Choudhary et al. 2011; Kim et al. 2012). The introduction of an oxime group at C6 in androstane series was explored in the development of aromatase inhibitors (Holland et al. 1992).

Concerning antiproliferative assays, previous studies showed that the presence of oximes in the steroid scaffold originated compounds with relevant potential anticancer interest. For example, 6*E*-hydroxyimino cholest-4-ene derivatives isolated from marine sponges showed relevant antiproliferative activities against several types of cancer cells (Rodriguez et al. 1997; Deive et al. 2001). Later, Cushman *et al.* developed several 2ME2 analogues with cancer cell growth and tubulin polymerization inhibitory effects. This series of compounds included 2-(2´,2´,2´-trifluoroethoxy)- and 2-ethoxy-6-oxoestradiol as well as their corresponding oximes, which have clearly higher antiproliferative effects than the ketone analogues in several cancer cell lines, including breast, prostate and colon tumoral cells. In addition, these compounds also inhibited tubulin polymerization and have low binding affinities to ERα (Cushman et al. 1995; Cushman et al. 1997). In estrane steroids, Rzheznikov and co-workers (Rzheznikov et al. 2003) synthesized 9α-hydroxy,11β-nitrooxyestrone-17-oxime and evidenced *in vivo* its antitumor effect against breast cancers. However, when compared with the corresponding 17-ketone analogue, the presence of the oxime group seems to have low influence in this activity. In addition, these two compounds stimulated the tumor growth by the end of a 15-day treatment course, possibly due to their estrogenic effects (Rzheznikov et al. 2003). Concerning substituted oximes, a large number of estrone-16-oxime ethers were synthesized and their antiproliferative effects were *in vitro* evaluated against several cell lines. Of these, among other compounds, interesting results were observed for 3-benzyloxy-16-propionyloximino-13α-methylestrone and 3-(4-methoxybenzyloxy)-16-methoximinoestrone as well as for the unsubstituted oximes 16-oximinoestrone and 3-sulfamoyloxy-16-oximinoestrone (Berényi et al. 2013). Sánchez-Sánchez *et al.* (Sánchez-Sánchez et al. 2016) also evidenced the antitumor effects of steroidal sapogenin oximes on HeLa cell lines and showed that the antiproliferative

activity was 2.3–2.8 times higher than the observed with diosgenin. More recently, C20 oxime ester derivatives were prepared from 16-dehydropregnenolone acetate and showed cytotoxicity against leukemia (NB4), prostate (PC-3) and HeLa cancer cells (Tang et al. 2019).

In view of the therapeutic importance of steroidal oximes, and considering our interest in developing modified estrane derivatives as anticancer agents (Canário et al. 2018; Canário et al. 2020), the present study focuses on the synthesis and antiproliferative evaluation of new E1 derivatives bearing an oxime group at C17. Their cytotoxic activities were tested using breast (MCF-7, T47D), prostate (LNCaP), liver (HepaRG), colon (Caco-2) and normal fibroblast (NHDF) cell lines. For the most promising compounds the IC_{50} was determined and then an estrogenicity assay, cell cycle analysis by flow cytometry after propidium iodide staining and fluorescence microscopy using Hoechst 33258 were performed. Molecular docking studies against the ERα, ST, 17β-HSD1 and β-tubulin were also accomplished.

5.2 Experimental Section

5.2.1 Chemistry

All chemicals received from suppliers were used without further purification. The following reagents were purchased from: E1: Cayman Chemical (Ann Arbor, MI, USA); hydroxylamine hydrochloride: Fluka (Buchs, Switzerland); methanol (MeOH): Fisher Chemical (Hampton, MA, USA); *N*-bromosuccinimide (NBS): (Alfa Aesar, Haverhill, MS, USA); ethanol (EtOH) 99.9%: Manuel Vieira & C^{a} (Torres Novas, Portugal). In addition, 2,3-dichloro-5,6-dicyano-*p*-benzoquinone (DDQ), morpholine, 17β-estradiol (E2), and dimethyl sulfoxide (DMSO) as well as the remaining chemical products referred in the text were obtained from Sigma-Aldrich (St. Louis, MO, USA). Deuterated DMSO (DMSO-d_6) and deuterated chloroform ($CDCl_3$) were purchased from Armar Chemicals (Leipzig, Germany). All reactions were monitored by thin layer chromatography (TLC) using Al-backed aluminum/silica gel plate 0.20 mm (Macherey-Nagel 60 F254, Duren, Germany). After elution, plates were visualized in a CN-15.LC UV chamber under ultraviolet (UV) radiation (254 nm). Then, the EtOH/concentrated sulfuric acid (95:5, v:v) solution was used, followed by heating at 120 °C, to reveal the plates. The evaporation of solvents was achieved by using a rotary vacuum drier from Büchi (R-215). Infrared (IR) spectra were collected on a Thermoscientific Nicolet iS10 equipped with a diamond attenuated total reflectance crystal at room temperature in the 4000-400 cm^{-1} range by averaging 16 scans at a spectral resolution of 2 cm^{-1}. Nuclear magnetic resonance (NMR) spectra (^{1}H-NMR and ^{13}C-NMR) were acquired on

a Bruker Avance 400 MHz spectrometer and were processed with the software TOPSPIN 4.07 (Bruker, Fitchburg, WI, USA). Chemical shifts are reported in parts per million (ppm) relative to tetramethylsilane (TMS) or solvent as an internal standard. Coupling constants (*J* values) are reported in hertz (Hz) and splitting multiplicities are described as s=singlet; brs=broad singlet; d=doublet and dd=double doublet. High resolution mass spectrometry (ESI-HRMS) was performed by the microanalysis service on a QSTAR XL instrument (Salamanca, Spain).

*5.2.1.1 Procedures for the synthesis of intermediates – compounds **2.1**, **2.3**, **2.5** and **5.2-5.3**.*

The intermediates **2.1, 2.3** and **2.5** were synthesized and structurally characterized as previously described (Canário et al. 2020).

*5.2.1.1.1 Synthesis of 3-hydroxy-2-nitroestra-1,3,5(10)-trien-17-one (**5.2**) and 3-hydroxy-2,4-dinitroestra-1,3,5(10)-trien-17-one (**5.3**)*

E1 (541 mg, 2 mmol) was added to 16.3 ml of glacial acetic acid and the mixture was vigorous stirred at 50ºC. Then, a solution of nitric acid 70% (178 µl) in glacial acetic acid (540.6 µl) was added dropwise and the mixture was stirred at room temperature for 48 h. After completion (TLC control), the reaction mixture was diluted in 150 mL of ethyl acetate and the resulting solution was washed with 50 mL of saturated NaCl solution, 50 mL of saturated $NaHCO_3$ solution and 50 mL of H_2O. Next, the solution was dried over anhydrous Na_2SO_4, filtered and concentrated under reduced pressure to yield the crude product, which was purified by column chromatography (eluent: gradient of ethyl acetate (EA)/petroleum ether (PE) 40 - 60 ˚C, 1:3; 1:1 and 3:1) to give compound **5.2** as yellow solid (261 mg, 41%) and compound **5.3** as orange solid (341 mg, 47%) (Stubenrauch and Knuppen 1976; Santaniello et al. 1983; Bose et al. 2007).

*5.2.1.1.2 3-Hydroxy-2-nitroestra-1,3,5(10)-trien-17-one (**5.2**)*

IR (υ_{max}/cm^{-1}): 896, 1258, 1306, 1372, 1429, 1478, 1519, 1563, 1628, 1733, 2858-2932, 3040, 3295; ^{1}H-NMR (400 MHz, $CDCl_3$) δ: 0.89 (s, 3H, C18-CH_3), 6.84 (s, 1H, C4-H), 7.96 (d, 1H, *J* = 1.1 Hz, C1-H), 10.39 (s, 1H, OH); ^{13}C-NMR (100 MHz, $CDCl_3$) δ: 13.97, 21.75, 25.90, 26.10, 29.83, 31.47, 35.98, 37.93, 43.66, 48.02, 50.56, 119.18, 121.77, 131.98, 133.31, 149.00, 153.12, 220.37.

*5.2.1.1.3 3-Hydroxy-2,4-dinitroestra-1,3,5(10)-trien-17-one (**5.3**)*

IR (υ_{max}/cm^{-1}): 902, 1246, 1376, 1455, 1532, 1571, 1629, 1729, 2872-2939, 3185; ^{1}H-NMR (400 MHz, $CDCl_3$) δ: 0.90 (s, 3H, C18-CH_3), 8.14 (d, 1H, *J* = 1.0 Hz, C1-H), 10.60

(s, 1H, OH); ^{13}C-NMR (100 MHz, $CDCl_3$) δ: 13.91, 21.64, 24.95, 25.06, 25.98, 31.33, 35.89, 37.21, 43.65, 47.85, 50.23, 122.87, 132.33, 133.72, 139.29, 141.87, 145.06, 219.76.

5.2.1.2 General procedure for the synthesis of oximes

To a solution of parent compound in EtOH (8.1 mL/1 mmol of parent compound) were added hydroxylamine hydrochloride (2.9 mmol), NaOH (2 mmol) and water (272 µL). The mixture was heated under reflux for 3 h and upon cooling poured into an aqueous solution of 1 N HCl (2.7 mL). The formed precipitate was filtered, washed with cold water, and air-dried to give the corresponding product. After, the solid was recrystallized using MeOH to afford the pure product (Hejaz et al. 1999). As compounds **5.5** and **5.8** did not precipitate after addition to HCl solution, the work up was performed as described below.

*5.2.1.2.1 Synthesis of 17-hydroxyiminoestra-1,3,5(10)-trien-3-ol (**5.1**)*

Compound **5.1** was prepared from compound **1** (270.37 mg, 1 mmol) to give white solid (265 mg; 93%). After recrystallization compound **5.1** was obtained as colorless crystals (Hejaz et al. 1999). IR (υ_{max}/cm^{-1}): 869, 918, 1151, 1237, 1283, 1348, 1373, 1460, 1497, 1583, 1618, 2868-2929, 3025, 3252, 3405; ^{1}H-NMR (400 MHz, DMSO-d_6) δ: 0.85 (s, 3H, C18-CH_3), 6.44 (d, 1H, J = 2.5 Hz, C4-H), 6.51 (dd, 1H, J_1 = 8.5 Hz, J_2 = 2.5 Hz, C2-H), 7.04 (d, 1H, J = 8.5 Hz, C1-H), 8.99 (brs, 1H, C3-OH), 10.08 (brs, 1H, NOH); ^{13}C-NMR (100 MHz, DMSO-d_6) δ: 17.32, 22.51, 24.89, 25.92, 26.84, 29.08, 34.27, 37.87, 43.36, 43.59, 52.49, 112.75, 114.94, 125.99, 130.15, 137.08, 154.96, 167.95.

*5.2.1.2.2 Synthesis of 17-hydroxyimino-2-nitroestra-1,3,5(10)-trien-3-ol (**5.4**)*

Compound **5.4** was prepared from compound **5.2** (157.68 mg, 0.5 mmol) to give a yellow solid (120 mg, 73%). After recrystallization from MeOH, compound **5.4** was obtained as yellow crystals. IR (υ_{max}/cm^{-1}): 927, 1017, 1095, 1259, 1298, 1373, 1433 1482, 1518, 1579, 1633, 2858-2961, 3283; ^{1}H-NMR (400 MHz, DMSO-d_6) δ: 0.85 (s, 3H, C18-CH_3), 6.83 (s, 1H, C4-H), 7.75 (s, 1H, C1-H), 10.11 (s, 1H, C3-OH), 10.54 (brs, 1H, NOH); ^{13}C-NMR (100 MHz, DMSO-d_6) δ: 17.21, 22.46, 24.87, 25.52, 26.11, 28.83, 33.97, 37.04, 42.86, 43.23, 52.34, 118.49, 121.45, 131.91, 134.07, 145.96, 150.25, 167.74. HRMS (ESI-TOF): *m/z* [M$^+$ + H] calcd for $C_{18}H_{22}N_2O_4$: 330.1580; found 330.1573.

*5.2.1.2.3 Synthesis of 17-hydroxyimino-2,4-dinitroestra-1,3,5(10)-trien-3-ol (**5.5**)*

Compound **5.5** was prepared from compound **5.3** (180.04 mg, 0.5 mmol). As the crude did not precipitate after the addition of HCl, the workup was performed in a different manner. For this, the reactional mixture was diluted in 100 mL of dichloromethane and washed with 50 mL of saturated NaCl solution, 50 mL of saturated $NaHCO_3$ solution

and 50 mL of H_2O, dried over anhydrous Na_2SO_4, filtered and concentrated under reduced pressure. For analysis and use in cell studies, a sample was recrystallized from MeOH to afford compound **5.5** as dark yellow crystals (130.7 mg, 73%). IR (υ_{max}/cm-1): 927, 1025, 1184, 1259, 1305, 1356, 1377, 1436, 1468, 1537, 1577, 1630, 2931, 3240, 3612; ^{1}H-NMR (400 MHz, DMSO-*d*$_6$) δ: 0.86 (s, 3H, C18-CH_3), 7.99 (s, 1H, C1-H), 10.12 (s, 1H, NOH); ^{13}C-NMR (100 MHz, DMSO-*d*$_6$) δ: 17.17, 22.39, 23.94, 24.85, 24.96, 25.43, 33.87, 36.14, 42.76, 43.17, 52.01, 122.79, 133.01, 135.25, 135.99, 141.98, 142.92, 167.62. HRMS (ESI-TOF): *m/z* [M^+ + H] calcd for $C_{18}H_{21}N_3O_6$: 375.1430; found 375.1424.

*5.2.1.2.4 Synthesis of 17-hydroxyimino-2,4-diiodooestra-1,3,5(10)-trien-3-ol (**5.6**)*

Compound **5.6** was prepared from compound **2.3** (99.06 mg, 0.19 mmol) to give a beige solid (69 mg, 34%). IR (υ_{max}/cm^{-1}): 800, 926, 1027, 1098, 1170, 1262, 1293, 1327, 1388, 1450, 2864-2927, 3270, 3451; ^{1}H-NMR (400 MHz, $CDCl_3$) δ: 0.94 (s, 3H, C18-CH_3), 7.59 (s, 1H, C1-H); ^{13}C-NMR (100 MHz, $CDCl_3$) δ: 17.23, 23.02, 25.75, 26.63, 28.13, 33.95, 37.28, 37.29, 44.01, 44.54, 52.88, 78.57, 92.24, 136.01, 136.28, 140.82, 151.64, 172.12. HRMS (ESI-TOF): *m/z* [M^+ + H] calcd for $C_{18}H_{21}I_2NO_2$: 536.9662; found 536.9632.

*5.2.1.2.5 Synthesis of 17-hydroxyimino-3-hydroxyestra-1,3,5(10),9(11)-tetraen-3-ol (**5.7**)*

Compound **5.7** was obtained from compound **2.1** (67.1 mg, 0.25 mmol) to give a white solid (55.2 mg, 78%). IR (υ_{max}/cm^{-1}): 926, 1155, 1246, 1279, 1354, 1426, 1465, 1494, 1575, 1613, 1627, 2831-2956, 3020, 3342; ^{1}H-NMR (400 MHz, DMSO-*d*$_6$) δ: 0.86 (s, 3H, C18-CH_3), 6.06 (m, 1H, C11-H), 6.45 (d, 1H, *J* = 2.5 Hz, C4-H), 6.54 (dd, 1H, J_1 = 8.7 Hz, J_2 = 2.5 Hz, C2-H), 7.42 (d, 1H, J = 8.7, C1-H), 9.25 (br s, 1H, OH); 10.18 (br s, 1H, NOH). ^{13}C-NMR (100 MHz, DMSO-*d*$_6$) δ: 18.03, 23.56, 25.32, 27.98, 29.32, 36.89, 37.47, 41.59, 49.88, 113.86, 114.87, 116.04, 125.11, 125.29, 135.18, 137.18, 156.18, 168.05. HRMS (ESI-TOF): *m/z* [M^+ + H] calcd for $C_{18}H_{21}NO_2$: 283.1572; found 283.1564.

*5.2.1.2.6 Synthesis of 17-hydroxyimino-2,4-dibromo-3-hydroxyestra-1,3,5(10)-trien-3-ol (**5.8**)*

Compound **5.8** was obtained from compound **2.5** (107.4 mg, 0.25 mmol). As the crude did not precipitate after the addition of HCl, the workup was performed in a different manner. For this, the reactional mixture was diluted in 150 mL of dichloromethane and washed with 50 mL of HCl 5%, 50 mL of saturated NaCl solution and 50 mL of H_2O, dried over anhydrous Na_2SO_4, filtered and concentrated under reduced pressure to give a white solid **5.8** (95 mg, 86%). IR (υ_{max}/cm^{-1}): 799, 927, 1019, 1097, 1173, 1260, 1398,

1463, 2869-2961, 3273, 3486; ^{1}H-NMR (400 MHz, $CDCl_3$) δ: 0.93 (s, 3H, C18-CH_3), 7.38 (s, 1H, C1-H); ^{13}C-NMR (100 MHz, $CDCl_3$) δ: 17.28, 23.04, 25.55, 26.56, 27.36, 31.13, 33.98, 37.27, 44.10, 44.43, 52.92, 106.64, 113.43, 128.69, 135.41, 136.67, 147.43, 171.72. HRMS (ESI-TOF): *m/z* [M^+ + H] calcd for $C_{18}H_{21}Br_2NO_2$: 440.9939; found 440.9932.

5.2.2 Bioactivity assays

5.2.2.1 Cell culture

Breast (MCF-7, T47-D), prostatic (LNCaP) and colon (Caco-2) cancer cells as well as normal human dermal fibroblasts (NHDF) were obtained from American Type Culture Collection (ATCC; Manassas, VA, USA). The hepatic (HepaRG) cell line was acquired to Life Technologies – Invitrogen™ (through Alfagene, Portugal). They were cultured in 75 cm^2 culture flasks at 37 °C in a humidified air incubator with 5% CO_2. MCF-7 cells were maintained with high-glucose Dulbecco's modified Eagle medium (DMEM) supplemented with 10 % fetal bovine serum (FBS; Sigma-Aldrich, St Louis, MO, USA) and 1% antibiotic/antimycotic mixture (10000 units/mL penicillin G, 100 mg/mL streptomycin and 25 μg/mL amphotericin B) (Sigma-Aldrich, St Louis, MO, USA). High glucose DMEM supplemented with 10% FBS and 1% of the antibiotic mixture of 10000 units/mL penicillin G and 100 mg/mL of streptomycin (Sigma-Aldrich, St Louis, MO, USA) was used for Caco-2 cells. LNCaP and T47-D cells were cultured in RPMI 1640 medium with 10% FBS and 1% antibiotic mixture. NHDF cells grew in RPMI 1640 medium supplemented with 10% FBS, 2 mM *L*-glutamine, 10 mM HEPES, 1 mM sodium pyruvate and 1% antibiotic/antimycotic. Lastly, hepatic cells were seeded in Williams' E medium supplemented with 10% FBS, 1% antibiotic mixture, 5 μg/mL insulin, and 5 × 10^{-5} M hydrocortisone hemisuccinate (Sigma–Aldrich, St Louis, MO, USA).

5.2.2.2 Preparation of stock solutions

The stock solutions of compounds were prepared in DMSO at 10 mM and stored at 4-8 °C. From these, the different diluted solutions of compounds were prepared in the corresponding complete culture medium before each experiment. The maximum DMSO concentration in cell studies was 1%.

5.2.2.3 Antiproliferative activities against six cell lines

The antiproliferative effect of compounds was evaluated by the 3-(4,5-dimethylthiazol-2-yl)-2,5-diphenyltetrazolium bromide (MTT; Sigma-Aldrich, St Louis, MO, USA) assay

in MCF-7, T47-D, LNCaP, HepaRG, Caco-2 and NHDF cells. After reaching near confluence, cells were trypsinized and counted with a hemocytometer by means of the trypan-blue exclusion of dead cells. Then, 100 μL of cell suspension (2×10^4 cells/mL) was seeded in 96-well culture plates and left to adhere and growth during 48 h. After this period, the medium was replaced by solutions of the compounds in study (30 μM for screening assays and 0.1, 1, 10, 25, 50 and 100 μM for concentration-response studies) in the appropriate cell culture medium for approximately 72 h. Then, cells were washed with 100 μL of phosphate buffer saline (PBS; NaCl 137 mM, KCl 2.7 mM, Na_2HPO_4 10 mM and KH_2PO_4 1.8 mM, pH 7.4), and 100 μL of the MTT solution (5 mg/mL), prepared in the appropriate serum-free medium, was added to each well, followed by incubation for approximately 4 h at 37 ºC. Afterward, MTT containing medium was removed and formazan crystals were dissolved in DMSO. Absorbance was measured at 570 nm using a microplate reader Bio-rad Xmark spectrophotometer. After background subtraction, cell proliferation values were expressed as percentage relatively to the absorbance determined in negative control cells. Untreated cells were used as the negative control and the clinical drug 5-fluorouracil (5-FU) was used as positive control. Each experiment was performed in quadruplicate and independently repeated.

5.2.2.4 E-screening assay in T47-D cells

Breast T47-D cells (2×10^4 cells/mL; 100 μL) were seeded in 96-well culture plates in RPMI 1640 medium supplemented with 10% FBS and allowed to attach. After overnight incubation, the medium was replaced every 3 days with fresh phenol red free RPMI 1640 medium supplemented with 5% of dextran-coated charcoal-treated fetal calf serum (DCC-FCS) and containing compound **5.7** (0.1, 0.01 and 0.001 μM). After 6 days of exposure, the proliferation of T47-D cells was estimated by the MTT assay as described in the previous section. Each experiment was performed in quadruplicate and independently repeated. After background subtraction, cell proliferation values were expressed as percentage relatively to the absorbance determined in negative control cells.

5.2.2.5 Analysis of LNCaP cells viability by flow cytometry

The analysis of LNCaP cells viability was performed by flow cytometry after staining with propidium iodide (PI) (solution of PI 1 mg/ml in 0.1% of sodium azide and water; Sigma Aldrich, St Louis, MO, USA). Briefly, 3 mL of cells suspension were seeded in 6-well plates (5×10^4 cells/mL) in complete culture medium. After 48 h they were treated with 50 μM of compound **5.7**. Untreated cells were used as negative control and 5-FU (50 μM) was used as positive control. Each experiment was performed in duplicate and

independently repeated. At the end of 24 h of incubation, the supernatant of each well was collected, cells were harvested by trypsinization and pooled with the supernatants. The resulting cell suspension was kept on ice, pelleted by centrifugation and resuspended in 400 µL of complete medium. Afterwards, 395 µL of the cell suspension was transferred to a FACS tube and 5 µL of PI and 0.5 µL of ethylenediamine tetraacetic acid (EDTA, 0.123 M) were added. A minimum of 20000 events was acquired using a BD Accuri C6 (San Jose, CA, USA) flow cytometer in the channels forward scatter (FSC), side scatter (SSC) and fluorescence channel-3 (FL3, for PI). Acquisition and analysis were performed with BD Accuri Software. In the FSC/FL3 contour plot, three regions were created, one corresponding to viable cells (R1), another to dead cells (R2) and a third to an indeterminate cell population between the other two regions (R3) excluding debris that were not considered in the analysis (data not shown). The percentage of viability is the percentage of cells in R1 as compared to the total number of events in R1, R2 and R3.

5.2.2.6 Cell cycle distribution of LNCaP cells

After 24 h of treatment with compound **5.7** at 50 µM (6-well plates, 5×10^4 cells/mL), LNCaP cells were collected and washed with PBS and resuspended in 450 µL of a cold solution of 0.5% bovine serum albumin (BSA; Amresco, Solon, OH, USA) and 1 mM EDTA in PBS, followed by fixation with 70% EtOH and kept at -20 °C. Afterward, fixed cells were washed twice with PBS and resuspended in a solution of PI (50 µg/mL) prepared in 0.5% BSA and 1 mM EDTA in PBS and then incubated with Ribonuclease A from bovine pancreas at a final concentration of 0.5 µg/µL (solution in 50% glycerol, 10 mM Tris-HCl, pH 8; Sigma Aldrich, St Louis, MO, USA) for 15 min in the dark. For comparison, untreated cells were used as negative control and cells treated with 5-FU at 50 µM were used as positive control. Each experiment was performed in duplicate and independently repeated. A minimum of 10000 events was acquired using BD Accuri Software and analysis was performed by Modfit software (Becton Dickinson, San Jose, CA, USA).

5.2.2.7 Fluorescence microscopy in LNCaP cells after DNA staining

Near-confluent LNCaP cells were seeded in a 6-well plate (5×10^4 cells/mL). After adherence and incubation for 24 h with compound **5.7** (50 µM), the dye Hoechst 33258 was added to the culture medium to achieve a final concentration of 1µg/ml. The cells were incubated for 15 min at 37 °C and were then photographed by means of a Nikon Eclipse microscope equipped with a fluorescence attachment containing the appropriate optical blocks and a QCapture CCD camera. Apoptosis was revealed by nuclear changes such as chromatin condensation and nuclear fragmentation.

5.2.2.8 Data analysis

Data were expressed as mean ± standard deviation (SD). *t*-Student test (two groups) and one-way ANOVA (three groups) were used followed by Bonferroni *post hoc* tests to determine statistically significant differences among the means. Difference between groups was considered statistically significant for a *p*-value lower than 0.05 ($p < 0.05$). The determination of IC_{50} was performed by sigmoidal fitting analysis [log(inhibitor) vs. normalized response - Variable slope], considering a confidence level of 95%.

5.2.3 Molecular docking studies

5.2.3.1 Preparation of proteins for molecular docking

The crystal structures of ERα (PDB ID: 1A52), ST (PDB ID: 1P49), 17β-HSD1 (PDB ID: 3KLM) and β-tubulin (PDB ID: 1SA0) were retrieved from Protein Data Bank (Tanenbaum et al. 1998; Hernandez-Guzman et al. 2003; Ravelli et al. 2004; Aka et al. 2010). The coordinates of all non-standard residues, including the co-crystalized ligand, were deleted using the software Chimera (v. 1.10.1). Then, non-polar hydrogens were merged in AutoDockTools (v. 1.5.6) and Kollman and Gasteiger partial charges were added. Lastly, the prepared structure was converted from the PDB format to PDBQT for posterior use in the docking simulations.

5.2.3.2 Preparation of ligands

All ligands used in docking simulations were built using ChemDraw (v. 12.0) software. Energy minimization and geometry optimization of these molecules were performed in Chem3D (v. 12.0) and the obtained structures were saved as PDB file format. The process of energy minimization was applied in a range from -20 to -40 $kcal.mol^{-1}$. Then, the ligands were completely prepared for docking choosing torsions and the structures were converted into PDBQT format using the software AutoDockTools.

5.2.3.3 Grid parameters

The grid parameters were selected using AutoDock vina and AutoDockTools based on the coordinates of the co-crystalized ligand for each case: E2, *N*-acetyl-*D*-glucosamine, 5α-dihydrotestosterone (DHT) and colchicine, with the respective macromolecule. The grid box was centered on the ligand with the following coordinates: for ERα, the coordinates were x=107.27, y=13.94, z=96.38; for ST were x=62.033, y=-12.215, z=52.512; for 17β-HSD1 were x=11.643, y=9.297, z=-11.887; and for β-tubulin were x=118.921, y=89.718, z=5.932. The size of grid box was 20 x 20 x 20 with 1.0 Å of spacing.

5.2.3.4 Docking simulations

After the preparation of macromolecules and ligands, molecular docking simulations were performed using AutoDock vina executable (Meng et al. 2011), which uses an iterated local search global optimizer. The parameter exhaustiveness of performed experiments was defined as 15. The results of molecular docking were analyzed and visualized in Discovery Studio Visualizer program from BIOVIA software.

5.2.3.5 Validation of the molecular docking performance

Scoring functions are essential for molecular docking performance. In order to validate the docking performance of AutoDock vina, the difference between the real and best-scored conformations were analyzed by re-docking ERα with E2, ST with *N*-acetyl-*D*-glucosamine, 17β-HSD1 with DHT and β-tubulin with colchicine. Low root-mean-square distance (RMSD) values (< 2.0 Å) were obtained for all the four cases, which means that the docking process was reliable and validated (Carugo 2003).

5.3 Results and discussion

5.3.1 Chemistry

Six steroidal oximes in estrane series were synthesized as shown in **Scheme 5.1**, five of which for the first time (compounds **5.4-5.8**), to the best of our knowledge. All compounds were characterized by spectral analysis (IR, ^{1}H- and ^{13}C-NMR) and HRMS was also obtained for the new prepared steroidal oximes. All spectral data are in agreement with the presented structures. The NOH signal in ^{1}H-NMR appeared near 10 ppm. In ^{13}C-NMR spectra, the signal of C17-ketone appeared near 220 ppm and the C17-NOH near 168-172 ppm. The presence of $\Delta^{9,11}$ double bond (compounds **2.1** and **5.7**) was associated to the signal of C11-H that appeared at 6.06 in the ^{1}H-NMR spectrum (Stéphan et al. 1995).

The nitration reaction was performed as described by Stubenrauch *et al.* (Stubenrauch and Knuppen 1976), which was applied by these authors to obtain 2-nitroestrone **5.2**. However, as an excess of the nitrating agent was used, 2,4-dinitroestrone **5.3** was also formed and the mixture of products was separated by column chromatography. The yields of these nitro-steroids were similar to the previously described ones (Stubenrauch and Knuppen 1976). The introduction of halogens (compounds **2.3** and **2.5**) and of $\Delta^{9,11}$ double bond (compound **2.1**) were effected using methodologies already applied by us (Canário et al. 2020). Finally, for the preparation of oximes we selected a method involving the use of EtOH, NaOH and hydroxylamine hydrochloride (Hejaz et al. 1999) as this is a more selective and greener strategy than other

approaches that use, for example, pyridine (Rzheznikov et al. 2003). In fact, these methods involve more toxic reagents/solvents, are more time consuming, have complex workups and can lead to lower reaction yields (Saikia et al. 2011; Kim et al. 2013; Jadhav et al. 2018).

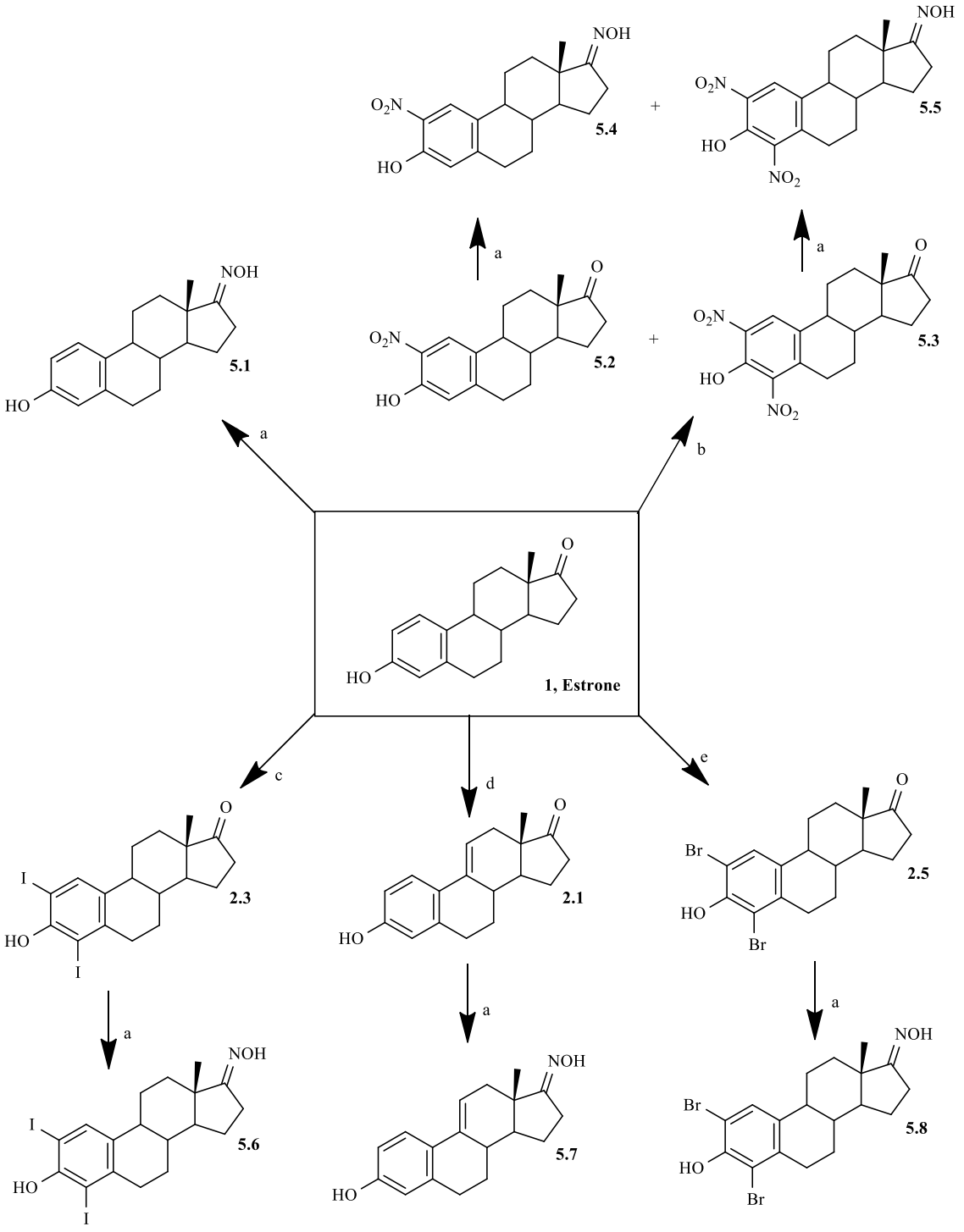

Scheme 5.1 Synthetic route to prepare estrone oxime derivatives. Reagents and conditions: (a) $NH_2OH{\cdot}HCl$, NaOH, EtOH, H_2O, reflux; (b) HNO_3, AcOH, T=50 °C; (c) I_2, morpholine, PhH, rt; (d) DDQ, MeOH, reflux; (e) *N*-bromosuccinimide, EtOH, rt.

5.3.2 Biological testing

5.3.2.1 Cell proliferation studies

All compounds were *in vitro* tested on MCF-7, T47-D, LNCaP, HepaRG, Caco-2 and NHDF cell lines by the MTT colorimetric assay. In this context, it is important to mention that the results for non-oxime compounds **2.1**, **2.3** and **2.5** were described in our previous research work (Canário et al. 2020).

Firstly, a screening study was performed at 30 μM for a first analysis of the cytotoxic effect of these compounds (**Figure 5.1**). This screening showed that several oximes led to a higher reduction in cell proliferation than the observed with parent compounds, which was particularly evident for compounds **5.4** and **5.7** in most cell lines. In addition, these two compounds and oxime **5.1** were the most cytotoxic in these experimental conditions. Furthermore, the cell lines mostly affected by all compounds were MCF-7 and HepaRG. On the other hand, only compound **5.7** promoted a significant reduction of LNCaP cells proliferation.

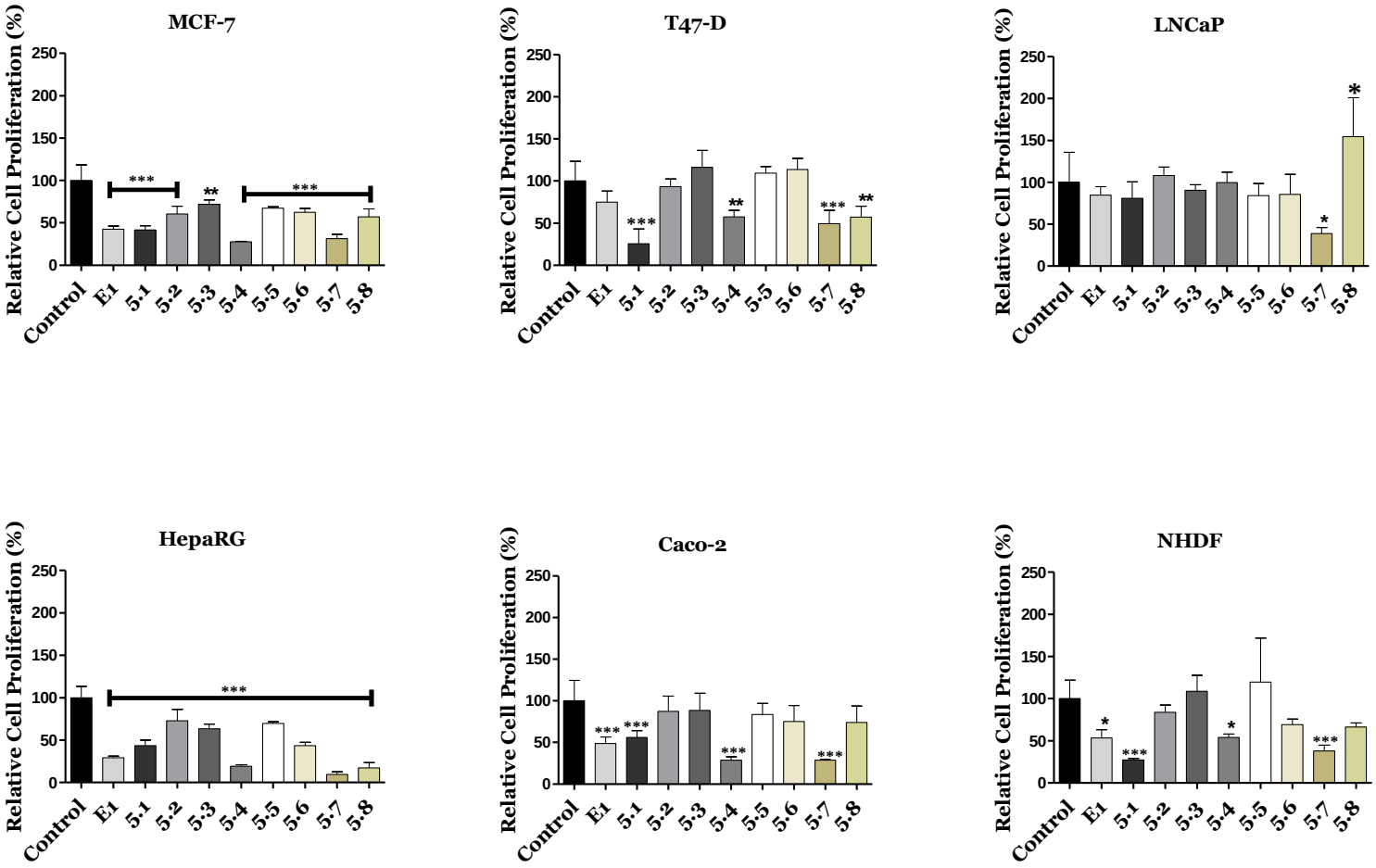

Figure 5.1 Relative cell proliferation of hormone-dependent (MCF-7, T47-D, LNCaP) and hormone-independent cancer cells (HepaRG, Caco-2 and NHDF) incubated for 72 h at 30 μM with the synthesized compounds, determined by the MTT assay, spectrophotometrically quantifying formazan at 570 nm. Data are expressed as a percentage of cell proliferation relative to the negative control and are indicated as means ± SD and are representative of at least two independent experiments. ***$p < 0.001$ *vs* control, **$p < 0.01$ *vs* control, *$p < 0,05$ *vs* control (Student *t*-test).

After the screening, for the cases where a reduction of cell proliferation was higher than 50%, the IC_{50} was determined (**Table 5.1**). Generally, the estimated IC_{50} values were in agreement with the results observed in the screening, confirming that the most potent compounds were oximes **5.1**, **5.4** and **5.7**. Of these, the most cytotoxic was $\Delta^{9,11}$-estrone oxime (compound **5.7**) on LNCaP cells (IC_{50} = 3.59 μM). In addition, the highest selectivity index was also observed for this derivative in these cells (**Table 5.2**). However, the variability of MTT assays was higher in LNCaP cells, as we and others have experienced with this poorly adherent cell line, and therefore the fit was less good and the uncertainty is higher in this case.

Table 5.1 Estimated IC_{50} values (μM) for various compounds in breast (MCF-7, T47-D), prostate (LNcaP), liver (HepaRG), colon (Caco-2) and normal fibroblast cells (NHDF)[a].

Compounds	MCF-7	T47-D	LNCaP	HepaRG	Caco-2	NHDF
1	41.93	ND	ND	29.53	42.69	61.82
5.1	26.65	29.26	ND	16.94	ND	43.88
5.4	16.75	ND	ND	12.32	18.51	ND
5.6	ND	ND	ND	28.00	ND	ND
5.7	25.63	43.45	3.59	18.35	24.33	30.84
5.8	ND	ND	ND	21.94	ND	ND
5-FU	1.71	0.54	7.79	1.78	1.31	3.61

[a]Cells were treated with different concentrations (0.1, 1, 10, 25, 50 and 100 μM) during 72 h. The cell proliferation effects were determined by the MTT assay. The data shown are representative of at least two independent experiments. 5-FU: 5-fluorouracil. ND: not determined.

Table 5.2 Selectivity index[a] of compounds **1**, **5.1**, **5.7** and 5-fluorouracil (5-FU).

Compounds	MCF-7	T47-D	LNCaP	HepaRG	Caco-2
1	1.47	ND	ND	2.09	1.45
5.1	1.65	1.50	ND	2.59	ND
5.7	1.20	0.71	8.59	1.68	1.27
5-FU	2.11	6.69	0.46	2.03	2.76

[a] Selectivity index is the ratio of the IC_{50} values of the treatments of non-tumor cells (NHDF) and tumor cells (MCF-7, T47-D, LNCaP, HepaRG and Caco); ND: not determined.

Although the structure of E1 oxime (compound **5.1**) is widely known (Hejaz et al. 1999; Allan et al. 2006), few studies concerning its biological activity have been published so far. Interestingly, our data showed a good antiproliferative activity of this compound against HepaRG cells (IC_{50} = 16.94 μM). When evaluating the effect of the presence of $\Delta^{9,11}$ double bond (compound **5.7** *versus* compound **5.1**), it is interesting to note that the effect depends on the cell line, being observed a higher cytotoxicity for compound **5.7** in MCF-7, LNCaP, Caco-2 and NHDF cells. Concerning the effect of A-ring modifications in these oximes, the introduction of 2-nitro group (compound **5.4**) allowed an improvement of the cytotoxicity when comparing with its absence (steroid **5.1**) in MCF-7, HepaRG and Caco-2 cells. In the other hand, the iodination and

bromination lead to a lower cytotoxicity than the non-functionalized A-ring (compound **5.1**) and 2-nitroestrone oxime **5.4**. However, similarly to our previously published results with 2,4-diiodo- and 2,4-dibromoestrone (Canário et al. 2020), interesting IC_{50} values were observed for A-ring halogenated E1 oximes **5.6** and **5.8** on HepaRG cancer cells. In this context, it is important to mention that the nitro group(s) are susceptible to reduction by nitro reductases and the $\Delta^{9,11}$ bond of compound **5.7** is prone to oxidation by the CYP P450 family which reinforces the importance of study its cytotoxic effect in hepatic cells (Tsuchiya et al. 2005). On the other hand, 2,4-dinitroestrone oxime (compound **5.5**) displayed low antiproliferative activity. Finally, considering the data on **Figure 5.1** and **Tables 5.1** and **5.2**, it is clear that the majority of these compounds had higher cytotoxicity against tumoral (MCF-7, T47-D, LNCaP, HepaRG and Caco-2) than non-tumoral (NHDF) cells.

To determine the potential estrogenic profile of the synthesized compound with the most relevant anti-proliferative activity (steroid **5.7**), its cell growing effect was measured on the estrogen-sensitive breast cancer T47-D cells (ER^+) in serum-free culture medium. This proliferative/estrogenic activity was expressed as the difference between the cell proliferation (in percentage) caused by a given compound and the basal cell proliferation fixed at 100% (**Figure 5.2**) (Ayan et al. 2012; Cortés-Benítez et al. 2017). E2 was also tested as reference compound. Unfortunately, similarly to the observed with E2, compound **5.7** also stimulated the cell proliferation at 0.001 and 0.01 μM when compared with the negative control.

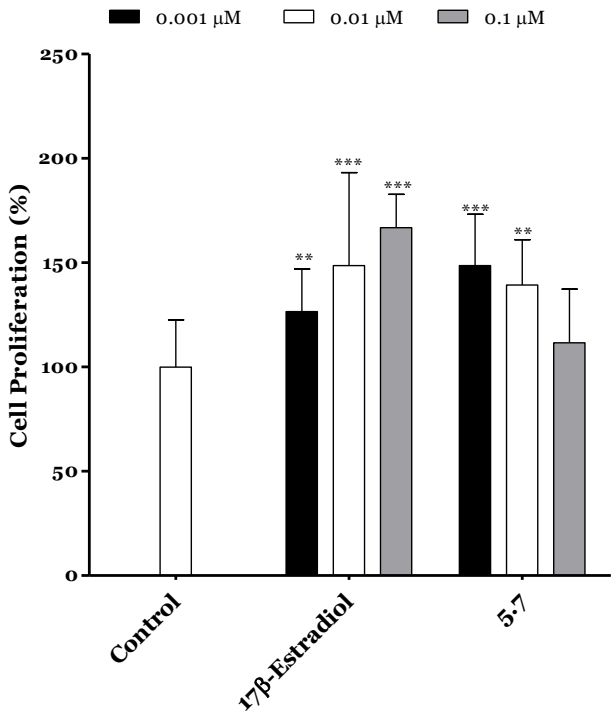

Figure 5.2 Proliferation of estrogen-sensitive T47-D cells incubated with 17β-estradiol and compound **5.7** for 24 h. Each bar represents the mean ± SD (originated from two independent experiments). ***p < 0.001, **p < 0.01 *vs* control (one way ANOVA post-hoc Bonferroni test).

In our previous study, it was also evidenced that $\Delta^{9,11}$-E1 (compound **2.1**) also stimulated the proliferation of T47-D cells (Canário et al. 2020) and therefore, its conversion into the oxime analogue did not eliminate this effect. In this context, Palomino *et al,* (Palomino et al. 1994) using X-ray crystallography and molecular modeling studies, showed that the presence of $\Delta^{9,11}$ double bond caused a flattening of B, C and D rings and consequently reduced the binding to ER in $1/5^{th}$ in comparison with E2. Despite this, as evidenced by our results, the presence of C9=C11 double bond did not eliminate the estrogenic effect characteristic of these compounds. In this context, other reports also showed that the presence of an oxime group did not eliminate this effect. In fact, OMATE had a stimulatory effect (0.15 g ± 0.01) on the uterine growth in ovariectomized rats, which was approximately 50% higher than that of EMATE (0.11 g ± 0.02) (Hejaz et al. 1999). In addition, and as previously referred, despite that 9α-hydroxy,11β-nitrooxyestrone-17-oxime had relevant anti-breast cancer effects, this compound also stimulated the tumor growth after a 15-day treatment period (Rzheznikov et al. 2003). This preliminary study seemed to suggest the estrogenic activity of compound **5.7**. Further studies will be necessary to elucidate this activity (e.g. using the luciferase assay) (Andruska et al. 2012).

5.3.2.2 Cell survival, cell cycle distribution evaluation and Hoechst 33258 staining

The possible mechanism of action of compound **5.7** was studied by flow cytometry after PI staining. This assay was performed in LNCaP cells at 24 h post treatment, and 5-FU was used as the positive control. In this cell line, it was observed that compound **5.7** led to 11% reduction in cell viability (**Figure 5.3**). This effect was similar to the one originated by 5-FU (12%). In addition to this flow cytometry study, cells were also observed using an optic microscope (**Figure 5.4**) and, after 24 h of treatment with compound **5.7**, it was possible to see small modifications in LNCaP cells, which lost their shape, becoming rounded, as it is characteristic to happen during mitosis.

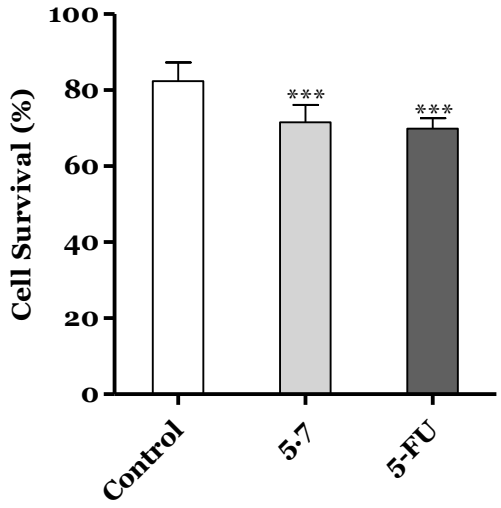

Figure 5.3 Percentage of LNCaP viable cells after 24 h treatment with 50 μM of compound **5.7** evaluated through propidium iodide flow cytometry assay. Control corresponds to untreated cells and 5-FU (50 μM) was used for comparison. The percentage of survival is the percentage of cells in R_1 (live cells) as compared to the total number of events in R_2 (dead cells) and R_3 (undetermined cells). Each bar represents the mean ± SD (originated from two independent experiments). ***$p < 0.001$ *vs* control (one way ANOVA post-hoc Bonferroni test).

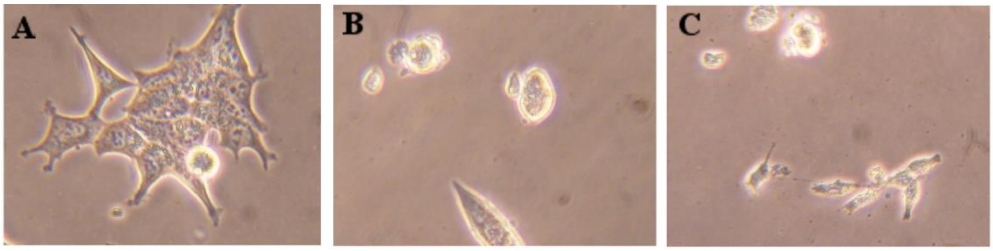

Figure 5.4 Photographs of the LNCaP cells (A, control) treated with 50 μM of compound **5.7** (B) and 5-FU (C) for 24 h. Amplification of 100x.

The arrest of cell cycle progression is one of the strategies used to stop the cancer proliferation (DiPaola 2002). In this context, some studies previously published

showed the effect of steroidal and non-steroidal oximes in cell cycle (Sánchez-Sánchez et al. 2016; Latif et al. 2019). As example, it was evidenced that E1-16-oxime ethers promoted the apoptotic HeLa cell death and modulated the cell cycle progression (arrest at G_1), leading to an increase in cellular shrinkage, nuclear condensation, membrane permeability, sub-diploid population and caspase-3 activity (Berényi et al. 2013). In addition, 16β-triazolyl-17α-estradiol 3-benzyl ethers of the 13α-E2 series led to a G_2/M cell cycle arrest and caspases-3 and 9 activation (Mernyák et al. 2015) and $\Delta^{9,11}$-E1 induced an arrest at G_0/G_1 in HepaRG cell cycle (Canário et al. 2020). Thus, the interference of compound **5.7** in cell cycle distribution was also evaluated by flow cytometry. Interestingly, it was found that the treatment with this steroid oxime (50 μM, 24 h) induced a G_2/M cell cycle arrest of LNCaP cells (**Figure 5.5**). Also, LNCaP cells were not able to pass through to the S and G_2/M phases treated by compound 5-FU, which are in agreement with literature for these cells (Demirci et al. 2019).

Apoptosis is essential for maintaining the physiologic balance between cell death and cell growth (Koff et al. 2015). Therefore, studies for understanding the cancer cell cycle, particularly the interplay with chromatin control, are providing opportunities for developing a new range of anti-cancer drugs (McLaughlin et al. 2003). In this context, using a preliminary assay, the Hoechst 33258 fluorescent dye was used by us to analyze nuclei morphology of LNCaP cells by fluorescence microscopy after exposition to 50 μM of compound **5.7** during 24 h (**Figure 5.6**). Interestingly, it was observed the presence of condensed DNA, typical of prophase, and a small proportion of condensed and fragmented nuclei, typical of apoptosis (Toné et al. 2007). β-Tubulin is a protein that polymerize into microtubules, which are involved in cell movement, intracellular trafficking and mitosis (Parker et al. 2014). Tubulin-binding drugs, such as paclitaxel and docetaxel (Yang and Horwitz 2017), kill cancerous cells by inhibiting microtubule dynamics leading to mitotic arrest and cell death. In this context, as it was observed that compound **5.7** promoted a cell cycle arrest at G_2/M (**Figure 5.5**) and also lead to the formation of condensed DNA typical of prophase, plus condensed and fragmented nuclei typical of apoptosis (**Figure 5.6**), it can be speculated that it can act by interference with β-tubulin, similarly to which occurs with other steroids of the estrane series like as estramustine and 2ME2 (Cabral et al. 1993; Cushman et al. 1995; Cushman et al. 1997). In the next section, we studied the interaction of compound **5.7** and β-tubulin by docking assay to try to better understand the cell cycle arrest.

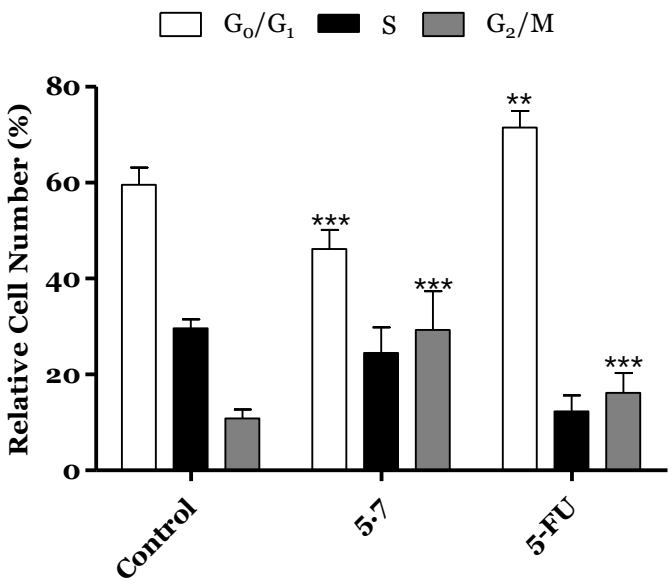

Figure 5.5 Cell cycle distribution analysis of LNCaP cancer cells after treatment with compound **5.7** at 50 μM for 24 h. Each bar represents the mean ± SD of four samples (originating from two independent experiments). $^{**}p < 0.01$ *vs* control; $^{***}p < 0.001$ *vs* control (one way ANOVA post-hoc Bonferroni test).

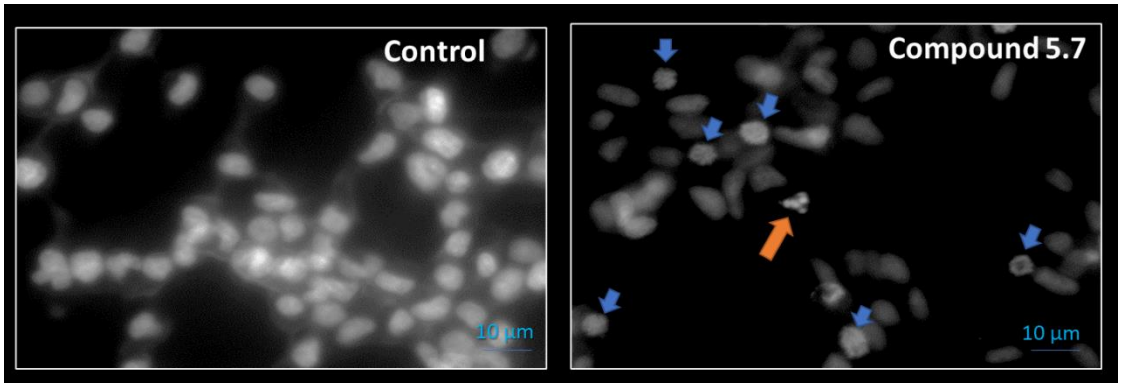

Figure 5.6 Fluorescence microscopy images of DNA staining (Hoechst 33258) in LNCaP cells treated with vehicle (Control) or with compound **5.7** at 50 μM for 24 h. Blue down-pointing arrows: condensed DNA onto visible chromosomes (prophase); Orange up-pointing arrow: condensed and fragmented nuclei (apoptosis).

5.3.3 Molecular docking studies

Taking into account the enzymes involved in steroidogenesis, and given the structural similarity of the compounds of our study and several of the above referred steroidal oximes acting by interaction with the mentioned targets, we aimed to evaluate the affinities of the steroids prepared by us and the proteins ERα, ST, 17β-HSD1 and β-tubulin. Molecular docking is a standard computational tool that has been successfully employed in drug design and discovery studies. Satisfactory docking results can be obtained when relatively small ligands with few rotatable bonds are docked towards

protein binding pockets in which flexibility does not play an important role. However, for complex molecules (with many rotatable bonds and flexibility), the use of methodology involving theoretical docking and molecular dynamic techniques are important to overtake these limitations, because they allow for evaluating and select the best molecule poses generated in the molecular docking, which can affect the results (Giacoppo et al. 2015; Lima et al. 2016; Paula et al. 2018). The three-dimensional structural coordinates of these three protein receptors were obtained from PDB and molecular docking was performed using the program AutoDock vina. To validate the standard docking method, simulations were carried out between crystallized ligands/drugs with the respective proteins and all control redocking simulations were able to reproduce the ligand-protein interaction geometries presented in the respective crystal structures with a RMSD ≤ 2.0 Å. Then, all compounds were docked for the referred targets, as observed in **Table 5.3**.

Table 5.3 Predicted affinity energies of compounds **1, 2.1, 2.3, 2.5, 5.1-5.8** calculated against the estrogen receptor α (ERα), steroid sulfatase (ST), 17β-hydroxysteroid dehydrogenase type 1 (17β-HSD1) and β-tubulin by AutodockTools with vina executable. Binding energies of co-crystalized ligand in the X-ray crystal structures were calculated by re-docking.

Compounds	Lowest energy (kcal.mol^{-1})			
	ERα	**ST**	**17β-HSD1**	**β-tubulin**
1	-10.3 [b]	-6.2 [b]	-8.1[b]	-9.0
5.1	-9.7	-6.7	-8.1	-8.9
5.2	-8.8	-7.0	-8.2	-8.7
5.3	-6.6	-7.0	-8.1	-8.5
5.4	-7.9	-6.9	-8.3	-8.9
5.5	-5.3	-6.8	-8.1	-8.4
2.3	-4.3 [b]	-6.0 [b]	-7.7 [b]	-8.4
2.1	-10.9 [b]	-5.9 [b]	-8.2 [b]	-9.0
2.5	-6.8 [b]	-6.3 [b]	-8.1 [b]	-9.0
5.6	-5.8	-6.6	-7.7	-8.5
5.7	-10.5	-6.5	-8.3	-9.1
5.8	-5.0	-6.3	-7.6	-8.5
E2	**-9.9** [a]	-	-	-
N-acetyl-*D*-glucosamine	-	**-7.2** [a]	-	-
5α-Dihydrotestosterone	-	-	**-8.3** [a]	-
Colchicine	-	-	**-**	**-8.4** [a]

[a] The RMSD between re-docked ligands and the corresponding X-ray crystal structure coordinates was ≤ 2.
[b] These values were described in a previous study (Canário et al. 2020).

The results observed in the docking simulations with ERα, ST and 17β-HSD1 for compounds **2.1**, **2.3** and **2.5** are presented in our previous work (Canário et al. 2020). According to the data presented in **Table 5.3**, compound **5.7** can bind ERα in a lower energy than the control (E2). In addition, in **Figure 5.7** can be observed that this compound can form two hydrogen bonds between its oxime group at C17 and Hist524 and between the hydroxyl group at C3 and Glu353 of ERα target. These interactions are similar to the observed with E2. Therefore, globally, these docking data seem to be in agreement with our experimental results (**Figure 5.2**).

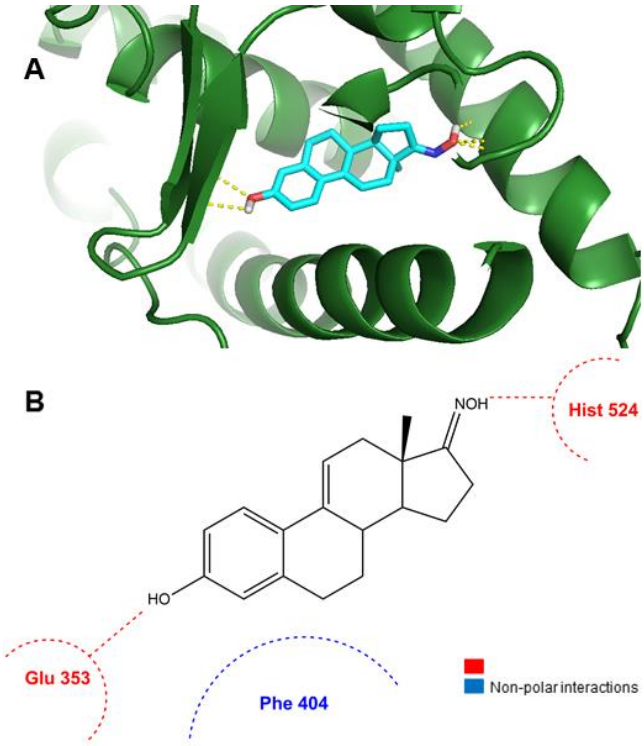

Figure 5.7 Analysis of predicted ERα binding orientations for the best raking compound, **5.7**. (**A**) 3D molecular and (**B**) 2D docking results showing the main interactions.

The predicted affinity energies of the synthesized compounds for ST are all higher than the energy obtained for co-crystalized ligand (**Table 5.3**). This suggests that these compounds have a poor affinity to this macromolecule. Concerning the energy values obtained in the docking studies with 17β-HSD1, generally they are very close to the determined affinity of the co-crystalized ligand (5α-dihydrotestosterone, DHT) (**Table 5.3**). Due to these interesting results, we also analyzed the interaction mode of the best ranked compounds, **5.4** and **5.7**, with 17β-HSD1. It is already known from the literature that the main interactions between DHT and this enzyme are a conventional hydrogen bond with Hist221 residue and Van der Waals interactions with Leu149, Val143 and Pro 187 residues (Day et al. 2008). However, the studied compounds just exhibit the Van der Waals interactions, lacking the hydrogen bond with Hist221, which can be determinant for their interaction with this target. Further *in vitro* studies will be necessary to elucidate the significance of this interaction. The most interesting binding was observed between compound **5.7** and β-tubulin, as shown in **Figure 5.8** and **Table 5.3**. Besides the good affinity energy value, which is lower than the determined for colchicine, compound **5.7** was also predicted to have the most important interactions with β-tubulin, such as the conventional hydrogen bond with CysB241, alkyl and Pi-alkyl interactions with LeuB248, and Van der Waals interaction with ValB318 (Dorléans et al. 2009; Kumar et al. 2016; Bueno et al. 2018). Interestingly, previous studies suggested that the tubulin ligand interactions through

amino acid residues Ala316 and Val318 are very crucial in inducing antitubulin effect (Kumar et al. 2016). The other studied compounds, despite having good binding energies, do not establish the conventional bonds to tubulin. Compounds **2.1** and **2.5** did not show a conventional hydrogen bond with CysB241, interacting only through Van der Waals, alkyl and Pi-alkyl interactions, which explains that the affinity energies may not be directly related to the established interactions required with the active site. Therefore, the cell cycle arrest at G_2/M originated by compound **5.7** (**Figure 5.5**), at prophase (**Figure 5.6**), can perhaps occur due to β-tubulin inhibition. However, future studies are needed to prove this hypothesis.

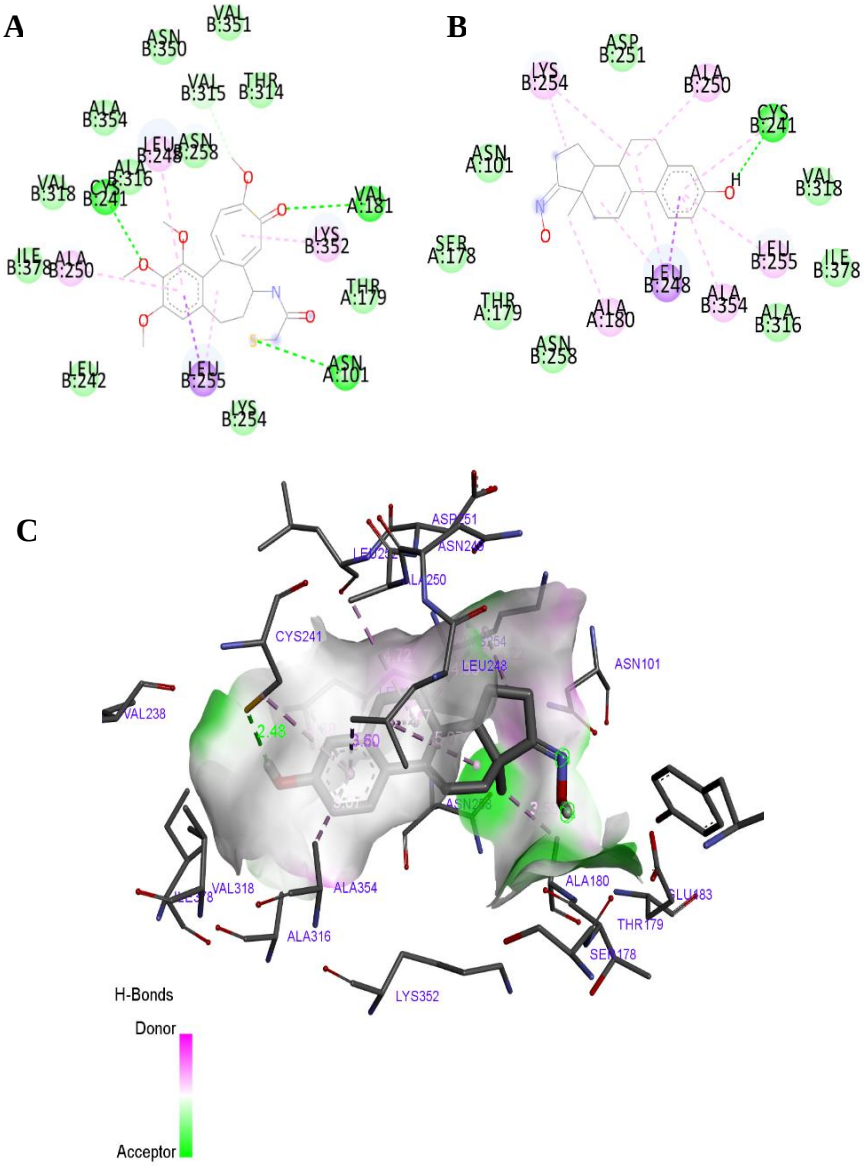

Figure 5.8 2D diagram of the active interaction between colchicine and β-tubulin (panel **A**). 2D diagram of predicted interactions between best ranked compound, **5.7**, and β-tubulin (panel **B**) and 3D representation (panel C). (**A, B**) Conventional hydrogen bonds are displayed in green, Van der Waals interactions in light green, Pi-sigma interactions are displayed in purple and alkyl and Pi-alkyl interactions in pink. (**C**) All contact and hydrogen bonds are shown as dotted lines, and represented with same colors above described.

5.4 Conclusions

Several E1 oxime derivatives were synthesized and revealed interesting effects against the proliferation of several tumor cell lines when compared with parent ketone compounds. Of these, oxime **5.7** showed the highest activity against LNCaP cancer cells as well as a very relevant selectivity index. In addition, it was also demonstrated that this compound originated cell cycle arrest in G_2/M on these cells in prophase and condensed and fragmented nuclei characteristic of apoptosis. However, in an *E-screening* assay this oxime also promoted the proliferation of T47-D cells. Docking studies evidenced that compound **5.7** also showed relevant affinities for ERα and β-tubulin, which could explain its mechanism of action and estrogenic effect. Interestingly, the oximes bearing halogens in A-ring (2,4-diiodoestrone oxime **5.6** and 2,4-dibromoestrone oxime **5.8**), evidenced a selectivity for HepaRG cancer cells. Another A-ring functionalized derivative, 2-nitroestrone oxime, but not its 2,4-dinitro analogue, showed higher cytotoxicity against HepaRG and MCF-7 cancer cells. Thus, the presence of an oxime group at C17 in functionalized E1 scaffold showed to be a good strategy to obtain new molecules with relevant anticancer effects.

Chapter 6
General discussion

Cancer is a leading cause of death worldwide, accounting for nearly 10 million deaths in 2020. The academia and pharmaceutical industry have made efforts to develop cancer therapies with higher selectivity and more tolerable side effects, allowing an increase in the survival and quality of life of the patients. Nowadays, different steroids are available for clinical treatment of cancer, such as fulvestrant, exemestane, cyproterone acetate, abiraterone acetate, estramustine, prednisolone and dexamethasone (Zucchini et al. 2015; Lossignol 2016; Lorente et al. 2021). Many other steroidal molecules have been synthesized and tested against different cancer cells showing cytotoxic activities, anti-angiogenic properties as well as cell cycle arrest, DNA fragmentation and apoptosis induction. Several of these compounds also inhibited their receptors (ER, AR), proteins involved in steroidogenesis like 17β-HDS1, STS, CYP19A1, CYP17A1 and other proteins involved in signaling pathways (e.g., caspases) and cell cycle like β-tubulin. 2ME2, EMATE, OMATE, SR-16234 are examples of steroidal molecules with interestingly activities against cancer (Gupta et al. 2013; Harada et al. 2017; Canário et al. 2018). Thus, the focus of this thesis was to find new oxime derivatives based on E1 scaffold because several oximes already synthesized showed interestingly cytotoxic activities against different cancer cells.

Following the guiding principles of this thesis, it is important to reflect and perform an integrated analysis of the obtained results, according with the proposed objectives. Therefore, this general and critical discussion intends to integrate the overall results, already discussed with more detail in the respective chapters.

The main goal of the present work was the discovery of new oxime derivatives based on E1 scaffold. For that, chemical modifications at C2, C3, C4, C9, C10, C11 and C16 were performed using different techniques, such as iodination, bromination, nitration, condensation, alkylation and acetylation to obtain intermediates, which were used to synthesize C17 E1 oximes. The reactions designed for this thesis are represented in **Scheme 6.1.**

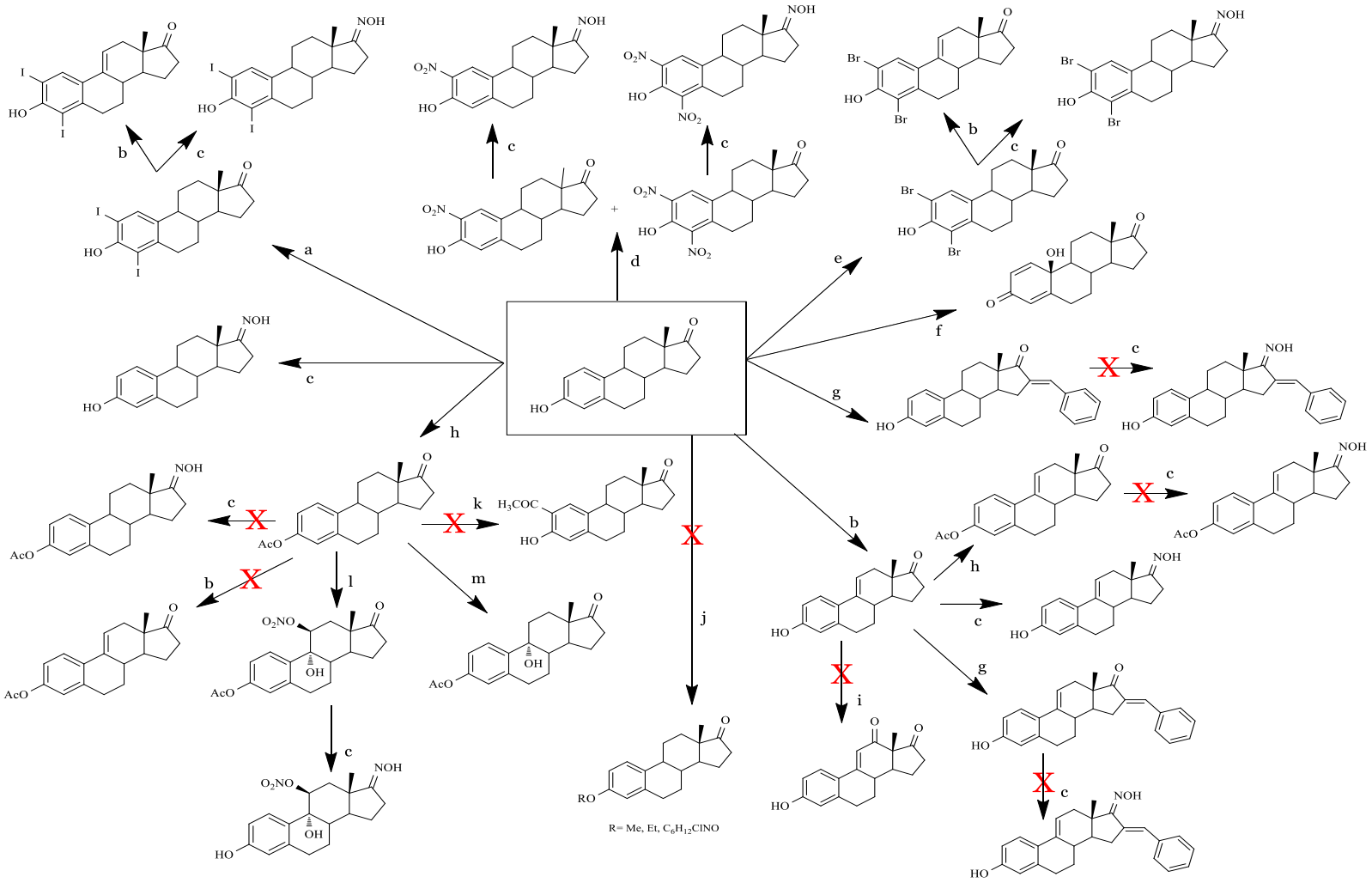

Scheme 6.1 Scheme representing the modifications in E1 scaffold. Reagents and conditions: (a) I_2, morpholine, PhH, rt; (b) DDQ, MeOH, reflux; (c) $NH_2OH{\cdot}HCl$, NaOH, EtOH, H_2O, reflux; (d) HNO_3, AcOH, T=50°C; (e) NBS, EtOH, rt; (f) $KMnO_4$, HCl, ethyl acetate, rt; (g) Benzaldehyde, KOH, MeOH, rt; (h) Ac_2O, DMAP, THF, rt; (i) $BiCl_3$, TBHP, CH_3CN, reflux; (j) IR, Na_2CO_3, acetone, reflux; (k) $ZrCl_4$, CH_2Cl_2; (l) CAN, H_2O, AcOH, rt; (m) Oxone™, acetone, CH_2Cl_2, H_2O, $NaHCO_3$, TBAHS, 15°C.

Fourteen intermediates and seven steroidal oximes in estrane series were successfully synthesized. The reactions used were adapted from the literature and were straightforward and relatively green, and allowed to obtain products with satisfactory yields. It is known that alterations at C2 are believed to reduce estrogenic activity of steroids, which is an undesirable side effect of these molecules (Brozic et al. 2008). Then, electrophilic aromatic substitutions such as iodination, nitration or bromination were performed in C2 and/or C4 positions of E1 (Palomino 1999). Of these three aromatic halogenations, bromination was the most straightforward to perform. Concerning iodination, two other greener strategies were tried before the successful use of I_2/morpholine/PhH. The combination of sodium iodide and sodium chlorite only allowed the synthesis of 2-iodoestrone in low yields and with the use of I_2 and copper (II) chloride di-hydrate ($CuCl_2.2H_2O$) it was very difficult to separate the isomers 2- and 4-iodoestrone by column chromatography (Cushman et al. 1995; Lista et al. 2008; Egan and Filer 2013). The nitration reaction was performed as described by Stubenrauch *et al.* (Stubenrauch and Knuppen 1976), which was applied by these authors to obtain 2-nitroestrone. However, as an excess of the nitrating agent was used, 2,4-dinitroestrone was also formed and the mixture of products was separated by column chromatography. However, it was very difficult to separate the isomers 2- and 4-nitroestrone by column chromatography and consequently the 4-nitroestrone was lost.

The protection of hydroxyl groups in the form of esters is one of the most common modifications and is extensively used in organic and medicinal chemistry. For this, the most frequently used reagents are acyl halides or anhydrides (Lugemwa et al. 2013). Since the 60s years, DMAP has been considered a powerful nucleophilic organic catalyst (Poisson et al. 2012). In this way, the hydroxyl group of the starting substrate (E1) was protected by acetylation with acetic anhydride in a reaction catalyzed by DMAP, aiming to obtain E1 acetate. It was important to mention that a protection of the 3-hydroxyl with an acetate group was necessary to perform subsequently C9 and C11 modifications.

Several C11-modified steroids were described in the literature with SERM activity, which makes this modification interesting to explore (Zhang et al. 2005). Then, concerning the steroid structure with aromatic A-ring, there were two benzylic positions susceptible to oxidation: the 6- and the 9-positions of the steroid nucleus. Tristriphenylphosphine rhodium chloride catalyst or photoexcited nitrobenzene were used to perform benzylic oxidations with low yields (Silvestre 2007). Alternatively, mild reaction conditions have been employed in selective hydroxylation, using *in situ* formed dioxiranes (Salvador et al. 2012). In this context, the hydroxylation of E1 acetate by

dimethyldioxirane enabled the selective oxyfunctionalization at C9α (Schwarz et al. 1999). Compounds oxidized at C9, especially the 9-hydroxyl derivatives, were important because they easily give rise, by dehydration, to the corresponding $\Delta^{9,11}$ derivatives, which are key intermediates in the synthesis of some compounds such as potent corticosteroids and progestagens (Silvestre 2007). Otherwise, the use of CAN as oxidant (Sykes et al. 1971) led to the hydroxylation of the C9 benzyl atom and nitration of the C11 homobenzyl position with acceptable yields (Golubovskaya and Rzheznikov 2007).

Other simple route for oxidation using DDQ was described by Brown *et al* (Brown et al. 1968), where the phenol is rapidly oxidized by DDQ at room temperature, to obtain $\Delta^{9,11}$-E1 without C3 protection and it was the procedure used by us.

Estrogen-related quinols were described in literature as potential drugs that can be used in estrogen replacement therapy (Prokai et al. 2004). There are many synthetic approaches reported to synthesize 10β-substituted-17β-hydroxyestra-1,4-dien-3-ones, but they often require many manipulation of E1 and E2 derivatives, lengthy protection/deprotection steps or functional group modifications, resulting in complex mixtures of products. Thus, using potassium permanganate it was possible to synthesize E1-quinol with cheap reagents and involving a simple work-up (Lista et al. 2006).

The introduction of aryl groups at C16 of steroidal scaffold also led to high antiproliferative effects (Bansal et al. 2011; Vosooghi et al. 2013) and modifications at C3 and C16 of E2 allowed to obtain compounds with 17β-HSD1 inhibition and a weak estrogenic effect on estrogen-sensitive breast cancer cells (Maltais et al. 2016). Thus, in our work, through a condensation reaction at C16, we synthesized a 16*E*-benzylidene steroid with the intention to explore these activities (Brito et al. 2019).

In the 90s, several compounds, particularly steroids, bearing oxime groups have shown relevant antiproliferative activity against several types of cancer cells (Deive et al. 2001). Oximes are usually prepared by condensation of an aldehyde or a ketone with hydroxylamine affording, respectively, aldoximes and ketoximes (Ãbele and Lukevics 2000). For the preparation of oximes, we selected a method involving the use of EtOH, NaOH and hydroxylamine hydrochloride (Hejaz et al. 1999), because is a more selective and greener strategy than other approaches that use, for example, pyridine (Rzheznikov et al. 2003). In fact, these last methods involve the use of more toxic reagents/solvents, are more time consuming, have complex workups and can lead to lower reaction yields (Saikia et al. 2011; Kim et al. 2013; Jadhav et al. 2018). Only for the synthesis of the oxime of 9α-hydroxy-11β-nitrooxy-E1 acetate was used pyridine

because the normal basic conditions used have not originated the oxime. However, the low yields obtained have not allowed to study this oxime in non-clinical assays.
Other reactions were performed to obtain E1 derivatives without success and, therefore, these compounds were not included in the present study. Concerning the synthesis for more intermediates, allylic oxidation to obtain 12-oxo-$\Delta^{9,11}$-E1 derivatives (Salvador and Silvestre 2005), the Fries rearrangement to obtain a 2-acetyl-E1 derivative (Rao and Cessac 2002), and *O*-alkylation at C3 of E1 (Wan et al. 2013) were performed. The synthesis of these compounds was not possible due to the low reactivity observed and the formation of complex mixtures of products (TLC control) that cannot be separated by chromatography. It is important to highlight that C-ring modifications of steroids usually were difficult to perform, mainly due to steric constraints and frequently the C-ring modified steroids are unstable. The synthesis of oximes in compounds with acetate group at C3 failed because the use of basic conditions also promoted the hydrolysis of the 3-acetate group. The oximes of 16*E*-benzylidene-E1 and 16*E*-benzylidene-$\Delta^{9,11}$-E1 were not synthesized probably due to sterically impairments.

The assessment of biological activity is very important to understand if compounds can be promising cytotoxic molecules. Therefore, *in vitro* assays were performed to access the cytotoxic activity of the synthesized compounds. The MTT colorimetric assay was chosen to evaluate the cytotoxicity of compounds on hormone-dependent (MCF-7, T47-D and LNCaP) and hormone-independent (HepaRG and Caco-2) cancer cells and on normal human dermal fibroblasts (NHDF). Firstly, a preliminary screening at 30 μM was performed for all compounds in all cell lines. When a reduction of cell proliferation was higher than 50%, the IC_{50} was determined. MTT assay was the method selected because it was easy to use, safe, cheap and has a high reproducibility (Aslantürk 2018).
The most relevant reduction of cell proliferation was observed with compounds $\Delta^{9,11}$-E1 (compound **2.1**) in HepaRG cells (IC_{50} = 6.67 μM), with 9α-hydroxy-11β-nitrooxy-E1 acetate (compound **3.3**) in hormone dependent cancer cells (IC_{50} = 5.87 μM for MCF-7; IC_{50} = 7.40 μM for T47-D and IC_{50} = 5.30 μM for LNCaP), with E1-quinol (compound **4.1**) in hormone dependent cancer cells (IC_{50} = 5.79 μM for MCF-7; IC_{50} = 7.72 μM for T47-D and IC_{50} = 4.11 μM for LNCaP) and with $\Delta^{9,11}$-E1 oxime (compound **5.7**) in LNCaP cells (IC_{50} = 3.59 μM). Concerning C-ring modifications, it was observed that the introduction of C9=C11 double bond in E1 increased the cytotoxic effects for all cell lines in study, except in T47-D cells. In fact, these results were expected because some reported studies showed that compounds with a double bond at C9=C11 combined with 2- and 4-substitutions in E1 nucleus had relevant antiproliferative activities (Milić et al. 2005).

The presence of the 11β-nitrooxy group, in addition to the 9α-hydroxyl (compound **3.3**), markedly increased the antiproliferative effect against all cell types studied, as shown by Rzheznikov (Rzheznikov et al. 2003) in breast cancer cells. Also, Lao *et al* (Lao et al. 2017) showed that C11α modifications in 2ME2 originated compounds with cytotoxic activities against hepatic HepG2 cancer cells, which showed the importance of C11 modifications.

Interestingly, the introduction of iodine in positions 2 and 4 of E1 and the 9α-hydroxylation of E1 acetate led to a higher antiproliferative activity against HepaRG cancer cells (IC_{50} = 29.67 μM, IC_{50} = 32.04 μM, respectively). In oximes, the introduction of a 2-nitro group (**compound 5.4**) allowed an improvement of the cytotoxicity, when compared with the analogs without this group (**steroid 5.1**), in MCF-7, HepaRG and Caco-2 cells. Also, interesting IC_{50} values were calculated for A-ring halogenated E1 oximes **5.6** (2,4-diiodoE1 oxime) and **5.8** (2,4-dibromoE1 oxime) on HepaRG cancer cells. The antiproliferative effects observed for these halogenated compounds were interesting, and could be explained by the fact that halogenated aromatic derivatives (e.g. halobenzenes) can be metabolically activated by CYP450 enzymes, which can transform them into reactive compounds, particularly quinones. Quinones are electrophilic and can bind tissue proteins and/or lead to the generation of reactive oxygen species harmful for hepatic cells (Brodie et al. 1971; Liu et al. 2003; Pizzo et al. 2015) However, further experimental studies would be necessary to elucidate these activities.

E1-quinol also showed a relevant antiproliferative effect (IC_{50} values ranging from 4.11 to 18.64 μM) when compared with E1 (IC_{50} values between 29.53 and 61.82 μM). In fact, these results were not expected because no relevant cytotoxicity (IC_{50} > 100 μM) was observed by Milic et al. (Milić et al. 2001) for this compound against melanoma (Fem-X), cervix carcinoma (HeLa) and leukemia (K_{562}) cells.

As expected by the analysis of IC_{50} values, a highest selectivity index was found for compounds $\Delta^{9,11}$-E1 oxime (SI>3) in LNCaP, 9α-hydroxy-11β-nitrooxy-E1 acetate (SI>2) in MCF-7, T47-D and LNCaP cells and E1-quinol (SI > 3) in LNCaP cells. These results were important because cancer drugs candidates should be selective for cancer cells, not harming normal cells.

Concerning the interesting antiproliferative results, it was important that new anticancer candidates did not show estrogenicity because this is an undesirable side effect that excludes the drug from being used in clinical practice. Then, a preliminary study using the *E*-screening assay was performed. This method is easy to use and can predict the estrogenic activity of molecules under study. All tested compounds ($\Delta^{9,11}$-E1; $\Delta^{9,11}$-16-benzylidene-E1, $\Delta^{9,11}$-E1 oxime, 9α-hydroxy-11β-nitrooxy-E1 acetate and E1-

quinol) favored cell proliferation, except 9α-OH-E1 acetate. These results were relatively expected because some studies showed the potential estrogenic effects of this type of compounds like 3,6β-dihydroxyestra-1,3,5(10),9(11)-tetraene-17β-yl propionate (Sakač et al. 2005), 2-methoxyestra-1,3,5(10),9(11)-tetraen-17-one, OMATE (Hejaz et al. 1999) and 9-hydroxy,11β-nitrooxyestrone-17-oxime (Rzheznikov et al. 2003). Otherwise, some reports demonstrated that a 2-bromoethyl side chain at C3 and a carbamoylbenzyl chain at C16 removed the residual estrogenic activity associated with the estrogen nucleus (Laplante et al. 2008; Maltais et al. 2011; Ayan et al. 2012). Also, 11β-estradiol carboxylates, esters and ethers showed that when the 11β-chain is increased in length from four to five non-hydrogen atoms, the estrogenic effect diminished and a SERM was obtained (Zhang et al. 2005). Unfortunately, our data showed that the introduction of $\Delta^{9,11}$, benzylidene group at C16 and oximes at C17 were not enough to reduce the estrogenic effect of these E1 derivatives. However, the results herein presented showed that the presence of a 9α-hydroxyl can be of interest to develop new anticancer estrane derivatives without estrogenic activity and therefore this structural modification should be considered in future studies intending to develop new compounds with antiproliferative potential.

For compounds with the best antiproliferative activities (**2.1**, **3.2**, **3.3, 4.1** and **5.7**), a cell viability assay and cell cycle distribution analysis by flow cytometry were performed to investigate the breakdown of cells in the G_0/G_1 phase versus S phase, G_2, or polyploidy state of the cell population. PI and carboxyfluorescein diacetate dyes were used to distinguish viable and non-viable cells. PI cannot enter into viable cells, opposed to carboxyfluorescein diacetate that are able to enter into these cells (Boyd et al. 2008). Compound **2.1** ($\Delta^{9,11}$-E1) led to a 34% reduction in cell viability after 24 h of treatment and induced an apparent G_0/G_1 cell cycle arrest in HepaRG cancer cells. As compound **3.2** (9αOH-E1 acetate) is not estrogenic (it did not promote a cell proliferation in our experimental conditions) and showed antiproliferative activity against liver cancer cells, the subsequent experiments (flow cytometry studies of cell cycle and analysis by the carboxyfluorescein succinimidyl ester assay) were performed in HepaRG cancer cells with the intention to understand its potentiality as antiproliferative agent in liver cancer. The results showed that 9αOH-E1 acetate induced a G_0/G_1 cell cycle arrest at 24h post-treatment in HepaRG cancer cells. Compound **3.3** (9α-hydroxy-11β-nitrooxy-E1 acetate) led to a drastic reduction of cell viability (92%) of HepaRG cancer cells. Unfortunately, despite the interesting potency and selectivity observed for compound **3.3**, due to the potential toxicity risks inherent to its potential use, we decided not to further explore its bioactivity. Also, compound **4.1** (E1-quinol) led to a drastic reduction (approximately 83%) of HepaRG cells

viability. Finally, the most promising compound, $\Delta^{9,11}$-E1 oxime (**compound 5.7**), induced a G_2/M cell cycle arrest of LNCaP cells. Concerning the interesting results evidenced for compound **5.7** ($\Delta^{9,11}$-E1 oxime), the Hoechst 33258 fluorescent dye was used by us to analyze nuclei morphology of LNCaP cells by fluorescence microscopy in order to understand which phase of mitosis was involved. It was observed the presence of condensed DNA, typical of prophase, and a small proportion of condensed and fragmented nuclei, typical of apoptosis (Toné et al. 2007), which elucidated better a potential mechanism of action for this compound. Additional studies would be necessary to further elucidate these activities. In this scope, as flow cytometry assays revealed that this steroid induced a G_2/M cell cycle arrest, the most logical future studies to be considered should involve the most relevant proteins influencing the cell cycle (e.g., caspases) as well as evaluation of interference in tubulin funcion.
These results are in agreement with proliferative assays and with literature for these types of compounds. Several results showing interference with cell cycle by E1-16-oxime ethers that promoted apoptotic HeLa cell death and modulated the cell cycle progression (arrest at G_1) (Berényi et al. 2013). Moreover, 16β-triazolyl-17α-estradiol 3-benzyl ethers of the 13α-E2 series led to a G_2/M cell cycle arrest and caspases-3 and -9 activation (Mernyák et al. 2015). 11α-Substituted 2ME2 derivatives showed a G_2/M cell cycle arrest as well as significant anti-estrogenic activity (Lao et al. 2017).

Molecular docking is a typical structure-based drug design protocol, which is used to study and predict the binding energies and interaction affinities between a ligand and receptor biomolecules (Ferreira et al. 2015). This method is usually fast and highly effective. Usually, the first potential targets considered to explain the possible mechanisms of action of steroids are those influencing hormonal biosynthesis (e.g. enzymes), effects (e.g. receptors) and proteins involved in cell cycle. Accordingly, in the context of the present work, ERα, AR, 17β-HSD1, STS, CYP19A1, CYP17A1 and β-tubulin were the proteins selected by us mainly because: a) they are potential targets involved in hormone-dependent cancers like breast and prostate cancers; b) several steroidal compounds similar to those prepared and evaluated by us were described as interacting with these proteins; c) we experimentally observed selective effects of compound **3.3** and **5.7** against hormone-dependent cell lines and that, on the contrary, compound **3.2** did not exhibit proliferative action in the *E*-screening assay. Also, we selected these structures because the target enzymes were complexed with endogenous molecules like E2, E1 and DHT, which are structurally similar to the tested compounds.
SAR studies for ERα showed that effective binding requires the presence of the polar hydroxyl groups at C3 and C17 of steroid nucleus (Palomino 1999). Bulky substituents

at positions C2 and C4 are not well tolerated by the receptor. Small hydrophobic substituents at positions 4, 12β, 14 and 16α enhance binding affinity; whereas, larger hydrophobic substituents are tolerated at positions 7α, 11β and 17α. Small polar groups at C11 create a negative influence on the affinity (Anstead et al. 1997). Compound **2.1** ($\Delta^{9,11}$-E1) can bind to ERα in a lower energy than the control (E2), binding with two hydrogen bonds between ketone group at C17 and Hist524 and between hydroxyl group at C3 and Glu353. $\Delta^{9,11}$-E1 oxime (compound **5.7**) can also bind ERα in a lower energy than the control. This compound can form two hydrogen bonds between its oxime group at C17 and Hist 524 and between the hydroxyl group at C3 and Glu353 of ERα target. These interactions are similar to the observed with E2. Regarding the results for compound **3.3** (9α-hydroxy-11β-nitrooxy-E1 acetate), this molecule does not establish the essential conventional hydrogen bonds with His524 and Glu353 residues, but establishes a Van der Waals interaction with Hist524, a weaker interaction when compared with the conventional hydrogen bond. Thus, the cytotoxicity originated by compound **3.3** can be associated to other mechanism of action than the interaction with ERα. Compound **4.1** (E1-quinol) shares with E2 some hydrophobic interactions, involving particularly the residues Leu387, Met388, Leu391 and Phe404. However, the conventional hydrogen bonds with the residues Glu353 and His524 are absent (Fukuzawa et al. 2006).

Regarding 17β-HSD1, the lowest energy compared to control DHT was obtained for compound **2.2** (16*E*-benzylidene-$\Delta^{9,11}$-E1). It is already known from the literature that the main interactions between DHT and this enzyme are a conventional hydrogen bond with Hist221 residue and Van der Waals interactions with Leu149, Val143 and Pro187 residues (Day et al. 2008). Compound **2.2** has a 16*E*-benzylidene group at C16, which contributes to interactions with 17β-HSD1 target. In this context, it was demonstrated that a flexible linker in C16 position afforded superior 17β-HSD1 inhibition than those with a rigid alkene linker (Allan et al. 2006). Compounds **3.1**, **3.3** and **3.4** just exhibit the Van der Waals, alkyl and pi-alkyl interactions, lacking the hydrogen bond with Hist221, which can be determinant for their interaction with this target. Modifications at C16 of E1 and C2 of E2 to develop 17β-HSD1 inhibitors were already explored (Poirier et al. 2006; Laplante et al. 2008; Maltais et al. 2011; Salaha et al. 2019). In addition, 2- and/or 4-halogenated 13*β* or 13*α*-estrone derivatives led to a competitive reversible inhibition of 17β-HSD1 and ST enzymes (Bacsa et al. 2018), which was not observed for our A-ring halogenations by docking analysis. Further experimental studies would be necessary to elucidate these activities.

Also, E1-quinol **4.1** does not interact through a hydrogen bond with the essential amino acid His221 forming instead two hydrogen bonds with the residues Tyr218 and Ser222 (Day et al. 2008).

Regarding ST enzyme, none of the studied compounds showed relevant interaction with this target. It is known that the presence of a free or *N*-unsubstituted sulfamate group ($H_2NSO_2O–$) is a pre-requisite for potent and irreversible ST inhibition as shown by inhibitors like EMATE (Woo et al. 2012). However, E1 derivatives substituted at the 4-position with a small electron withdrawing group as nitro group or fluorine atom showed a good reversible and non-competitive inhibitory activity (Phan et al. 2011). However, the modifications performed in E1 did not allow to obtain ST inhibitors by docking analysis. Further experimental studies would be necessary to elucidate these activities.

The most interesting binding was observed between compound **5.7** ($\Delta^{9,11}$-E1 oxime) and β-tubulin. Besides the good affinity energy value, which is lower than the determined for colchicine, compound **5.7** is also predicted to have the most important interactions with β-tubulin, such as the conventional hydrogen bond with Cys B 241, alkyl and Pi-alkyl interactions with Leu B 248, and Van der Waals interaction with Val B 318 (Dorléans et al. 2009; Kumar et al. 2016; Bueno et al. 2018). Interestingly, previous studies suggested that the tubulin ligand interactions through amino acid residues Ala316 and Val318 are crucial in inducing antitubulin effect (Kumar et al. 2016). The other studied compounds, despite having good binding energies, do not establish the conventional bonds to tubulin. Therefore, the cell cycle arrest at G_2/M originated by compound **5.7**, at prophase can perhaps occur due to β-tubulin inhibition. However, future studies are needed to prove this hypothesis.

Overall, satisfactory docking results are obtained when relatively small ligands with few rotatable bonds are docked towards protein binding pockets in which flexibility does not play an important role. However, for complex molecules (with many rotatable bonds and flexibility), the use of methodology involving theoretical docking and molecular dynamic techniques are important to overtake these limitations, because they allow to evaluate and select the best molecule poses generated in the molecular docking, which can affect the results as shown by the difference obtained for molecular docking predictions and experimental results (Giacoppo et al. 2015; Lima et al. 2016; Paula et al. 2018).

Finally, *in silico* evaluation of drug-likeness properties, specifically the Lipinski's rule of five, and a prediction of the ADMET properties were performed for compound **4.1** (E1-quinol). These assays were performed because a novel bioprecursor prodrug (10β,17β-

dihydroxyestra-1,4-dien-3-one) approach for CNS-selective estrogen therapy was described with good oral bioavailability (Prokai-Tatrai and Prokai 2019). Otherwise, E1-quinol also showed a relevant antiproliferative effect against melanoma, cervix carcinoma and leukemia cells (Milić et al. 1999; Milić et al. 2001). Thus, despite the interesting potency and selectivity observed it is important to understand the potential toxicity risks inherent to its potential use.

The results showed a high Caco-2 permeability; high intestinal absorption; not be a P-glycoprotein substrate or inhibitor; not interact with the renal protein organic cation transporter 2 (OCT2); low probability to penetrate into the CNS; be a substrate of CYP3A4 isoform and low maximum tolerated dose in humans. The strong interactions with ERα and 17β-HSD1 and a relatively low maximum tolerated dose are relevant data to be considered in future studies involving this compound.

Considering the biological results obtained, the SARs for synthesized compounds are summarized in **Figure 6.1**.

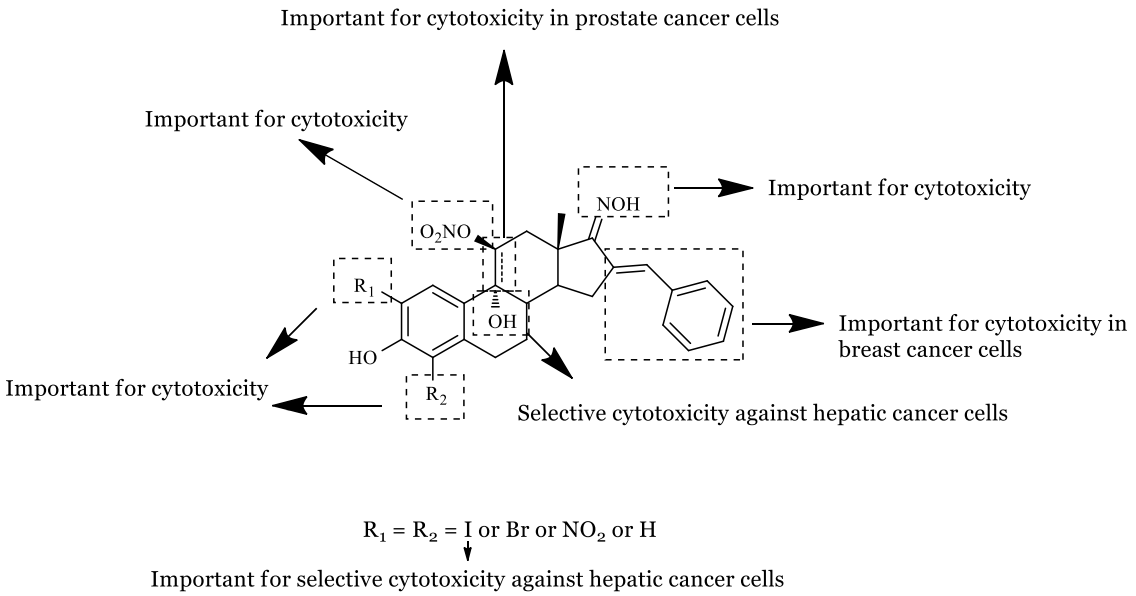

Figure 6.1 Structure activity relationship (SAR) analysis for estrone C17 oxime derivatives.

It was found that the 3-hydroxyl group was important for bioactivity of this type of compounds (comparing E1 with E1 acetate; and $\Delta^{9\text{-}11}$-E1 with $\Delta^{9\text{-}11}$-E1 acetate). Concerning A-ring halogenations, the introduction of iodine in positions 2 and 4 of E1 allowed a selective cytotoxicity against HepaRG cells. However, the presence of iodine and bromine in positions 2 and 4 of $\Delta^{9,11}$-E1 was not a favorable structural change for the development of potential antiproliferative agents. Both C9=C11 double bond and 16*E*-benzylidene groups led to an increase in the cytotoxicity in breast cancer cell lines.

The introduction of the group -ONO_2 at C11 showed to be a good strategy to improve cytotoxicity of compounds and 9α group seemed to be important to avoid estrogenicity. $\Delta^{9,11}$ and NOH group at C17 were important for cytotoxicity of LNCaP cells and probably to promote G_2/M arrest of cell cycle.

Chapter 7
Conclusion

The discovery of new oxime derivatives based on E1 scaffold was successfully achieved with the synthesis and biological assessment of five new oximes at C17. The structural design of the target molecules under investigation in this work was based on investigational and clinically relevant steroids, aiming at developing compounds with better antiproliferative activities. For that, modifications at C2, C3, C4, C9, C10, C11, C16 and C17 were performed through iodination, bromination, nitration, alkylation, condensation and acetylation reactions on E1 scaffold. The synthesis used allowed to obtain the products with good yields and applied straightforward and greener chemical processes. However, many reactions have failed avoiding the synthesis of more oximes, probably because steroids with an aromatic A-ring are difficult to modify namely due to steric reasons. For evaluating the antiproliferative effects of compounds synthesized, cell viability assays, cell cycle analysis, fluorescence microscopy and molecular docking predictions on ERα, 17β-HSD1, ST and β-tubulin were performed. These several assays are reliable, fast and inexpensive, representing a set of favorable characteristics that support their choice.

The most relevant key findings brought out from all the experimental work carried out under the scope of the present thesis are succinctly provided below:

- 3-Hydroxyl E1 derivatives showed to be more potent as antiproliferative molecules than 3-acetate E1 derivatives.
- 2,4-Diiodo derivatives showed to have selectivity for liver cancer cells.
- The halogenation of $\Delta^{9,11}$-E1 showed to have no benefit for antiproliferative activities.
- 9α-Hydroxy,11β-nitrooxy E1 acetate and E1-quinol showed to be the most cytotoxic molecules against hormone-dependent cancer cells, but they were also cytotoxic to liver cancer cells.
- 16*E*-Benzylidene-$\Delta^{9,11}$-E1 increased the cytotoxic activity on breast cancer cells.
- All compounds tested, except compound 9α-OH-E1 acetate, showed to be estrogenic compounds.
- $\Delta^{9,11}$-E1 Oxime showed the highest antiproliferative activity against prostate cancer cells.
- The possible mechanism of action for $\Delta^{9,11}$-E1 oxime was the β-tubulin inhibition predicted by molecular docking and due to biological effects observed as G_2/M cell cycle arrest.

Hence, several E1 derivatives were prepared and revealed interesting effects against the proliferation of several cancer cell lines. The small modification on E1 originated big differences in activity as observed by cell death, reduction of cell viability and cell cycle arrest at G_0/G_1 or G_2/M and the differences observed in molecular docking predictions. Further studies to understand the mechanisms of action that can be involved in the cytotoxicity of these new chemical entities were necessary.

In conclusion, the results obtained in this study provide new information on the cytotoxic activity of this class of steroids: the presence of a $\Delta^{9,11}$, the 9α-OH group and the presence of an oxime group at C17 in functionalized E1 scaffold showed to be a good starting point to obtain new molecules with relevant anticancer effects.

References

Ãbele E, Lukevics E. 2000. Recent advances in the chemistry of oximes. Org Prep Proced Int. 32(3):235–264.

Abida W, Patnaik A, Campbell D, Shapiro J, Bryce AH, McDermott R, Sautois B, Vogelzang NJ, Bambury RM, Voog E, et al. 2020. Rucaparib in men with metastatic castration-resistant prostate cancer harboring a BRCA1 or BRCA2 gene alteration. J Clin Oncol. 38(32):3763–3772.

Abou-Salim MA, Shaaban MA, Hameid MKAE, Elshaier YAMM, Halaweish F. 2019. Design, synthesis and biological study of hybrid drug candidates of nitric oxide releasing cucurbitacin-inspired estrone analogs for treatment of hepatocellular carcinoma. Bioorg Chem. 85:515–533.

ACS. 2018. Cancer Facts & Figures 2018. Atlanta: American Cancer Society. p. 1–68.

ACS. 2020. The history of cancer. [accessed 2020 Dec 8]. https://www.cancer.org/cancer/cancer-basics/history-of-cancer/cancer-causes-theories-throughout-history.html.

Adan A, Alizada G, Kiraz Y, Baran Y, Nalbant A. 2017. Flow cytometry: basic principles and applications. Crit Rev Biotechnol. 37(2):163–176.

Adan A, Kiraz Y, Baran Y. 2016. Cell proliferation and cytotoxicity assays. Curr Pharm Biotechnol. 17(14):1213–1221.

Ajithkumar TV, Gilbert DC. 2017. Modern challenges of cancer clinical trials. Clin Oncol. 29(12):767–769.

Aka JA, Mazumdar M, Chen C-Q, Poirier D, Lin S-X. 2010. 17β-Hydroxysteroid dehydrogenase type 1 stimulates breast cancer by dihydrotestosterone inactivation in addition to estradiol production. Mol Endocrinol. 24(4):832–845.

Aliau S, Delettre G, Mattras H, El Garrouj D, Nique F, Teutsch G, Borgna J-L. 2000. Steroidal affinity labels of the estrogen receptor α. 4. Electrophilic 11β-Aryl derivatives of estradiol. J Med Chem. 43(4):613–628.

Allan GM, Lawrence HR, Cornet J, Bubert C, Fischer DS, Vicker N, Smith A, Tutill HJ, Purohit A, Day JM, et al. 2006. Modification of estrone at the 6, 16, and 17 positions: novel potent inhibitors of 17β-hydroxysteroid dehydrogenase type 1. J Med Chem. 49(4):1325–1345.

Allison KH. 2012. Molecular pathology of breast cancer: What a pathologist needs to know. Am J Clin Pathol. 138(6):770–780.

Alsayari A, Kopel L, Ahmed MS, Pay A, Carlson T, Halaweish FT. 2017. Design, synthesis, and biological evaluation of steroidal analogs as estrogenic/anti-estrogenic agents. Steroids. 118:32–40.

Alvarez FS, Watt AN. 1972. The reaction of steroidal 3-keto-19-carboxylic acids and 19-nor steroidal dienones in solutions of iodine in pyridine. J Org Chem. 37(23):3725–3729.
Amelichev SA, Shashkov AS, Zavarzin I V, Rakitin OA. 2011. Synthesis of 17-(1,2,3-dithiazole) androstene derivatives. Mendeleev Commun. 21(4):186–187.
Amr AEE, Elsayed EA, Al-Omar MA, Eldin HOB, Nossier ES, Abdallah MM. 2019. Design, synthesis, anticancer evaluation and molecular modeling of novel estrogen derivatives. Molecules. 24(3):e416.
Andruska N, Mao C, Cherian M, Zhang C, Shapiro DJ. 2012. Evaluation of a luciferase-based reporter assay as a screen for inhibitors of estrogen-ERα-induced proliferation of breast cancer cells. J Biomol Screen. 17(7):921–932.
Anstead GM, Carlson KE, Katzenellenbogen JA. 1997. The estradiol pharmacophore: ligand structure-estrogen receptor binding affinity relationships and a model for the receptor binding site. Steroids. 62(3):268–303.
Arantes-Rodrigues R, Colaço A, Pinto-Leite R, Oliveira PA. 2013. *In Vitro* and *in vivo* experimental models as tools to investigate the efficacy of antineoplastic drugs on urinary bladder cancer. Anticancer Res. 33(4):1273–1296.
Archampong D, Sweetland H. 2014. Endocrine therapy in cancer care. Surgery. 33(3):122–126.
Aslantürk ÖS. 2018. *In vitro* cytotoxicity and cell viability assays: principles, advantages, and disadvantages. in: Genotoxicity - a predictable risk to our actual world. IntechOpen. p. 1–18.
Ayan D, Maltais R, Roy J, Poirier D. 2012. A new nonestrogenic steroidal inhibitor of 17β-hydroxysteroid dehydrogenase type 1 blocks the estrogen-dependent breast cancer tumor growth induced by estrone. Mol Cancer Ther. 11(10):2096–2104.
Ayaz O, Howlett SE. 2015. Testosterone modulates cardiac contraction and calcium homeostasis: Cellular and molecular mechanisms. Biol Sex Differ. 6(9):e1-15.
Bacsa I, Herman BE, Jójárt R, Herman KS, Wölfling J, Schneider G, Varga M, Tömböly C, Rižner TL, Szécsi M, et al. 2018. Synthesis and structure–activity relationships of 2- and/or 4-halogenated 13β- and 13α-estrone derivatives as enzyme inhibitors of estrogen biosynthesis. J Enzyme Inhib Med Chem. 33(1):1271–1282.
Bacsa I, Jójárt R, Schneider G, Wölfling J, Maróti P, Herman BE, Szécsi M, Mernyák E. 2015. Synthesis of A-ring halogenated 13α-estrone derivatives as potential 17β-HSD1 inhibitors. Steroids. 104:230–236.
Bader A, Bkhaitan MM, Abdalla AN, Abdallah QMA, Ali HI, Sabbah DA, Albadawi G, Abushaikha GM. 2021. Design and synthesis of 4-*O*-podophyllotoxin sulfamate derivatives as potential cytotoxic agents. Evid Based Complement Alternat Med. 2021:

e6672807.
Balogh J, Victor D, Gordon S, Li X, Ghobrial RM, Jr Monsour HP. 2016. Hepatocellular carcinoma: a review. J Hepatocell Carcinoma. 3:41–53.
Banfalvi G. 2017. Methods to detect apoptotic cell death. Apoptosis. 22(2):306–323.
Bansal R, Guleria S. 2008. Synthesis of 16E-[3-methoxy-4-(2-aminoethoxy)-benzylidene] androstene derivatives as potent cytotoxic agents. Steroids. 73(14):1391–1399.
Bansal R, Guleria S, Thota S, Hartmann RW, Zimmer C. 2011. Synthesis and biological evaluation of 16*E*-arylidenosteroids as cytotoxic and anti-aromatase agents. Chem Pharm Bull. 59(3):327–331.
Barakat R, Oakley O, Kim H, Jin J, Ko CMJ. 2016. Extra-gonadal sites of estrogen biosynthesis and function. BMB Rep. 49(9):488–496.
Bardia A, Aftimos P, Bihani T, Anderson-Villaluz AT, Jung J, Conlan MG, Kaklamani VG. 2019. EMERALD: Phase III trial of elacestrant (RAD1901) *vs* endocrine therapy for previously treated ER$^+$ advanced breast cancer. Future Oncol. 15(28):3209–3218.
Barnes JL, Zubair M, John K, Poirier MC, Martin FL. 2018. Carcinogens and DNA damage. Biochem Soc Trans. 46(5):1213–1224.
Baskar R, Lee KA, Yeo R, Yeoh KW. 2012. Cancer and radiation therapy: Current advances and future directions. Int J Med Sci. 9(3):193–199.
Batista VS, Crabtree RH, Konezny SJ, Luca OR, Praetorius JM. 2012. Oxidative functionalization of benzylic C-H bonds by DDQ. New J Chem. 36(5):1141–1144.
Baudino TA. 2015. Targeted cancer therapy: the next generation of cancer treatment. Curr Drug Discov Technol. 12(1):3–20.
Beato M, Klug J. 2000. Steroid hormone receptors: An update. Hum Reprod Update. 6(3):225–236.
Begam AJ, Jubie S, Nanjan MJ. 2017. Estrogen receptor agonists/antagonists in breast cancer therapy: A critical review. Bioorg Chem. 71:257–274.
Belfiore CJ, Hawkins DE, Wiltbank MC, Niswenders GD. 1994. Regulation of cytochrome P450scc synthesis and activity in the ovine *corpus luteum*. J Steroid Biochem Mol Biol. 51(5–6):283–290.
Berényi Á, Minorics R, Iványi Z, Ocsovszki I, Ducza E, Thole H, Mernyák E, Frank É, Schneider G, Zupkó I. 2013. Synthesis and investigation of the anticancer effects of estrone-16-oxime ethers *in vitro*. Steroids. 78(1):69–78.
Bereshchenko O, Bruscoli S, Riccardi C. 2018. Glucocorticoids, sex hormones, and immunity. Front Immunol. 9:e1332.
Berridge MV, Tan AS. 1993. Characterization of the cellular reduction of 3-(4,5-dimethylthiazol-2-yl)-2,5-diphenyltetrazolium bromide (MTT): subcellular localization,

substrate dependence, and involvement of mitochondrial electron transport in MTT reduction. Arch Biochem Biophys. 303(2):474–482.
Bessudo A, Wang X, Strauss JF, Slater DE, Pieczonka C, Guo P, Liu J, Yue Y, Lu C. 2021. A phase I dose-escalation study of LAE001/prednisone plus afuresertib in patients with metastatic castration-resistant prostate cancer (mCRPC) following standard of care (SOC) treatment. Ann Oncol. 32(5):644–645.
Bézivin C, Tomasi S, Dévéhat FLL, Boustie J. 2003. Cytotoxic activity of some lichen extracts on murine and human cancer cell lines. Phytomedicine. 10(6–7):499–503.
Bidram E, Esmaeili Y, Ranji-Burachaloo H, Al-Zaubai N, Zarrabi A, Stewart A, Dunstan DE. 2019. A concise review on cancer treatment methods and delivery systems. J Drug Deliv Sci Technol. 54:e101350.
Bose A, Sanjoto WP, Villarreal S, Aguilar H, Banik BK. 2007. Novel nitration of estrone by metal nitrates. Tetrahedron Lett. 48(23):3945–3947.
Bovicelli P, Lupattelli P, Mincione E, Prencipe T, Curci R. 1992. Oxidation of natural targets by dioxiranes. Oxyfunctionalization of steroids. J Org Chem. 57(7):2182–2184.
Boyd V, Cholewa OM, Papas KK. 2008. Limitations in the use of fluorescein diacetate/propidium iodide (FDA/PI) and cell permeable nucleic acid stains for viability measurements of isolated Islets of Langerhans. Curr Trends Biotechnol Pharm. 2(2):66–84.
Bray F, Ferlay J, Soerjomataram I, Siegel RL, Torre LA, Jemal A. 2018. Global cancer statistics 2018: GLOBOCAN estimates of incidence and mortality worldwide for 36 cancers in 185 countries. CA Cancer J Clin. 68(6):394–424.
Brito V, Alves G, Almeida P, Silvestre S. 2021. Highlights on steroidal arylidene derivatives as a source of pharmacologically active compounds: a review. Molecules. 26(7):e2032.
Brito V, Santos AO, Almeida P, Silvestre S. 2019. Novel 4-azaandrostenes as prostate cancer cell growth inhibitors: Synthesis, antiproliferative effects, and molecular docking studies. C R Chim. 22(1):73–83.
Brodie BB, Reid WD, Cho AK, Sipes G, Krishna G, Gillette JR. 1971. Possible mechanism of liver necrosis caused by aromatic organic compounds. Proc Natl Acad Sci. 68(1):160–164.
Brown W, Findlay JWA, Turner AB. 1968. Dehydrogenation of steroidal phenols via quinone methides. Chem Commun. 10:10–11.
Brozic P, Risner TL, Gobec S. 2008. Inhibitors of 17β-Hydroxysteroid dehydrogenase type 1. Curr Med Chem. 15(2):137–150.
Bucevičius J, Lukinavičius G, Gerasimaite R. 2018. The use of hoechst dyes for DNA staining and beyond. Chemosensors. 6(18):1–12.

Bueno O, Gallego JE, Martins S, Andrea EP, Gago F, Gómez-sanjuan A, Camarasa M, Barasoain I, Steinmetz MO, Díaz JF, et al. 2018. High-affinity ligands of the colchicine domain in tubulin based on a structure-guided design. Sci Rep. 8(1):1–17.

Buyyounouski MK, Choyke PL, McKenney JK, Sartor O, Sandler HM, Amin MB, Kattan MW, Lin DW. 2017. Prostate cancer–major changes in the american Joint Committee on Cancer eighth edition cancer staging manual. CA Cancer J Clin. 67(3):245–253.

Cabral F, Billstrom A, Hartley-Asp B. 1993. Estramustine depolymerizes microtubules by binding to tubulin. Cancer Res. 53(19):4573–4581.

Canário C, Matias M, Brito V, Santos AO, Falcão A, Silvestre S, Alves G. 2020. $\Delta^{9,11}$-Estrone derivatives as potential antiproliferative agents: synthesis, *in vitro* biological evaluation and docking studies. C R Chim. 23(2):201–217.

Canário C, Matias M, Brito V, Santos AO, Falcão A, Silvestre S, Alves G. 2021. New Estrone oxime derivatives: synthesis, cytotoxic evaluation and docking studies. Molecules. 26(9):e2687.

Canário C, Silvestre S, Falcão A, Alves G. 2018. Steroidal oximes: useful compounds with antitumor activities. Curr Med Chem. 25(6):660–686.

Capper CP, Rae JM, Auchus RJ. 2016. The metabolism, analysis, and targeting of steroid hormones in breast and prostate cancer. Horm Cancer. 7(3):149–164.

Carugo O. 2003. How root-mean-square distance (r.m.s.d.) values depend on the resolution of protein structures that are compared. J Appl Crystallogr. 36(1):125–128.

Chan HJ, Petrossian K, Chen S. 2016. Structural and functional characterization of aromatase, estrogen receptor, and their genes in endocrine-responsive and -resistant breast cancer cells. J Steroid Biochem Mol Biol. 161:73–83.

Chang J, Bhasin SS, Bielenberg DR, Sukhatme VP, Bhasin M, Huang S, Kieran MW, Panigrahy D. 2019. Chemotherapy-generated cell debris stimulates colon carcinoma tumor growth via osteopontin. FASEB J. 33(1):114–125.

Chen H, Liang X, Sun T, Qiao X, Zhou Z, Li Z, He C, Ya H, Yuan M. 2018. Synthesis and biological evaluation of estrone 3-*O*-ether derivatives containing the piperazine moiety. Steroids. 134:101–109.

Cheung KL. 2007. Endocrine therapy for breast cancer: an overview. Breast. 16(4):327–343.

Choudhary MI, Alam MS, Atta-Ur-Rahman, Yousuf S, Wu YC, Lin AS, Shaheen F. 2011. Pregnenolone derivatives as potential anticancer agents. Steroids. 76(14):1554–1559.

Chuffa LGA, Lupi-Júnior LA, Costa AB, Amorim JP de A, Seiva FRF. 2017. The role of sex hormones and steroid receptors on female reproductive cancers. Steroids. 118:93–108.

Claussner A, Nédélec L, Nique F, Philibert D, Teutsch G, Velde PV. 1992. 11β-

amidoalkyl estradiols, a new series of pure antiestrogens. J Steroid Biochem Mol Biol. 41(3):609–614.
Combs CA, Shroff H. 2017. Fluorescence microscopy: A concise guide to current imaging methods. Curr Protoc Neurosci. 79:2.1.1-2.1.25.
Cornel KMC, Krakstad C, Delvoux B, Xanthoulea S, Jori B, Bongers MY, Konings GFJ, Kooreman LFS, Kruitwagen RF, Salvesen HB, et al. 2017. High mRNA levels of 17β-hydroxysteroid dehydrogenase type 1 correlate with poor prognosis in endometrial cancer. Mol Cell Endocrinol. 442:51–57.
Cortés-Benítez F, Roy J, Maltais R, Poirier D. 2017. Impact of androstane A- and D-ring inversion on 17β-hydroxysteroid dehydrogenase type 3 inhibitory activity, androgenic effect and metabolic stability. Bioorganic Med Chem. 25(7):2065–2073.
Crowley F, Sterpi M, Buckley C, Margetich L, Handa S, Dovey Z. 2021. A review of the pathophysiological mechanisms underlying castration-resistant prostate cancer. Res Reports Urol. 13:457–472.
Cui W, Aouidate A, Wang S, Yu Q, Li Y, Yuan S. 2020. Discovering anti-cancer drugs via computational methods. Front Pharmacol. 11:e733.
Cushman M, He H-M, Katzenellenbogen JA, Lin CM, Hamel E. 1995. Synthesis, antitubulin and antimitotic activity, and cytotoxicity of analogs of 2-methoxyestradiol, an endogenous mammalian metabolite of estradiol that inhibits tubulin polymerization by binding to the colchicine binding site. J Med Chem. 38(12):2041–2049.
Cushman M, He HM, Katzenellenbogen JA, Varma RK, Hamel E, Lin CM, Ram S, Sachdeva YP. 1997. Synthesis of analogs of 2-methoxyestradiol with enhanced inhibitory effects on tubulin polymerization and cancer cell growth. J Med Chem. 40(15):2323–2334.
D'Accolti L, Fusco C, Lampignano G, Capitelli F, Curci R. 2008. Oxidation of natural targets by dioxiranes. Part 6: on the direct regio- and site-selective oxyfunctionalization of estrone and of 5α-androstane steroid derivatives. Tetrahedron Lett. 49(39):5614–5617.
Dasgupta P, Henshaw C, Youlden DR, Clark PJ, Aitken JF, Baade PD. 2020. Global trends in incidence rates of primary adult liver cancers: a systematic review and meta-analysis. Front Oncol. 10:e171.
Daśko M, Demkowicz S, Biernacki K, Ciupak O, Kozak W, Masłyk M, Rachon J. 2020. Recent progress in the development of steroid sulphatase inhibitors–examples of the novel and most promising compounds from the last decade. J Enzyme Inhib Med Chem. 35(1):1163–1184.
Day JM, Tutill HJ, Purohit A, Reed MJ. 2008. Design and validation of specific inhibitors of 17β-hydroxysteroid dehydrogenases for therapeutic application in breast

and prostate cancer, and in endometriosis. Endocr Relat Cancer. 15(3):665–692.
Deive N, Rodriguez J, Jiménez C. 2001. Synthesis of cytotoxic 6*E*-hydroximino-4-ene steroids: structure/activity studies. J Med Chem. 44(16):2612–2618.
Deluca D, Möller G, Rosinus A, Elger W, Hillisch A, Adamski J. 2006. Inhibitory effects of fluorine-substituted estrogens on the activity of 17beta-hydroxysteroid dehydrogenases. Mol Cell Endocrinol. 248(1–2):218–224.
Demirci S, Hayal TB, Kıratlı B, Şişli HB, Demirci S, Şahin F, Doğan A. 2019. Design and synthesis of phenylpiperazine derivatives as potent anticancer agents for prostate cancer. Chem Biol Drug Des. 94(3):1584–1595.
Deshpande A, Sicinski P, Hinds PW. 2005. Cyclins and cdks in development and cancer: A perspective. Oncogene. 24(17):2909–2915.
DeVore NM, Scott EE. 2012. Structures of cytochrome P450 17A1 with prostate cancer drugs abiraterone and TOK-001. Nature. 482(7383):116–119.
Dias TR, Alves MG, Almeida SP, Silva J, Barros A, Sousa M, Silva BM, Silvestre SM, Oliveira PF. 2015. Dehydroepiandrosterone and 7-oxo-dehydroepiandrosterone in male reproductive health: Implications of differential regulation of human Sertoli cells metabolic profile. J Steroid Biochem Mol Biol. 154:1–11.
Dimri M, Satyanarayana A. 2020. Molecular signaling pathways and therapeutic targets in hepatocellular carcinoma. Cancers (Basel). 12(2):e491.
DiPaola RS. 2002. To arrest or not to G_2/M cell-cycle arrest. Clin cancer Res. 8:3311–3314.
Dong JT. 2006. Prevalent mutations in prostate cancer. J Cell Biochem. 97(3):433–447.
Dorléans A, Gigant B, Ravelli RBG, Mailliet P, Mikol V, Knossow M. 2009. Variations in the colchicine-binding domain provide insight into the structural switch of tubulin. Proc Natl Acad Sci USA. 106(33):13775–13779.
Dutour R, Roy J, Cortés-Benítez F, Maltais R, Poirier D. 2018. Targeting cytochrome P450 (CYP)1B1 enzyme with four series of A-ring substituted estrane derivatives: design, synthesis, inhibitory activity, and selectivity. J Med Chem. 61(20):9229–9245.
Dwivedy I, Gupta A, Grover A, Srivastava V, Singh MM, Ray S. 2008. Synthesis and *in vivo* evaluation of 11-substituted estradiol derivatives as anti-implantation agents. Bioorganic Med Chem Lett. 18(14):4102–4105.
Edgren RA, Stanczyk FZ. 1999. Nomenclature of the gonane progestins. Contraception. 60(6):313.
Ediriweera MK, Tennekoon KH, Samarakoon SR. 2019. *In vitro* assays and techniques utilized in anticancer drug discovery. J Appl Toxicol. 39(1):38–71.
Egan JA, Filer CN. 2013. Biologically active equine estrogens and sulfate conjugates

labelled with tritium at high specific activity. Appl Radiat Isot. 71(1):68–71.
Ekins S, Mestres J, Testa B. 2007. *In silico* pharmacology for drug discovery: Methods for virtual ligand screening and profiling. Br J Pharmacol. 152(1):9–20.
El-Kady DS, Abd Rabou AA, Tantawy MA, Abdel-Rahman AAH, Abdel-Megeed AAS, AbdElhalim MM, Elmegeed GA. 2019. Synthesis and evaluation of novel cholestanoheterocyclic steroids as anticancer agents. Appl Biochem Biotechnol. 188(3):635–662.
Elder K, Michael Dixon J, Blackmur JP, Laurie J. 2021. Endocrine therapy for cancer. Surgery. 39(4):208–214.
EMA. 2010. European public assessment reports: Taxotere (Docetaxel) EMA/350414/2010. p :1–3.
EMA. 2015. European public assessment reports: Abraxane (paclitaxel) EMA/99258/2015. p :1–3.
EMA. 2016a. European public assessment reports: Kadcyla (trastuzumab emtansine) EMA/192622/2016. p :1–3.
EMA. 2016b. The EU regulatory system for medicines. A consistent approach to medicines regulation across the European Union. p:1–6.
EMA. 2018a. European public assessment reports: Perjeta (pertuzumab) EMA/377646/2018. p: 1-3
EMA. 2018b. European public assessment reports: Tyverb (lapatinib) EMA/516307/2018. p:1–3.
EMA. 2020a. European public assessment reports: Lynparza (olaparib) EMA/502202/2020. p:1–3.
EMA. 2020b. European public assessment reports: Enhertu (trastuzumab deruxtecan) EMA/692819/2020. p:1–3.
Evans G, Sutton EL. 2015. Oral contraception. Med Clin North Am. 99(3):479–503.
Faguet GB. 2015. A brief history of cancer: Age-old milestones underlying our current knowledge database. Int J Cancer. 136(9):2022–2036.
Falzone L, Salomone S, Libra M. 2018. Evolution of cancer pharmacological treatments at the turn of the third millennium. Front Pharmacol. 9:e1300.
Fan F, Wood K V. 2007. Bioluminescent assays for high-throughput screening. Assay Drug Dev Technol. 5(1):127–136.
Farzaneh S, Zarghi A. 2016. Estrogen receptor ligands: A review (2013–2015). Sci Pharm. 84(3):409–427.
Feng Q, He B. 2019. Androgen receptor signaling in the development of castration-resistant prostate cancer. Front Oncol. 9:e858.
Feng Y, Spezia M, Huang S, Yuan C, Zeng Z, Zhang L, Ji X, Liu W, Huang B, Luo W, et

al. 2018. Breast cancer development and progression: Risk factors, cancer stem cells, signaling pathways, genomics, and molecular pathogenesis. Genes Dis. 5(2):77–106.
Ferreira LG, Dos Santos RN, Oliva G, Andricopulo AD. 2015. Molecular docking and structure-based drug design strategies. Molecules. 20(7):13384–13421.
Fischer DS, Allan GM, Bubert C, Vicker N, Smith A, Tutill HJ, Purohit A, Wood L, Packham G, Mahon MF, et al. 2005. E-Ring modified steroids as novel potent inhibitors of 17β-hydroxysteroid dehydrogenase type 1. J Med Chem. 48(18):5749–5770.
Fishbein A, Hammock BD, Serhan CN, Panigrahy D. 2021. Carcinogenesis: Failure of resolution of inflammation? Pharmacol Ther. 218:e107670.
Fishbein A, Wang W, Yang H, Yang J, Hallisey VM, Deng J, Verheul SML, Hwang SH, Gartung A, Wang Y, et al. 2020. Resolution of eicosanoid/cytokine storm prevents carcinogen and inflammation-initiated hepatocellular cancer progression. Proc Natl Acad Sci USA. 117(35):21576–21587.
Freireich E. 1984. Landmark perspective: Nitrogen mustard therapy. JAMA. 251(17):2262–2263.
Fuentes N, Silveyra P. 2019. Estrogen receptor signaling mechanisms. Adv Protein Chem Struct Biol. 116(7):135–170.
Fujita K, Nonomura N. 2019. Role of androgen receptor in prostate cancer: A review. World J Men´s Heal. 37(3):288–295.
Fukuzawa K, Mochizuki Y, Tanaka S, Kitaura K, Nakano T. 2006. Molecular interactions between estrogen receptor and its ligand studied by the ab initio fragment molecular orbital method. J Phys Chem B. 110(32):16102–16110.
Gabbard RB, Hamer LF, Segaloff A. 1981. Structure-activity relationships of four 11-hydroxyestrones isomeric at the C-9 and C-11 positions. Steroids. 37(3):243–255.
Gao H. 1997. Approaches to partial syntheses of 11-oxo steroids. A brief review. Org Prep Proced Int. 29(5):499–539.
Ghosh D, Griswold J, Erman M, Pangborn W. 2009. Structural basis for androgen specificity and oestrogen synthesis in human aromatase. Nature. 457(7226):219–223.
Ghosh D, Pletnev VZ, Zhu DW, Wawrzak Z, Duax WL, Pangborn W, Labrie F, Lin S-X. 1995. Structure of human estrogenic 17β-hydroxysteroid dehydrogenase at 2.20 Å resolution. Structure. 3(5):503–513.
Giacoppo JOS, França TCC, Kuča K, Cunha EFF, Abagyan R, Mancini DT, Ramalho TC. 2015. Molecular modeling and *in vitro* reactivation study between the oxime BI-6 and acetylcholinesterase inhibited by different nerve agents. J Biomol Struct Dyn. 33(9):2048–2058.
Global Cancer Observatory. 2018. Cancer Statistics Reports for the UK. [accessed 2019

Oct 21], https://www.cancerresearchuk.org/health-professional/cancer-statistics/worldwide-cancer/incidence#heading-One
Golubovskaya LE, Ivanenko TI, Rzheznikov VM. 2009. Steroidal nitrates. Part III. Synthesis and antiestrogen activity of the 11α-nitroxy analog of ethynylestradiol. Pharm Chem J. 43(10):560–562.
Golubovskaya LE, Rzheznikov VM. 2007. Oxidation of estra-1,3,5(10)-triene-3,11α,17β-triol triacetate with ceric ammonium nitrate. Russ J Org Chem. 43(11):1730–1732.
Gordon J, Brown M, Reynolds M. 2018. Cell-based methods for determination of efficacy for candidate therapeutics in the clinical management of cancer. Diseases. 6:e85.
Granados-Romero JJ, Valderrama-Treviño AI, Contreras-Flores EH, Barrera-Mera B, Herrera Enríquez M, Uriarte-Ruíz K, Ceballos-Villalba JC, Estrada-Mata AG, Alvarado Rodríguez C, Arauz-Peña G. 2017. Colorectal cancer: a review. Int J Res Med Sci. 5(11):4667–4676.
Groner AC, Brown M. 2017. Role of steroid receptor and coregulator mutations in hormone-dependent cancers. J Clin Invest. 127(4):1126–1135.
Guo H, Wu H, Yang J, Xiao Y, Altenbach H-J, Qiu G, Hu H, Wu Z, He X, Zhou D, et al. 2011. Synthesis, characterization and biological evaluation of some 16*E*-arylidene androstane derivatives as potential anticancer agents. Steroids. 76(7):709–723.
Guo Z. 2017. The modification of natural products for medical use. Acta Pharm Sin B. 7(2):119–136.
Gupta A, Kumar BS, Negi AS. 2013. Current status on development of steroids as anticancer agents. J Steroid Biochem Mol Biol. 137:242–70.
Gyovai A, Minorics R, Kiss A, Mernyák E, Schneider G, Szekeres A, Kerekes E, Ocsovszki I, Zupkó I. 2018. Antiproliferative properties of newly synthesized 19-nortestosterone analogs without substantial androgenic activity. Front Pharmacol. 9:e825.
Haidar S, Klein CD, Hartmann RW, Chemie M, Saarlandes U, Box PO, Saarbrücken D-. 2001. Synthesis and evaluation of steroidal hydroxamic acids as inhibitors of P450 17 (17alpha-hydroxylase/C17-20-lyase). Arch Pharm Pharm Med Chem. 334(4):138–140.
Hajdu SI. 2011a. A note from history: Landmarks in history of cancer, Part 1. Cancer. 117(5):1097–1102.
Hajdu SI. 2011b. A note from history: Landmarks in history of cancer, Part 2. Cancer. 117(12):2811–2820.
Hajdu SI. 2012a. A note from history: Landmarks in history of cancer, Part 3. Cancer. 118(4):1155–1168.
Hajdu SI. 2012b. A note from history: Landmarks in history of cancer, Part 4. Cancer.

118(20):4914–4928.
Hajdu SI, Darvishian F. 2013. A note from history: Landmarks in history of cancer, Part 5. Cancer. 119(8):1450–1466.
Halperin I, Ma B, Wolfson H, Nussinov R. 2002. Principles of docking: An overview of search algorithms and a guide to scoring functions. Proteins Struct Funct Genet. 47(4):409–443.
Hanahan D. 2022. Hallmarks of Cancer: New Dimensions. Cancer Discov. 12(1):31–46.
Hanahan D, Weinberg R. 2000. The Hallmarks of Cancer. Cell. 100(1):57–70.
Hanahan D, Weinberg RA. 2011. Hallmarks of cancer: The next generation. Cell. 144(5):646–674.
Hanson RN, Hua E, Adam Hendricks J, Labaree D, Hochberg RB. 2012. Synthesis and evaluation of 11β-(4-substituted phenyl) estradiol analogs: Transition from estrogen receptor agonists to antagonists. Bioorganic Med Chem. 20(12):3768–3780.
Hanukoglu I. 1992. Steroidogenic enzymes: Structure, function, and role in regulation of steroid hormone biosynthesis. J Steroid Biochem Mol Biol. 43(8):779–804.
Haque MM, Desai K V. 2019. Pathways to endocrine therapy resistance in breast cancer. Front Endocrinol (Lausanne). 10:e573.
Harada T, Ohta I, Endo Y, Sunada H, Noma H, Taniguchi F. 2017. SR-16234, a novel selective estrogen receptor modulator for pain symptoms with endometriosis: An open-label clinical trial. Yonago Acta Med. 60(4):227–233.
Hartmann RW, Hector M, Haidar S, Ehmer PB, Reichert W, Jose J. 2000. Synthesis and evaluation of novel steroidal oxime inhibitors of P450 17 (17alpha-hydroxylase/C17-20-lyase) and 5alpha-Reductase Types 1 and 2. J Med Chem. 43(22):4266–4277.
Hejaz HAM, Purohit A, Mahon MF, Reed MJ, Potter BVL. 1999. Synthesis and biological activity of the superestrogen (*E*)-17-Oximino-3-*O*-sulfamoyl-1,3,5(10)-estratriene: X-ray crystal structure of (*E*)-17-Oximino-3-hydroxy-1, 3, 5(10)-estratriene. J Med Chem. 42(16):3188–3192.
Henderson BE, Feigelson HS. 2000. Hormonal carcinogenesis. Carcinogenesis. 21(3):427–433.
Herington AC, Chopin LK, Jeffery P, Amorim L, Veveris-Lowe T, Bui L, Clements JA. 2010. Hormone-dependent cancers: New approaches to identification of potential diagnostic and/or therapeutic biomarkers. Asia-Pacific J Mol Biol Biotechnol. 18(1):63–66.
Hernandez-Guzman FG, Higashiyama T, Osawa Y, Ghosh D. 2001. Purification, characterization and crystallization of human placental estrone/dehydroepiandrosterone sulfatase, a membrane-bound enzyme of the

endoplasmic reticulum. J Steroid Biochem Mol Biol. 78(5):441–450.
Hernandez-Guzman FG, Higashiyama T, Pangborn W, Osawa Y, Ghosh D. 2003. Structure of human estrone sulfatase suggests functional roles of membrane association. J Biol Chem. 278(25):22989–22997.
Hilal T, Gonzalez-Velez M, Prasad V. 2020. Limitations in clinical trials leading to anticancer drug approvals by the US food and drug administration. JAMA Intern Med. 180(8):1108–1115.
Holland HL, Kumaresan S, Tan L, Njar VCO. 1992. Synthesis of 6-Hydroximino-3-oxo steroids, a new class of aromatase inhibitor. J Chem Soc Perkin Trans 1. 5:585–587.
Hollingshead MG, Alley MC, Camalier RF, Abbott BJ, Mayo JG, Malspeis L, Grever MR. 1995. *In vivo* cultivation of tumor cells in hollow fibers. Life Sci. 57(2):131–141.
Holst JP, Soldin OP, Guo T, Soldin SJ. 2004. Steroid hormones: relevance and measurement in the clinical laboratory. Clin Lab Med. 24(1):105–118.
Hong Y, Chen S. 2011. Aromatase, estrone sulfatase, and 17β-hydroxysteroid dehydrogenase: Structure-function studies and inhibitor development. Mol Cell Endocrinol. 340(2):120–126.
Hori-Tanaka Y, Yura K, Takai-Igarashi T, Tanaka H. 2015. Structural classification of steroid-binding sites on proteins by coarse-grained atomic environment and its correlation with their biological function. Steroids. 96:81–88.
Howard N, Clementino M, Kim D, Wang L, Verma A, Shi X, Zhang Z, DiPaola RS. 2019. New developments in mechanisms of prostate cancer progression. Semin Cancer Biol. 57:111–116.
Hu J, Zhang Z, Shen WJ, Azhar S. 2010. Cellular cholesterol delivery, intracellular processing and utilization for biosynthesis of steroid hormones. Nutr Metab. 7(47):1–25.
Huang SY, Grinter SZ, Zou X. 2010. Scoring functions and their evaluation methods for protein-ligand docking: Recent advances and future directions. Phys Chem Chem Phys. 12(40):12899–12908.
Hudson DL, Guy AT, Fry P, O'Hare MJ, Watt FM, Masters JRW. 2001. Epithelial cell differentiation pathways in the human prostate: identification of intermediate phenotypes by keratin expression. J Histochem Cytochem. 49(2):271–278.
Icard P, Fournel L, Wu Z, Alifano M, Lincet H. 2019. Interconnection between metabolism and cell cycle in cancer. Trends Biochem Sci. 44(6):490–501.
Ireson CR, Alavijeh MS, Palmer AM, Fowler ER, Jones HJ. 2019. The role of mouse tumour models in the discovery and development of anticancer drugs. Br J Cancer. 121(2):101–108.
Ispán D, Szánti-Pintér E, Papp M, Wouters J, Tumanov N, Zsirka B, Gömöry Á, Kollár

L, Skoda-Földes R. 2018. The use of switchable polarity solvents for the synthesis of 16-arylidene steroids via Claisen–Schmidt condensation. European J Org Chem. 2018(24):3236–3244.
Jadhav AD, Gade EH, Angarkhe BL, Durrani A. 2018. An efficient one pot synthesis of oxime by classical method. Int J Chem Phys Sci. 7:12–16.
Janssen. 1996. Summary of product characteristics: Caelyx (pegykated liposomal doxorrubicin). p:1–40.
Janssen. 2018. Full prescribing information: Zytiga (abiraterone acetate). p:1–34.
Jesus M, Martins APJ, Gallardo E, Silvestre S. 2016. Diosgenin: Recent highlights on pharmacology and analytical methodology. J Anal Methods Chem. 2016:e 4156293.
Jindal DP, Chattopadhaya R, Guleria S, Gupta R. 2003. Synthesis and antineoplastic activity of 2-alkylaminoethyl derivatives of various steroidal oximes. Eur J Med Chem. 38(11–12):1025–1034.
Jones KL, Buzdar AU. 2004. A review of adjuvant hormonal therapy in breast cancer. Endocr Relat Cancer. 11(3):391–406.
Jurášek M, Černohorská M, Řehulka J, Spiwok V, Sulimenko T, Dráberová E, Darmostuk M, Gurská S, Frydrych I, Buriánová R, et al. 2018. Estradiol dimer inhibits tubulin polymerization and microtubule dynamics. J Steroid Biochem Mol Biol. 183:68–79.
Kamdje AHN, Etet PFS, Vecchio L, Muller JM, Krampera M, Lukong KE. 2014. Signaling pathways in breast cancer: Therapeutic targeting of the microenvironment. Cell Signal. 26(12):2843–2856.
Kargbo RB. 2020. PROTAC compounds targeting androgen receptor for cancer therapeutics: prostate cancer and Kennedy's disease. ACS Med Chem Lett. 11(6):1092–1093.
Karnik AV, Hasan M. 2021. Steroids stereochemistry. In: Stereochemistry: A Three-Dimensional Insight. 1st Edition. Elsevier. p. 338–339.
Katt ME, Placone AL, Wong AD, Xu ZS, Searson PC. 2016. *In vitro* tumor models: advantages, disadvantages, variables, and selecting the right platform. Front Bioeng Biotechnol. 4(12):1–14.
Kattan SW, Nafie MS, Elmgeed GA, Alelwani W, Badar M, Tantawy MA. 2020. Molecular docking, anti-proliferative activity and induction of apoptosis in human liver cancer cells treated with androstane derivatives: Implication of PI3K/AKT/mTOR pathway. J Steroid Biochem Mol Biol. 198:e105604.
Kerwin JF, Lancaster JR, Feldman PL. 1995. Nitric oxide: a new paradigm for second messengers. J Med Chem. 38(22):4343–4362.
Khanna V, Ranganathan S. 2009. Physiochemical property space distribution among

human metabolites, drugs and toxins. BMC Bioinformatics. 10(15):1–18.
Kim BR, Sung GH, Kim JJ, Yoon YJ. 2013. A development of rapid, practical and selective process for preparation of *z*-oximes. J Korean Chem Soc. 57(2):295–299.
Kim S, Kim Y, Ma E. 2012. Synthesis and 5α-reductase inhibitory activity of C_{21} steroids having 1,4-diene or 4,6-diene 20-ones and 4-azasteroid 20-oximes. Molecules. 17(1):355–68.
Kim S, Ma E. 2009. Synthesis of pregnane derivatives, their cytotoxicity on LNCaP and PC-3 cells, and screening on 5α-reductase inhibitory activity. Molecules. 14(11):4655–4668.
Kinghorn AD, Blanco EJC, Lucas DM, Rakotondraibe HL, Orjala J, Soejarto DD, Oberlies NH, Pearce CJ, Wani MC, Stockwell BR, et al. 2016. Discovery of anticancer agents of diverse natural origin. Anticancer Res. 36(11):5623–5637.
Kitchen DB, Decornez H, Furr JR, Bajorath J. 2004. Docking and scoring in virtual screening for drug discovery: methods and applications. Nat Rev Drug Discov. 3(11):935–949.
Kiwerska K, Szyfter K. 2019. DNA repair in cancer initiation, progression, and therapy—a double-edged sword. J Appl Genet. 60(3):329–334.
Klein T, Henn C, Negri M, Frotscher M. 2011. Structural basis for species specific inhibition of 17β-hydroxysteroid dehydrogenase type 1 (17β-HSD1): Computational study and biological validation. PLoS One. 6(8):e22990.
Koff JL, Ramachandiran S, Bernal-Mizrachi L. 2015. A time to kill: Targeting apoptosis in cancer. Int J Mol Sci. 16(2):2942–2955.
Kontomanolis EN, Koutras A, Syllaios A, Schizas D, Mastoraki A, Garmpis N, Diakosavvas M, Angelou K, Tsatsaris G, Pagkalos A, et al. 2020. Role of oncogenes and tumor-suppressor genes in carcinogenesis: A review. Anticancer Res. 40(11):6009–6015.
Koveitypour Z, Panahi F, Vakilian M, Peymani M, Forootan FS, Esfahani MHN, Ghaedi K. 2019. Signaling pathways involved in colorectal cancer progression. Cell Biosci. 9(97):1–14.
Kumar BS, Raghuvanshi DS, Hasanain M, Alam S, Sarkar J, Mitra K, Khan F, Negi AS. 2016. Recent Advances in chemistry and pharmacology of 2-methoxyestradiol: An anticancer investigational drug. Steroids. 110:9–34.
Kümler I, Knoop AS, Jessing CAR, Ejlertsen B, Nielsen DL. 2016. Review of hormone-based treatments in postmenopausal patients with advanced breast cancer focusing on aromatase inhibitors and fulvestrant. ESMO open. 1(4):e000062.
Kunnumakkara AB, Bordoloi D, Sailo BL, Roy NK, Thakur KK, Banik K, Shakibaei M, Gupta SC, Aggarwal BB. 2019. Cancer drug development: The missing links. Exp Biol

Med. 244(8):663–689.
Lao K, Wang Y, Chen M, Zhang J, You Q, Xiang H. 2017. Design, synthesis and biological evaluation of novel 2-methoxyestradiol analogs as dual selective estrogen receptor modulators (SERMs) and antiangiogenic agents. Eur J Med Chem. 139:390–400.
Laplante Y, Cadot C, Fournier M-A, Poirier D. 2008. Estradiol and estrone C-16 derivatives as inhibitors of type 1 17β-hydroxysteroid dehydrogenase: Blocking of ER^+ breast cancer cell proliferation induced by estrone. Bioorganic Med Chem. 16(4):1849–1860.
Latif AD, Gonda T, Vágvölgyi M, Kúsz N, Kulmány Á, Ocsovszki I, Zomborszki ZP, Zupkó I, Hunyadi A. 2019. Synthesis and *in vitro* antitumor activity of naringenin oxime and oxime ether derivatives. Int J Mol Sci. 20(9):e2184.
Lee CI, Goodwin A, Wilcken N. 2017. Fulvestrant for hormone-sensitive metastatic breast cancer (review). Cochrane Database Syst Rev. 3(1):CD011093.
Lee CS, Ryan EJ, Doherty GA. 2014. Gastro-intestinal toxicity of chemotherapeutics in colorectal cancer: The role of inflammation. World J Gastroenterol. 20(14):3751–3761.
Lee HR, Hwang KA, Park MAH, Yi B-R, Jeung EB, Choi KC. 2012. Treatment with bisphenol A and methoxychlor results in the growth of human breast cancer cells and alteration of the expression of cell cycle-related genes, cyclin D1 and p21, via an estrogen receptor-dependent signaling pathway. Int J Mol Med. 29(5):883–890.
Lee YT, Tan YJ, Oon CE. 2018. Molecular targeted therapy: Treating cancer with specificity. Eur J Pharmacol. 834:188–196.
Leese MP, Leblond B, Newman SP, Purohit A, Reed MJ, Potter BVL. 2005. Anti-cancer activities of novel D-ring modified 2-substituted estrogen-3-*O*-sulfamates. J Steroid Biochem Mol Biol. 94(1–3):239–251.
Lespérance M, Barbeau X, Roy J, Maltais R, Lagüe P, Poirier D. 2018. Chemical synthesis of C3-oxiranyl/oxiranylmethyl-estrane derivatives targeted by molecular modeling and tested as potential inhibitors of 17β-hydroxysteroid dehydrogenase type 1. Steroids. 140:104–113.
Lespérance M, Roy J, Djiemeny Ngueta A, Maltais R, Poirier D. 2021. Synthesis of 16β-derivatives of 3-(2-bromoethyl)-estra-1,3,5(10)-trien-17β-ol as inhibitors of 17β-HSD1 and/or steroid sulfatase for the treatment of estrogen-dependent diseases. Steroids. 172:e108856.
Liang CD, Baran JS. 1976. Synthesis and conformational stabilities of 11-oxo-9α- and 9β-estradiol 3-benzyl ether. Tetrahedron. 32:2067–2069.
Liga Portuguesa Contra o Cancro. 2021. Cancro da Mama. [accessed 2021 Jan 17]. https://www.ligacontracancro.pt/cancro-da-mama/.

Lima WEA, Pereira AF, Castro AA de, Cunha EFF, Ramalho TC. 2016. Flexibility in the molecular design of acetylcholinesterase reactivators: probing representative conformations by chemometric techniques and docking/QM calculations. Lett Drug Des Discov. 13(5):360–371.

Ling Y, Li J, Kato K, Liu Y, Wang X, Klus GT, Marat K, Nnane IP, Brodie AMH. 1998. Synthesis and *in vitro* activity of some epimeric 20α-hydroxy, 20-oxime and aziridine pregnene derivatives as inhibitors of human 17α-hydroxylase/C17,20-lyase and 5α-reductase. Bioorg Med Chem. 6(10):1683–1693.

Lipinski CA. 2000. Drug-like properties and the causes of poor solubility and poor permeability. J Pharmacol Toxicol Methods. 44(1):235–249.

Lista L, Manini P, Napolitano A, Pezzella A, D'Ischia M. 2006. Practical one-pot conversion of 17β-estradiol to 10β-hydroxy-(*p*-quinol) and 10β-chloro-17β-hydroxyestra-1,4-dien-3-one. Steroids. 71(8):670–673.

Lista L, Pezzella A, Napolitano A, D'Ischia M. 2008. Mild and efficient iodination of aromatic and heterocyclic compounds with the NaClO2/NaI/HCl system. Tetrahedron. 64(1):234–239.

Liu JF, Gordon M, Veneris J, Braiteh F, Balmanoukian A, Eder JP, Oaknin A, Hamilton E, Wang Y, Sarkar I, et al. 2019. Safety , clinical activity and biomarker assessments of atezolizumab from a Phase I study in advanced/recurrent ovarian and uterine cancers. Gynecol Oncol. 154(2):314–322.

Liu X, Zhang F, Liu H, Burdette JE, Li Y, Overk CR, Pisha E, Yao J, Van Breemen RB, Swanson SM, et al. 2003. Effect of halogenated substituents on the metabolism and estrogenic effects of the equine estrogen, equilenin. Chem Res Toxicol. 16(6):741–749.

Liu Y, Yin T, Feng Y, Cona MM, Huang G, Liu J, Song S, Jiang Y, Xia Q, Swinnen J V, et al. 2015. Mammalian models of chemically induced primary malignancies exploitable for imaging-based preclinical theragnostic research. Quant Imaging Med Surg. 5(5):708–729.

Lobaccaro C, Pons JF, Duchesne MJ, Auzou G, Pons M, Nique F, Teutsch G, Borgna JL. 1997. Steroidal affinity labels of the estrogen receptor. 3. Estradiol 11β-*n*-alkyl derivatives bearing a terminal electrophilic group: Antiestrogenic and cytotoxic properties. J Med Chem. 40(14):2217–2227.

Lorente D, Llacer C, Lozano R, Velasco G, Romero-Laorden N, Rodrigo M, Sánchez-Iglesias Á, Capua C, Castro E, Ferrer C, et al. 2021. Prognostic score and benefit from abiraterone in first-line metastatic, castration-resistant prostate cancer. Eur Urol. 80(5):641–649.

Lossignol D. 2016. A little help from steroids in oncology. J Transl Intern Med. 4(1):52–54.

Lozano R, Castro E, Aragón IM, Cendón Y, Cattrini C, López-Casas PP, Olmos D. 2021. Genetic aberrations in DNA repair pathways: a cornerstone of precision oncology in prostate cancer. Br J Cancer. 124(3):552–563.
Lu DY, Lu T-R, Zhu H, Ding J, Xu B, Wu SY, Yarla NS. 2017. Anticancer drug development, getting out from bottleneck. Int J Mol Biol. 2(1):28–33.
Lu Y, Chen J, Xiao M, Li W, Miller DD. 2012. An overview of tubulin inhibitors that interact with the colchicine binding site. Pharm Res. 29(11):2943–2971.
Luch A. 2005. Nature and nurture - Lessons from chemical carcinogenesis. Nat Rev Cancer. 5(2):113–125.
Lugemwa FN, Shaikh K, Hochstedt E. 2013. Facile and efficient acetylation of primary alcohols and phenols with acetic anhydride catalyzed by dried sodium bicarbonate. Catalysts. 3(4):954–965.
Lunn WHW, Farkas E. 1968. The adamantyl carbonium ion as a dehydrogenating agent, its reactions with estrone. Tetrahedron. 24(5):6773–6776.
Madan RA, Schmidt KT, Karzai F, Peer CJ, Cordes LM, Chau CH, Steinberg SM, Owens H, Eisner J, Moore WR, et al. 2020. A Phase 2 study of seviteronel (INO-464) in patients with metastatic castration-resistant prostate cancer post-enzalutamide treatment. Clin Genitourin Cancer. 18(4):258–267.
Maitland NJ. 2021. Resistance to antiandrogens in prostate cancer: Is it inevitable, intrinsic or induced? Cancers (Basel). 13(327):1–32.
Majtnerova P, Capek J, Petira F, Handl J, Rousar T. 2021. Quantitative spectrofluorometric assay detecting nuclear condensation and fragmentation in intact cells. Sci Rep. 11:e11921.
Majumder A, Singh M, Tyagi SC. 2017. Post-menopausal breast cancer: From estrogen to androgen receptor. Oncotarget. 8(60):102739–102758.
Makar S, Saha T, Swetha R, Gutti G, Kumar A, Singh SK. 2020. Rational approaches of drug design for the development of selective estrogen receptor modulators (SERMs), implicated in breast cancer. Bioorg Chem. 94: e103380.
Maltais R, Ayan D, Poirier D. 2011. Crucial role of 3-bromoethyl in removing the estrogenic activity of 17β-HSD1 inhibitor 16β-(*m*-carbamoylbenzyl)estradiol. ACS Med Chem Lett. 2(9):678–681.
Maltais R, Ayan D, Trottier A, Barbeau X, Lagüe P, Bouchard JE, Poirier D. 2014. Discovery of a non-estrogenic irreversible inhibitor of 17β-Hydroxysteroid dehydrogenase type 1 from 3-substituted-16β-(*m*-carbamoylbenzyl)-estradiol derivatives. J Med Chem. 57(1):204–222.
Maltais R, Trottier A, Barbeau X, Lagüe P, Perreault M, Thériault J, Lin S, Poirier D. 2016. Impact of structural modifications at positions 13, 16 and 17 of 16β-(*m*-

carbamoylbenzyl)-estradiol on 17β-hydroxysteroid dehydrogenase type 1 inhibition and estrogenic activity. J Steroid Biochem Mol Biol. 161:24–35.
Mandal A. 2019. Cancer Classification. [accessed 2021 Dec 4]. https://www.news-medical.net/health/Cancer-Classification.aspx.
Mandigo AC, Tomlins SA, Kelly WK, Knudsen KE. 2022. Relevance of pRB loss in human malignancies. Clin Cancer Res. 28(2):255–264.
Manna PR, Dyson MT, Stocco DM. 2009. Regulation of the steroidogenic acute regulatory protein gene expression: Present and future perspectives. Mol Hum Reprod. 15(6):321–333.
Markossian S, Grossman A, Brimacombe K, Arkin M, Auld D, Austin CP, Baell J, Chung TDY, Coussens NP, Dahlin JL, et al. 2016. Assay Guidance Manual. Eli Lilly & Company and the National Center for Advancing Translational Sciences.
Mazzanti R, Arena U, Tassi R. 2016. Hepatocellular carcinoma: Where are we? World J Exp Med. 6(1):21–36.
McLaughlin F, Finn P, La Thangue NB. 2003. The cell cycle, chromatin and cancer: Mechanism-based therapeutics come of age. Drug Discov Today. 8(17):793–802.
McNamara KM, Nakamura Y, Miki Y, Sasano H. 2013. Phase two steroid metabolism and its roles in breast and prostate cancer patients. Front Endocrinol (Lausanne). 4(116):1–7.
Meng X-Y, Zhang H-X, Mezei M, Cui M. 2011. Molecular docking: a powerful approach for structure-based drug discovery. Curr Comput Aided-Drug Des. 7(2):146–157.
Meng X, Lei Y, Zhang X, Sun K, Zhang L, Wang Z. 2021. Cancer immunotherapy: Classification, therapeutic mechanisms, and nanomaterial-based synergistic therapy. Appl Mater Today. 24:e101149.
Mernyák E, Kovács I, Minorics R, Sere P, Czégány D, Sinka I, Wolfling J, Schneider G, Újfaludi Z, Boros I, et al. 2015. Synthesis of trans-16-triazolyl-13α-methyl-17-estradiol diastereomers and the effects of structural modifications on their *in vitro* antiproliferative activities. J Steroid Biochem Mol Biol. 150:123–134.
Messinger J, Husen B, Koskimies P, Hirvelä L, Kallio L, Saarenketo P, Thole H. 2009. Estrone C15 derivatives- a new class of 17β-hydroxysteroid dehydrogenase type 1 inhibitors. Mol Cell Endocrinol. 301(1–2):216–224.
Miki Y, Iwabuchi E, Ono K, Sasano H, Ito K. 2018. Exploring protein–protein interaction in the study of hormone-dependent cancers. Int J Mol Sci. 19(10):1–17.
Milić D, Gašić M, Muster W, Csanádi J, Šolaja B. 1997. The synthesis and biological evaluation of A-ring substituted steroidal *p*-quinones. Tetrahedron. 53(41):14073–14084.
Milić D, Kop T, Juranić Z, Gašić MJ, Tinant B, Pocsfalvi G, Šolaja BA. 2005. Synthesis

and antiproliferative activity of A-ring aromatised and conduritol-like steroidal compounds. Steroids. 70(14):922–932.
Milić DR, Kapor A, Markov B, Ribar B, Strümpel M, Juranić Z, Gašić MJ, Šolaja BA. 1999. X-ray crystal structure of 10β-hydroxy-4β,5β-epoxyestr-1-en3,17-dione and antitumor activity of its congeners. Molecules. 4(12):338–352.
Milić DR, Kop T, Juranić Z, Gašić MJ, Šolaja BA. 2001. Synthesis and antiproliferative activity of epoxy and bromo compounds derived from estrone. Bioorg Med Chem Lett. 11(16):2197–2200.
Miller WL. 2017. Steroidogenesis: Unanswered Questions. Trends Endocrinol Metab. 28(11):771–793.
Miller WL, Auchus RJ. 2011. The molecular biology, biochemistry, and physiology of human steroidogenesis and its disorders. Endocr Rev. 32(1):81–151.
Miller WL, Strauss JF. 1999. Molecular pathology and mechanism of action of the steroidogenic acute regulatory protein, STAR. J Steroid Biochem Mol Biol. 69(1–6):131–141.
Mirzaei S, Qayumov M, Gangi F, Behravan J, Ghodsi R. 2020. Synthesis and biological evaluation of oxazinonaphthalene-3-one derivatives as potential anticancer agents and tubulin inhibitors. Iran J Basic Med Sci. 23(11):1388–1395.
Mohammadian M, Mahdavifar N, Mohammadian-Hafshejani A, Salehiniya H. 2018. Liver cancer in the world: epidemiology, incidence, mortality and risk factors. World cancer Res J. 5(2):e1082.
Mohs RC, Greig NH. 2017. Drug discovery and development: Role of basic biological research. Alzheimer's Dement Transl Res Clin Interv. 3(4):651–657.
Morozkina SN, Shavva AG. 2016. Estrone sulfatase inhibitors as new anticancer agents. In: Chemistry and Biological Activity of Steroids. IntechOpen. p. 1–26.
Mosmann T. 1983. Rapid colorimetric assay for cellular growth and survival: Application to proliferation and cytotoxicity assays. J Immunol Methods. 65(1–2):55–63.
Moss GP. 1989. Nomenclature of steroids. Pure Appl Chem. 61(10):1783–1822.
Mould DR, Hutson PR. 2017. Critical considerations in anticancer drug development and dosing strategies: the past, present, and future. J Clin Pharmacol. 57(10):116–128.
Muntha P. 2016. Drug discovery & development - A Review. Res Rev Pharm Pharm Sci. 5(1):135–142.
Murray TBJ. 2021. Chapter 3: The Pathogenesis of Prostate Cancer. In: Prostate Cancer. Brisbane: Exon Publications, p. 29–42.
Murugan R, Scriven EF V. 2003. Applications of dialkylaminopyridine (DMAP) catalysts in organic synthesis. Aldrichima Acta. 36(1):21–27.

Napolitano E, Fiaschi R, Carlson SKE, Katzenellenbogen JA. 1995. 11β-Substituted estradiol derivatives. 2. Potential carbon-11- and iodine-labeled probes for the estrogen receptor. J Med Chem. 38:2774–2779.
NCCN. 2021. NCCN Guidelines Version 1.2022 Breast Cancer.
NCCN. 2022a. NCCN Guidelines Version 3.2022 Prostate Cancer.
NCCN. 2022b. NCCN Guidelines Version 1.2022 Hepatobiliary Cancers.
NCCN. 2022c. NCCN Guidelines Version 1.2022 Colon Cancer.
Nguyen LH, Goel A, Chung DC. 2020. Pathways of colorectal carcinogenesis. Gastroenterology. 158(2):291–302.
NIH. 2022. Phases of Cancer Clinical Trials. [accessed 2022 May 22]. https://www.cancer.gov/about-cancer/treatment/clinical-trials/what-are-trials/phases.
Nogales E, Downing KH, Amos LA, Löwe J. 1998. Tubulin and FtsZ form a distinct family of GTPases. Nat Struct Biol. 5(6):451–458.
Noppe H, Le Bizec B, Verheyden K, De Brabander HF. 2008. Novel analytical methods for the determination of steroid hormones in edible matrices. Anal Chim Acta. 611(1):1–16.
Nussbaumer P, Billich A. 2004. Steroid sulfatase inhibitors. Med Res Rev. 24(4):529–576.
Odes EJ, Randolph-Quinney PS, Steyn M, Throckmorton Z, Smilg JS, Zipfel B, Augustine TN, Beer FD, Hoffman JW, Franklin RD, et al. 2016. Earliest hominin cancer: 1.7-million-year old osteosarcoma from Swartkrans cave, South Africa. S Afr J Sci. 112(7–8):1–6.
Ohe T, Hirobe M, Mashino T. 2000. Novel metabolic pathway of estrone and 17β-estradiol catalyzed by cytochrome P450. Drug Metab Dispos. 28(2):110–112.
Page PCB, Hussain F, Bonham NM, Morgan P, Maggs JL, Park BK. 1991. Regioselective synthesis of A-ring halogenated derivatives of 17α-ethynyloestradiol. Tetrahedron. 47(16–17):2871–2878.
Palmieri C, Januszewski A, Stanway S, Coombes RC. 2011. Irosustat: A first-generation steroid sulfatase inhibitor in breast cancer. Expert Rev Anticancer Ther. 11(2):179–183.
Palomino E. 1999. Chemical modulation of activity in steroidal estrogens. Crit Rev Biochem Mol Biol. 34(6):387–398.
Palomino E, Heef MJ, Horwitz JP, Polin L, Brooks SC. 1994. Skeletal conformations and receptor binding of some 9,11-modified estradiols. J Steroid Biochem Mol Biol. 50(1–2):75–84.
Pan L, Chai HB, Kinghorn AD. 2012. Discovery of new anticancer agents from higher plants. Front Biosci - Sch. 4(1):142–156.

Panigrahy D, Gartung A, Yang J, Yang H, Gilligan MM, Sulciner ML, Bhasin SS, Bielenberg DR, Chang J, Schmidt BA, et al. 2019. Preoperative stimulation of resolution and inflammation blockade eradicates micrometastases. J Clin Invest. 129(7):2964–2979.

Parker AL, Kavallaris M, McCarroll JA. 2014. Microtubules and their role in cellular stress in cancer. Front Oncol. 4:e153.

Parsons HA, Macrae ER, Guo H, Li T, Barry WT, Tayob N, Wulf GM, Isakoff SJ, Krop IE. 2021. Phase II single-arm study to assess trastuzumab and vinorelbine in advanced breast cancer patients with HER2-negative tumors and HER2-positive circulating tumor cells. JCO Precis Oncol. 5:896–903.

Patil Shirish, Patil Sudhir, Kokare N, Pujari A. 2019. Review : the *in vivo* screening methods of anticancer. World J Pharm Pharm Sci. 8(2):202–215.

Paula RL, Almeida JSFD, Cavalcante SFA, Gonçalves AS, Simas ABC, Franca TCC, Valis M, Kuca K, Nepovimova E, Granjeiro JM. 2018. Molecular modeling and *in vitro* studies of a neutral oxime as a potential reactivator for acetylcholinesterase inhibited by paraoxon. Molecules. 23(11):e2954.

Payne AH, Hales DB. 2004. Overview of steroidogenic enzymes in the pathway from cholesterol to active steroid hormones. Endocr Rev. 25(6):947–970.

Pearce A, Haas M, Viney R, Pearson S, Haywood P, Brown C, Ward R. 2017. Incidence and severity of self-reported chemotherapy side effects in routine care: A prospective cohort study. PLoS One. 10: e0184360.

Peltoketo H, Isomaa V, Mäentausta O, Vihko R. 1988. Complete amino acid sequence of human placental 17β-hydroxysteroid dehydrogenase deduced from cDNA. FEBS Lett. 239(1):73–77.

Pereira K, Côté P-L, Cantin L, Blanchet J, Labrie F, Breton R. 2006. Comparison of crystal structures of human androgen receptor ligand-binding domain complexed with various agonists reveals molecular determinants responsible for binding affinity. Protein Sci. 15(5):987–999.

Peters RH, Crowe DF, Avery MA, Chong WKM, Tanabe M. 1989. 11β-Nitrate estrane analogues: potent estrogens. J Med Chem. 32(10):2306–2310.

Petrelli F, Coinu A, Borgonovo K, Cabiddu M, Ghilardi M, Lonati V, Barni S. 2014. The value of platinum agents as neoadjuvant chemotherapy in triple-negative breast cancers: A systematic review and meta-analysis. Breast Cancer Res Treat. 144(2):223–232.

Pfizer. 2016. Summary of product characteristics: Ibrance (Palbociclib). p:1–106.

Phan C, Liu Y, Kim B, Mostafa Y, Taylor D. 2011. Inhibition of steroid sulfatase with 4-substituted estrone and estradiol derivatives. Bioorg Med Chem. 19(20):5999–6005.

Pires V., Blundell TL, Ascher DB. 2015. pkCSM: Predicting Small-Molecule Pharmacokinetic and Toxicity Properties Using Graph-Based Signatures. J Med Chem. 58(9):4066–4072.

Pizzo F, Gadaleta D, Lombardo A, Nicolotti O, Benfenati E. 2015. Identification of structural alerts for liver and kidney toxicity using repeated dose toxicity data. Chem Cent J. 9(1):1–11.

Poirier D. 2011. Contribution to the development of inhibitors of 17β-hydroxysteroid dehydrogenase types 1 and 7: Key tools for studying and treating estrogen-dependent diseases. J Steroid Biochem Mol Biol. 125(1–2):83–94.

Poirier D, Chang HJ, Azzi A, Boivin RP, Lin SX. 2006. Estrone and estradiol C-16 derivatives as inhibitors of type 1 17β-hydroxysteroid dehydrogenase. Mol Cell Endocrinol. 248(1–2):236–238.

Poirier D, Dionne P, Auger S. 1998. A 6β-(thiaheptanamide) derivative of estradiol as inhibitor of 17β-hydroxysteroid dehydrogenase type 1. J Steroid Biochem Mol Biol. 64(1–2):83–90.

Poirier D, Mérand Y, Labrie C, Labrie F. 1996. D-ring alkylamide derivatives of estradiol: Effect on ER-binding affinity and antiestrogenic activity. Bioorganic Med Chem Lett. 6(21):2537–2542.

Poirier D, Roy J, Maltais R. 2021. Estrogen-Biosynthesis Pathways: *In vitro* (metabolism) and *in vivo* (xenograft) studies in T-47D breast cancer models. Cancers (Basel). 13(8):e1841.

Poisson T, Oudeyer S, Levacher V. 2012. Efficient C-3 functionalization of 4-dimethylaminopyridine (DMAP). A straightforward access to new chiral nucleophilic catalysts. Tetrahedron Lett. 53(26):3284–3287.

Pokhrel M, Ma E. 2011. Synthesis and screening of aromatase inhibitory activity of substituted C19 steroidal 17-oxime analogs. Molecules. 16(12):9868–9885.

Ponce-Cusi R, Calaf GM. 2016. Apoptotic activity of 5-fluorouracil in breast cancer cells transformed by low doses of ionizing α-particle radiation. Int J Oncol. 48(2):774–782.

Prokai-Tatrai K, Prokai L. 2019. A novel prodrug approach for central nervous system-selective estrogen therapy. Molecules. 24(22):1–17.

Prokai L, Prokai K, Simpkins J. 2003. Patent Application Publication, Pub. No.: US 2003/0229060A1. 1(19).

Prokai L, Prokai K, Simpkins J. 2004. Patent Application Publication, Pub. No.: US 2004/0138190 A1. 1(405).

Purohit A, Williams G, Howarth N, Potter B, Reed M. 1995. Inactivation of steroid sulfatase by an active site-directed inhibitor, estrone-3-*O*-sulfamate. Biochemistry. 34(36):11508–11514.

Purohit A, Williams G, Roberts C, Potter B, Reed M. 1999. *In vivo* inhibition of *o*estrone sulphatase and dehydroepiandrosterone sulphatase by oestrone-3-O-sulphamate. Int J Cancer. 63(1):106–111.

Qiu W, Campbell RL, Gangloff A, Dupuis P, Boivin RP, Tremblay MR, Poirier D, Lin SX. 2002. A concerted, rational design of type 1 17β-hydroxysteroid dehydrogenase inhibitors: estradiol-adenosine hybrids with high affinity. FASEB J. 16(13):1829–1831.

Quinkert G., Weber W-D., Schwartz U. 1982. United States Patent. 4,357,278.(2).

Raj K, Mathi P, Prasad MVVV, Botlagunta M, Ravi M, Ramachandran D. 2018. *De novo* design of selective Sortase-A inhibitors: Synthesis, structural and *in vitro* characterization. Chem Data Collect. 15–16:126–133.

Ramalingam S, Ramamurthy VP, Njar VCO. 2017. Dissecting major signaling pathways in prostate cancer development and progression: Mechanisms and novel therapeutic targets. J Steroid Biochem Mol Biol. 166:16–27.

Rao PN, Cessac JW. 2002. A new, practical synthesis of 2-methoxyestradiols. Steroids. 67(13–14):1065–1070.

Rasmussen LM, Zaveri NT, Stenvang J, Peters RH, Lykkesfeldt AE. 2007. A novel dual-target steroid sulfatase inhibitor and antiestrogen: SR 16157, a promising agent for the therapy of breast cancer. Breast Cancer Res Treat. 106(2):191–203.

Ravelli RBG, Gigant B, Curmi PA, Jourdain I, Lachkar S, Sobel A, Knossow M. 2004. Insight into tubulin regulation from a complex with colchicine and a stathmin-like domain. Nature. 428:198–202.

Rawla P, Sunkara T, Barsouk A. 2019. Epidemiology of colorectal cancer: Incidence, mortality, survival, and risk factors. Prz Gastroenterol. 14(2):89–103.

Reed MJ, Purohit A, Woo LWL, Newman SP, Potter BVL. 2005. Steroid sulfatase: Molecular biology, regulation, and inhibition. Endocr Rev. 26(2):171–202.

Resende FA, Oliveira APS, Camargo MS, Vilegas W, Varanda EA. 2013. Evaluation of estrogenic potential of flavonoids using a recombinant yeast strain and MCF7/BUS cell proliferation assay. PLoS One. 8(10):e74881.

Riss TL, Moravec RA, Niles AL, Duellman S, Benink HA, Worzella TJ, Minor L. 2013. Cell Viability Assays. In: Assay Guidance Manual. Eli Lilly & Company and the National Center for Advancing Translational Sciences.

Rižner TL. 2016. The important roles of steroid sulfatase and sulfotransferases in gynecological diseases. Front Pharmacol. 7(30):1–16.

Rodriguez J, Nunez L, Peixinho S, Jiménez C. 1997. Isolation and synthesis of the first natural 6-hydroximino 4-en-3-one- steroids from the sponges. Tetrahedron Lett. 38(10):1833–1836.

Romagosa C, Simonetti S, López-Vicente L, Mazo A, Lleonart ME, Castellvi J, Cajal

SRY. 2011. P16Ink4a overexpression in cancer: A tumor suppressor gene associated with senescence and high-grade tumors. Oncogene. 30(18):2087–2097.
Ruyck J, Brysbaert G, Blossey R, Lensink M. 2016. Molecular docking as a popular tool in drug design, an *in silico* travel. Adv Appl Bioinforma Chem. 9(1):1–11.
Rzheznikov VM, Golubovskaya LE, Minailova ON, Osetrova IP, Smirnova ZS. 2003. Steroidal nitrates: synthesis and antitumor activity of 9α, 11β-dihydroxyestra-1,3,5(10)-triene 11-nitrates. Pharm Chem J. 37(1):10–12.
Saeidnia S, Manayi A, Abdollahi M. 2013. The pros and cons of the *in silico* pharmaco-toxicology in drug discovery and development. Int J Pharmacol. 9(3):176–181.
Saikia L, Baruah J, Thakur A. 2011. A rapid, convenient, solventless green approach for the synthesis of oximes using grindstone chemistry. Org Med Chem Lett. 1(12):1–6.
Sainsbury R. 2013. The development of endocrine therapy for women with breast cancer. Cancer Treat Rev. 39(5):507–517.
Sajjad H, Imtiaz S, Noor T, Siddiqui YH, Sajjad A, Zia M. 2021. Cancer models in preclinical research: A chronicle review of advancement in effective cancer research. Anim Model Exp Med. 4(2):87–103.
Sakač MN, Penov Gaši KM, Popsavin M, Djurendić EA, Andrić S, Kovačević RM. 2005. Synthesis and estrogenic activity screening of some 6,9-disubstituted estradiol derivatives. Collect Czechoslov Chem Commun. 70(4):479–486.
Salaha M, Abdelsamieb AS, Frotschera M. 2019. Inhibitors of 17β-hydroxysteroid dehydrogenase type 1, 2 and 14: Structures, biological activities and future challenges. Mol Cell Endocrinol. 489:66–81.
Salmaso V, Moro S. 2018. Bridging molecular docking to molecular dynamics in exploring ligand-protein recognition process: An overview. Front Pharmacol. 9:e923.
Salto-Tellez M, Cree IA. 2019. Cancer taxonomy: pathology beyond pathology. Eur J Cancer. 115:57–60.
Salvador JAR, Carvalho JFS, Neves MAC, Silvestre SM, Leitão AJ, Silva MMC, Sá e Melo ML. 2013. Anticancer steroids: linking natural and semi-synthetic compounds. Nat Prod Rep. 30(2):324–374.
Salvador JAR, Silvestre S, Moreira VM. 2012. Recent developments in oxidative processes in steroid chemistry. Curr Org Chem. 16(10):1243–1276.
Salvador JAR, Silvestre SM. 2005. Bismuth-catalyzed allylic oxidation using *t*-butyl hydroperoxide. Tetrahedron Lett. 46(15):2581–2584.
Sam KM, Boivin RP, Tremblay MR, Auger S, Poirier D. 1998. C16 and C17 derivatives of estradiol as inhibitors of 17β-hydroxysteroid dehydrogenase type 1: chemical synthesis and structure-activity relationships. Drug Des Discov. 15(3):157–180.
Sánchez-Sánchez L, Hernández-Linares MG, Escobar ML, López-Muñoz H, Zenteno E,

Fernández-Herrera MA, Guerrero-Luna G, Carrasco-Carballo A, Sandoval-Ramírez J. 2016. Antiproleferative, cytotoxic and apoptotic activity of steroidal oximes in cervicouterine cell Lines. Molecules. 21:e1533.
Santaniello E, Ravasi M, Ferraboschi P. 1983. A-Ring nitration of estrone. J Org Chem. 48(5):739–740.
Schäcke H, Döcke W-D, Asadullah K. 2002. Mechanisms involved in the side effects of glucocorticoids. Pharmacol Ther. 96(1):23–43.
Schiffer L, Barnard L, Baranowski ES, Gilligan LC, Taylor AE, Arlt W, Shackleton CHL, Storbeck KH. 2019. Human steroid biosynthesis, metabolism and excretion are differentially reflected by serum and urine steroid metabolomes: A comprehensive review. J Steroid Biochem Mol Biol. 194:e105439.
Schmid P, Adams S, Rugo HS, Schneeweiss A, Barrios CH, Iwata H, Diéras V, Hegg R, Im S-A, Wright GS, et al. 2018. Atezolizumab and nab-paclitaxel in advanced triple-negative breast cancer. N Engl J Med. 379(22):2108–2121.
Schrecengost R, Knudsen KE. 2013. Molecular pathogenesis and progression of prostate cancer. Semin Oncol. 40(3):244–258.
Schwarz S, Schumacher M, Nanninga A, Weber G, Thieme I, Undeutsch B, Elger W. 1999. 17β-Hydroxy-11α-(3'-sulfanylpropyl)oxy-estra-1,3,5(10)-trien-3-yl sulfamate - A novel hapten structure: Toward the development of a specific enzyme immunoassay (EIA) for estra-1,3,5(10)-triene-3-yl sulfamates. Steroids. 64(7):460–471.
Sheikh A, Hussain SA, Ghori Q, Naeem N, Fazil A, Giri S, Sathian B, Mainali P, Al Tamimi DM. 2015. The spectrum of genetic mutations in breast cancer. Asian Pacific J Cancer Prev. 16(6):2177–2185.
Shen G, Wang C, Luo Y, Wang J, Wang R, Xu W, Zhang Yi, Zhang Yu, Zhang D, Jin C. 2020. NF-κB Signalling pathways in lung cancer A549 cells. Evidence-Based Complement Altern Med. 29:e00594.
Siddiqui IA, Sanna V, Ahmad N, Sechi M, Mukhtar H. 2015. Resveratrol nanoformulation for cancer prevention and therapy. Ann N Y Acad Sci. 1348(1):20–31.
Siegel RL, Miller KD, Jemal A. 2020. Cancer statistics, 2020. CA Cancer J Clin. 70(1):7–30.
Silvestre SM. 2007. Capítulo 4: Oxidação de alcenos a enonas utilizando clorito de sódio, na ausência de catalisadores metálicos. In: Novos processos de oxidação ambientalmente aceitáveis usando esteróides como substratos. p. 160–204.
Simeón JLL, Morales JET, Navarro FAV, Manchado FC, Montoto LGP. 2004. Actividad catalítica del acetato de vanadilo en la acetilación de alcoholes secundarios. Rev CENIC Ciencias Químicas. 35(3):141–145.
Simpkins JW, Yang SH, Liu R, Perez E, Zu YC, Covey DF, Green PS. 2004. Estrogen-

like compounds for ischemic neuroprotection. Stroke. 35(1):2648–2651.
Simpson ER. 2002. Aromatization of androgens in women: Current concepts and findings. Fertil Steril. 77(4):S1–S9.
Simpson ER. 2003. Sources of estrogen and their importance. J Steroid Biochem Mol Biol. 86(3–5):225–230.
Sinka I, Kiss A, Mernyák E, Wölfling J, Schneider G, Ocsovszki I, Kuo C-Y, Wang H-C, Zupkó I. 2018. Antiproliferative and antimetastatic properties of 3-benzyloxy-16-hydroxymethylene-estradiol analogs against breast cancer cell lines. Eur J Pharm Sci. 123:362–370.
Sivoňová MK, Jurečeková J, Tatarková Z, Kaplán P, Lichardusová L, Hatok J. 2017. The role of CYP17A1 in prostate cancer development: structure, function, mechanism of action, genetic variations and its inhibition. Gen Physiol Biophys. 36(5):487–499.
Skehan P, Storeng R, Scudiero D, Monks A, Mcmahon J, Vistica D, Warren JT, Bokesch H, Kenney S, Boyd MR. 1990. New colorimetric cytotoxicity assay for anticancer-drug screening. J Natl Cancer Inst. 82(13):1107–1112.
Soronen P, Laiti M, Törn S, Härkönen P, Patrikainen L, Li Y, Pulkka A, Kurkela R, Herrala A, Kaija H, et al. 2004. Sex steroid hormone metabolism and prostate cancer. Steroid Biochem Mol Biol. 92(4):281–286.
Soto AM, Sonnenschein C, Chung KL, Fernandez MF, Olea N, Serrano FO. 1995. The *E-SCREEN* assay as a tool to identify estrogens: an update on estrogenic environmental pollutants. Env Heal Perspect. 103(7):113–122.
Stanczyk FZ. 2009. Production, Clearance, and Measurement of Steroid Hormones. In: The Global Library of Women's Medicine. Sapiens Publishing, LTD.
Stander A, Joubert F, Joubert A. 2011. Docking, synthesis, and *in vitro* evaluation of antimitotic estrone analogs. Chem Biol Drug Des. 77(4):173–181.
Stathis A, Siu LL, Tourneau C Le. 2012. Capter 1: Preclinical Drug Development: Translating Basic Research into Clinical Work. In: Clinical Pharmacology of Anti-Cancer Agents. ESMO. p. 1–8.
Stein CJ, Colditz GA. 2004. Modifiable risk factors for cancer. Br J Cancer. 90(2):299–303.
Stéphan E, Zen R, Authier L, Jaouen G. 1995. Improved synthesis of a protected 11-oxoestrone. Steroids. 60(12):809–811.
Stockert JC, Blazquez-Castro A. 2017. Fluorescence Microscopy in Life Sciences. Bentham Science Publishers Ltd.
Stubenrauch G, Knuppen R. 1976. Convenient large scale preparation of catechol estrogens. Steroids. 28(5):733–741.
Sung H, Ferlay J, Siegel RL, Laversanne M, Soerjomataram I, Jemal A, Bray F. 2021.

Global Cancer Statistics 2020: GLOBOCAN Estimates of Incidence and Mortality Worldwide for 36 Cancers in 185 Countries. CA Cancer J Clin. 71(3):209–249.
Sutherland RL, Watts CKW, Musgrove EA. 1995. Cell cycle control by steroid hormones in breast cancer: Implications for endocrine resistance. Endocr Relat Cancer. 2(1):87–96.
Suvarna V. 2010. Phase IV of Drug Development. Perspect Clin Res. 1(2):57–60.
Sykes PJ, Rutherford FJ, Laing SB, Phillipps GH, Turnbull JP. 1971. Oxidation of ring A-aromatic steroids to 9,11β-diol 11-nitrates with ceric ammonium nitrate. Tetrahedron Lett. 12(37):3393–3396.
Tanenbaum DM, Wang Y, Williams SP, Sigler PB. 1998. Crystallographic comparison of the estrogen and progesterone receptor's ligand binding domains. Proc Natl Acad Sci USA. 95(11):5998–6003.
Tang JJ, Li G, Gao JM. 2019. Synthesis and cytotoxicity of novel steroidal C-20 oxime ester derivatives from 16-DPA. Arab J Chem. 12(8):2084–2090.
Taylor RA, Toivanen R, Risbridger GP. 2010. Stem cells in prostate cancer: Treating the root of the problem. Endocr Relat Cancer. 17(4):273–285.
Tolosa L, Pinto S, Donato MT, Lahoz A, Castell JV, O'connor JE, Gómez-Lechón MJ. 2012. Development of a multiparametric cell-based protocol to screen and classify the hepatotoxicity potential of drugs. Toxicol Sci. 127(1):187–198.
Toné S, Sugimoto K, Tanda K, Suda T, Uehira K, Kanouchi H, Samejima K, Minatogawa Y, Earnshaw WC. 2007. Three distinct stages of apoptotic nuclear condensation revealed by time-lapse imaging, biochemical and electron microscopy analysis of cell-free apoptosis. Exp Cell Res. 313(16):3635–3644.
Tremblay MR, Auger S, Poirier D. 1995. Synthesis of 16-(bromoalkyl)-estradiols having inhibitory effect on human placental estradiol 17β-hydroxysteroid dehydrogenase (17-β-HSD type 1). Bioorganic Med Chem. 3(5):505–523.
Tremblay MR, Boivin RP, Luu-The V, Poirier D. 2005. Inhibitors of type 1 17β-hydroxysteroid dehydrogenase with reduced estrogenic activity: modifications of the positions 3 and 6 of estradiol. J Enzyme Inhib Med Chem. 20(2):153–163.
Trott O, Olson AJ. 2010. AutoDock Vina: Improving the speed and accuracy of docking with a new scoring function, efficient optimization, and multithreading. J Comput Chem. 31(2):455–461.
Tsuchiya Y, Nakajima M, Yokoi T. 2005. Cytochrome P450-mediated metabolism of estrogens and its regulation in human. Cancer Lett. 227(2):115–124.
Ulm M, Ramesh A V., McNamara KM, Ponnusamy S, Sasano H, Narayanan R. 2019. Therapeutic advances in hormone-dependent cancers: Focus on prostate, breast and ovarian cancers. Endocr Connect. 8(2):10–26.

Valente KP, Khetani S, Kolahchi AR, Sanati-Nezhad A, Suleman A, Akbari M. 2017. Microfluidic technologies for anticancer drug studies. Drug Discov Today. 22(11):1654–1670.

Veronesi U, Boyle P, Goldhirsch A, Orecchia R, Viale G. 2005. Breast cancer. Lancet. 365(9472):1727–1741.

Villanueva A, Newell P, Chiang DY, Friedman SL, Llovet JM. 2007. Genomics and signaling pathways in hepatocellular carcinoma. Semin Liver Dis. 27(1):55–76.

Vosooghi M, Yahyavi H, Divsalar K, Shamsa H, Kheirollahi A, Safavi M, Ardestani SK, Sadeghi-Neshat S, Mohammadhosseini N, Edraki N, et al. 2013. Synthesis and *in vitro* cytotoxic activity evaluation of (*E*)-16-(substituted benzylidene) derivatives of dehydroepiandrosterone. Daru. 21(1):e34.

Wan Z, Musa MA, Joseph P, Cooperwood JS. 2013. Synthesis and biological activity of 3-*N*-substituted estrogen derivatives as breast cancer agents. Mini Rev Med Chem. 13(9):1381–1388.

Wang LH, Wu CF, Rajasekaran N, Shin YK. 2018. Loss of tumor suppressor gene function in human cancer: An overview. Cell Physiol Biochem. 51(6):2647–2693.

Wang P, Henning SM, Heber D. 2010. Limitations of MTT and MTS-based assays for measurement of antiproliferative activity of green tea polyphenols. PLoS One. 5(4):e10202.

Wang P, McInnes C, Zhu BT. 2013. Structural characterization of the binding interactions of various endogenous estrogen metabolites with human estrogen receptor α and β subtypes: a molecular modeling study. PLoS One. 8(9):1–11.

Wendlandt AE, Yelton SM, Lou D, Watt DS, Noonan DJ. 2010. Synthesis and functional analysis of novel bivalent estrogens. Steroids. 75(12):825–833.

WHO. 2013. International Classification of Diseases for Oncology, Third Edition. WHO.

WHO. 2020. Cancer. [accessed 2020 Nov 29]. https://www.who.int/health-topics/cancer#tab=tab_1.

Wolpin BM, Mayer RJ. 2008. Systemic treatment of colorectal cancer. Gastroenterology. 134(5):1296–1310.

Woo LWL, Leblond B, Purohit A, Potter BVL. 2012. Synthesis and evaluation of analogues of estrone-3-*O*-sulfamate as potent steroid sulfatase inhibitors. Bioorg Med Chem. 20(8):2506–2519.

Woo LWL, Purohit A, Potter BVL. 2011. Development of steroid sulfatase inhibitors. Mol Cell Endocrinol. 340(2):175–185.

Wu F, Zhou Y, Li L, Shen X, Chen G, Wang X, Liang X, Tan M, Huang Z. 2020. Computational approaches in preclinical studies on drug discovery and development.

Front Chem. 8:e726.
Yang CPH, Horwitz SB. 2017. Taxol®: The first microtubule stabilizing agent. Int J Mol Sci. 18(8): e1733.
Yaşar P, Ayaz G, User SD, Güpür G, Muyan M. 2017. Molecular mechanism of estrogen–estrogen receptor signaling. Reprod Med Biol. 16(1):4–20.
Zhang J, Labaree DC, Hochberg RB. 2005. Nonpolar and short side chain groups at C-11β of estradiol result in antiestrogens. J Med Chem. 48(5):1428–1447.
Zloh M, Kirton SB. 2018. The benefits of in silico modeling to identify possible small-molecule drugs and their off-target interactions. Future Med Chem. 10(4):423–432.
Zucchini G, Geuna E, Milani A, Aversa C, Martinello R, Montemurro F. 2015. Clinical utility of exemestane in the treatment of breast cancer. Int J Womens Health. 7:551–563.